THE MEASUREMENT OF THE DEFORMATION PROPERTIES

OF

·COWDEN TILL AT SMALL STRAINS

by

Peter Chiu Yin Yung

Diploma (H.K.B.C.), M.Eng. (Sheffield)

.

SUMMARY

The work described in this thesis was firstly concerned with developing and evaluating automated soil testing equipment and associated instrumentation. The equipment consists principally of a triaxial stress path cell of the Bishop-Wesley type, a microcomputer and two pressure controllers. Inductive displacement transducers have been mounted inside the cell to measure axial and radial strains locally on the specimen boundary and axial strains between the end caps. The local axial strain measurements have proved superior to the end cap measurements which can be adversely affected by bedding errors and misalignment of the transducers relative to the loading axis.

Following the development, the system was used to investigate the stress-strain behaviour of Cowden Till, particularly at small strains (0.01 - 0.10%). Cylindrical blocks of 250mm diameter were retrieved from the site and stored under isotropic stress. Eight specimens of 100mm diameter were trimmed from these blocks and subjected to either a drained or undrained compression test under load-controlled conditions.

Cowden Till has been shown to exhibit strongly non-linear stress-strain behaviour, even at small strains, and most of the shear strain is irreversible. The stress-strain characteristics were in acceptable agreement with those derived from a 865mm diameter plate loading test with under-plate instrumentation. Although the interpretation of the plate test is still being investigated, it is concluded that plate tests provide no better information about the stiffness of the material than triaxial tests of the type described in this thesis.

The experimental stress-strain behaviour during compressive loading has been compared with the predictions of some mathematical models. The non-linear elastic model of Atkinson (1973) appears to be applicable to Cowden Till, for which the behaviour is approximately isotropic. Simple stiffness

predictions on the basis of critical state soil mechanics are inadequate at small strains. However, the model of Pender (1978) predicts the behaviour reasonably well.

An attempt has been made to analyse the compression (bedding error) which occurs at the end of a triaxial specimen as the axial strain is increased. A quantification of the compression is hindered by the random nature of surface variations and by the limitations of present theories.

CONTENTS

LIST OF FIGURES

ACKNOWLEDGEMENTS

ABBREVIATIONS AND NOTATION

Abbreviation of Units

C	Celsius
cm	centimeter
hr	hour
gm	gramme
kg	kilogramme
kgf	kilogramme force
kN	kilonewton
MN	maganewton
m	metre
mm	millimeter
V	volt
μm	micron
%	percentage

List of Abbreviations

AC	Alternating Current
ASCE	American Society of Civil Engineers
ASME	American Society of Mechanical Engineers
BS	British Standard
BRE	Building Research Establishment
DC	Direct Current
ICE	Institution of Civil Engineers (London, UK)
ICI	Imperial Chemical Industries
ICSMFE	International Conference on Soil Mechanics and Foundation Engineering
IEEE	Institution of Electrical and Electronic Engineers

LL	Liquid Limit (Atterberg)
LVDT	Linear Variable Differential Transformer (displacement transducer)
MC	Moisture Content
PL	Plastic Limit (Atterberg)
OCR	Overconsolidation Ratio
UK	United Kingdom
VDU	Video Display Unit

Notation - Capitals

A	cross-sectional area of triaxial specimen
A_o	initial cross-sectional area of triaxial specimen
A_s	pore water pressure parameter for unloading during sampling
B	increase in specimen pore water pressure divided by increase in applied cell pressure in triaxial tests
B	diameter of sampling tube
B	diameter of loading plate in plate load tests
D	diameter of triaxial specimen
E	Young's modulus of elasticity
$E*$	composite Young's modulus for bodies making contact
E_A	apparent Young's modulus (with effect of end restraint)
E_T	true Young's modulus
E', E_u	Young's modulus in terms of effective stress and total stress respectively
E'_v, E'_H	Young's modulus for vertically and horizontally orientated specimens respectively
$(E')_{0.1}$, $(E_u)_{0.1}$	secant Young's modulus in terms of effective stress and total stress respectively at indicated axial strain level
$(E')_{ur}$, $(E_u)_{ur}$	secant Young's modulus in terms of effective and total stress respectively from unload-reload cycle

$(E')_{50}$, $(E_u)_{50}$	secant Young's modulus in terms of effective and total stress respectively at half of maximum deviator stress
G	elastic undrained shear modulus
G'	shear modulus in terms of effective stress
G_{ur}	shear modulus from unload-reload cycle
G_{50}	secant shear modulus at half of maximum deviator stress
G'_v	shear modulus in a vertical plane (in a cross-anisotropic medium)
K	slope of stress path in (p', q) plane
K'	bulk modulus in terms of effective stress
K_o	coefficient of lateral earth pressure at rest
L	length of triaxial specimen
L_o	initial length of triaxial specimen
L_a	lower Bellofram sealed area
L_g	gauge length within central half of triaxial specimen
L_p	lower chamber pressure
N_c	bearing capacity factor
N_p	pressuremeter constant
P	load applied in a plate loading test
R	rate of change of deviator stress with respect to time
R	radius of triaxial specimen
U_a	upper Bellofram sealed area
V	volume of triaxial specimen
V_o	initial volume of traixial specimen
v^e	elastic volumetric strain
v^p	plastic volumetric strain
V_p	volume of pressuremeter

V_{po} volume of pressuremeter at $p = p_{ho}$

W weight

W average work done per unit area

Z vertical distance below ground surface

Z_p depth of borehole

Notation - Lower Case

a_o initial amplitude of sinusoidal bedding surface

a_1 amplitude of sinusoidal bedding surface during deformation

c' effective cohesion of soil

c_u undrained shear strength of soil

c_v, c_s coefficients of consolidation and swelling respectively

d differential operator

d depth beneath plate in a plate loading test

d perpendicular distance between axis of tilting and centre of top cap

k_b stiffness of clay matrix

m_v, m_s coefficient of volume decrease and expansion respectively

n degree of effective stress anisotropy

p total mean normal stress $(= \frac{1}{3}(\sigma_1' + \sigma_2' + \sigma_3'))$

p' effective mean normal stress $(= \frac{1}{3}(\sigma_1' + \sigma_2' + \sigma_3'))$

p_o' value of p' at start of a shearing process

p_o amplitude of a sinusoidal pressure distribution

p_L pressure in a pressuremeter test when cavity expands indefinitely

p'_{cs} value of p' at critical state

p'_k value of p' after perfect sampling

p'_{max}	preconsolidation pressure
p_n	normal pressure applied to an elastic medium to produce a sinusoidal surface deflection
p_p	current pressure in a pressuremeter test
$\bar{p}$	mean pressure applied in order to eliminate bedding
$\bar{p}_T$	value of $\bar{p}$ for total elimination of bedding
p_{ho}	total horizontal in-situ stress
p'_{vo}, p_{vo}	effective and total in-situ overburden pressure respectively
q	deviator stress
q_f	value of deviator stress at failure
q_n	net applied pressure in plate loading test
q_p	bearing pressure in plate loading test
q_u	ultimate bearing pressure in plate loading test
q_{max}	maximum value of q
r	radial distance
s	shear strength of material
t	time
t	thickness of sampling tube
u	pore water pressure
v	specific volume of soil
w	half width of contact during bedding deformation
x	horizontal distance
z	vertical distance

Notation - Capital Greek Symbols

Γ	specific volume of soil at critical state with $p' = 1.0$ kN/m^2
Δ	large increment of ...
M	slope of critical state line when it is projected on to a constant volume plane

Notation - Lower Case Greek Symbols

ϕ'	effective angle of shearing resistance
θ	angle between axis of tilting and line joining submersible LVDTs
α	angle of upper axial target ring with horizontal
β	angle of lower axial target ring with horizontal
ξ	semi-angle wedges in idealization of bedding
δ	small increment of ...
γ	angle of tilting of top cap
γ_{max}	maximum shear strain at edge of borehole in a pressuremeter test
τ	shear stress at wall of borehole in a pressuremeter test
ν	Poisson's ratio
ν'	Poisson's ratio in a drained test
ν_u	Poisson's ratio in a constant volume test
ν_1'	value of ν' for strain in any horizontal direction due to a horizontal stress applied at right angles in a cross-anisotropic medium
ν_3'	value of ν' for strain in the horizontal direction due to a vertical stress in a cross-anisotropic medium
ρ	settlement of plate in a plate loading test
λ	slope of normal consolidation line (negative)
λ_b	wavelength of idealized sinusoidal bedding
κ	slope of overconsolidation line (negative)
σ', σ	effective and total normal stress respectively
σ_1', σ_2', σ_3'	effective major, intermediate and minor principal stresses respectively
σ_1, σ_2, σ_3	total major, intermediate and minor principal stresses respectively
σ_v', σ_H	effective vertical and horizontal normal stresses respectively

σ_v, σ_H	total vertical and horizontal normal stresses respectively
η	stress ratio ($= \dfrac{q}{p'}$)
ε_A	axial strain
$(\varepsilon_A)_{50}$	value of ε_A at half of q_{max}
ε_c	cavity strain in pressuremeter test
ε_f	axial strain at failure
ε_s	shear strain
ε_v	volumetric strain
ε^p	plastic shear strain
ε_E	end cap axial strain (average of two sides)
ε_L	local axial strain (average of two sides)
ε_R	local radial strain
ε_{EL}, ε_{ER}	end cap axial strain on left and right sides respectively
ε_{LL}, ε_{LR}	local axial strain on left and right sides respectively
ε_{RL}, ε_{RR},	local radial strain on left and right sides respectively

Notational - Miscellaneous

o	degree
$[C]$	compliance matrix
$[G]$	matrix relating current stresses and plastic strains
$\{\delta\sigma'\}$, $\{\delta\sigma\}$	vectors of effective and total stress increment respectively
$\{\delta\varepsilon\}$	vector of strain increment
$\{\delta\varepsilon^p\}$	components of plastic strain increment
$F(\sigma')$	yield function
$Q(\sigma')$	plastic potential function
$f(z)$	depth correction factor

h(x)	vertical distance between two elastic bodies making contact at a horizontal distance x
p(x)	pressure distribution within contact zone at a horizontal distance x
$\bar{u}_z(x)$	profile of bedding surface with horizontal distance
| |	absolute value of ...
ln	natural logarithm

CHAPTER 1

INTRODUCTION

1.1   DEFORMATION PROBLEMS IN GEOTECHNICAL ENGINEERING

Engineering design relies on the successful prediction of any

behaviour which may make a structure unfit for the purpose it is intended

to serve. A structure may be said to reach various conditions, or "limit

states", in which its usefulness is restricted in some way. The two limit

states generally considered are the "ultimate limit state" which entails

collapse of the structure and the "serviceability limit state" in which

deformations become unacceptable for normal use. In a geotechnical context

the requirement for ultimate limit state design is that the ratio of the

shear strength of the soil to the mobilized shear stress (the usual

definition of the factor of safety) must be adequate. The serviceability

limit state requires an acceptable deformation of the structure, associated

with the working loads. The acceptable limits for frame buildings and

load-bearing walls have been summarized by Burland, Broms and De Mello

(1977).

In considering the ultimate limit state of a geotechnical structure,

analyses such as the upper and lower bound plasticity methods and limit

equilibrium techniques are often used. In these analyses the soil is

assumed to behave in a rigid-perfectly plastic manner and the prediction

of deformations under working loads is therefore not possible. The

serviceability limit state of a geotechnical structure is generally much

more difficult to consider. Calculations tend to be restricted to the

prediction of settlements of foundations on clayey soils due to applied

loads. These are usually predicted by one-dimensional consolidation

theory in conjunction with a stress distribution obtained from the theory

of elasticity. Settlements of clays are more likely to cause problems

than those of granular soils or rocks, which are usually estimated by empirical means.

Despite the frequently restricted nature of the design calculations carried out in practice, modern numerical methods can be used to analyse complex boundary value problems with irregular geometry, boundary stresses and displacements. The finite element method involves the subdivision of the soil mass into a number of elements and the solving of a set of simultaneous equations so that equilibrium and strain compatibility conditions are satisfied. The stress-strain behaviour of the soil has to be idealized by a suitable mathematical model and therefore a more complete knowledge of the stress-strain behaviour is needed. With such an approach, a wider variety of geotechnical structures can be analysed and their behaviour under working loads more realistically predicted.

One way to determine the deformation behaviour of the soil is to test it in the laboratory by applying stress changes as close as possible to those applied in the field. In the stress path method, Lambe (1964, 1967, 1979), representative elements within the soil mass are chosen and for each element the stress history and changes of stress under the applied loads are estimated. Laboratory tests are then performed so as to follow the estimated stress paths, and the strains measured in these tests are used to define the deformation characteristics of the soil. Finally, the deformations in the field are estimated.

It is of interest from a theoretical point of view to understand the deformation behaviour of the ground throughout the whole stress range up to and including failure. However, in most geotechnical structures the shear stresses under working conditions are purposely kept well below those at failure and deformations are relatively small. Therefore, from a practical point of view, it is the stress-strain behaviour within the small strain range that is of most interest. For example, Simpson et al. (1979) showed that for large, stable excavations in stiff clay, where

movements of the retaining wall do not exceed about 0.2% of the wall height (e.g. Peck, 1969), the shear strain in the surrounding soil exceeds 0.1% only very locally. This is similar to the range of strain used by Marsland (1971a, b) to determine tangent moduli from plate loading tests, but much less than the strains normally studied in the laboratory for determination of stiffness parameters. Indeed, the instrumentation used in routine laboratory tests is not capable of accurately measuring deformations within the small strain range (0.01% - 0.10%). With the advance of electronic technology, however, sufficiently accurate devices have been developed for use in conjunction with triaxial specimens. The development of the electrolevel gauge (Symes and Burland, 1984; Jardine et al., 1984) is an example. The gauge measures the deformation of a triaxial specimen locally in the central region and hence minimizes the effects of end restraint and bedding errors. These problems will be discussed in more detail in Sections 2.2.2 and 2.2.3. With the electro-level gauge axial strains can be measured to ±0.002%. Jardine et al. (1985) have demonstrated that the stiffness parameters measured at small strain levels in the laboratory agree remarkably well with those found from plate loading tests in London Clay.

There are, however, possible complications in the interpretation of the deformation behaviour of clays at small strains. Lewin (1970) and Som (1968) have reported "threshold effects" (i.e. there is a marked increase of stiffness when a small stress increment is applied following a delay at constant stress or an abrupt change in the direction of the stress path). Furthermore, any sample of soil taken from the ground must experience a change of stress state and, in addition, some mechanical disturbance due to the sampling process and subsequent preparations for testing. All this may contribute to a change of its original behaviour. A more detailed discussion of such effects will be presented in Section 2.2.

1.2   MODELS OF SOIL BEHAVIOUR

The conceptual or mathematical representation of material behaviour is known as a model. A mathematical model consists of constitutive equations which express relationships between the external agencies and the responses of the material, governed by the internal constitution of the material. The constitutive relationships generally involve stress, strain, time and temperature. Soil models are needed not only for the purpose of making predictions of the behaviour of geotechnical structures but also for analysing and interpreting field and laboratory tests.

A complete mathematical model for soil should be sufficiently general to describe the deformation of the soil irrespective of the drainage conditions and the total stress path being followed. Ideally the model should also be simple and accurate. However, the criteria of generality, simplicity and accuracy are, in most cases, contradictory. It is often possible to refine a model to improve its accuracy but only at the expense of simplicity or generality. The acceptable error is a function of the engineering situation. In engineering practice the accuracy of a prediction is controlled to some extent by the soil model and the idealization of the boundary conditions, but is also affected by the quality of sampling, the choice of representative samples for testing and the interpretation of test results.

Because of the widely varying behaviours of natural soils, numerous mathematical models have been proposed. The concepts of continuum mechanics have been widely used and most of the models are based on the theories of elasticity and plasticity.

1.2.1   Elastic Models

The theory of linear elasticity may be represented in matrix form as:-

$$\{\delta\varepsilon\} = [C] \{\delta\sigma\} \tag{1.1}$$

where $\{\delta\sigma\}$ and $\{\delta\varepsilon\}$ are the vectors of stress and strain increment respectively and $[C]$ is a compliance matrix. Equation (1.1) relates the six stress increment components to the six strain increment components in a continuum and the symmetric matrix $[C]$ consists of up to 21 independent elastic coefficients.

Within the elastic domain all deformations are recoverable and therefore the energy stored during loading is recovered during unloading. The deformations associated with a given stress state do not depend on how that stress state was reached but only on the change of stress that occurred (i.e. the deformations are stress path independent). The principle of superposition is therefore applicable.

If the material properties are the same in all directions (i.e. the material is isotropic), it can be shown that only two independent elastic constants are required to describe the elastic model. Furthermore, for triaxial loading conditions, equation (1.1) can be expressed as:-

$$\begin{Bmatrix} \delta\varepsilon_s \\ \delta\varepsilon_v \end{Bmatrix} = \begin{bmatrix} \dfrac{1}{3G'} & 0 \\ 0 & \dfrac{1}{K'} \end{bmatrix} \begin{Bmatrix} \delta q \\ \delta p' \end{Bmatrix} \tag{1.2}$$

where ε_s and ε_v are the shear strain and volumetric strain respectively and q and p' denote the deviator stress and effective mean normal stress respectively. Correspondingly G' and K' are known as the effective shear modulus and effective bulk modulus respectively.

1.2.2 Plastic Models

In the theory of plasticity the plastic strain increment is related not to the stress increment but to the current stress. This may be expressed as:-

$$\{\delta\varepsilon^p\} = [G] \{\sigma'\} \tag{1.3}$$

where $\{\delta\varepsilon^p\}$ and $\{\sigma'\}$ are the components of the plastic strain increment and current effective stress respectively. $[G]$ contains a yield function and

a flow rule and may or may not include a hardening law. These terms will be defined in the subsequent paragraphs.

Plastic strains are not recovered during unloading and thus the total strain occurring in a material during loading may be separated into elastic (recoverable) and plastic (irrecoverable) components. Materials are said to yield and undergo plastic deformations when the current effective stresses satisfy a yield criterion (function) which takes the mathematical form $F(\sigma') = 0$. The yield criterion can be expressed in terms of the principal stresses and forms a surface in principle stress space $(\sigma_1', \sigma_2', \sigma_3')$ where σ_1', σ_2' and σ_3' are the three effective principal stresses. If the material is isotropic the yield surface is symmetrical about the space diagonal.

A flow rule relates increments of plastic strain to the current state of stress during yielding. This contrasts with the theory of elasticity in which increments of (elastic) strain are related to the increments of stress.

Plastic deformation causes a permanent change in the state of the material. As work is done upon the material the yield surface expands and the material is said to strain harden. The incremental relationship between the stress and the size of the yield surface is known as a hardening law. It is convenient to define a plastic potential function $Q(\sigma') = 0$ such that the corresponding plastic strain increment vectors are orthogonal to the plastic potential. If the plastic potential function is equal to the yield function, the plastic strain increment vectors are also normal to the yield surface and the material is said to possess an associated flow rule.

1.2.3 Critical State Models

Critical state soil mechanics, Schofield and Wroth (1968), provides a conceptual framework within which to interpret the behaviour of soils

at and before failure. It is assumed that soil, when loaded, yields and approaches a critical state at which unlimited distortion occurs with no further change in effective stress or volume. As it yields the soil behaves isotropically and obeys an associated flow rule. Hardening occurs as the volume permanently reduces. The traditional Mohr Coulomb and Hvorslev strength criteria are also incorporated into critical state soil mechanics.

Within this framework a family of mathematical models has been developed. The two most well known models are Cam Clay (Schofield and Wroth, 1968) and Modified Cam Clay (Roscoe and Burland, 1968). The basic difference between these two models concerns the energy dissipation relationship. In the Cam Clay model energy is dissipated only during plastic shear strain, whereas in the Modified Cam Clay model energy can be dissipated during both plastic volumetric strain and plastic shear strain. It is not appropriate here to give a detailed mathematical account of these models. Instead a brief qualitative description will be given.

The key feature of the models, based on the experimental work of Rendulic (1938) and the later work of Henkel (1960), is that a surface, the "state boundary surface", can be defined in (p', q, v) space where v denotes the specific volume of the soil, outside of which a point representing the state of soil cannot lie. As long as the soil is in a normally consolidated condition, its state point will lie on this surface; the state point will lie within the surface if the effective stress is reduced and the soil becomes overconsolidated. In the latter case, the state point is constrained to lie on an "elastic wall" directly above the appropriate swelling curve on the (v, p') plane. Within the state boundary surface the soil behaviour is thus purely elastic and the bulk, shear and Young's moduli $(K', G'$ and $E')$ can be related to v, p' and the effective Poisson's ratio v'. The elastic behaviour is non-linear.

Plastic strains only occur when a state point traverses the state boundary surface. The projection of the intersection of each elastic wall with the state boundary surface onto the (p', q) plane forms a yield locus. The mathematical expression for the yield locus can be derived from energy considerations, knowing that for an associated flow rule the slope of the plastic strain increment vector must be perpendicular to the yield locus. As the soil yields, elastic volumetric strains may occur simultaneously but elastic shear strains are assumed to be negligible.

For any soil there is an isotropic pressure (preconsolidation pressure), p'_{max}, which if exceeded, causes plastic contraction in the absence of deviatoric stress. For overconsolidated soil the Cam Clay model predicts that p' equals the effective critical pressure, p'_{cs}, when the overconsolidation ratio $(\dfrac{p'_{max}}{p'})$ is 2.72. For a lower over-consolidation ratio the state of the soil is said to be on the "wet" side of the critical state line (i.e. when sheared the soil tends to reduce in volume and expel water). Conversely, the soil is said to be on the "dry" side if the above ratio is exceeded. If such soil is sheared, so that it approaches the critical state from the dry side, the soil will tend to dilate and take in water. This latter behaviour is associated with strain softening rather than strain hardening and it is then unsafe to apply the continuum equations of the Cam Clay model. The most likely mode of softening is the generation of rupture surfaces, so that strains become severely localized. Thus the application of the Cam Clay model is limited to normally or lightly overconsolidated soils. Even then, the model excludes some potentially important aspects of behaviour such as anisotropy and creep.

A model for overconsolidated soil is perhaps of more value to the engineering profession than one for normally consolidated soil because soil is more frequently encountered in the former state. As seen above, prior to yield overconsolidated soil is treated as a non-linear elastic

material by the critical state theories, the elastic moduli being stress dependent. On the other hand, Wroth (1971) and Atkinson (1975) suggest that, since on loading overconsolidated soil from a given stress state there is a range of stress over which the stress-strain curve is approximately linear, constant equivalent elastic moduli can be used to advantage. However, this view could be contested because of the degree of non-linearity that is often observed in test data (e.g. Jardine et al., 1984). A clear defect of any elastic model is its inability to account adequately for dilatancy. To overcome this problem Pender (1978) presented a model for overconsolidated soil which was based on critical state concepts but involved a non-associated flow rule.

1.3   SCOPE OF PRESENT RESEARCH

1.3.1 General Objectives

The discrepancies between the deformation (stiffness) parameters measured in the laboratory and in-situ are well known, the laboratory stiffnesses often being only a fraction of those measured in-situ. Sample disturbance, due to mechanical distortion or stress changes, is thought to be the main reason (Broms, 1980).

As the serviceability limit state is often the controlling factor in design, the importance of measuring the stiffness parameters at small strain levels is readily apparent. Yet, this is difficult to do by means of in-situ tests, where a direct measurement of strain is unlikely to be made. For example, in the plate loading test only the displacement of the rigid loading plate is usually measured; the strain is sometimes arbitrarily defined as the ratio of the displacement of the plate to its diameter. Thus, although the stress range over which the stiffness has been measured may be known, the strain range is usually unknown. For this and other reasons the measurement of stiffness parameters at small

strains may be considerably easier in the laboratory, despite the problems of sampling disturbance referred to above.

A primary objective of the present research was to carry out a limited number of carefully conducted laboratory tests in order to minimize the discrepancy between laboratory and in-situ values of the stiffness parameters. An evaluation of the test techniques and results was to be made by referring to existing field data. As few data presently exist on the small strain deformation behaviour of natural soils, it was hoped that data from these tests would contribute towards the general knowledge of such behaviour. Because of the difficulty of obtaining suitable samples of natural soil, collaboration was sought and obtained with the Building Research Establishment (BRE). Samples of a glacial clay were retrieved from the BRE test site at Cowden (see Section 1.3.2).

During the last five years an attempt has been made in the Civil Engineering Department of Sheffield University to build up a triaxial testing facility capable of supplying high quality stress-strain data in support of other research being conducted within the Department. In line with this objective, the development of a computer-controlled test system and small strain measurement techniques formed a major part of the research. The development and evaluation of this equipment were intended to be complete before the tests referred to above were commenced.

It was considered important that the small strain measurement system developed at Sheffield was significantly different from those already existing at other research institutions, in order to permit independent corroboration or criticism of results being obtained elsewhere.

1.3.2 Collaboration with the Building Research Establishment (BRE)

As mentioned above, the BRE has a well established test site at Cowden, on the North Sea (Holderness) coast. The development of the oil and gas fields in the North Sea necessitated a careful evaluation of the

geotechnical parameters of the glacial and post-glacial deposits on which the off-shore structures were founded. These soils have a wide range of geotechnical properties due to the complex depositional and post depositional processes which occur in the glacial environment. Varying depositional environments have resulted in large variations in composition, fabric and stress history. Unfortunately this complicated the geotechnical investigations. Nevertheless, since very few data were available on the full scale behaviour of glacial soils similar to those found beneath the North Sea, the BRE decided to conduct an extensive research programme on the glacial soil at Cowden (Gallagher, 1984).

It was originally hoped that block samples for the present work could be retrieved from shallow (3m deep) excavations at the Cowden site. These would have suffered a minimum of mechanical disturbance. However, this plan proved overambitious and it was later agreed that BRE would supply 250mm diameter tube samples, using a special sampler previously used in London Clay but untried at Cowden. Eventually, such samples were retrieved from about 5m depth. It was also agreed that data obtained in the present investigation would be exchanged for BRE's in-situ test information, only some of which has been published. The large diameter plate tests with "under-plate" instrumentation were of particular importance (Marsland and Eason, 1974).

CHAPTER 2

INVESTIGATIONS OF THE DEFORMATION BEHAVIOUR OF CLAY
SOILS WITH PARTICULAR REFERENCE TO COWDEN TILL

2.1   INTRODUCTION

In this chapter the problems associated with the laboratory
determination of soil deformation characteristics are first discussed.
The most common techniques, particularly those employed by the BRE on
the soil from Cowden are then reviewed. The engineering properties of
the upper levels of the Cowden Till (0 - 10m depth) are briefly
summarized in Section 2.3.

2.2   THE DETERMINATION OF SOIL DEFORMATION CHARACTERISTICS

Soil deformation parameters have traditionally been obtained in
the laboratory from triaxial tests. Other tests using more complex
apparatus (biaxial, true triaxial or simple shear) have also been
performed, but with much less frequency. Much fundamental work on the
deformation properties of soils has been done by researchers at Cambridge
University, Roscoe (1970), and for this work reconstituted or remoulded
samples have usually been used because of their reproducibility.
Relatively few test programmes have been carried out for the sole
purpose of investigating the deformation properties of undisturbed natural
clay, compared with those aimed at investigating the shear strength of
such material.

Laboratory tests have an advantage over field tests in that the
boundary conditions can be better controlled. These include drainage
conditions, stresses and displacements and the changes of stress or
displacement with time. However, when an attempt is made to obtain
parameters from "undisturbed" soil samples, some potentially serious
difficulties exist.

Firstly, there is the question of whether a single specimen is able to represent the behaviour of a whole soil mass. Many soil masses contain heterogeneities such as pockets and veins of different materials together with discontinuities (fissures, bedding planes etc.). Such features impose considerable limitations on the use of relatively small specimens in laboratory tests, Rowe (1971) and Marsland (1971c).

Secondly, complex and adverse changes may be brought about by sampling. Even if considerable care is taken to avoid mechanical disturbance of the soil structure, there is always a total stress release during withdrawal of the sample from the ground. The effect of sampling on the subsequent behaviour of the material will depend very much on whether the material can be considered to behave elastically during this unloading (i.e. whether the changes can be reversed).

A process of sampling without mechanical disturbance is sometimes referred to as "perfect sampling" and the sample so obtained as a "perfect" sample. If the soil is removed without volume change, an effective stress difference of $(1 - K_o) \, p'_{vo}$ is released, where K_o denotes the coefficient of lateral earth pressure at rest and p'_{vo} denotes the vertical in-situ effective stress, and a certain shear strain will occur. The mean normal effective stress p'_k retained in the sample by perfect sampling would then be given by the expression (Skempton, 1961):-

$$p'_k = p'_{vo} \left\{ K_o - A_s \, (K_o - 1) \right\} \qquad (2.1)$$

where A_s is the pore water pressure parameter for the corresponding stress change. It may be noted that for normally consolidated clays (with $K_o < 1$) p'_k will be less than p'_{vo} and that for some overconsolidated clays (with $K_o > 1$) p'_k will be greater than p'_{vo}. For overconsolidated clays, Skempton and Sowa (1963) have shown experimentally that there is little difference in the strengths obtained in undrained triaxial tests between perfect samples and

samples which have not been subjected to a deviatoric stress relief. The measured values of A_s were close to one-third, indicating that elastic behaviour occurred during perfect sampling, and the measured values of p'_k were close to those predicted by equation (2.1). Kirkpatrick et. al., (1986) investigated the change with time of the effective stress retained in overconsolidated specimens after perfect sampling. This was done by measuring the pore water pressure present in triaxial specimens by increasing the cell pressure in stages under undrained conditions. They concluded that both the effective stress and undrained strength decayed with the elapsed time after sampling. This was not full understood but was linked to cavitation and diffusion effects in the pore water.

Mechanical disturbance during sampling can also cause a change in p'_k (Hvorslev, 1949) as a result of shear strains being generated near the surface of the sampling tube. To minimize this effect the use of a 250mm diameter piston sampler was suggested by Rowe (1968). Its length was limited to 600mm and its wall thickness to 6.3mm. The wall thickness was reduced to 4mm near the cutting edge. However, even with this sampler, poor results were obtained in a low permeability, laminated clay where a significant proportion of the sample was badly distorted.

The sequence of strains, or strain path, followed by soil being sampled by a driven tube was first evaluated by Baligh (1984). Figure 2.1(a) illustrates the sequence of strains for an element on the centre-line of such a sampler. As it enters the tube the element undergoes compression followed by extension. The magnitude of the strains depends on the geometry of the sampler. For a 250mm diameter tube with a wall thickness of 6.3mm, as referred to above, a maximum strain of about 0.35% is predicted. Around the periphery, even more severe shear distortions are predicted. Further straining occurs when the sample is extruded from the

tube prior to testing. Figures 2.1(b) and (c) show qualitatively the
stress path followed during sampling with σ'_v and σ'_H denoting the
effective vertical and horizontal stresses. For overconsolidated clay
an increase of effective mean normal stress is anticipated as a result
of sampling. The opposite applies for normally consolidated clay. The
potential severity of these effects is readily apparent. However, for
overconsolidated clay it is possible that the effects may not be too
serious providing the strain cycle (a to h) in Figure 2.1(c) does not
exceed a certain magnitude (threshold value) and the in-situ stress
state is close to isotropic. There is, as yet, no theory or experimental
evidence regarding the strain threshold but Hight et al. (1985) proposed
a value of 0.1% as a limit for clayey soils.

Other factors, such as the drying out of samples during storage
and temperature differences between the ground and the laboratory, can
also affect the deformation characteristics of specimens. However,
provided that good practices are adopted, these factors should be of
minor importance.

2.2.1 <u>Triaxial Test</u>

The main features of the triaxial test were originally described
in detail by Bishop and Henkel (1962) and, apart from the development of
the stress path apparatus (Bishop and Wesley, 1975), the testing techniques
and procedures have remained much the same. However, a considerable
number of electronic devices have been introduced to measure forces,
pressures and displacements.

In the triaxial test axial loads are applied to a cylindrical
specimen via stiff top and bottom caps and radial pressures are applied
by a confining fluid acting on a flexible rubber membrane. In the
conventional cell axial displacements are generally controlled and the
deviatoric component of load is measured by an internal load cell or an

external proving ring. This procedure enables post-peak behaviour to be observed, although only to a limited extent since non-uniform strains usually develop in the sample. In the Bishop - Wesley apparatus the stresses are controlled and the resulting displacements are measured. The axial and radial stresses can be varied continuously, thereby allowing an axially symmetric total stress path to be followed. However, the observation of post-peak behaviour is not possible as the strain rate becomes too high.

In standard tests only axial displacements are measured, and this is done by installing a dial gauge or a displacement transducer outside the cell. The relative movement between the loading ram and the cell is measured. Other, more refined techniques for the measurement of strain will be described in Section 2.2.3.

As the specimen strains the conventional assumption is that it deforms as a right cylinder either in compression or extension, so that the stresses and strains are uniform. The axial strain, ε_A, is simply

$$\varepsilon_A = \frac{\delta L}{L_o} \qquad (2.2)$$

where δL is the measured change in the height of the specimen and L_o is the initial height. The cross-sectional area A used to compute the axial stress will then be as given by Bishop and Henkel (1962):-

$$A = A_o \frac{1 - \frac{\delta V}{V_o}}{1 - \varepsilon_A} \qquad (2.3)$$

where A_o and V_o are the intial area and volume respectively and δV is the change in volume. However the right cylinder assumption is strictly valid only for a specimen tested with perfectly frictionless end caps. The effect of the friction between the end caps and the specimen is to introduce non-uniform distributions of stress and strain in the specimen, as

discussed in the following section.

The use of lubricated ("free") ends in triaxial tests has been discussed by Rowe and Barden (1964). End friction can be reduced by inserting one or more greased rubber membranes between the specimen and the end caps. Not only does such a technique improve the stress and strain distributions within the specimen, but since a shorter length of specimen can be used there is a more economical use of material and a considerable reduction in the time of testing. However the compressibility of the greased membranes can introduce bedding errors which would necessitate careful calibration (Sarsby et al., 1980). Also the ordinary method of measuring pore water pressure at the base of the specimen has to be modified. The size of the ceramic plug mounted in the base pedestal has to be reduced and this may result in increased response times.

2.2.2 Stress and Strain Distributions in the Triaxial Test

A summary of the previous research findings concerning the stress and strain conditions in cylindrical triaxial tests is presented in this section. In the analytical solutions only the effects of end restraint on isotropic materials are considered and perfect contact is assumed to exist between the specimen and the end caps. As the emphasis in the experimental work described in this thesis is placed on small strain behaviour, only the effects of end restraint on the initial portion of the stress-strain curves is of interest.

Many workers (e.g. Pickett, 1944; Balla, 1960 and Moore, 1966) have attempted to solve this problem using various analytical techniques allied to the theory of elasticity. The solution of Balla (1960) is the most complete since it allows for the variation of material properties (ν'), loading conditions (σ_1, σ_3) and friction characteristics between the specimen and the end caps (smooth or adhesive contact). In Balla's solution the effect of end restraint dies out significantly with distance

from the ends of the specimen and at about one quarter of the specimen height the difference between the results for frictionless ends and completely restrainted ones is no more than ±5%. Balla also noted that the effect of end restraint increases as the Poisson's ratio increases and as the aspect ratio $\frac{L}{D}$ decreases, where D denotes the specimen diameter.

Gerrard and Wardle (1971) obtained a finite element solution based on linear elasticity, Figure 2.2. They showed that at an applied stress ratio of 4 (i.e. $\frac{\sigma_1}{\sigma_3} = 4$) the stresses and strains are uniformly distributed within the central half of a specimen having rough end caps and an aspect ratio of 2. The variation of the stresses is within ±6% of the applied vertical stress (shaded areas in Figure 2.2). They also noted that the apparent Young's modulus, computed using the average vertical strain, is 4% higher than the true value for a material with a Poisson's ratio of 0.35. Results from Radhakrishnan (1972) obtained using a non-linear finite element solution, also indicate that a remarkably uniform state of stress and strain exists, except close to the ends of the specimen. Again this applied for a fixed end condition and an aspect ratio of 2. The vertical and radial (and hence shear) stresses in the central half of the specimen depart from the conventionally calculated ones by a maximum of ±3% only. Using the same numerical technique but different soil parameters, Costa Filho (1980) showed that within the central third of a London Clay specimen the stresses are likely to be within ±5% of the conventionally calculated ones.

The above evidence, from both linear and non-linear analysis, suggests that, in the central half of a triaxial specimen with an aspect ratio of 2 and completely restrained ends, the stress and strain distributions may be considered to be relatively free from end effects.

Girijavallabhan (1970) and Maguire (1975) showed that, for a

linearly elastic specimen with a Poisson's ratio of 0.5 and an aspect ratio of 2, the conventional neglect of end restraint leads to an overestimation of the true modulus by approximately 10%, Figure 2.3, and suggested that conventional moduli should be corrected by the factors shown in Table 2.1. A similar effect was noted by Gerrard and Wardle (see above). However, using a non-linear elastic finite element analysis, Perloff and Pombo (1969) found an almost negligible difference between the stress-strain curves from specimens with unconstrained ends and those with restrained ends up to an axial strain level of 0.5%.

Experimental evidence provided by Blight (1965), Barden and McDermott (1965) and Duncan and Dunlop (1968) indicates a marginally steeper stress-strain curve for clay specimens with conventional ends rather than lubricated ones. The pore pressure developed in a sample of aspect ratio 2 did not depend on whether the end conditions were lubricated or not, providing the specimen was deformed slowly. X-ray determination of strain uniformity in Kaolin was carried out by Balasubramanian (1976). The strains were found to be approximately uniform in the initial stages of the test but non-uniformities then started to develop. The lubrication of the end caps delayed the onset of non-uniformity. In undrained compression tests with ordinarily rough ends, the specimen was reasonably uniform up to an axial strain of about 4%, whereas by using lubricated ends that value was increased to around 9%.

2.2.3 Recent Improvements in the Measurement of Strains in the Triaxial Test

As already mentioned, axial displacements for the computation of axial strains are measured outside the cell in conventional tests. The displacement is therefore not only affected by end restraint, as discussed in the previous section, but also includes any compression of items such as internal load cell, porous stones, filter paper and end caps. Furthermore,

if the contacts between the specimen and the end caps are imperfect, so-called bedding errors occur and an additional deformation is measured. All these factors introduce errors into the computation of axial strains. Although some sources of error, such as the compressibility of an internal load cell, are systematic and might be eliminated by careful calibration, bedding errors are more random in nature. Bedding errors are likely to be accentuated in stiff clays, particularly glacial deposits, due to the increased difficulty of the trimming process. However, several researchers have realized that, if measurements of strains are made locally on the central part of the specimen, bedding errors are eliminated. In the central region strains are also relatively free from end effects, as shown in the previous section, and this provides an additional incentive for making the measurements there. Local measurements involve the placing of marks or targets on or through the sample membrane. Miller (1980) found that small relative displacements between sample and membrane occur near and beyond failure when significant bulging occurs or discontinuities develop. However at low strains such relative displacements were not observed.

Several local measurement systems have been developed using a variety of electronic transducers. Brown and Snaith (1974) and Boyce and Brown (1976) described systems for the measurement of both axial and radial strains. Their techniques were used on 150mm diameter specimens of bituminous materials and crushed limestone. Six studs were placed into the specimen and sealed where they passed through the membrane. Four small linear variable differential transformers (LVDTs), attached directly to the studs, were used to measure axial strain. Flexible strain-gauged rings were used to measure radial strain. The difficulty in using an LVDT system of the type just described is that, if the sample tilts as it deforms, there is a potential danger of bending of the LVDT armatures.

Daramola (1978) developed a system for the measurement of small strains in sands in the stress path cell. This same system was used by Costa Filho (1980) for tests on London Clay. Two LVDTs were attached to opposite sides of the specimen, measuring the relative vertical displacement between the mounting points and the pedestal at one third and two thirds of the specimen height. An additional LVDT was used to measure the relative displacement between the top cap and the pedestal. From these measurements the average strains in the upper, central and lower thirds of the specimen could be computed, although errors due to non-uniform deformation could not be eliminated.

Burland and Symes (1982) described the use of an electrolevel gauge for local axial strain measurements. The gauge consists of an electrolyte sealed in a glass capsule. Three coplanar electrodes protrude into the capsule and are partially immersed in the electrolyte. The impedance between the central electrode and the outer ones varies as the capsule is tilted. Since the gauge is suspended on a mechanism attached to the specimen, the relative movement of the mounting points can be deduced. Jardine, Symes and Burland (1984) further improved the gauges, which enable axial strain over the gauge length to be resolved to within ±0.002%. The gauges can be used in stress path cells designed for testing 38mm diameter specimens.

Clayton and Khatruch (1986) developed a local strain gauge making use of the Hall effect. The gauge is made in two parts. The upper part consists of a spring-mounted pendulum which holds two bar magnets. This is suspended from a pad fixed to the specimen by means of a pin penetrating into the soil. The lower part consists of a Hall effect semiconductor, mounted on the specimen in a similar way. As the distance between the mounting points of the upper and lower parts of the gauge changes, a change in voltage is produced across the semiconductor. The device is capable of measuring axial strain to ±0.002%.

2.2.4 Field Tests - Plate Loading Tests

Field tests have been developed to overcome the previously mentioned problems in laboratory tests of sample size and sampling disturbance. However the installation of the testing device in the ground usually causes some form of disturbance and the interpretation of the tests is normally subject to some uncertainties in the boundary conditions. Thus the chief merit of field tests often lies in their ability to test a larger volume of soil.

Some field tests assist the identification of soil types (including localized changes) or the determination of strength or density but provide little or no information about deformation properties. The pressuremeter and plate load tests are suitable for obtaining deformation parameters but in both cases some allowance has to be made for the stress relief associated with excavation before testing. The introduction of the self-boring pressuremeter represented a major advance since the disturbance of the ground is kept to a minimum. It should be noted that the plate load test largely measures the vertical deformation characteristics of the ground whereas the pressuremeter measures the horizontal characteristics. However, the interpretation of these tests is at present limited by assumptions that the soil deposit is homogenous and isotropic.

The plate load test has long been employed for the in-situ determination of soil properties. Tests with either load or rate of penetration control may be carried out. Tests may be performed at the ground surface and at the bottom of excavations or boreholes. Due to the importance of determining the variation of deformation characteristics with depth (Burland et al. 1973), plate tests have been made more frequently inside boreholes (Marsland, 1971a). Thus the discussion in this section will concentrate on borehole plate tests. Different test arrangements and sizes of loading plate are available but only those adopted by the BRE at the Cowden site will be described.

Over the last fifteen years the BRE has developed and made extensive use of loading tests on 865mm diameter rigid plates installed at the bottom of 900mm diameter boreholes. Figure 2.4 illustrates the arrangement of the test. Vertical loads are applied through a loading column by hydraulic jacks which are attached to tension piles located 3.5m from the centre of the test borehole. The settlement of the plate is transferred to ground level using a tensioned invar tape where it is measured by displacement transducers attached to a 12m long reference beam. To prepare for a test the borehole is advanced to within 500mm of the test depth by a rotary drilling rig fitted with a helical auger. The last 500mm of soil are removed using a 900mm diameter flat bottom bucket auger. Disturbed material (typically 25-50mm thick) is excavated by hand and the plate bedded on a thin layer of quick setting plaster. The interval of time between drilling to the test depth and applying a bearing pressure equal to the in-situ vertical stress is typically two to three hours, with partial loading by the self weight of the loading column in one to two hours. The usual test procedures is to load the plate at a constant rate of penetration of 2.5mm per minute. Unload-reload cycles are included in some tests at selected stress levels, before failing the soil. The failure or ultimate bearing pressure is taken to be the pressure applied when the total settlement has reached 15% of the plate diameter. At this stage it is believed that more than 90% of the actual ultimate bearing capacity would have been mobilized based on experience in London Clay (Marsland, 1972).

The main difficulties in interpreting the results concern the possibility of ground disturbance and stress relief during excavation to gain access to the test position and the uncertainty in drainage conditions when the test is being performed. In order to study these effects, Marsland and Eason (1974) developed an "under-plate" instrumentation system to measure local deformations beneath the plate.

From the load-settlement curve of the plate both strength and deformation properties can be estimated. The conventional interpretation assumes that prior to failure the soil beneath the plate behaves as a linear elastic, isotropic and homogeneous material, deforming under undrained conditions. In order to compare in-situ plate tests with strength measurements made in the laboratory, it is necessary to use a relationship between the ultimate bearing pressure and the shear strength of the clay. For a saturated clay loaded under undrained conditions,

$$q_u = c_u N_c + p_{vo} \tag{2.4}$$

where

q_u = ultimate bearing pressure

c_u = undrained shear strength,

N_c = bearing capacity factor (dependent on geometry), and

p_{vo} = total overburden pressure.

The values of N_c published by Terzaghi (1943) are only suitable for shallow foundations where the depth of the foundation is not greater than the width. Thus they are unsuitable for the majority of the plate tests conducted in boreholes. A series of carefully conducted tests on deep model plates by Marsland (1972) gave values of N_c ranging from 9.0 to 9.8 with an average value of 9.24. These values were measured at a plate penetration equal to 15% of the plate diameter. Subsequently, Marsland and Randolph (1977) obtained experimental values of N_c in the range 8.70 to 9.65, with an average value of 9.25. This time, the values were deduced from the ultimate bearing capacities measured in full scale plate loading tests in London Clay and the corresponding shear strengths measured in triaxial tests on 98mm diameter samples. The plate tests were made on 865mm diameter plates at a depth of 6.1m. At that depth, good undisturbed samples were obtained and the fissures were

sufficiently closely spaced for the strengths of 98mm diameter specimens to provide a reasonable measure of the large scale (mass) strength.

Approximate theoretical values of N_c can be obtained by considering the base failure of a foundation to be analogous to the expansion of a spherical cavity in a uniform isotropic elastic-perfectly plastic material. For a flat base loaded to cause undrained failure in clay, Gibson (1950) obtained the relationship:-

$$q_u = \left[\frac{4}{3} (\ln \frac{G}{c_u} + 1) + 1 \right] c_u + p_{vo} \qquad (2.5)$$

where G is the elastic undrained shear modulus. Hence by comparison with equation (2.4)

$$N_c = \frac{4}{3} \left[\ln (\frac{G}{c_u}) + 1 \right] + 1 \qquad (2.6)$$

The values of N_c so obtained range from about 5 for a material with a $\frac{G}{c_u}$ ratio of 7 to 9 or above for one with a $\frac{G}{c_u}$ ratio greater than 150. Values of $\frac{G}{c_u}$ (determined from the initial parts of load-settlement curves measured during constant rate of penetration tests on 865 mm diameter plates) range from 120 to 130 for London Clay and from 100 to 290 for the top 12m of the Cowden Till (Marsland and Powell, 1979). The largest corresponding N_c values, as determined by equation (2.6), are in reasonable agreement with those obtained by Meyerhof (1951, 1961). By considering a pile penetrating into a rigid-plastic medium, Meyerhof obtained N_c = 9.34 when the effects of shear stresses on the sides of the pile were neglected and N_c = 9.74 when their effects were taken into account.

On the basis of all the above studies, the value N_c = 9.6 was recommended by Marsland and Powell (1979) in evaluating the shear strength of Cowden Till. If this recommended value is inserted into equation (2.4), together with the measured ultimate bearing pressure and the overburden pressure, the value of c_u may be determined.

The Young's modulus can be computed using the theory for a circular rigid punch pushed into the surface of a semi-infinite elastic medium. Timoshenko and Goodier (1971) gave the expression:-

$$\rho = \frac{P(1 - \nu^2)}{BE} \tag{2.7}$$

where
ρ = settlement of the plate,

B = plate diameter,

ν = Poisson's ratio of the material ($\nu = 0.5$ for undrained conditions),

P = load applied to the plate, and

E = Young's modulus of the material.

However, due to the generally observed non-linearity of the load-settlement curve (Marsland, 1979), E has to be determined for a specific pressure range. It is common to define the secant modulus applying from zero load to one half of the failure pressure. As already noted failure generally corresponds to a plate settlement of 15% of the plate diameter. Once E has been determined, the shear modulus G is readily obtained ($G = \frac{E}{2(1 + \nu)}$).

If the plate test is carried out at the bottom of a borehole, equation (2.7) has to be modified to take into account the stiffening effect of the soil above the base of the borehole. The secant modulus may be calculated using the following equation:-

$$E = \frac{\Delta q_p}{\Delta \rho} \cdot \frac{\pi}{4} \cdot (1 - \nu^2) \cdot f(z) \cdot B \tag{2.8}$$

where
Δq_p = increase in bearing pressure,

$\Delta \rho$ = associated settlement of plate, and

$f(z)$ = $\dfrac{\text{settlement of loaded plate at depth } z}{\text{settlement of loaded plate at surface}}$.

The term f(z) is a depth correction factor determined by Burland (1969) using a finite element analysis for a linear elastic medium, Figure 2.5. At depths greater than six times the plate diameter, the correction factor is of the order of 0.85.

According to Marsland and Randolph (1977) a rational stress range over which to determine the secant modulus would start from the in-situ stress condition and end when the maximum shear stress had increased by c_u, because by this point in an elastic-perfectly plastic material a plastic zone would certainly have started to develop and elastic theory would cease to be applicable. Poulos and Davies (1973) show that the maximum shear stress developed on the centre-line below a symmetrically loaded rigid circular punch on an elastic material is approximately 30% of the average applied pressure. For the maximum shear stress to increase by c_u, the applied pressure must increase by 3.33 c_u (i.e. the net applied pressure $q_n = 3.33 \ c_u$). Combining this relationship with equation (2.4)

$$\frac{q_n}{q_u - p_{vo}} = \frac{3.33 \ c_u}{c_u N_c}$$

where $N_c = 9.6$ as recommended above. Consequently

$$q_n \simeq \frac{1}{3} (q_u - p_{vo})$$

At Cowden, the stress range defined in this way, from $q_n = 0$ to $q_n = \frac{1}{3} (q_u - p_{vo})$, has been adopted in determining secant moduli from plate loading tests. However it must be remembered that when a plate load is applied to a material such as Cowden Till, with non-linear stress-strain properties, the variation of strain beneath the plate causes a local variation in the operational secant modulus that is not reflected in the above interpretation.

2.2.5 Field tests - Pressuremeter Tests

Compared with the plate load test, the development of the pressuremeter as an in-situ test is fairly recent. This development was pioneered by Menard (1957). Test procedures and interpretations have been comprehensively reviewed by Baguelin et al. (1972). At Cowden three types of pressuremeter have been used by the BRE, namely the Menard type (Menard 1957), the self-boring pressuremeter (Windle and Wroth, 1977) and the push-in pressuremeter (Henderson et al., 1977). Only a brief description of the equipment and test procedures adopted at Cowden is presented in this section. For more details, reference should be made to Powell and Uglow (1985).

The Menard pressuremeter consists of a rubber sheathed central measuring cell which is capable of being expanded to twice its original volume. This is covered by a long rubber sheath which extends over "guard" cells at the ends. The central cell is designed so as to apply a radial pressure in the borehole and simultaneously to measure the increase in the diameter of the hole; the outer guard cells expand under a slightly lower radial pressure than the central cell and protect the central region from end effects. The central measuring cell is full of water pressurized by gas. The gas pressure is measured on a Bourdon gauge at the ground surface and the volume change is measured by a burette. At Cowden a test pocket approximately 1m deep with a slightly larger diameter than the probe was freshly drilled and the probe was inserted as quickly as possible. The pressure was increased in increments (typically 50 kN/m^2) which was maintained for 1 minute each. Volume change readings were recorded after 15 seconds, 30 seconds and 1 minute.

It is not possible to install a Menard pressuremeter without causing some disturbance to the surrounding soil. The soil immediately around the borehole also suffers from stress relief and a change in drainage conditions. All of this affects the determination of the

deformation characteristics and the in-situ horizontal stress. In order to overcome the problems of disturbance the self-boring pressuremeter has been developed.

The self-boring pressuremeter consists of a rubber sheathed pressuremeter section placed behind a drilling head. Gas pressure is used to expand the membrane and is monitored by a pressure transducer, while the movement of the membrane is monitored by strain gauges attached to feelers within the probe. After insertion at Cowden, the probe was left for an average of 30 minutes before the membrane was expanded at a constant radial strain rate of 1% per minute. The rate was kept constant by a control unit, which also limited the maximum expansion to about 20% of the original volume. An unload-reload cycle was included when about 2 - 3% of radial strain had been reached. In principle, this type of test is well suited to investigating the in-situ deformation properties of soils. However, at Cowden some stones tended to prevent the advancement of the pressuremeter and had to be removed by withdrawing the pressuremeter and boring temporarily with flight augers.

The push-in pressuremeter was initially developed for off-shore site investigation and consists of three main units: the pressuremeter itself, the pressure developer and the control and data acquisition system. The pressuremeter comprises a hollow stainless steel cylinder onto which is mounted the inflateable membrane. At the lower end, the cylinder is fitted with a cutting shoe so that soil can pass unrestricted up the inside of the cylinder. The inflateable membrane is protected by long stainless steel strips attached at the lower end to the cutting shoe. At the upper end, the strips are attached to a split ring, which is free to move axially in order to accommodate the expansion of the membrane. At Cowden the membrane was inflated at a constant rate of 2% volume increase per minute, by means of oil pumped from the pressure developer, to a

maximum expansion of 20% of the original volume. The volume of oil delivered was measured by recording the displacement of a ram within the pressure developer, and its pressure was monitored by pressure transducers. At least one unload-reload loop was included over a range of up to 3% volumetric strain.

Undrained shear strengths have been obtained from pressuremeter results in a number of ways. The two commonest methods are due to Gibson and Anderson (1961) and Palmer (1972).

Gibson and Anderson (1961) derived the following expression for the net limiting pressure, p_L, needed to expand an infinitely long cylindrical cavity in an elastic-perfectly plastic soil:-

$$p_L - p_{ho} = \left[\ln \left(\frac{G}{c_u} \right) + 1 \right] c_u = N_p \cdot c_u \qquad (2.9)$$

where p_L = pressure when the cavity expands indefinitely,

p_{ho} = original total horizontal stress, and

N_p = pressuremeter constant.

A relationship can be established between N_p and the bearing capacity factor N_c. From a comparison of equations (2.6) and (2.9) it follows that

$$N_p = \frac{3}{4} (N_c - 1) \qquad (2.10)$$

In relating N_p and N_c it is assumed that the ratio $(\frac{G}{c_u})$ is unaffected by any anisotropy of the clay. If $N_c = 9.25$, as suggested in Section 2.2.4, $N_p = 6.18$. The value of p_L is determined by extrapolating plots of p_p versus $\ln (\frac{\Delta V_p}{V_p})$ to the point at which $\ln(\frac{\Delta V_p}{V_p}) = 0$,

where p_p = current pressure of pressuremeter,

V_p = current volume of pressuremeter,

$$\Delta V_p = (V_p - V_{po}), \text{ and}$$

$$V_{po} = \text{volume of pressuremeter at } p = p_{ho}.$$

Palmer (1972) developed a method of deriving the stress-strain curves for clays from the pressure-volume curves measured in pressuremeter tests. The soil is simply assumed to be incompressible. Palmer shows that the shear stress, τ, in the soil next to the wall of the expanding borehole is given in terms of the radial expansion of the borehole, ε_c (cavity strain), and the corresponding pressure gradient, $\dfrac{dp_p}{d\varepsilon_c}$, by :-

$$\tau = \frac{1}{2} \varepsilon_c (1 + \varepsilon_c)(2 + \varepsilon_c) \frac{dp_p}{d\varepsilon_c} \tag{2.11}$$

where $\varepsilon_c = \dfrac{\text{increase in radius of borehole due to increase in pressure } (p - p_{ho})}{\text{radius of borehole at } p = p_{ho}}$

At large strains, it is more accurate to express the shear stress in terms of the volume increase ratio, $\dfrac{\Delta V_p}{V_p}$, so that

$$\tau = \frac{dp_p}{d\left(\ln \dfrac{\Delta V_p}{V_p}\right)} \tag{2.12}$$

The value of c_u is assumed to equal the largest shear stress so calculated. Equation (2.11) can also be used to derive the shear modulus. Providing ε_c is small, values of secant shear moduli can be obtained using the expression :-

$$G = \frac{1}{2} \frac{\Delta p_p}{\Delta \varepsilon_c} \tag{2.13}$$

since the maximum shear strain at the edge of the borehole is approximately equal to $2\varepsilon_c$. For unload-reload loops the shear modulus, G_{ur}, is more safely calculated as:-

$$G_{ur} = \frac{1}{2}(1 + \varepsilon_c) \frac{\Delta p_p}{\Delta \varepsilon_c} \qquad (2.14)$$

since ε_c may not be small.

Applying the same argument as adopted for the plate test, the appropriate stress range over which to determine the secant modulus will be from $p = p_{ho}$ to $p = p_{ho} + c_u$. At the end of this range the maximum shear stress in an elastic-perfectly plastic soil has increased by an amount equal to c_u.

To permit the evaluation of the undrained strength and modulus from the pressuremeter test, p_{ho} has first to be determined. For the Menard pressuremeter the standard method (Menard, 1957) of estimating p_{ho} is to assume that it corresponds to the start of the linear region of the pressure-volume curve and also to the point where the change in volume after the application of each pressure increment (creep) drops to a low, constant value, see Figure 2.6(b). However, Marsland and Randolph (1977) suggested that this method underestimates the value of p_{ho} by a considerable amount for overconsolidated clay and suggested an iterative graphical approach. This involves adjusting p_{ho} and calculating c_u by equation (2.12) until the value of $(p_{ho} + c_u)$ so obtained corresponds to the pressure at which the $p_p - \varepsilon_c$ curve becomes significantly non-linear (see Figure 2.6(c)). For the self-boring pressuremeter p_{ho} is estimated by observing the pressure at which the membrane starts to expand radially, as shown in Figure 2.6(a). Because of the method of insertion of the push-in pressuremeter the surrounding soil is considered to be significantly overstressed and therefore p_{ho} has to be estimated by other means. The estimation of p_{ho} at Cowden is discussed in Section 2.3.3.

2.2.6 Back Analysis

In view of the difficulties associated with both the laboratory and field tests previously described, back analysis of instrumented structures has sometimes been attempted to provide estimates of the operational deformation parameters of specific clay deposits. In the field the soil has usually remained at a constant stress state for a long time following the last period of erosion, deposition or tectonic movement. Thus because of creep, threshold effects (see Section 1.1), may be present which would not be evident in many laboratory or field tests because of disturbance and stress relief prior to the test. Threshold effects may also be caused by cementing of the soil grains.

Gallagher (1984) reported a back analysis of two pile tests at Cowden. Both piles were 0.457m in diameter and about 9.5m long. The shear modulus of the soil was backfigured from the load-displacement response of the piles using the method developed by Randolph and Wroth (1978) in which the soil is assumed to be linearily and isotropically elastic. The modulus was taken as the secant value from zero load to 50% of the pile capacity.

2.3   ENGINEERING PROPERTIES OF COWDEN TILL

Existing information for the Cowden site is summarized in this section. Unless otherwise stated, the data were extracted from Gallagher (1984). Only the uppermost 10m of the soil profile will be discussed as the samples supplied by the BRE for the present research ranged in depth from 3 to 7m (see Section 3.5.2).

2.3.1 Location of Site and General Geology

The BRE test site is on the Holderness coast at the Cowden Royal Air Force base, 2km north of Aldborough, North Humberside (see Figure 2.7). The Ordnance Survey map reference is TA 245 403. The site is located on

an extensive deposit of glacial tills, about 60m thick, which overlies chalk. The area was glaciated during several major ice advances but much of the material deposited during the earlier advances was re-incorporated in the ice and re-deposited as the ice advanced from the North Sea during the Devensian Period. Consequently, all the tills are thought to be less than 18,500 years old (Catt and Penny, 1966).

2.3.2 Description of Soil Profile

The upper part of the soil profile (first 10m) mainly consists of fairly uniform gravelly clay of low to medium plasticity. A weathered zone extends to about 4m where the colour changes from brown to very dark greyish brown. The water table is within 1m of the ground surface. Typical classification data are given in Figures 2.8 and 2.9. The till is well graded and contains around 30% of clay-sized particles. The Atterberg limits tend to reduce with depth.

A microfabric study by Hadidi (1984) showed that there is little contact between one coarse (i.e. sand or gravel) particle and another. No consistent preferred orientation of the clay particles was observed; rather, the particles tended to orientate sympathetically to the larger particle surfaces. This study therefore suggests that the behaviour of the till is dominated by the clay matrix. Hadidi also studied the macro-fabric of the till using core samples of 98mm diameter taken from a borehole at 1m intervals. Some fissures were identified in the first 4 to 5m but no macro discontinuities were found below this depth. The fissures are near vertical, planar, smooth and sometimes stained with iron oxide. They are of moderate size ($0.01 - 1.00m^2$) and of very low intensity ($3m^2/m^3$).

2.3.3 In-Situ Stresses, Permeability and Consolidation Properties

The total vertical stresses, Figure 2.10, were estimated from the bulk densities measured on 98mm diameter x 150mm long samples, retrieved by pushing in thin walled sampling tubes. The effective vertical stresses, also shown in the figure, were then computed by subtracting the measured pore pressures, discussed below. The horizontal stresses have been determined by a number of methods including:-

(i) Self-boring presuremeter. Direct measurement of total lateral stress (Wroth and Hughes, 1973).

(ii) Push-in stress cell ("spade" cell). Direct measurement of total lateral stress and pore pressure (Tedd and Charles, 1981; 1983).

(iii) Menard pressuremeter. Interpretation to obtain total horizontal stress (Menard, 1957; Marsland and Randolph, 1977).

(iv) Measurement of initial suction of samples (Skempton, 1961).

(v) Estimation from oedometer results (Schmidt, 1966; Ladd et al., 1977).

Typical horizontal stress profiles produced by these methods are shown in Figure 2.11. The coefficient of lateral earth pressure at rest K_o and overconsolidation ratio (OCR) derived by method (iv) or (v) are shown in Figures 2.12 and 2.13 respectively.

The work outlined above suggests that the horizontal and vertical stresses are approximately equal over much of the depth. Results from oedometer tests, "corrected" spade cells and suction measurements show reasonable agreement and their mean has been considered as a best estimate of p_{ho} for comparison with pressuremeter tests. The push-in pressure-meter overstresses the ground during insertion, as is evident from the

resulting stress-strain curve (Powell and Uglow, 1985), and the estimated values of p_{ho} (not shown in Figure 2.11) are considered to be unrepresentative. The values of p_{ho} assessed from self-boring pressuremeter tests using the "lift-off" method are seen to be scattered quite widely in Figure 2.11. In general they appear to considerably overestimate the horizontal stresses. This may be indicative of the difficulties of using the self-boring technique in the Cowden Till and the possibility of significant overstressing during insertion. Values of p_{ho} obtained from Menard pressuremeter tests using the Menard (1957) approach are considerably lower than any of the other estimates. The graphical iterative method of Marsland and Randolph (1977) gave values only slightly lower than the best estimates. One difficulty arising in using this method is that the stress-strain relationship of the Cowden Till shows greater curvature at low strains than that of London Clay, for which the method was developed.

The pore water pressures at different depths were measured using both standpipe and twin tube hydraulic piezometers attached to mercury manometers. The average pore water pressure profile obtained from the piezometers is shown in Figure 2.10. It indicates a watertable about 1m below ground level and an approximately linear increase of pore pressure with depth down to 7m. Below this depth the pore water pressures are significantly reduced by drainage towards some sand and gravel layers at a lower elevation. Values of in-situ permeability were obtained from measurements of flow when a constant excess head was applied to the piezometer tips. The in-situ permeabilities of the unweathered tills below 4.5m depth vary between 0.0005 and 0.007m per year, while in the weathered zone they generally exceed 0.05m per year.

Altogether sixteen oedometer tests were reported by Gallagher (1984). These tests were carried out in accordance with the recommendations

of the British Standards Institution (1975). On the basis of the laboratory determined values of the coefficients of volume decrease (m_v) and volume expansion (m_s), together with the in-situ measurements of permeability, the average coefficients of consolidation (c_v) and of swelling (c_s) were reported as:-

$$c_v = 4.04 \times 10^{-7} \text{ m}^2/\text{second}$$

and

$$c_s = 5.40 \times 10^{-7} \text{ m}^2/\text{second}$$

2.3.4 Strength and Deformation Properties

The BRE has conducted triaxial compression tests on samples of Cowden Till obtained by four different sampling techniques, namely pushing, hammering, vibrocore and rotary. Most of the tests were made on unconsolidated 100mm diameter x 150mm long specimens with lubricated ends under undrained conditions, although a few consolidated specimens were tested under both drained and undrained conditions. Full details are given by Gallagher (1984) and Marsland and Powell (1985). Typically, no peak was observed on the stress-strain curve and the undrained strength was measured at an axial strain of 15%. The effective strength parameters from different specimens and test types may conveniently be compared by plotting the maximum shear strength against the corresponding mean effective stress, as in Figure 2.14. Values of the angle of effective shearing resistance ϕ' are given in the figure, the effective cohesion c' being taken to zero. Given the scatter in the data, no real difference can be detected between the results from unconsolidated pushed samples and those from consolidated ones. The rotary cores give results similar to those obtained from the pushed samples; the vibro cores give somewhat higher strengths. To some extent this may be due to the slightly higher densities that were evident in the vibro cores.

The measurements of the undrained shear strength, c_u, is affected

by factors such as mechanical disturbance, stress relief, the volume of soil tested relative to its macrofabric and the rate of testing. Values of c_u from good quality pushed samples were found to be close to the values from large diameter plate tests, Figure 2.15. It is however possible that this agreement may be fortuitous due to the combination of the various factors mentioned above. Values of c_u from different types of pressuremeter test (and methods of interpretation) are compared with those from plate tests in Figures 2.16(a) and (b). Results from all types of pressuremeters are in general higher than those from the plate tests, with the limit-pressure approach (equation (2.9)) giving the more consistent results. The less satisfactory Palmer interpretation (equation (2.12)) is considered to be more sensitive than the limit-pressure approach to errors in the initial in-situ stresses and mechanical disturbance of the soil around the borehole. Based on the above evidence it has been concluded that there is no significant variation of c_u with depth.

Marsland and Powell (1979) reported the shear moduli obtained from unconsolidated triaxial tests on 200mm long x 98mm diameter specimens trimmed from pushed samples. The tests were conducted under undrained conditions with the cell pressure equal to the total overburden pressure. The moduli have been corrected for equipment compliance and form a lower bound when compared with other techniques, Figure 2.17. Very variable secant shear moduli were obtained from all three types of pressuremeter. In evaluating the results from the Menard pressuremeter, p_{ho} was estimated by the method of Marsland and Randolph (1977). Values of G derived from the self-boring and push-in pressuremeters were obtained from the entire unload-reload stage of the test irrespective of the stress or strain range. The initial loading stage could not be used because of overstressing during insertion. The values from the pressuremeters were generally intermediate between those from triaxial tests and those from plate loading tests, with the results from back analysis exceeding all other

values by a large margin. Broadly similar trends were exhibited by the reload shear moduli, Figure 2.18. In the case of the self-boring and push-in pressuremeters the reload moduli have been calculated over a limited strain range at the start of reloading. According to Powell and Uglow (1985), the shear strain levels associated with the reload moduli from these two types of pressuremeter and from the plate load tests are comparable.

The following conclusion is extracted from Gallagher (1984): "The available evidence suggests that the elastic properties are not strongly dependent on depth, at least over the upper 10m, are independent of the direction of loading (i.e. tension or compression), are strongly dependent on the stress or strain range over which they are determined and strongly dependent on the test technique used".

Critical state parameters (see Section 1.2.3) for Cowden Till have been determined by Atkinson et al. (1985) from tests on reconstituted and remoulded samples. The published parameters were:-

$$\lambda = 0.084$$

$$\kappa = 0.015$$

$$\Gamma = 1.95$$

$$M = 1.1$$

where
λ = gradient of normal consolidation line on the v versus ln p' plot,

κ = gradient of the swelling line on the same plot,

Γ = specific volume at the critical state with $p' = 1.0 \ kN/m^2$, and

M = slope of critical state line when it is projected on to a constant volume plane.

Poisson's ratio	Modulus correction factor
0.15	0.9970
0.20	0.9911
0.25	0.9829
0.30	0.9760
0.35	0.9638
0.40	0.9562
0.45	0.9316
0.49	0.9186

TABLE 2.1 Modulus correction factors (after Girijavallabhan, 1970)
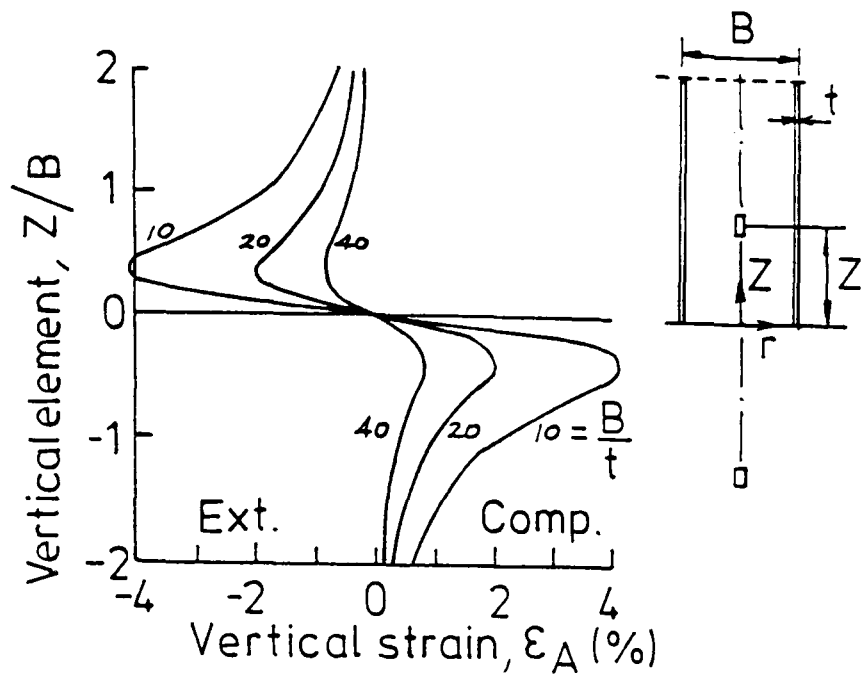
(a) Strain paths
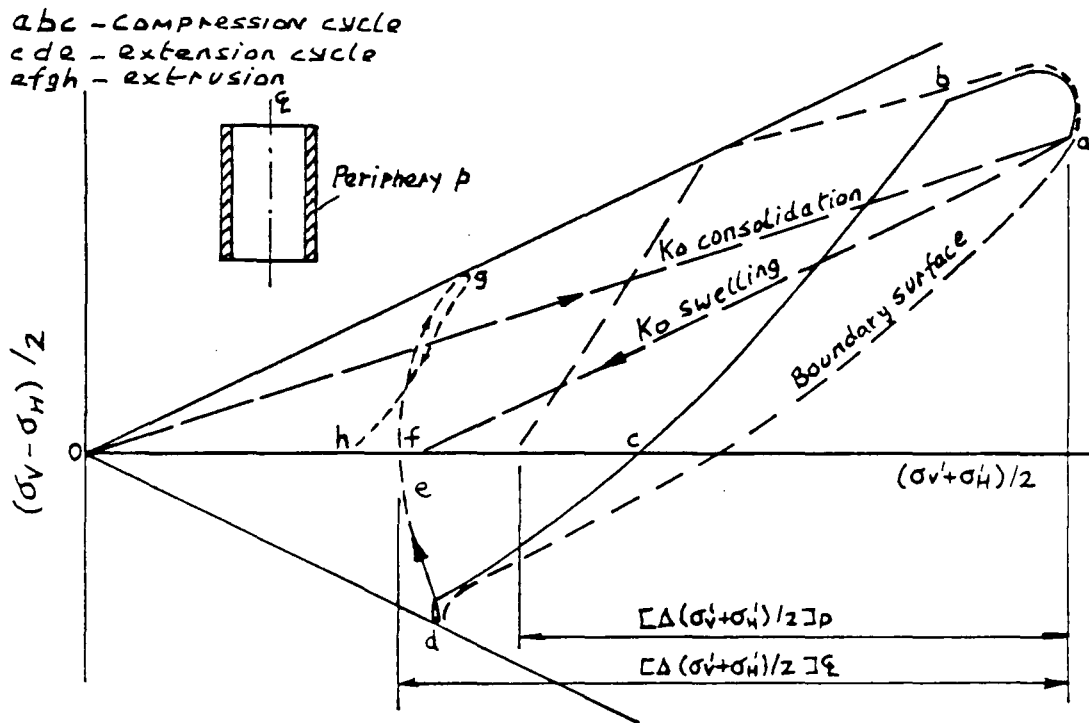
(b) Stress paths for normally consolidated clays
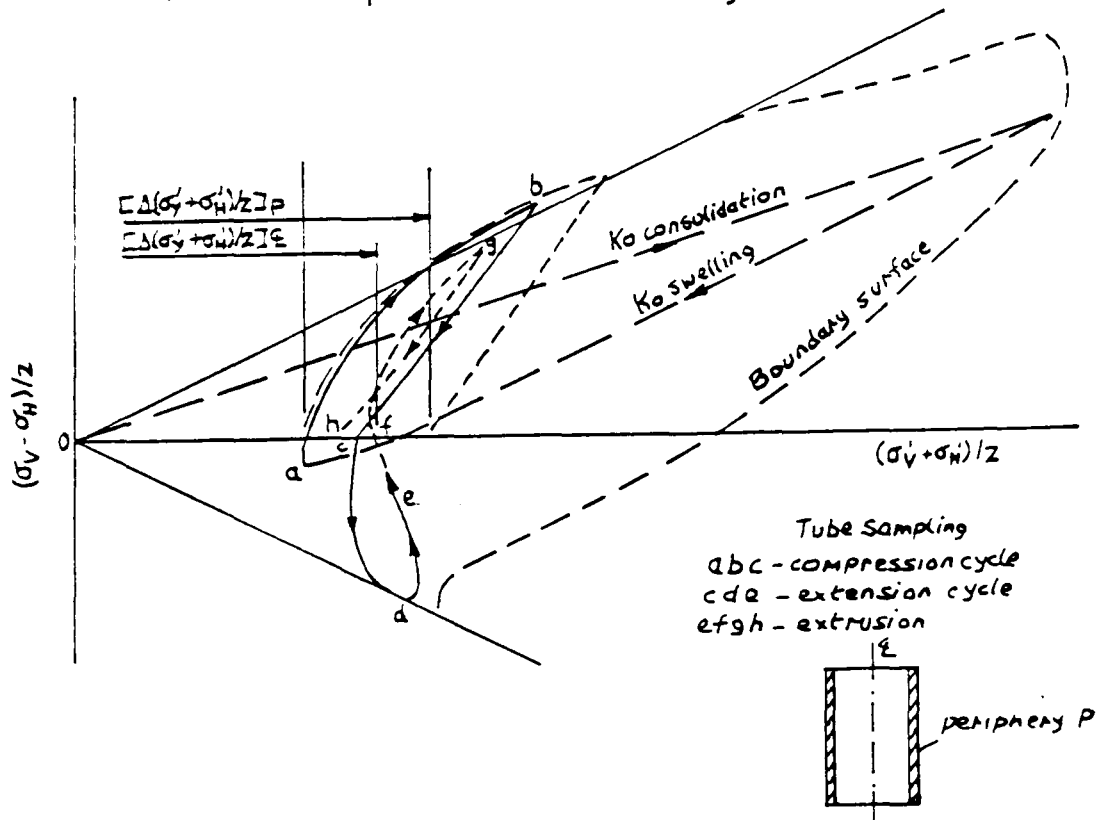
(c) Stress paths for overconsolided clays

FIG. 2·1   STRESS AND STRAIN PATHS DURING TUBE SAMPLING
(AFTER HIGHT ET AL, 1985)
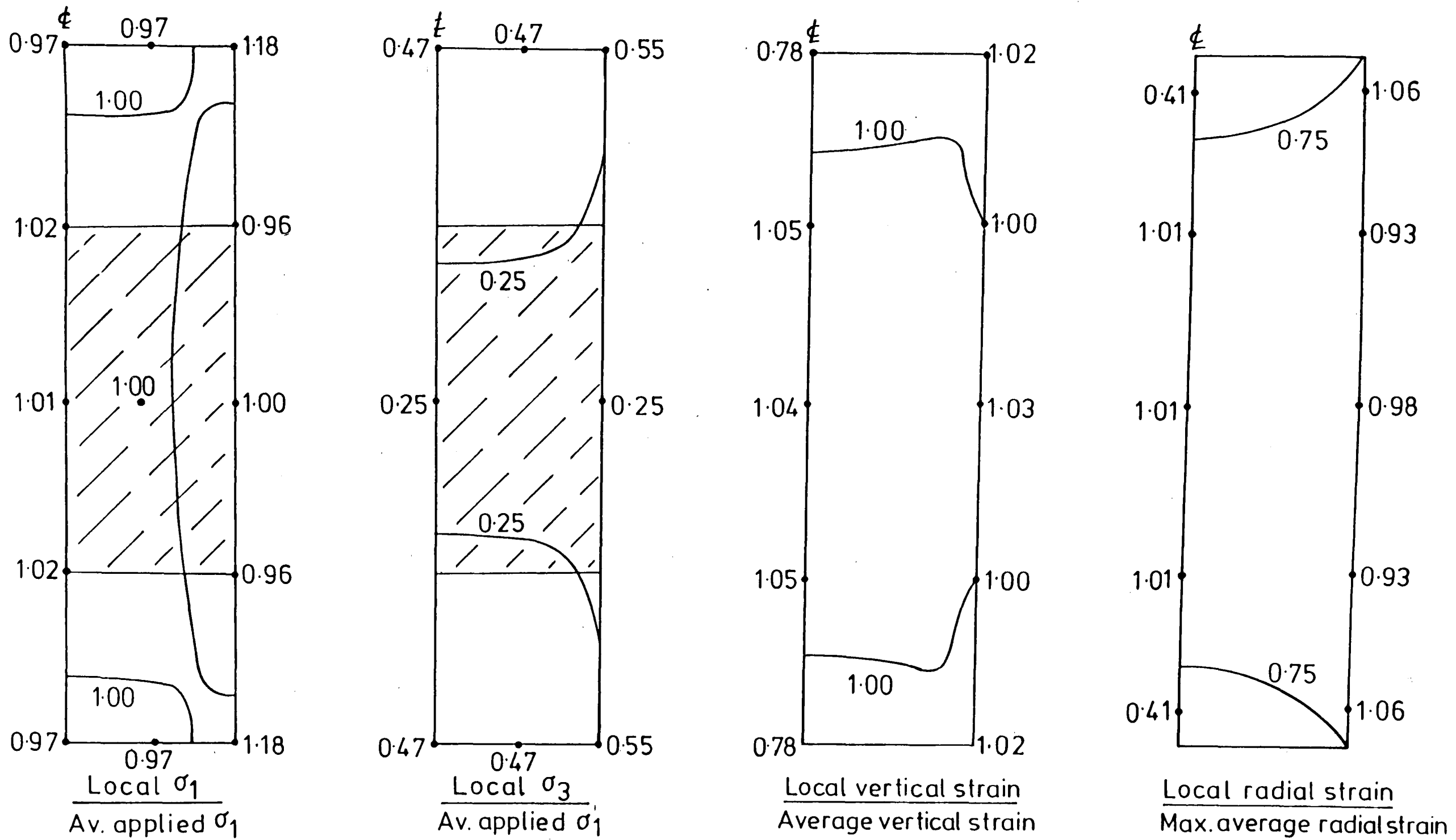
FIG. 2·2   STRESS/STRAIN DISTRIBUTION IN TRIAXIAL TEST (AFTER GERRARD & WARDLE, 1971)

Legend

— ●— Girijavallabhan (1970)

×— —× Moore (1966)

(a) Young's modulus

Moore (1966)

$v_A = v_T$

Legend

E Young's modulus

v Poisson's Ratio

Suffixes A = Apparent

T = True
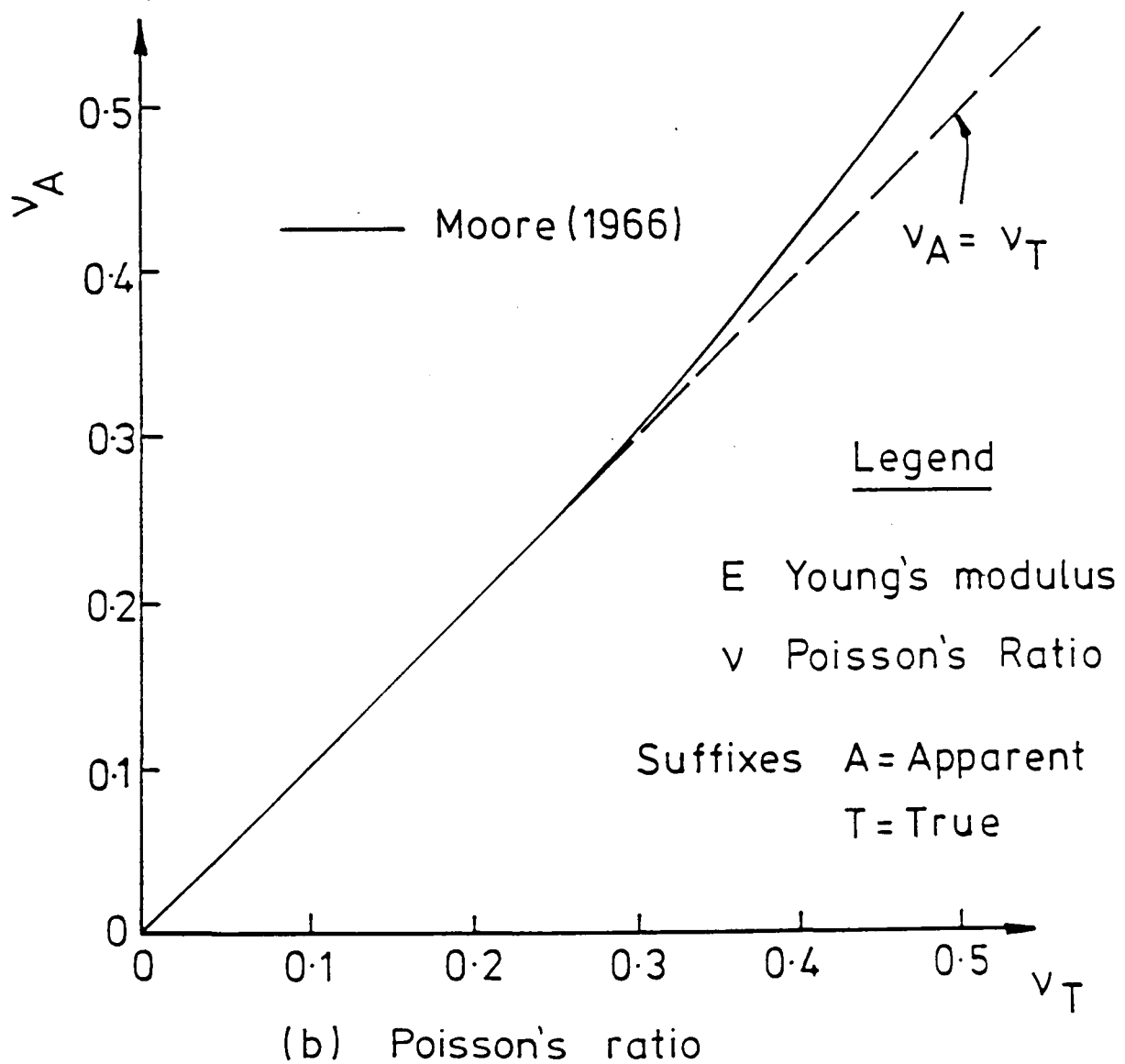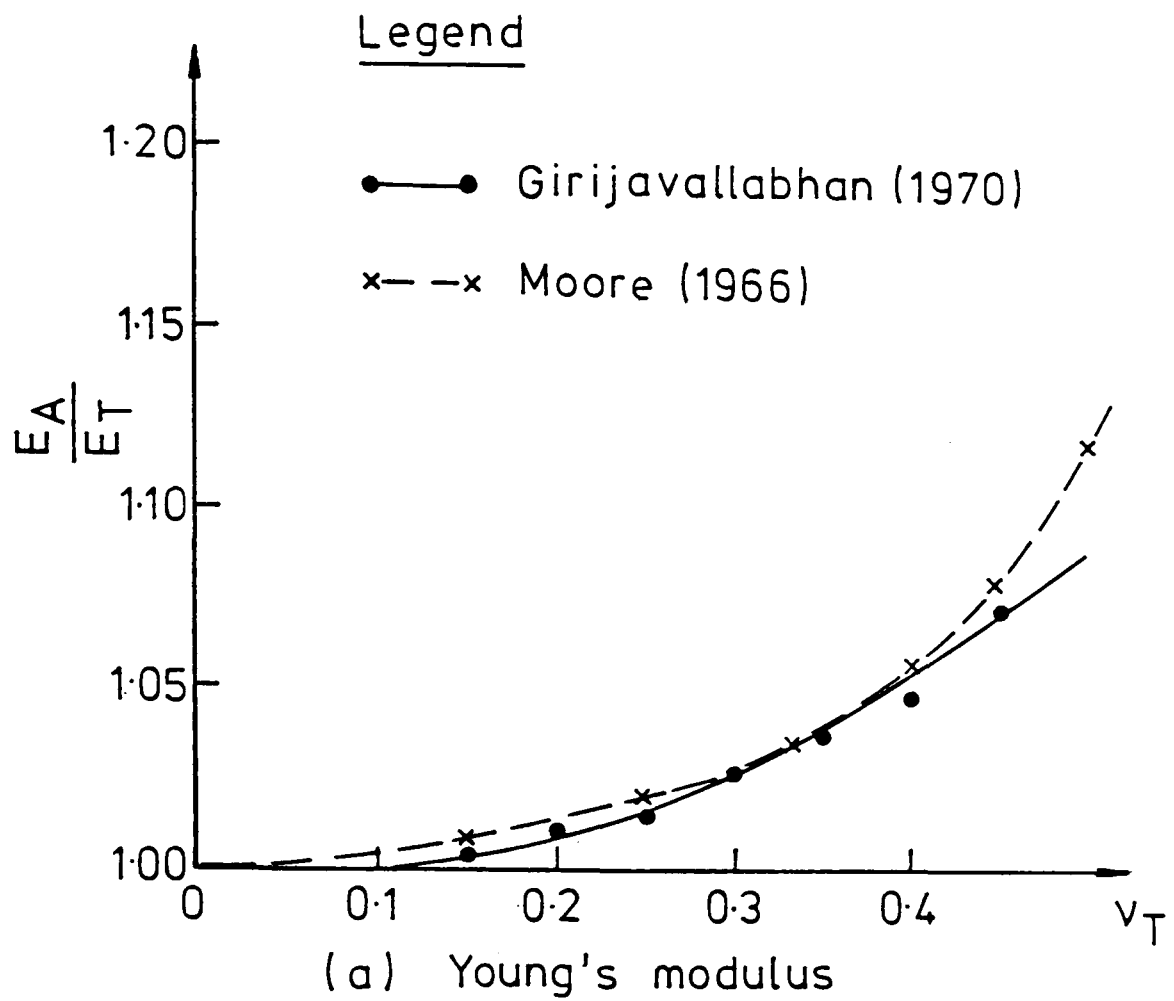
(b) Poisson's ratio

FIG. 2·3   EFFECTS OF END RESTRAINT IN TRIAXIAL TEST
(L/D = 2) ON YOUNG'S MODULUS AND POISSON'S RATIO
(AFTER MAGUIRE , 1975)

Detachable loading head

Hydraulic jacks

Settlement reference

Main loading frame

Reference beam

Spreader beam

Tension pile

Loading column (extends to 30m)

Loading plate
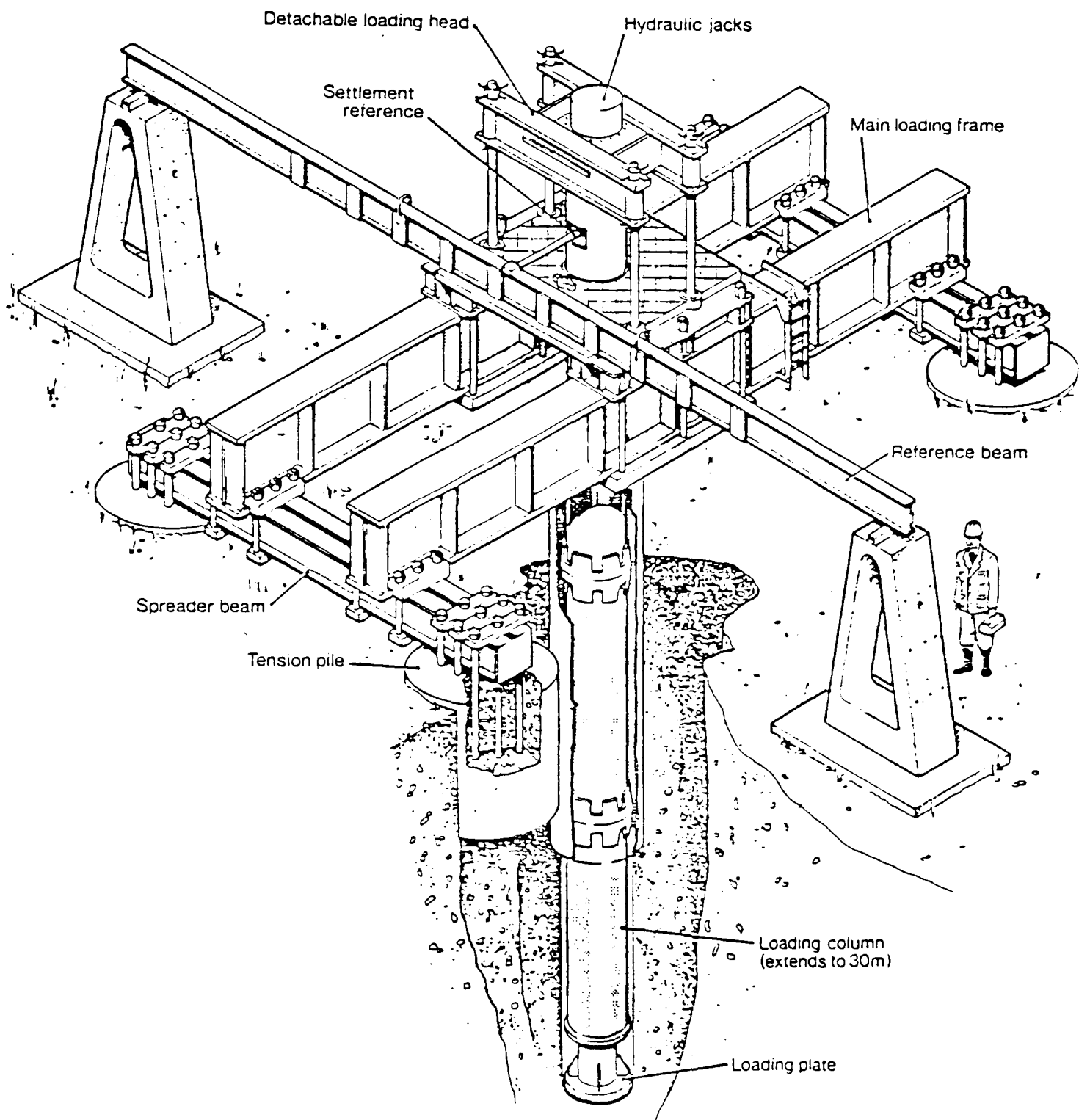
FIG. 2·4   DIAGRAMMATIC ARRANGEMENT OF PLATE LOAD TEST

(AFTER MARSLAND & POWELL, 1979)
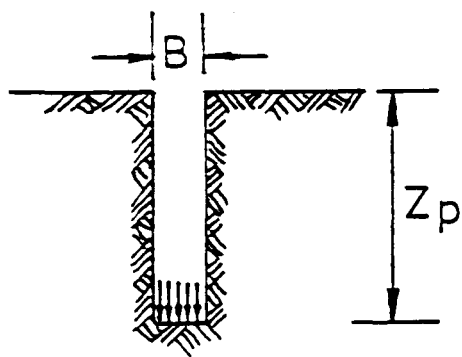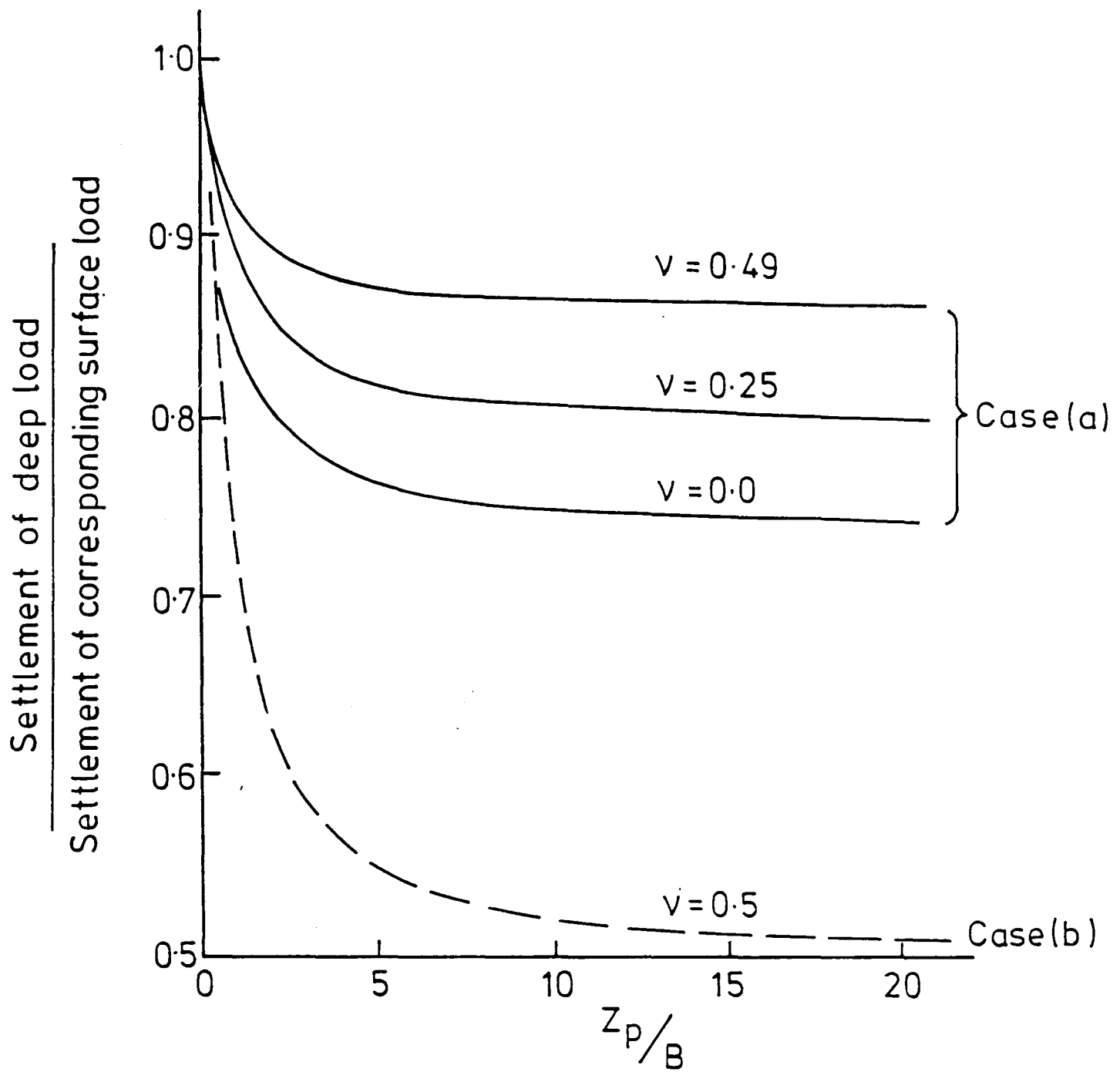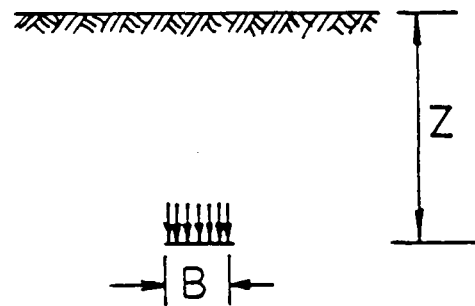
FIG. 2·5   DEPTH CORRECTION FACTORS
(AFTER BURLAND, 1969)

(a)   Self-boring pressuremeter

(b)   Menard pressuremeter (Menard,1957)

(c)   Menard pressuremeter (Marsland & Randolph,1977)
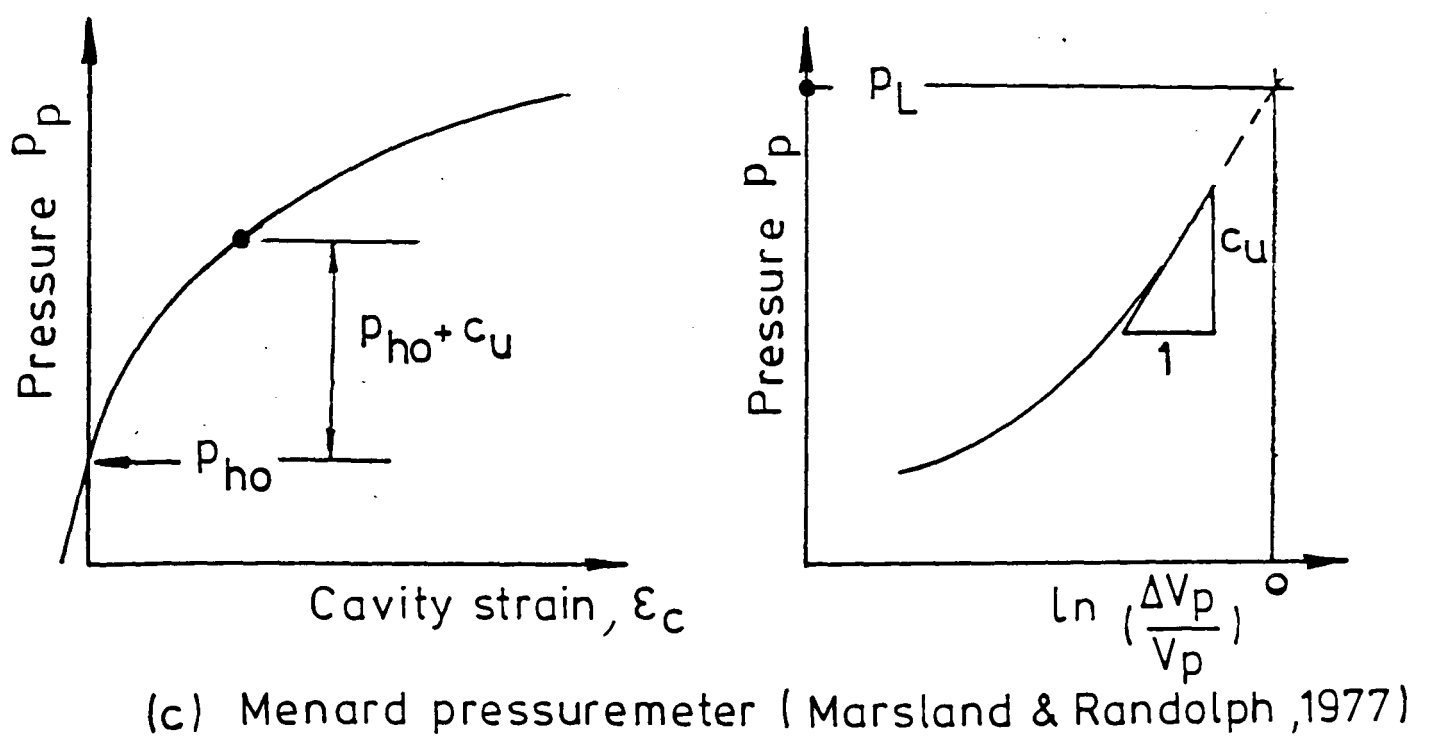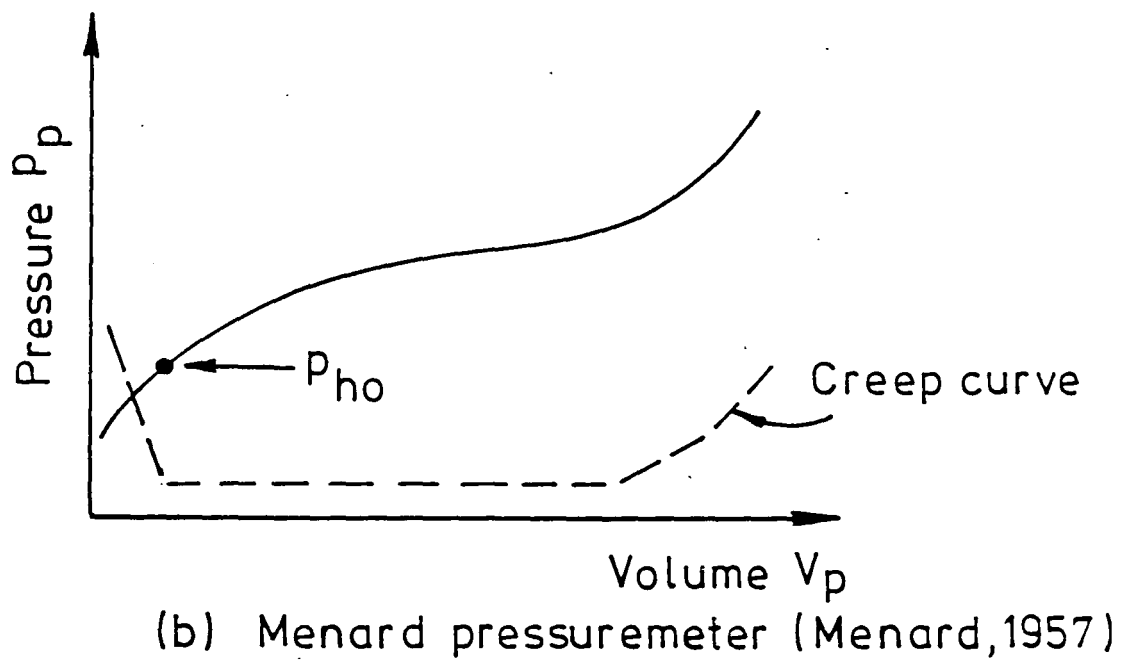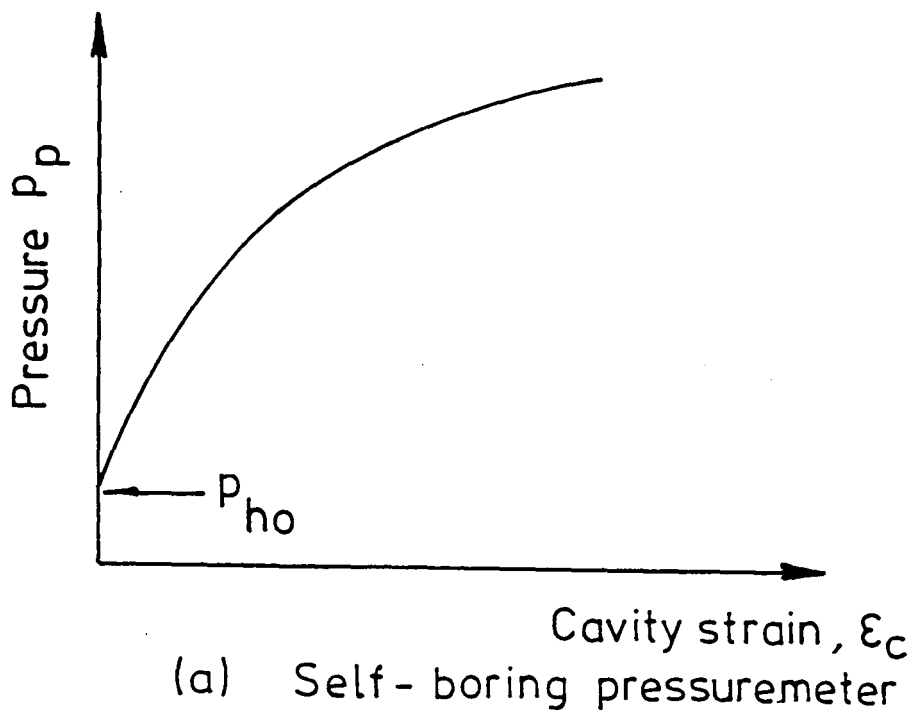
FIG. 2·6   ESTIMATION OF TOTAL HORIZONTAL IN-SITU STRESS
FROM PRESSUREMETER TESTS

Hull • Hornsea

BRE Site
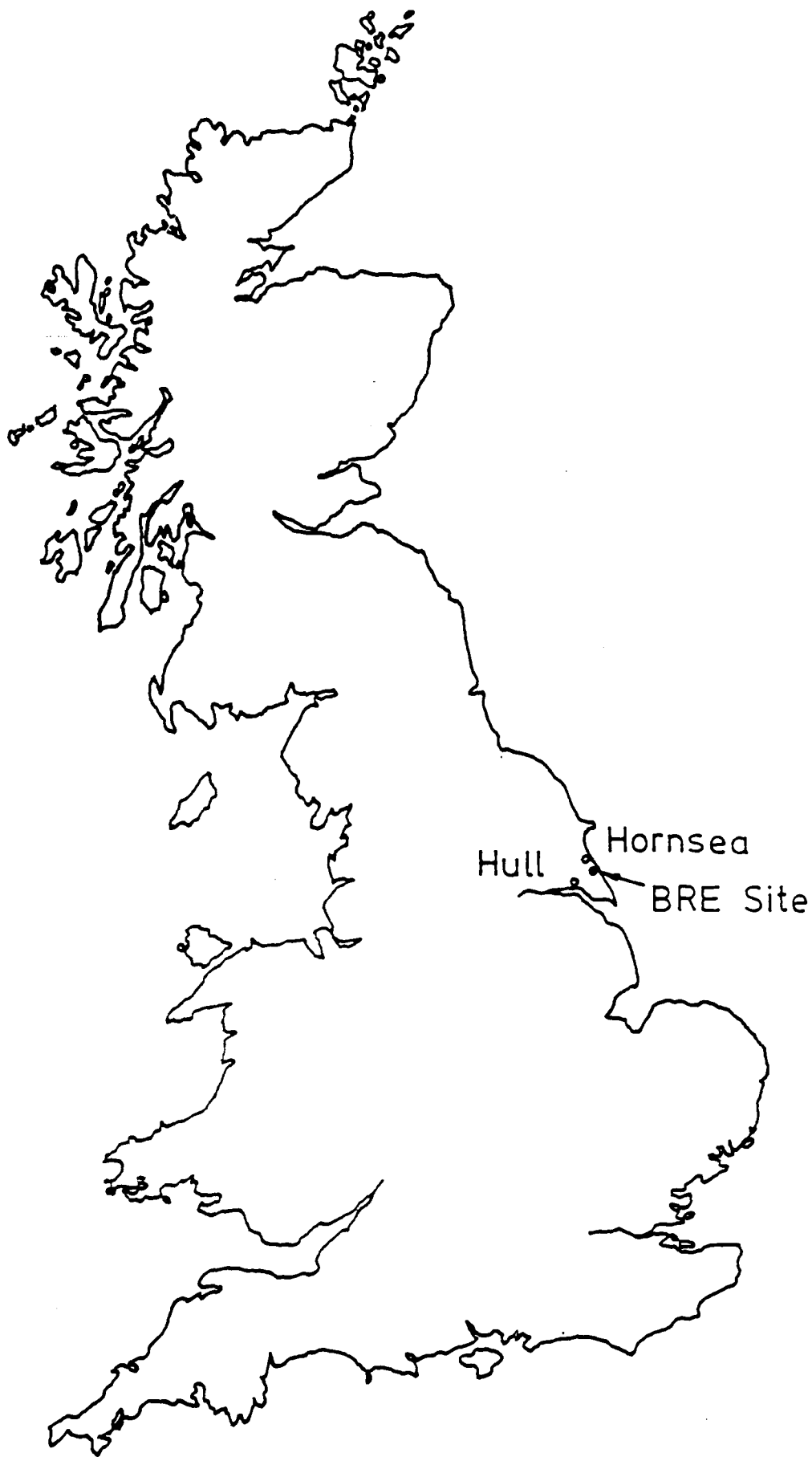
FIG. 2·7   LOCATION OF BRE (COWDEN) TEST SITE
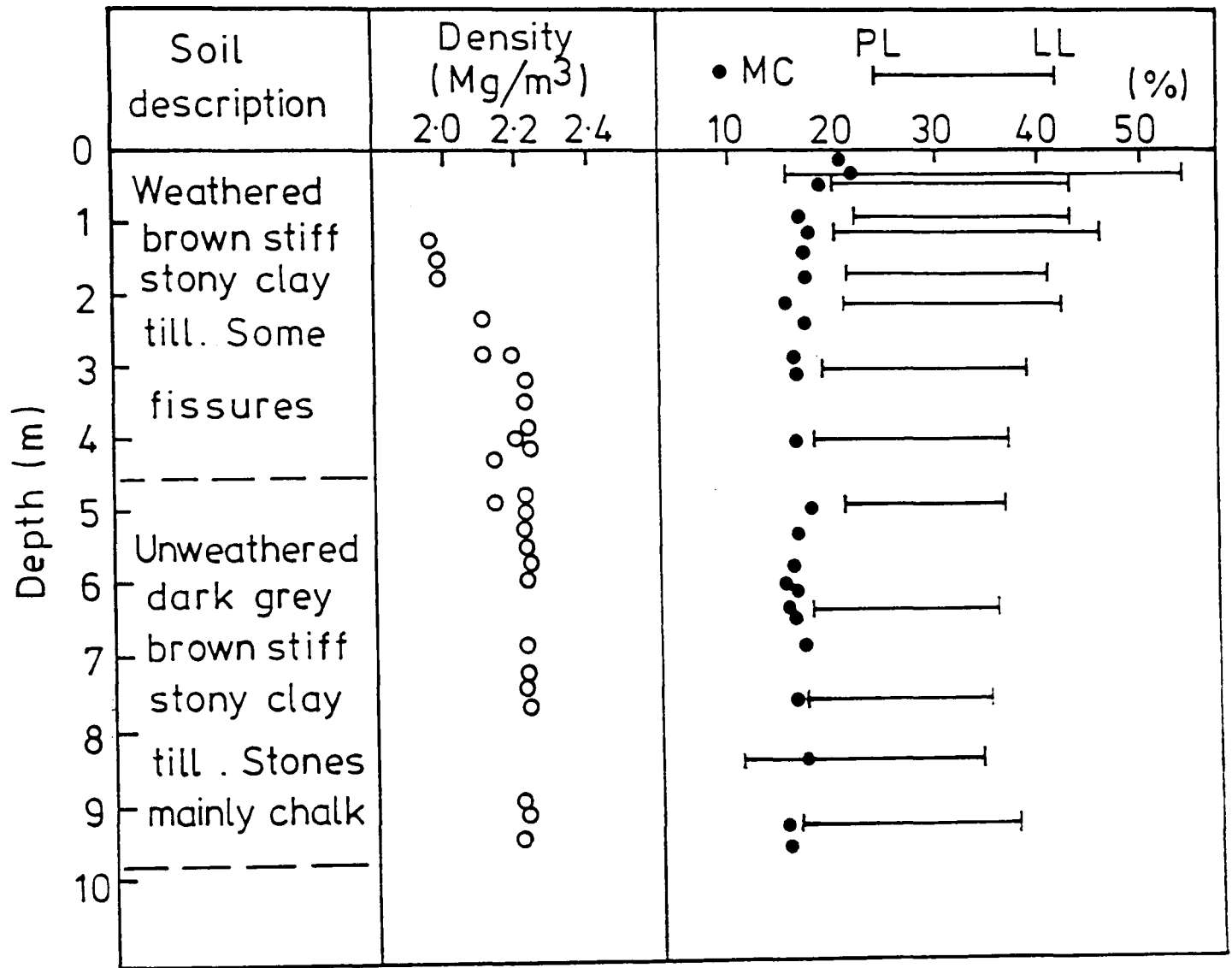
FIG. 2·8   TYPICAL SOIL PROFILE AT COWDEN
(AFTER MARSLAND AND POWELL, 1985)
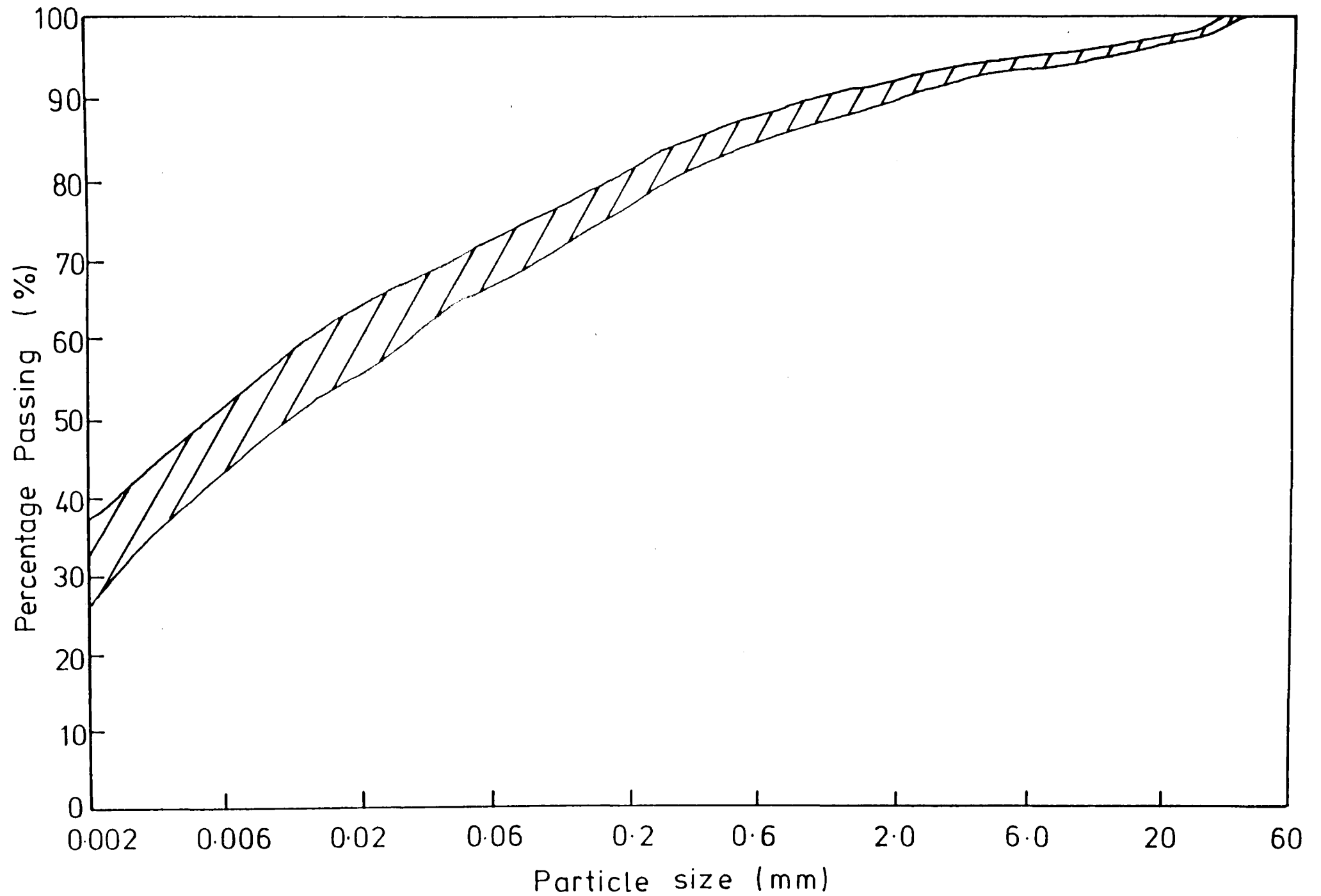
FIG. 2·9 PARTICLE SIZE DISTRIBUTION OF COWDEN TILL
(AFTER POWELL , MARSLAND & AL − KHAFAGI , 1983)
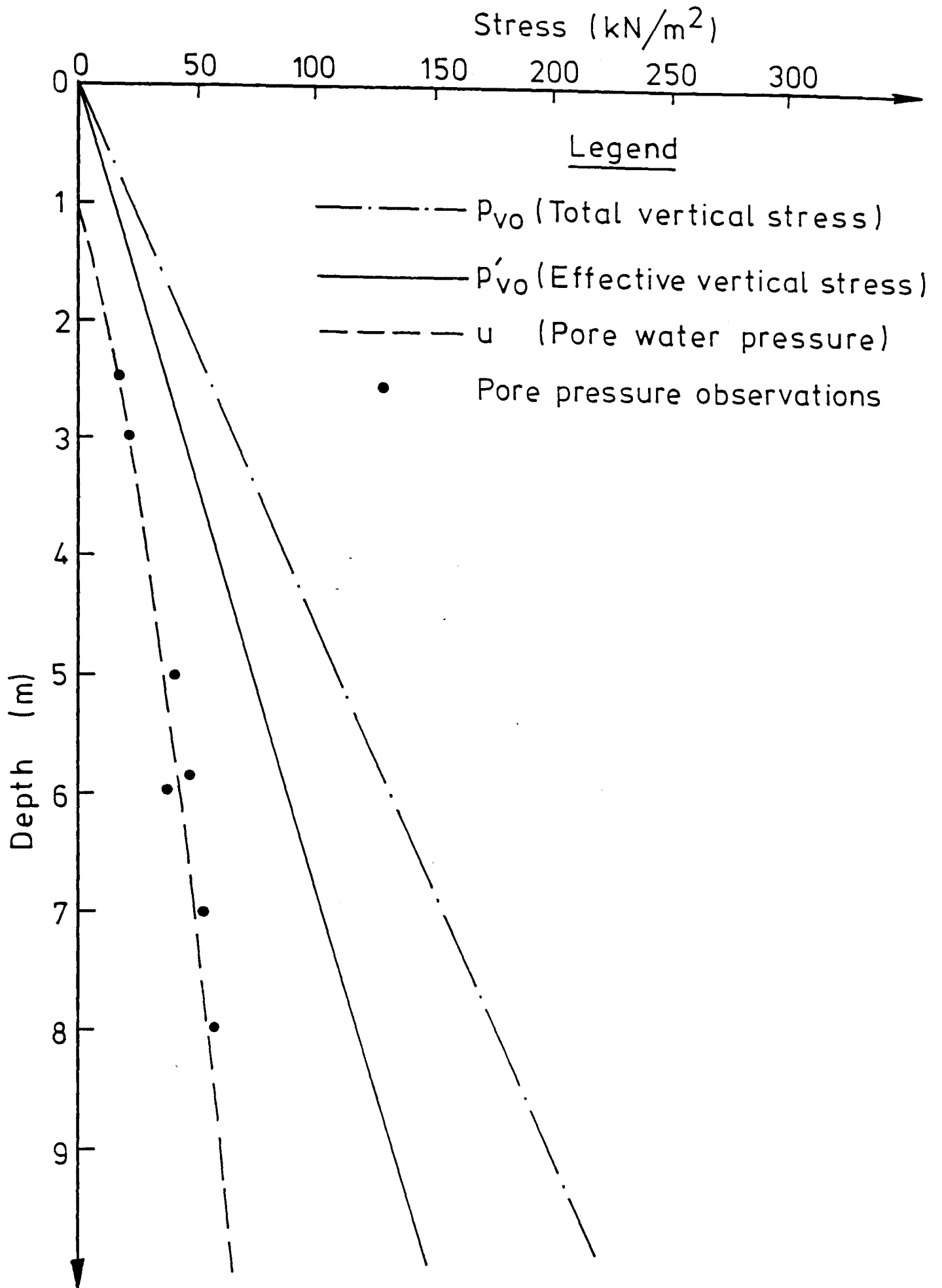
FIG. 2·10   VERTICAL STRESS DISTRIBUTION
(AFTER MARSLAND & POWELL, 1985)
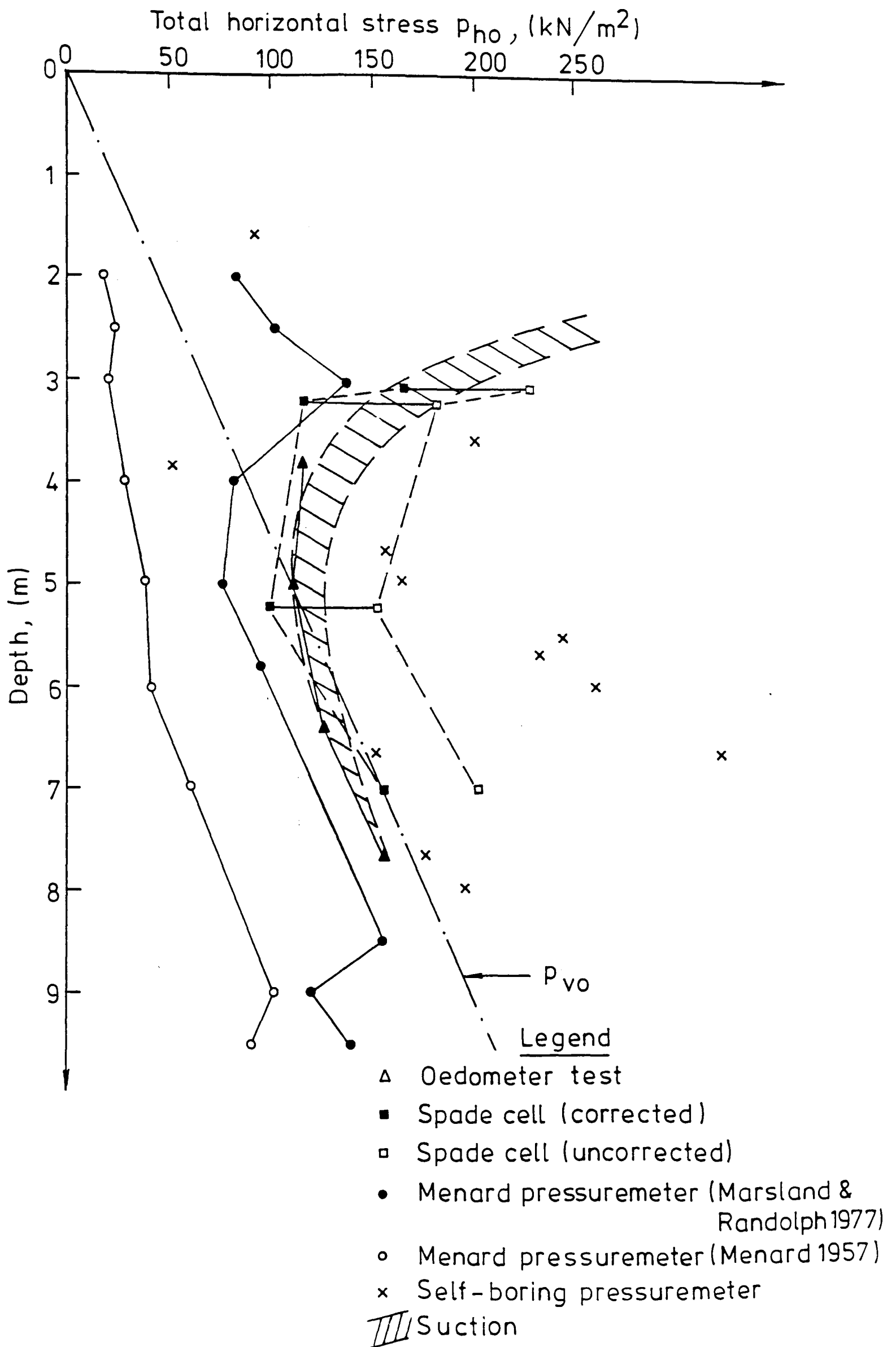
FIG. 2·11   TOTAL HORIZONTAL STRESS DISTRIBUTION
AFTER POWELL, MARSLAND & AL-KHAFAG,1983)
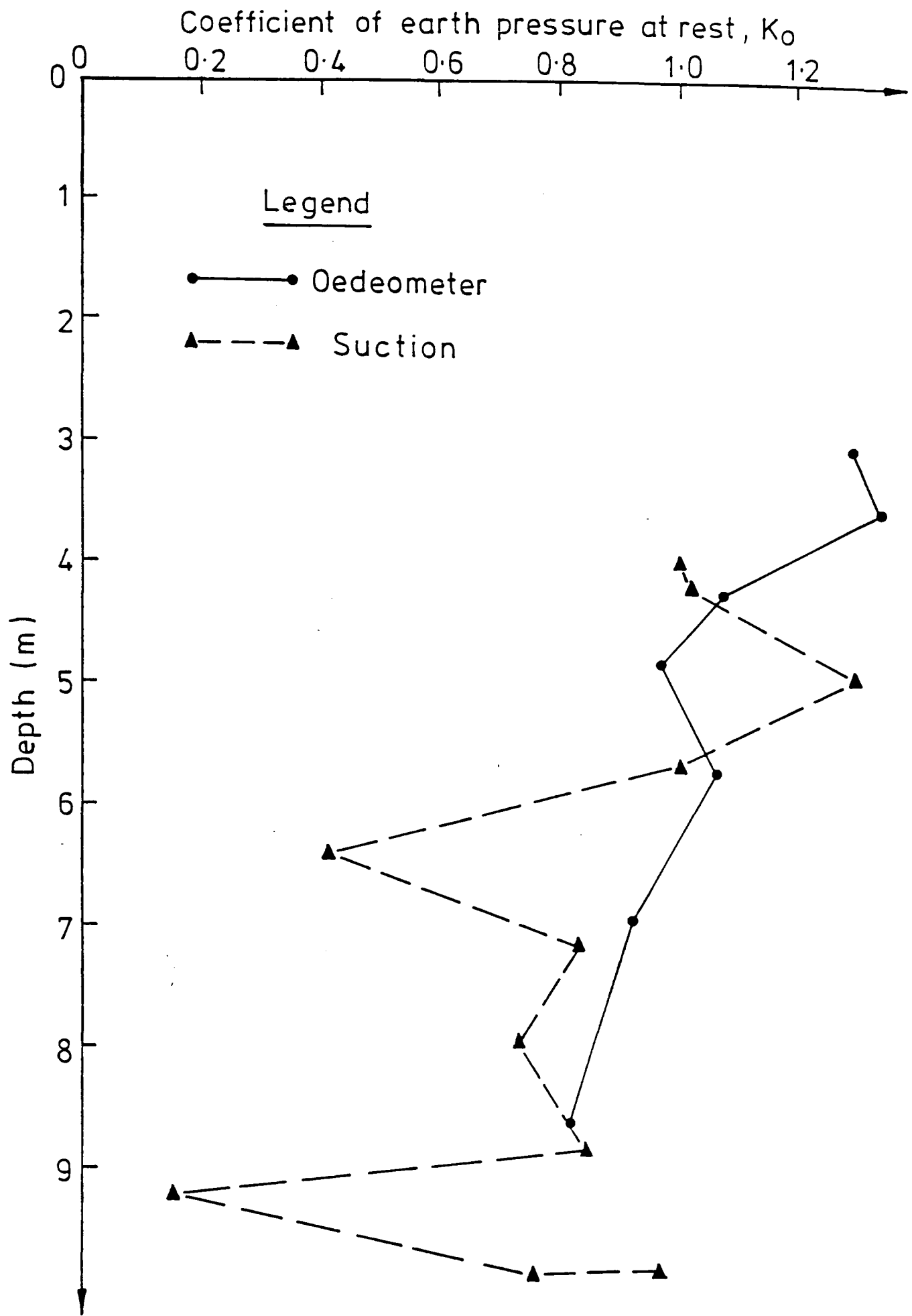
FIG. 2·12   COEFFICIENT OF EARTH PRESSURE AT REST (K₀)

(AFTER GALLAGHER, 1984)
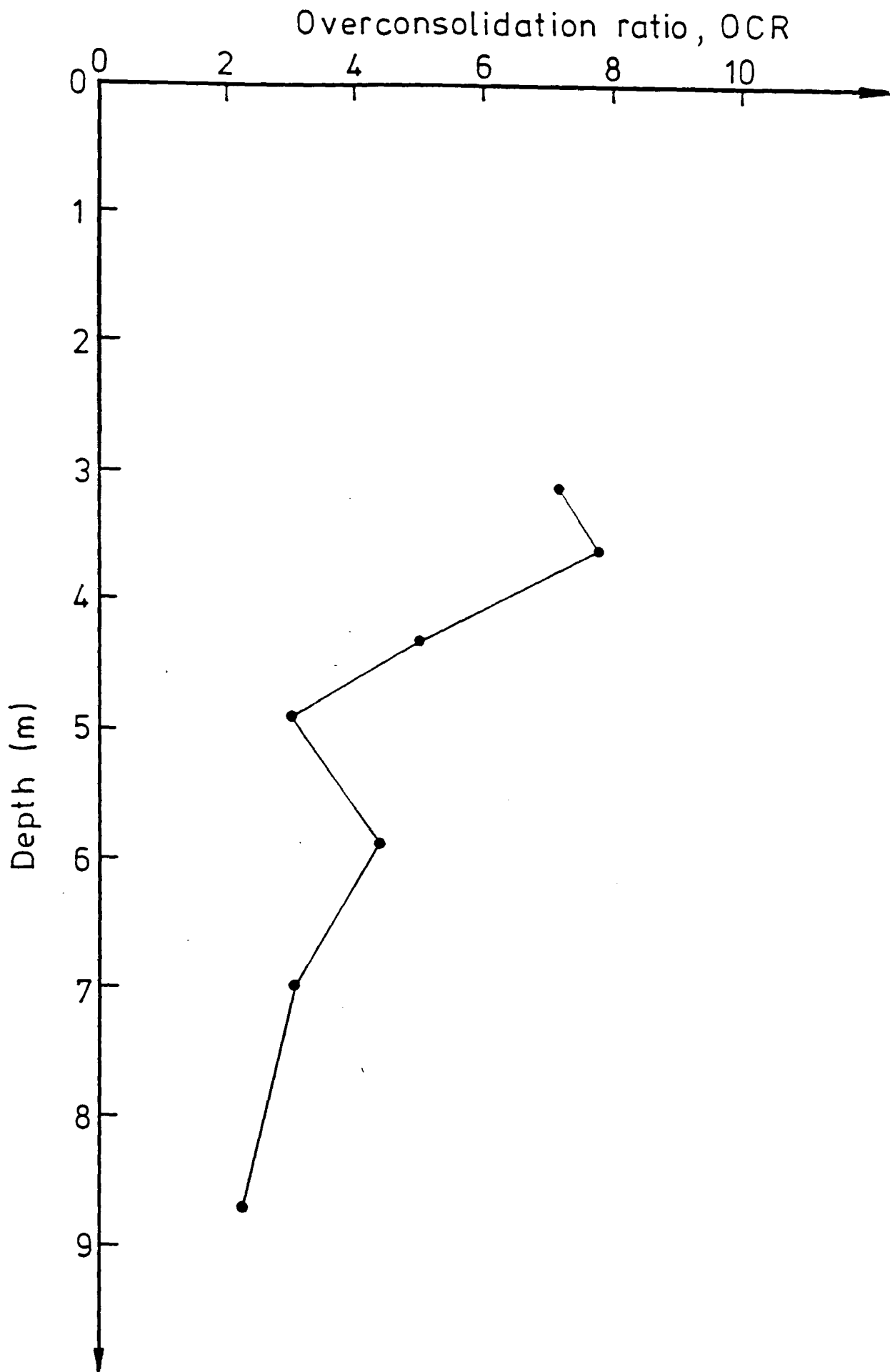
FIG. 2·13   OVERCONSOLIDATION RATIO (FROM OEDOMETER TESTS)
(AFTER GALLAGHER, 1984)
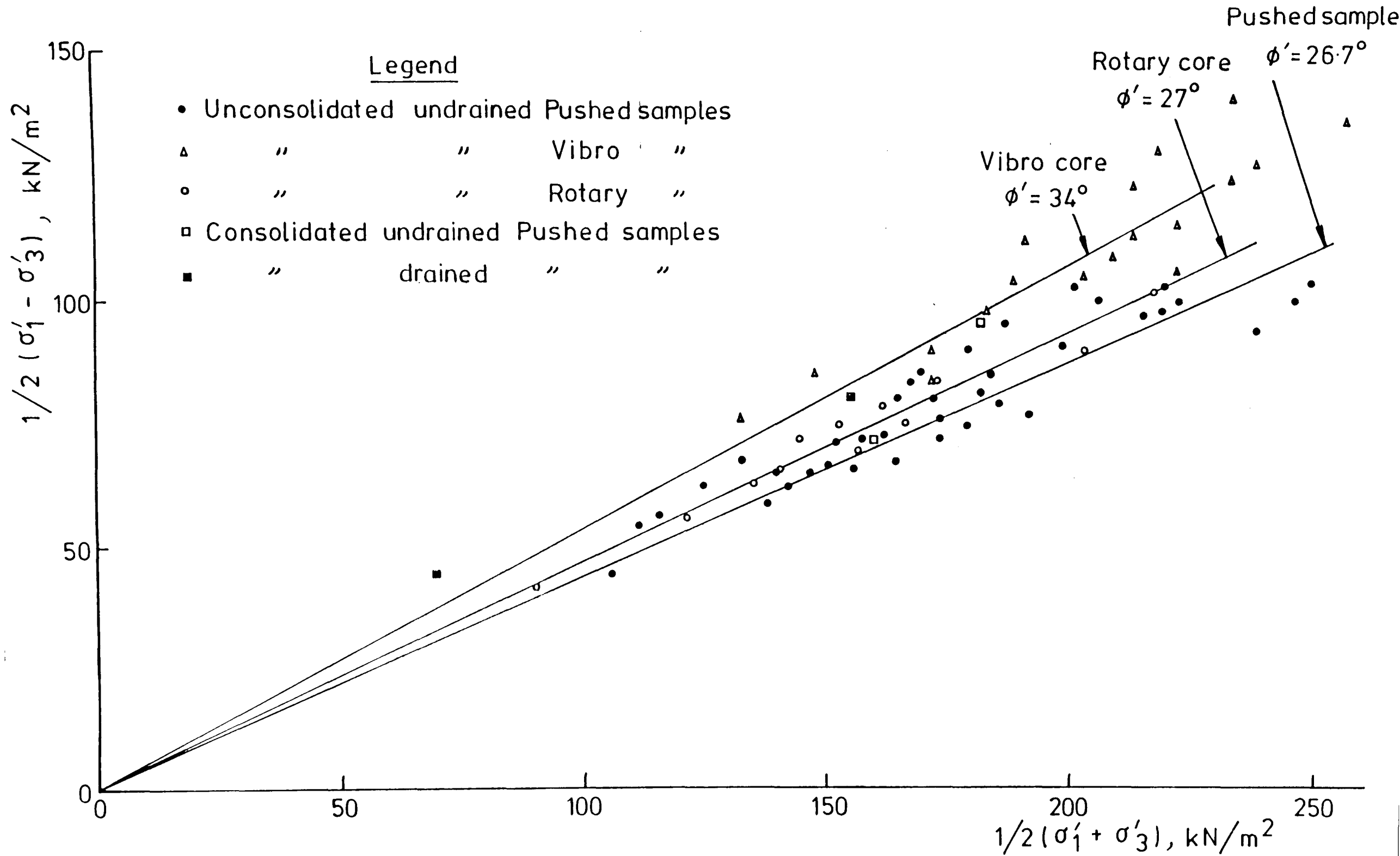
FIG. 2·14   FAILURE ENVELOPES FROM DIFFERENT TRIAXIAL SAMPLES (AFTER MARSLAND & POWELL, 1985)
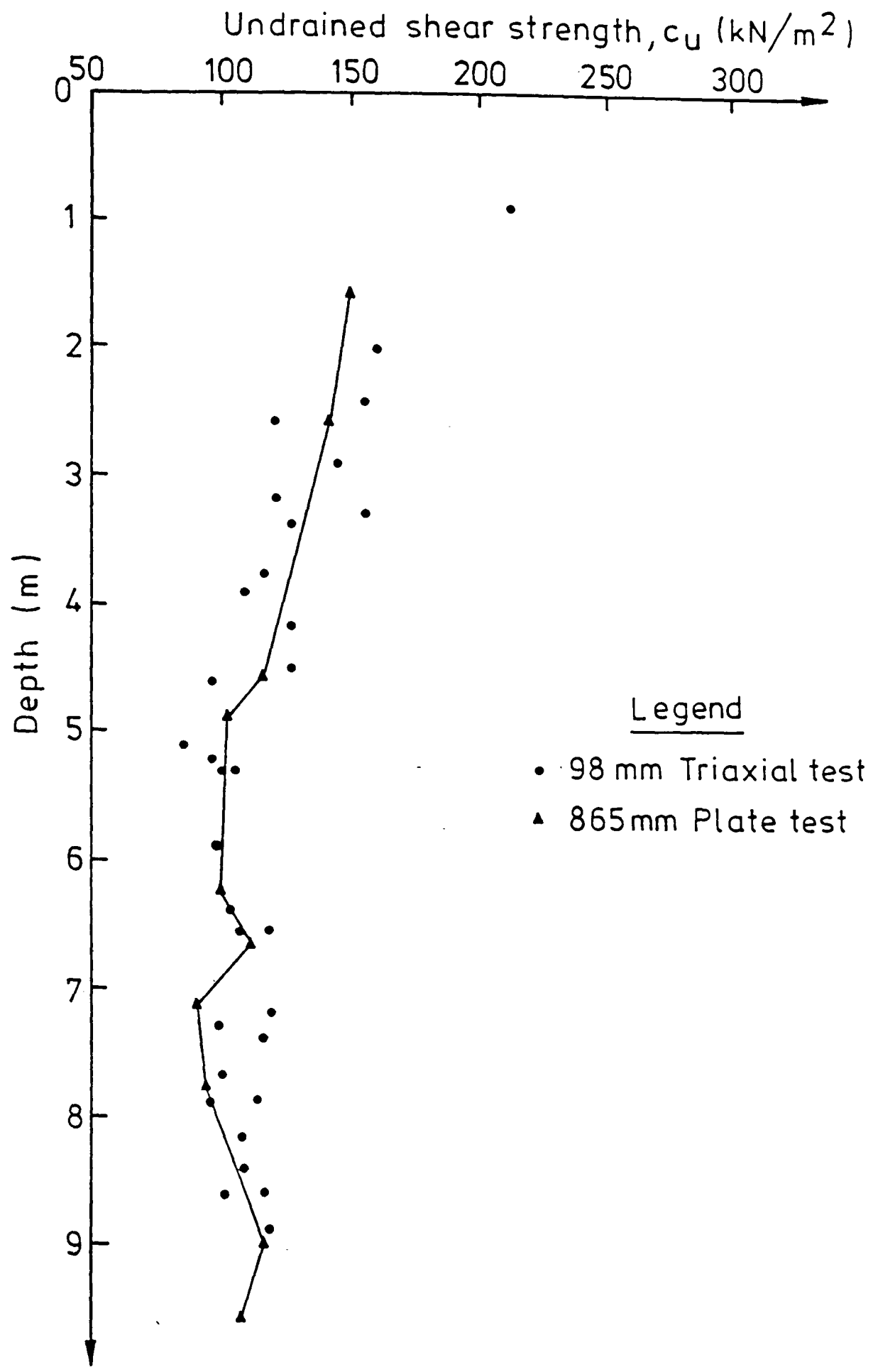
FIG. 2·15 COMPARISON OF UNDRAINED SHEAR STRENGTHS
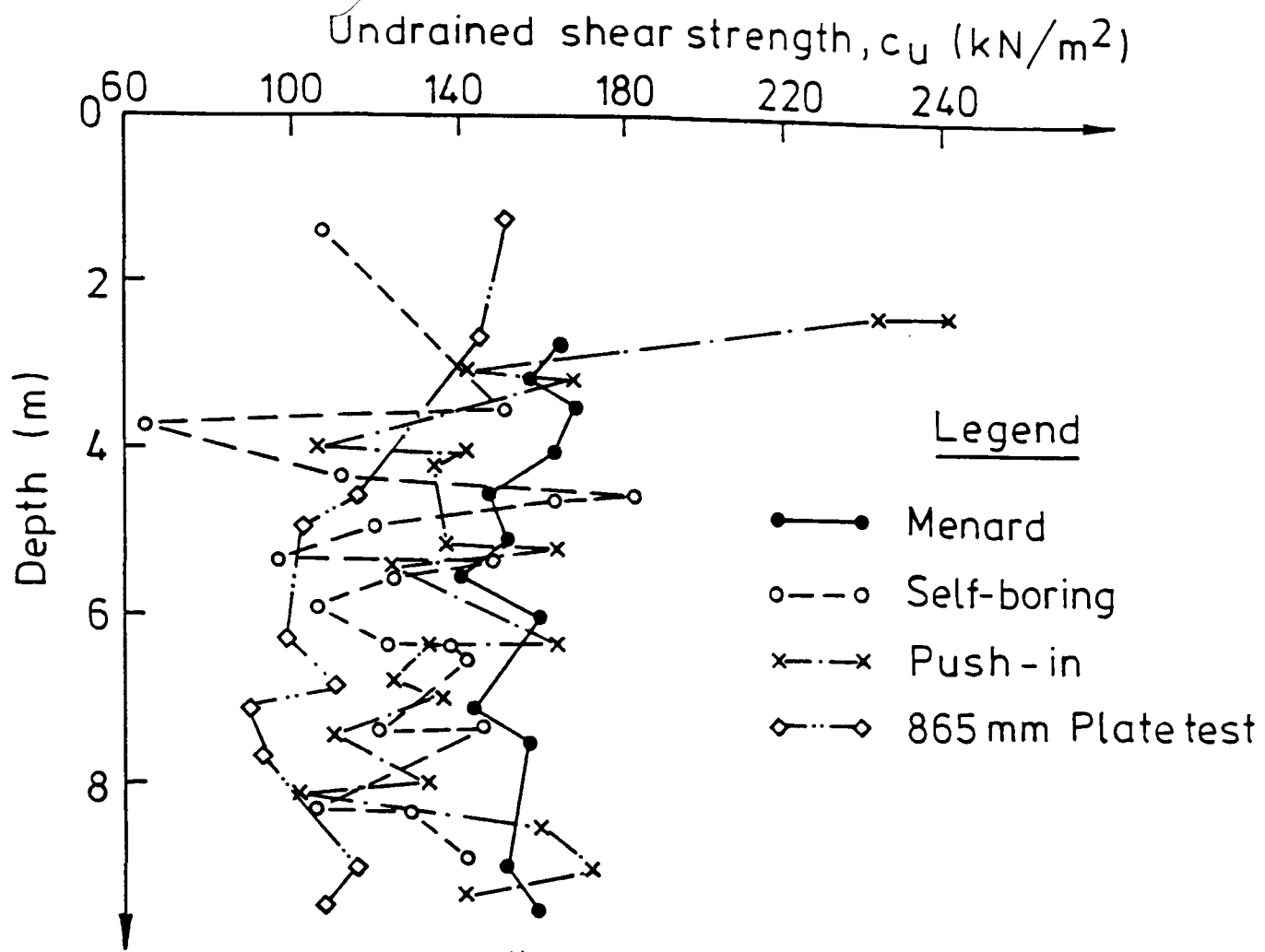
(a) Limit approach (Gibson & Anderson, 1961)
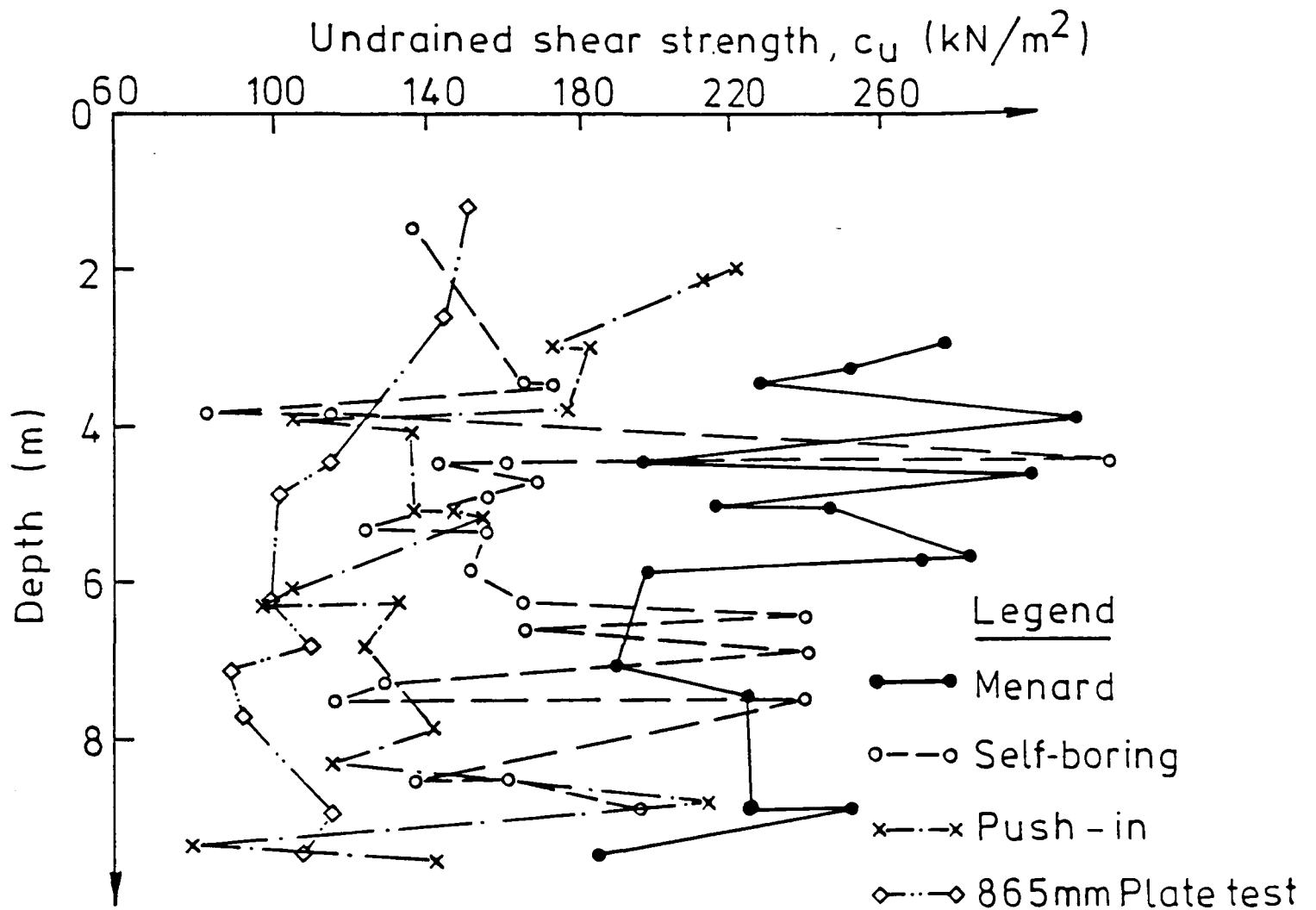
(b) Peak approach (Palmer, 1972)

FIG. 2·16 UNDRAINED SHEAR STRENGTH FROM PRESSUREMETER
TESTS (AFTER POWELL & UGLOW, 1985)

Secant shear modulus, G (MN/m²)

Depth (m)

Back analysis
from field scale
model piles

98 mm Triaxial test
G from $q = 0$ to $q = \frac{1}{2} q_u$

Menard pressuremeter test
G from $q = p_{ho}$ to $q = p_{ho} + c_u$
(p_{ho} estimated as Marsland
and Randolph, 1977)

Self-boring pressuremeter test
G from full unload-reload loop

Push-in pressuremeter test
G from full unload-reload loop

865 mm Plate test
G from $q = p_{vo}$ to $q = \frac{1}{3}(q_u - q_{vo})$
$+ p_{vo}$

FIG. 2·17   SUMMARY OF SECANT SHEAR MODULI
(AFTER MARSLAND AND POWELL, 1979)
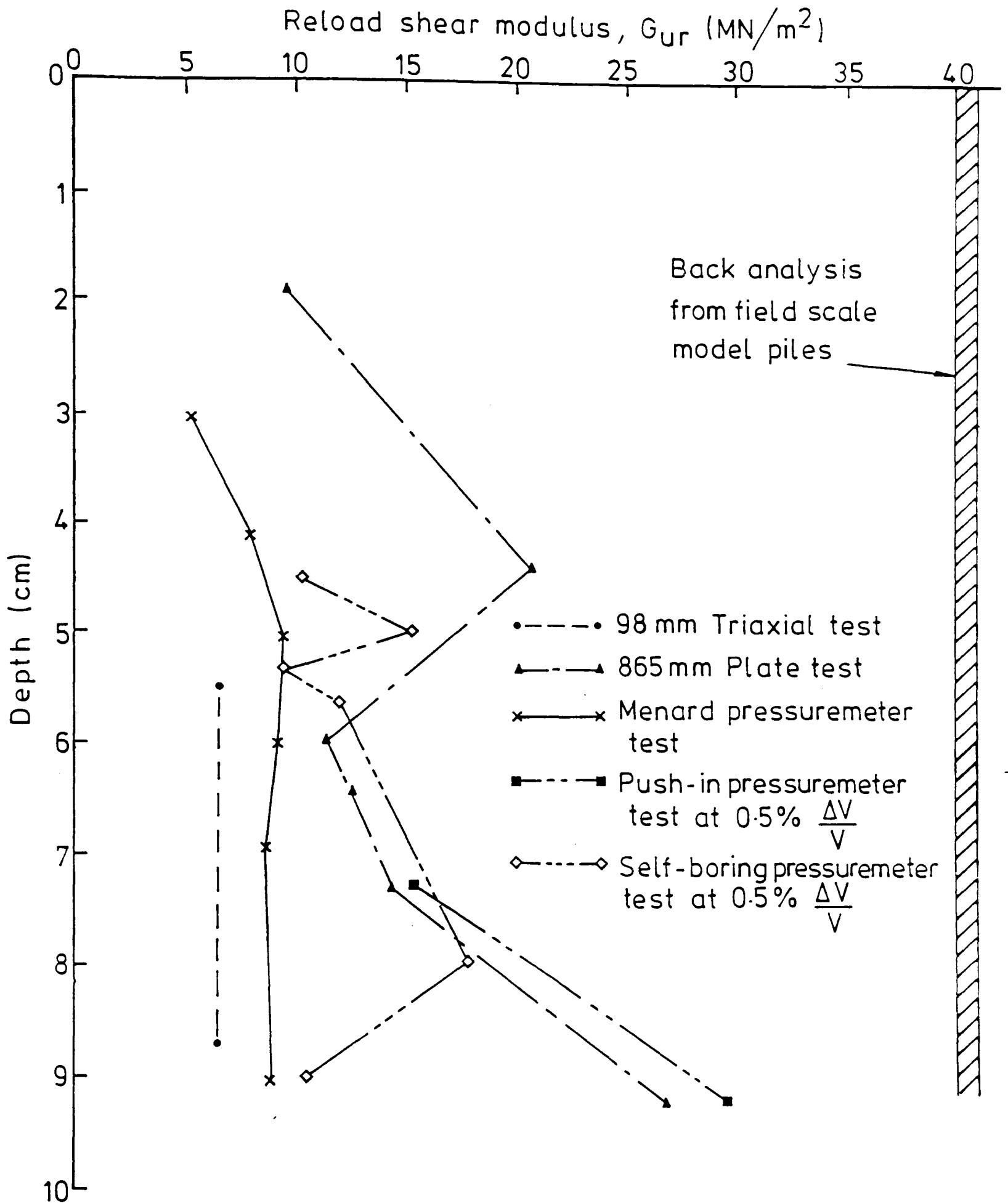
FIG. 2·18 SUMMARY OF RELOAD SHEAR MODULI
(AFTER POWELL AND UGLOW, 1985)

CHAPTER 3

EQUIPMENT AND EXPERIMENTAL TECHNIQUES

3.1   INTRODUCTION

The tests reported in Chapter 5 were performed in a triaxial

stress path cell for 100mm diameter specimens. As mentioned in Section

1.3.1, the development of computer programmes to control the tests and of

strain measurement techniques formed a significant part of the research.

The development of the computer programmes will be described in Chapter 4.

In this chapter a description will be given of the stress path cell and

ancillary equipment, specimen preparation and testing procedures, and

the instrumentation that has been developed to measure small strains.

3.2   STRESS PATH CELL

The cell, manufactured by Shape Instruments Ltd., Berkshire,

England, is similar in principle to that described by Bishop and Wesley

(1975) but is of larger size. It is capable of carrying out triaxial

stress path tests on samples of up to 100mm in diameter and 200mm in

height.

The cell is shown diagrammatically in Figure 3.1. Vertical load

is applied to the specimen by moving the base pedestal upwards and

pushing the top cap of the specimen against a stationary load cell. The

pedestal is mounted at the top end of a loading ram, at the bottom end

of which is a piston and a lower pressure chamber. Bellofram rolling

seals are used to retain fluid both in the cell and in the lower chamber,

and the ram travels up and down in a Rotolin linear bearing. It has a

maximum travel of about 50mm. A cross-arm is attached to the ram so that

vertical movement of the loading ram relative to the cell body may be

measured by an external displacement transducer.

Although the design is similar in principle to that of Bishop and Wesley (1975), there are several differences of practical detail. Firstly, the linear bearing is submerged in the lower chamber. This means that oil must be used as the chamber fluid so as to protect the bearing from corrosion. In Bishop and Wesley's apparatus, the linear bearing is positioned differently and is not submerged in any fluid. Consequently water can be used in both the cell and the lower chamber. Had this design been used for the present cell, it would have resulted in a tall and cumbersome apparatus.

Secondly, the flexible pore pressure and drainage leads are taken out through holes in the base of the cell. The lower loading platen is attached to the pedestal by screw threads so that it can be easily changed. In Bishop and Wesley's apparatus, these connections are made via holes drilled down the centre of the loading ram and out through a spacer block immediately above the lower pressure chamber. The flexible leads are connected at the exit points of the holes.

Thirdly, while the vertical strain is measured externally in both versions of the apparatus by means of cross-arms on the loading ram, in the present apparatus only one cross-arm is used (i.e. the measurement is one-sided) and the base of the cell is used as a reference point; in Bishop and Wesley's apparatus, opposite cross-arms are used (i.e. the measurement is two-sided) and the top of the cell is the reference point.

Fourthly, in the present apparatus the cross-sectional area sealed by the lower Bellofram is significantly larger than the area sealed by the upper Bellofram, whereas in Bishop and Wesley's apparatus these are equal. The area of the lower seal is about five times larger than that of the upper one. Consequently, a pressure of about a fifth of the cell pressure is required in the lower chamber to keep the loading ram in

equilibrium. This arrangement has the advantage that tests on strong materials at high cell pressure are possible and such specimens can be sheared to failure without applying excessively larger lower chamber pressures. However, because of the load multiplication effect, the lower chamber pressure control must be more precise.

Figure 3.2 shows the general layout of the hydraulic connections to the cell. As the cell was operated in the present work, drainage of the specimen and the application of back pressure took place via the top cap, whereas pore water pressure was measured at the bottom of the specimen.

Following delivery of the cell a number of faults were detected and these had to be rectified. Modifications were also needed to accommodate additional instrumentation.

The major fault was leakage around both the upper and lower Bellofram seals. In the original design the flanges of the Belloframs were clamped by flat metal rings screwed to the cell body. These leaks were rectified by inserting a number of O-rings, as indicated in Figure 3.3. Unfortunately, these modifications were only successfully completed following the tests described in Chapter 5 for which the leakage imposed certain pressure limitations.

To allow for the local strain instrumentation, three new holes had to be drilled out and threaded in the cell base. As the aluminium used in the construction of the cell was soft, these threads were easily broken and ultimately had to be sealed using Loctite glue. However, the major modification was the heightening of the cell by inserting a spacing ring of 50mm height which rested on the original cell base. This increased the clearance at the top of the specimen so that instrumentation to measure axial strains between the end caps could be installed. The tie rods on the outside of the cell had to be extended by 50mm also.

It should be noted that, where the load cell makes contact with the specimen top cap, the latter has a flat surface instead of the usual curved recess. The potential dangers of using a curved recess are two fold, should there be any misalignment. Firstly, the top of the specimen will move sideways until alignment is achieved and this would probably cause non-uniformity of strain at small strain levels. Secondly, vertical movement of the entire specimen is needed to achieve true contact and this increases the carefully pre-arranged distances between the proximity transducers used for local axial strain measurement and their targets (see Section 3.4.2). The measurements are then less accurate. For these reasons it was considered best to tolerate some eccentricity of loading.

3.3   PRINCIPLE OF STRESS PATH CONTROL

The response of a specimen to a given total stress path is dictated by the drainage conditions. Under fully drained conditions the effective stress path is the same as the total stress path. In order to follow a given total stress path, both the axial stress (σ_1) and lateral stress (σ_3) generally need to be controlled. One of these, σ_3, can be controlled directly. The other, σ_1, responds to changes in the lower chamber pressure (L_p). The following relationship between σ_1, σ_3 and L_p was determined by Bishop and Wesley (1975) by considering the equilibrium of the loading ram:-

$$\sigma_1 = L_p \left(\frac{L_a}{A}\right) + \sigma_3 \left(1 - \frac{U_a}{A}\right) - \frac{W}{A} \qquad (3.1)$$

where U_a =   area sealed by upper Bellofram,

L_a =   area sealed by lower Bellofram,

A =   cross-sectional area of sample, and

W =   total weight of loading ram, sample, pedestal, cross-arm (i.e. all moving parts).

As W must be countered by a certain value of L_p at the start of the stress path, it is more useful to express equation (3.1) in terms of the subsequent stress changes:-

$$\Delta\sigma_1 \;=\; \Delta L_p \left(\frac{L_a}{A}\right) + \Delta\sigma_3 \left(1 - \frac{U_a}{A}\right) \tag{3.2}$$

With the help of this equation, it is easy to determine the way in which L_p must be varied in relation to σ_3 in order for the required stress path to be followed. A control system may be programmed accordingly.

In practice both the Rotolin bearing and Bellofram seals offer some resistance to movement of the loading ram and a correction for this friction is required in predicting the axial stress σ_1. If the friction is variable, equation (3.2) becomes invalid. It is clearly advantageous to use the load cell not only for the measurement of deviator stress but also its control. A more detailed discussion of this aspect is given in Section 4.3.

A method of controlling stress paths in real time has been developed. Suppose it is desired to follow a linear stress path in the (p', q) plane with a slope of $K\left(= \dfrac{dq}{dp'}\right)$ and that this is to be achieved by varying the deviator stress with time, t, at a rate $R\left(= \dfrac{dq}{dt}\right)$. Then for a small incremental change

$$K \;=\; \frac{\delta q}{\delta p'} \;=\; \frac{\delta\sigma_1 - \delta\sigma_3}{\frac{1}{3}(\delta\sigma_1 + 2\delta\sigma_3)}$$

Hence

$$\delta\sigma_3 \;=\; \left(\frac{3 - K}{2K + 3}\right)\delta\sigma_1$$

Since

$$R \;=\; \frac{\delta q}{\delta t} \;=\; \frac{\delta\sigma_1 - \delta\sigma_3}{\delta t}$$

$$\delta\sigma_3 \;=\; \left(\frac{3 - K}{3K}\right)\cdot R \cdot \delta t \tag{3.3}$$

and

$$\delta q \;=\; R \cdot \delta t \tag{3.4}$$

The target cell pressure and deviator stress are evaluated from

equations (3.3) and (3.4) after a change of time δt and are compared

with the actual values. Corrections of the latter are only worthwhile

if the differences from the target values exceed certain tolerance

limits. If the limits are too small, oscillation of the stresses will

occur. If the limits are too large the desired stress path will not be

accurately followed. The implementation of the scheme outline above and

the tolerance limits found to be satisfactory are described in Section 4.3.

3.4 INSTRUMENTATION

3.4.1 Standard or Semi-Standard Instrumentation

It has been stated previously (Section 1.3.1) that attention was

to be concentrated on the measurement of small strains. The instrumentation

used to measure small local strains in the central part of the specimen will

be discussed in the following section. The remaining instrumentation was

of a commonly used type and only a brief description will be given.

The deviator load was measured using a submersible load cell

designed at Imperial College with a maximum capacity of 1350 kgf (13.2 kN).

The principles of its design have been described by El-Ruwayih (1975) and

subsequent modifications introduced to improve its performance have been

discussed by Hight (1983). The cell, lower chamber and pore water pressure

were measured using pressure transducers (Bell and Howell, type 4-306-

0119-olMO) with a range of 0 - 700 kN/m^2. A linear displacement

potentiometer (Novatech, type R102) was used to measure the vertical

displacement of the loading ram. It was installed outside the cell and

had a stroke length of 50mm. As mentioned in Section 2.2.3, bedding errors

and the compressibility of the loading system are measured inadvertently

by an externally placed instrument. The external measurement of axial

strain was therefore regarded as relatively crude. A volume change unit

developed at Imperial College and described in detail by Maswoswe (1985) was employed to measure specimen volume changes during the tests. It has a capacity of 100 cm^3.

In addition to the external and local measurements of axial strain already referred to, axial strains were also measured between the specimen end caps. While the compressibility of the load cell is not included in such a measurement, errors remain due to bedding, end restraint and the compressibility of porous stones or filter papers. The vertical displacement between the end caps was measured by two submersible LVDTs with flexible leads (Sangamo, type 920915). These had a range of 10mm and were mounted on opposite sides of the specimen. As shown in Figure 3.4, the body of the transducer was mounted on a bracket connected to the bottom end cap. The armature rested under its own weight on a metal plate attached to the top cap. This arrangement ensured that the restraint to movement of the top cap was negligible and that the armatures of the transducers would be undamaged in the event of lateral movement.

Very thorough calibrations of all the instrumentation were carried out at the start and end of the test programme, which was of about one year's duration. It was found that the calibration factors determined at the start of the experiments were valid throughout. The calibration results are summarized in Table 3.1. At this point several terms used in metrology need to be clarified. The term "resolution" is defined as the smallest change in mechanical input which produces a detectable change in the output signal. The overall resolution is affected by the resolution of the analogue to digital converters used. In general, the "accuracy" of a measurement is unlikely to be as small as the resolution of the measuring instrument, accuracy being defined by the British Standards Institution (1986) as the closeness between the result of a measurement and the true value. If the measurement is actually the average of a large number of observations, it follows that any

inaccuracy is caused solely by systematic errors. The term "precision" is used to express the scatter of measurements around a mean value and therefore involves only random errors, British Standards Institution (1978).

3.4.2 Instrumentation for Local Strain Measurement

As discussed in Sections 2.2.2 and 2.2.3, the effects of end restraint can be minimized and bedding errors eliminated if local measurements of strain are made in the central region of the specimen. For sufficiently accurate measurements of small strains to be made over the central half of a 200mm high specimen, the relative displacement of two points on the specimen must be measured to within ±0.01mm. This gives a possible ±10.0% error at the 0.1% axial strain level, although a higher accuracy would be preferable. Not only is high accuracy required but also the restraint imposed on the specimen by the measuring device and possible damage to that device at large strains have to be considered. In these latter respects the LVDT systems reviewed in Section 2.2.3 were considered to be less than satisfactory. The use of other devices reviewed in Section 2.2.3 was rejected because of a desire to develop an independent system of small strain measurement (see Section 1.3.1). It was therefore decided to make use of proximity transducers which, although used previously to measure radial strains (e.g. Khan and Koag, 1979) appeared not to have been fully exploited.

Proximity transducers are non-contacting inductive devices. A magnetic field is generated by a coil within the transducer. The field thus generated interacts with a suitable target material placed at a certain distance from the transducer. As the target distance changes there is a measurable change of inductance caused by the circulation of eddy currents within the target. The arrangement of the proximity transducers within the stress path cell is illustrated

in Figure 3.4. Two pairs of transducers (Sangamo, type DT18M) measure the axial strains on opposite sides of the specimen and one pair (Sangamo, type DT19M) measure the radial strain across a diameter.

There are some disadvantages associated with these particular types of transducer. Firstly, the range is limited to 6mm. Secondly, within this range the output varies non-linearly with the target distance (see Figure 3.5) so that calibration and data processing are more complicated. To obtain acceptable accuracy for small strain measurements the target distance must be restricted to 1mm. Thirdly, the stiff cable (metallic sheath) attached to the transducer can only be bent with difficulty and to a radius of not less than 19mm.

According to the manufacturer, measurements can be made against most metallic surfaces, although some non-magnetic alloys have low conductivity and a small wafer of "soft" iron has to be applied to the sensing surface. Factors considered in the choice of target in this research were size, weight, conductivity and susceptibility to oxidation or corrosion. The last consideration ruled out the use of materials such as cast iron, brass and aluminium. Trials using tin and ordinary stainless steel did not achieve the accuracy required due to their non-magnetic nature. The material finally adopted was magnetic stainless steel of about 1mm thickness, which satisfied all the criteria.

The transducers are fully submersible, with an operating pressure range of 0 - 7 MN/m^2, and have an operating temperature range of $-40^{\circ}C$ to $+180^{\circ}C$. The transducers were calibrated in air but it was checked that the calibrations did not change when they were submerged in water. The following calibration procedure was also adopted for other types of displacement transducer, mentioned in Section 3.4.1. All these transducers were calibrated using slip gauges conforming to British Standards Institution (1950). Each transducer was mounted vertically in a rigid stand and slip gauge assemblies of thicknesses known with an

accuracy of ±0.0002mm were inserted under the transducer. In the case of the proximity transducers, a 40mm square magnetic stainless steel target was glued on to a 30mm high perspex block with the same plan dimensions as those of the slip gauges. This perspex block was placed on top of a known height of slip gauges. The mean of ten successive output readings (sampled at about 0.1 second intervals) was taken as a measurement and the height of the slip gauges was then changed.

Figure 3.5 shows a typical proximity transducer calibration curve. A method of linearization was developed by transforming the output to $\ln (V_d - V_z)$, where V_d is the original output when the target is at a known distance from the transducer and V_z is the corresponding output when there is no target. The value of V_z was determined by calculating the mean of 3000 measurements (each measurement being the mean of ten readings). The transformed, approximately linear, calibration curve is shown in Figure 3.6. The data were then analysed by fitting a fourth order polynomial to each successive 0.5mm range by the method of least squares. The precision of the transducer in each range was determined by examining the deviations of the data. Table 3.2 shows the precisions typically achieved. The accuracy of the strains measured by the proximity transducers will be discussed in Section 5.2.

Unfortunately the research could not be conducted in a temperature controlled environment as would have been desirable. Therefore, the temperature variations were continuously monitored for 18 months; the maximum deviation during that period was ±3°C about a mean of 20°C. This is a very small variation by comparison with the operating range of the transducers (-40°C to +180°C). It is therefore concluded that the effect of temperature variation upon the transducers was negligible.

The proximity transducers were mounted on rigid brackets (see Figure 3.4). The axial strain targets were positioned so as to move

away from the transducers in a compression test. However, the radial
strain targets moved towards the transducers and had to be designed to
collapse at large strains. For radial strain measurement, a 30mm
square target was glued with rapid hardening Araldite onto a thin-
walled plastic tube (20mm diameter x 50mm long x 0.2mm wall thickness).
The dimensions of the target were sufficiently generous to allow it to
be easily aligned with the corresponding proximity transducer (the
minimum target size being about 16mm). The whole target arrangement,
weighing about 9gm, was then glued onto the membrane, again with
Araldite, so that the target faced the transducer. The design ensures
that, should the target make contact with the transducer due to radial
strain during compression, further deformation will be absorbed by
flexing of the thin-walled tube. Therefore there will be no damage
to the transducers and no significant restraint to the specimen. For
axial strain measurement, two pieces of target material, 35mm long x
30mm wide, were glued by silicon rubber onto a perspex ring of outside
diameter 150mm, inside diameter 130mm and thickness 6mm, Figure 3.7.
Four stainless steel rods, 30mm long x 3mm diameter, pass through
radial holes in the ring, each provided with a steel bushing. The
clearance between the rod and the bushing was kept to a minimum and
was packed with silicon grease. At the inner end of each rod a footing,
20mm long x 5mm wide, with a curvature designed for a 100mm diameter
specimen was welded to the rod and at the outer end a special cap was
fitted. A rubber band was passed around the outside of the ring and
over these caps in order to press the footings lightly against the
specimen (see Figure 3.7 and Plate 3.3). Since the whole arrangement
only weighed about 56gm this was easily achieved. However, due to the
roughness of the surface of Cowden Till specimens, contact between the
footings and the specimen was incomplete and the footings were subsequently

glued onto the membrane with Araldite. It was realized that three footings would be a better number than four in the event of a specimen deforming non-uniformly, but geometric (space) considerations favoured the above design. During compression of the specimen the ring bearing the targets remains stationary in plan view. Radial strain is absorbed by movement of the rods through the bushings, since the rubber band exerts a negligible resistance. The maximum radial strain that can be absorbed in this way is about 24%. In the axial direction the ring, footings and targets move as a unit during compression. At very large strains it is possible for the lower targets to collide with some of the stiff transducer cables and to break off the ring.

3.5 SAMPLE PREPARATION

3.5.1 Drilling and Sampling

Samples of Cowden Till were supplied by the BRE in the form of 250mm diameter tube samples. A borehole was first drilled by flight auger and then cleaned by bucket auger. A double-tube core barrel method of sampling, developed by the BRE, was used. At the lower end of the sampling tube a cutting ring was fitted such that the area ratio was about 38%. On the upper end a swivel mechanism was fitted to which a larger concentric tube (outside diameter about 300mm) bearing a helical auger was also connected. During sampling this outer tube was rotated to remove soil from around the sampling tube which was advanced without rotation. The vertical reaction required was provided by a truck via the drilling rod connected to the top of the swivel mechanism.

In the course of drilling two difficulties were encountered. Firstly, large stones tended to prevent advancement of the borehole, especially during sampling, so that the borehole had to be abandoned. Secondly, due to a faulty connection of a non-return valve near the

swivel mechanism, the soil was not able to be retained in the sampling tube by suction but fell back into the borehole. When sampling was successful, disturbed material at the ends of the sample was removed before it was sealed with wax. The samples were delivered to Sheffield within a few days.

3.5.2 Extrusion and Storage of 250mm Diameter Samples

It has been mentioned previously, in Section 2.2, that the effective stresses within a soil sample will change as it is removed from the ground. While this is unavoidable, it is desirable that a stress regime similar to that existing in the ground is re-imposed as quickly as possible. In the present investigation, the samples were stored under pressure before they were tested. The period of storage varied from 15 to 53 weeks.

First of all, it was necessary to design equipment to permit extrusion of the 250mm diameter samples. Figure 3.8 and Plate 3.1 show the arrangements adopted for extrusion using a 500 kN Amsler testing machine available in the Structures Laboratory of the Department. The square frame (A) was first connected to the cross-head of the machine and raised to a suitable height. The sample tube was then lowered by overhead crane onto the square plate (B) and inserted under the machine. Four tie rods were used to connect the sample tube both to the square frame and to the plate so that the whole assembly could be raised together on the cross-head. A piston (C) was then put onto the loading ram under the assembly. Finally the sample was extruded by lowering the cross-head. The first 30mm was discarded and the end surface trimmed flat. A further 250mm length of soil was then extruded and sawn off with a coarse steel blade. The time spent on cutting and trimming a surface was typically about one hour. In total eight such cylindrical blocks of soil were retrieved from six 250mm diameter tube samples.

The samples ranged in depth from 3.8m to 6.7m. The estimated vertical effective stresses (p'_{vo}) of the individual samples are summarized in Table 3.3. From Figures 2.10, 2.11 and 2.13 it can be seen that the value of the coefficient of lateral earth pressure K_o, was about unity. This was fortunate since it meant that the in-situ stress condition was approximately isotropic and it was relatively easy to store the soil under such conditions. Although Table 3.3 shows a variation of in-situ stress among the samples, it was decided for simplicity to store all the soil under the same stress. A value of 90 kN/m^2 was chosen.

For the purposes of storage the samples were treated as large triaxial specimens. Following extrusion, some grooves on the sides of the samples, presumed to be due to the sampling operation, were clearly visible. The maximum size observed was about 50mm long x 10mm wide x 5mm deep. In preparing the end surfaces, some medium to large gravel particles had to be removed, creating additional cavities. In order to maintain the desired effective stress and avoid the effect of local uneven straining, all these cavities were filled with moist sand. A full drainage system was also employed so that any leakage during storage could be checked. This was achieved by covering the sides of the sample with Whatman Grade 54 filter paper. The end surfaces were then covered with filter paper discs followed by a layer of non-woven synthetic filter fabric (ICI, Terram NP4) and a porous plastic disc. Such an arrangement was thought to minimize the risk of local distortion and provide effective drainage. Perspex end caps were put in place, with the top one having a drainage connection. A membrane of thickness 1mm was positioned around the sample and was sealed to the end caps in the usual way with two O-rings at each end. The samples were lifted by crane into steel tanks, Plate 3.2. After

the tanks had been filled with water and the back pressure line deaired,

a cell pressure of 290 kN/m^2 and a back pressure of 200 kN/m^2 were

applied. Any passage of water to or from the back pressure system was

observed with a twin burette system. The purpose of this was to check

for leakage rather than to measure the volume change characteristics

of the soil.

3.5.3 Preparation and Setting up of 100mm Diameter Specimens

A sample, prepared as described in the previous section, was taken

from the storage tank and cut longitudinally or transversely depending

on the test programme (see Section 5.4.1).One half was kept in reserve

in case the trimming of the other half was unsuccessful for any reason

(e.g. presence of stones). The specimen was trimmed to a diameter of

about 100mm in a soil lathe and the ends were cut as flat and parallel

as possible using a split mould as a guide. However, it was considered

risky to remove coarse particles that only protruded slightly from the

end surfaces as their sizes were unknown. Considerable care was taken

over the trimming operations, which took an average of six hours to

complete. If the trimming process was interrupted, the sample was covered

with polythene cling film and moist paper.

After being weighed and measured, the specimen was placed on the

bottom cap of the stress path cell which had been covered with a saturated

coarse porous stone protected by a filter paper disc. Another porous stone

protected with filter paper was placed on top of the specimen. The use of

coarse porous stones was convenient, since deairing was straightforward,

and permissible, since no measurement of the initial pore water suction

within the specimen (Skempton, 1961) was required.

Spiral filter paper strips were used on the side of the specimen

to accelerate drainage without affecting the stiffness of the specimen

(Berre, 1983). Four wet strips of filter paper, 15mm wide, were installed

using metal guides to obtain an inclination of 1 : 1.3. A thin layer of silicon grease was then smeared on the O-ring grooves in the end caps to help seal the membrane. A membrane was immediately placed on the specimen and sealed to the bottom cap with two O-rings.

To permit the measurement of "local" strains, the two perspex rings with the targets already glued on (see Section 3.4.2) were placed around the specimen before the membrane was sealed with two O-rings to the top cap. Two collapsable radial strain targets (see again Section 3.4.2) were then glued onto the specimen opposite the corresponding proximity transducers. With the aid of a subroutine of the control algorithm (see Section 4.3), the distances between the radial strain targets and the transducers were adjusted by moving the transducers so that they were within 1mm of the targets. Perspex spacers, 20mm long x 20mm wide x 3mm thick, were then rested on the axial strain transducers and the perspex rings moved down until the targets rested on the spacers. The four mounting pads of each perspex ring were glued onto the membrane and later the perspex spacers were removed. To permit the measurement of "end cap" axial strains, two small stainless steel plates were screwed to the top cap and two steel brackets were erected on the bottom cap (see Figure 3.4). A perspex block holding a submersible LVDT was connected to the top of each bracket so that the armature of the LVDT rested on the small plate attached to the top cap. By adjusting the position of the perspex block on the bracket the LVDT was set to the desired starting point within the calibrated range. This completed the setting up of the instrumentation, as photographed in Plate 3.3.

The cell top was too heavy to be lifted by hand and a pulley system had therefore to be used to remove or replace it. Replacement of the cell top had to be done with care in order to avoid disturbing the instrumentation. The cell was filled with tap water and the specimen was then ready for testing.

3.6   TEST PROCEDURES

First of all, a cell pressure of 95 kN/m^2 was applied under undrained conditions and the specimen was left for between 24 and 48 hours, until the reading of the pore pressure transducer was essentially constant. The stable pore pressure was typically about 35 kN/m^2. This probably reflected the pressure in air trapped within the membrane.

Next, the specimen was saturated by raising the back pressure and the cell pressure incrementally so as to keep the effective confining stress the same as that measured in the previous stage. To save time, these increments were applied simultaneously and the degree of saturation was only checked in the final stages (back pressure approaching 300 kN/m^2). Saturation was checked in the usual manner by measuring the pore pressure parameter B ($= \frac{\Delta u}{\Delta \sigma_3}$ where Δu = increase in pore pressure and $\Delta \sigma_3$ = increase in cell pressure). Only a value of B $\geqslant$ 0.95 was regarded as acceptable. Typically, such a value was only achieved after an elapsed time of about four hours. The time lag was mainly attributed to the presence of undissolved air. However, because of pressure limitations in the apparatus (associated with the leakage problems discussed in Section 3.2) it was not possible to improve this response by further increasing the back pressure. The whole saturation process took about four days.

The specimen was then allowed to reconsolidate under an effective isotropic stress of 90 kN/m^2 (i.e. the stress under which it had been stored) until the volume change was negligible. However, the total volume change during consolidation was small (< $5cm^3$) and the coefficient of consolidation c_v could not be satisfactorily determined in the conventional manner. One of the difficulties of interpreting the consolidation data was that the spiral drains covered only about 20% of the specimen's peripheral area and therefore full radial drainage could not be assumed. Also, on the basis of pore pressure, not all of

the samples could be fully consolidated (see Sections 5.4.2 and 5.4.3) indicating, as suggested above, that some air was still undissolved under a typical back pressure of 300 kN/m^2. The reconsolidation stage took about five days.

Following consolidation, specimens were sheared under either drained or undrained conditions. In an undrained test, unless a central pore pressure measurement is made, sufficient time must be allowed for pore pressure to equalize within the specimen. In a drained test the rate of shearing should be slow enough to allow the almost complete dissipation of excess pore pressure developed within the specimen. If the value of c_v is known, testing times can be estimated in accordance with theory, Bishop and Henkel (1962). Unfortunately, as mentioned above, no reliable c_v values could be determined from the triaxial consolidation stages. Atkinson (1984) has developed an alternative approach for determining the loading rate under undrained conditions but this requires the gradient of the undrained stress path in the (p', q) plane to be known in advance and therefore could not be applied in the present work. A general rate of deviator stress increase of 1 kN/m^2/hour has been recommended by Atkinson et al. (1985) for clayey soils under both drained and undrained conditions. In the present work, the choice of loading rate was a matter of judgement. After two trial tests (see Section 5.3.2) the final rates adopted were 0.7 kN/m^2/hour and 2 kN/m^2/hour for drained and undrained conditions respectively.

In most tests a conventional total stress path was followed (i.e. the deviator stress was increased while the cell pressure was kept constant). However, different total stress paths were used in certain stages of two tests. In all tests, when the deviator stress reached about 50 kN/m^2, the specimen was subjected to an unload-reload cycle before the test was continued. Although the emphasis was placed on

retrieving data at small strains, an attempt was made to shear the

specimens to failure so as to maximize the information retrieved.

Details of the test programme and test conditions will be presented

in Section 5.4.1.
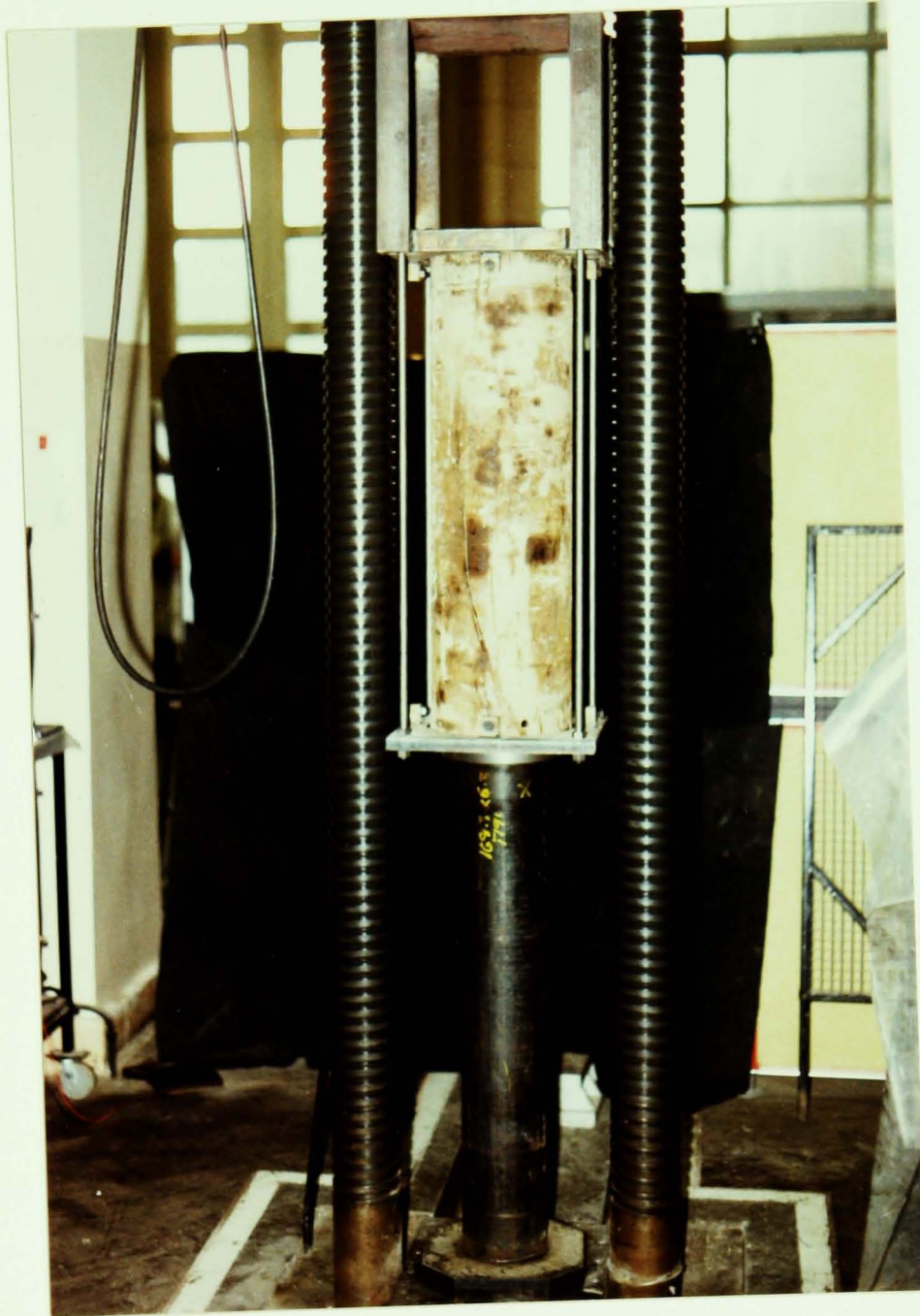
PLATE 3·1 EXTRUSION OF 250 mm DIAMETER TUBE SAMPLE
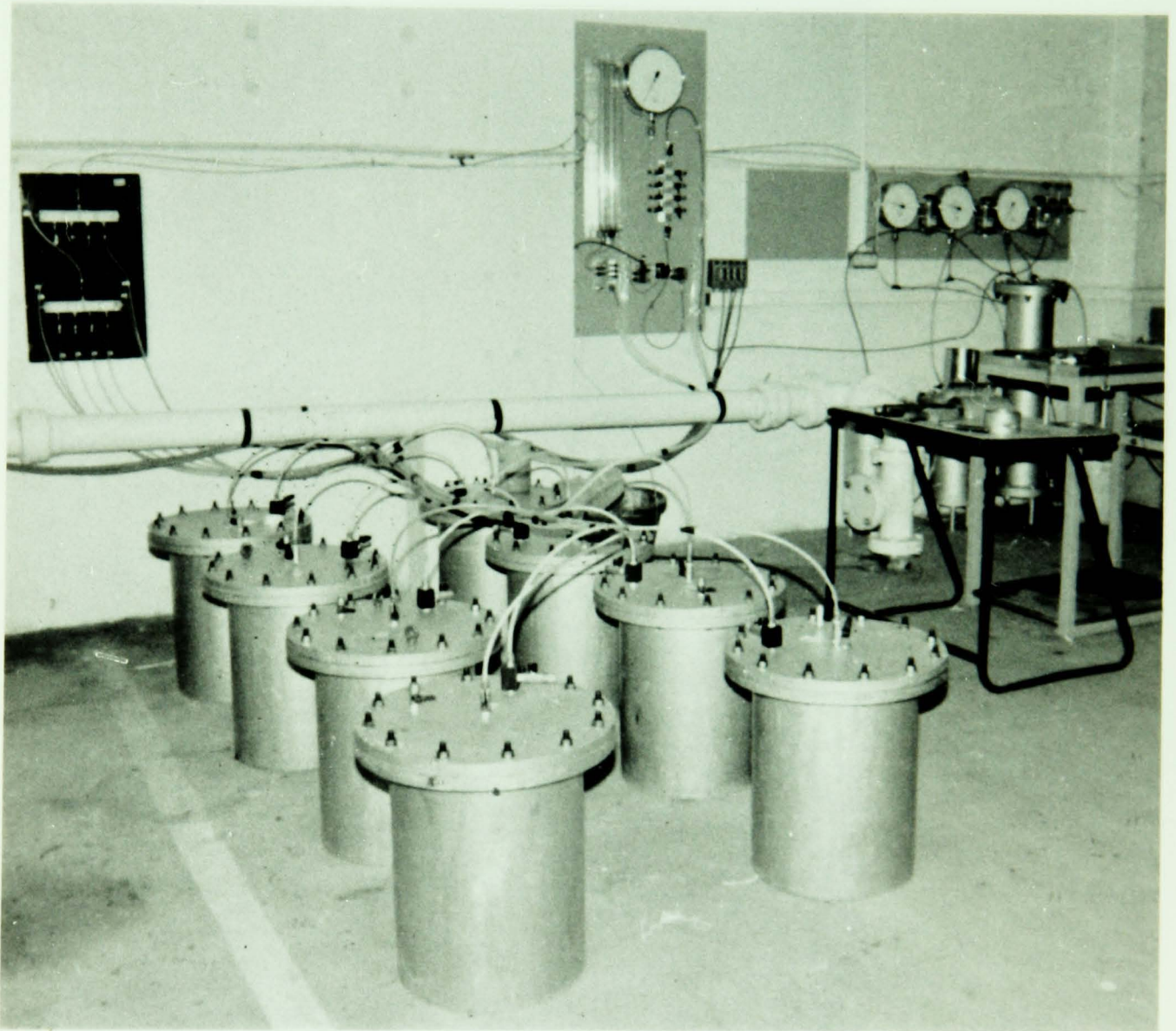
PLATE 3·2 STORAGE SYSTEM OF 250 mm DIAMETER SPECIMEN
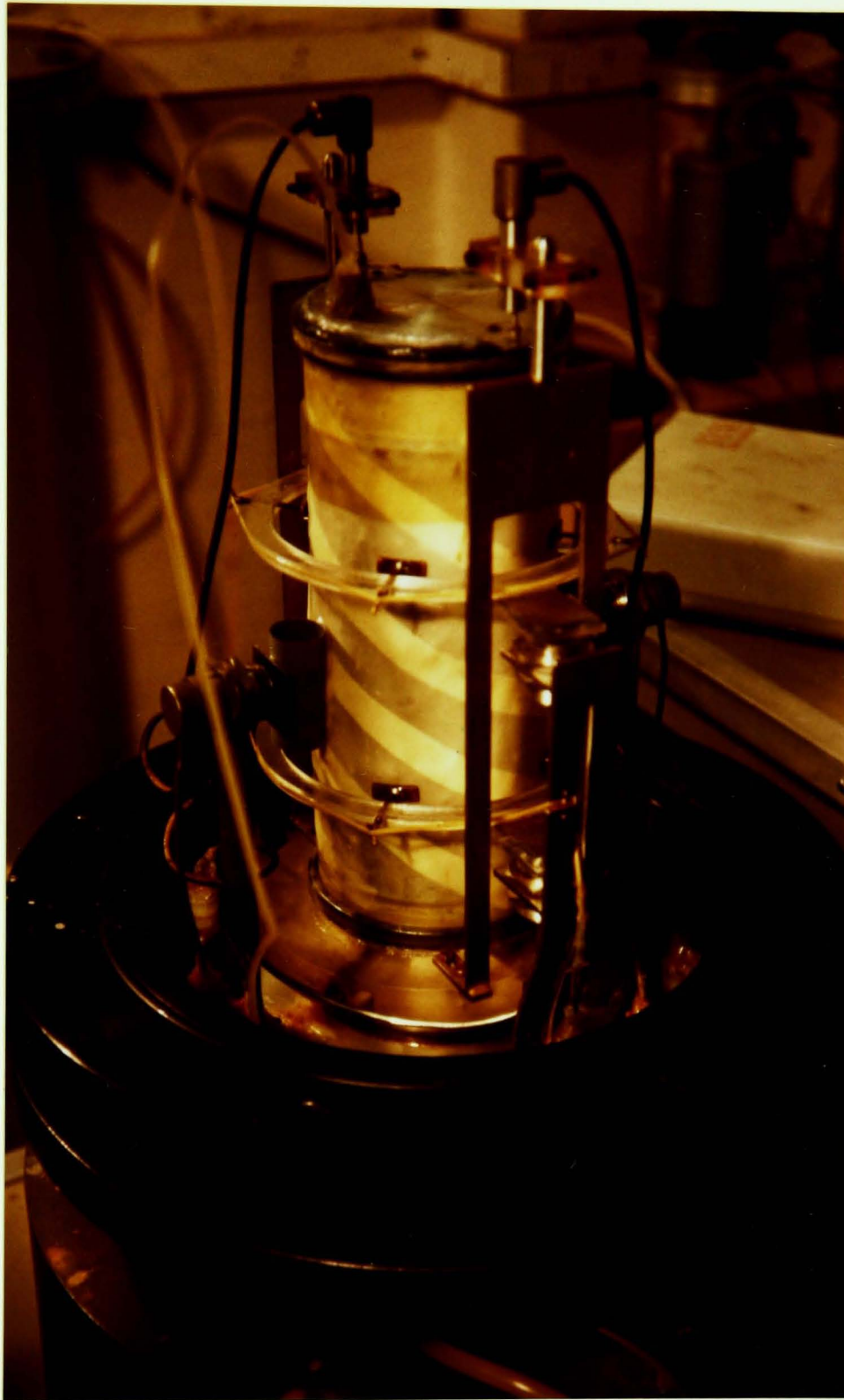
PLATE 3·3 INSTRUMENTATION WITHIN STRESS PATH CELL

Item	Resolution	Precision
Load cell	0.003 kN	0.006 kN
Volume change unit	0.032 cm^3	0.228 cm^3
Cell pressure transducer	0.30 kN/m^2	0.62 kN/m^2
Pore pressure transducer	0.28 kN/m^2	0.70 kN/m^2
Lower chamber pressure transducer	0.31 kN/m^2	0.70 kN/m^2
External displacement transducer	0.013 mm	0.19 mm
Submersible LVDT: serial no.: 25880	0.002 mm	0.074 mm
Submersible LVDT: serial no.: 25883	0.002 mm	0.066 mm

TABLE 3.1   Results of calibration (proximity transducers not included)

Range (μm)	Precision (μm)
0-500	1.8
500-1000	1.9
1000-1500	3.1
1500-2000	4.1
2000-2500	5.9
2500-3000	6.6
3000-3500	9.5
3500-4000	12.2
4000-4500	16.9
4500-5000	19.0
5000-5500	29.1
5500-6000	36.9

TABLE 3.2 Typical precision of
proximity transducer

Sample no.	Borehole no.	Depth (m)	Estimated p'_{vo} from Figure 2.10 (kN/m^2)	Moisture content (%)	no. of samples retrieved	Sequence of sample retrieved during extrusion	Test no. (see Chapter 5)
1	4	4.0-4.6	60-67	17.70	2	1	T8DV
						2	TR1
1	5	3.8-4.7	55-70	17.10	3	1	RT6DH
						2	RT5UV
						3	
2	5	5.0-5.8	75-85	16.80	2	1	
						2	T2UH
3	5	6.0-6.7	88-98	16.70	2	1	T7DV
						2	TR2
4	6	4.0-4.8	60-70	17.20	2	1	T4DH
						2	T3DV
5	6	4.8-5.3	70-78	17.95	1	1	T1UV

TABLE 3.3   Details of 250 mm diameter samples retrieved

Adjusting screw

Load cell

Perspex

Tie rod

Specimen

Holes for drainage
& transducer leads

'Bellofram'
seals

Loading ram
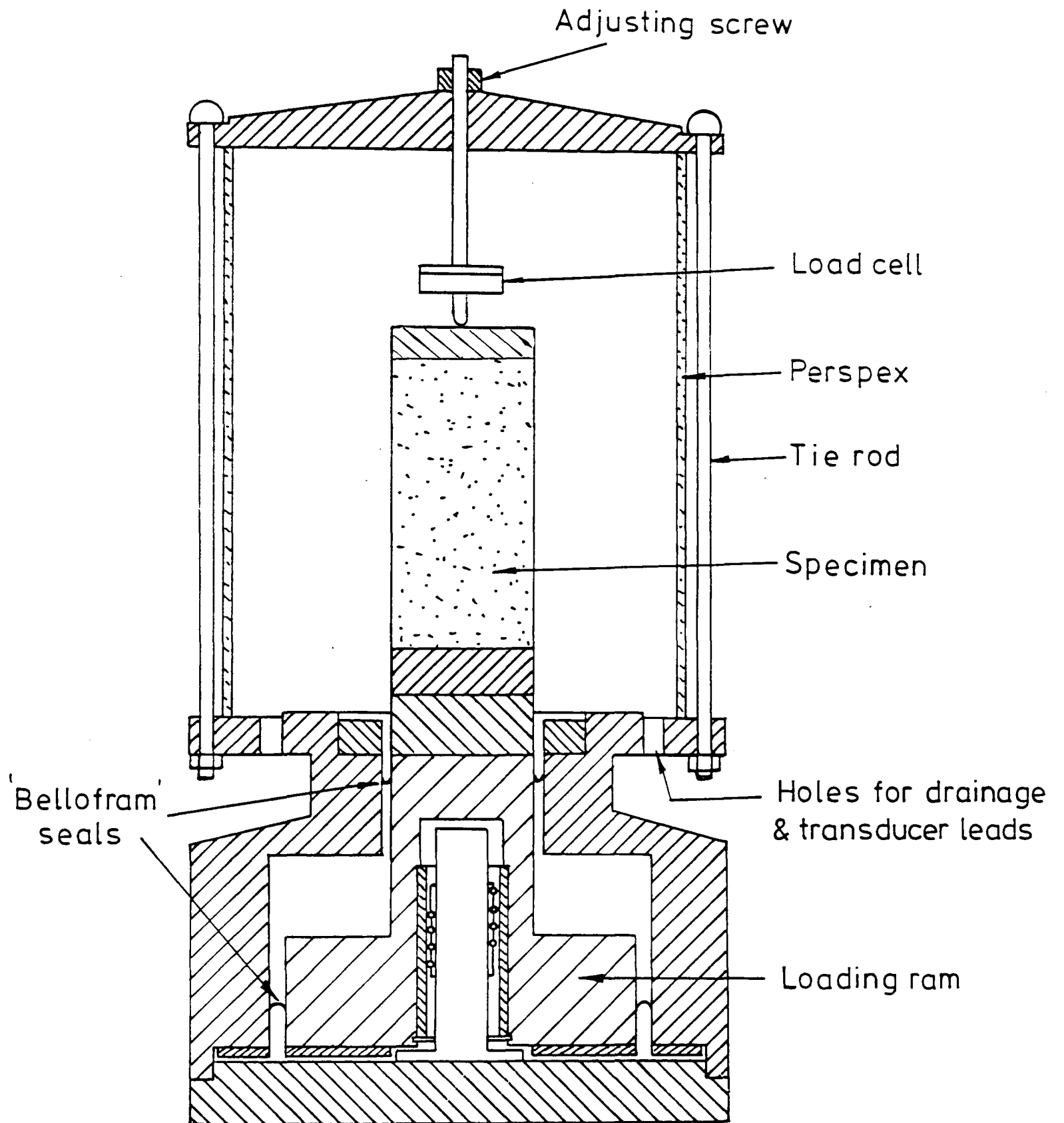
FIG. 3·1   DIAGRAMMATIC ARRANGEMENT OF STRESS PATH CELL

Air main

Load cell

Air control valve

Pressure gauge

Back pressure regulator

Deaired water

Cell pressure transducer

Volume change unit

Pore pressure transducer

Lower chamber pressure transducer

Oil
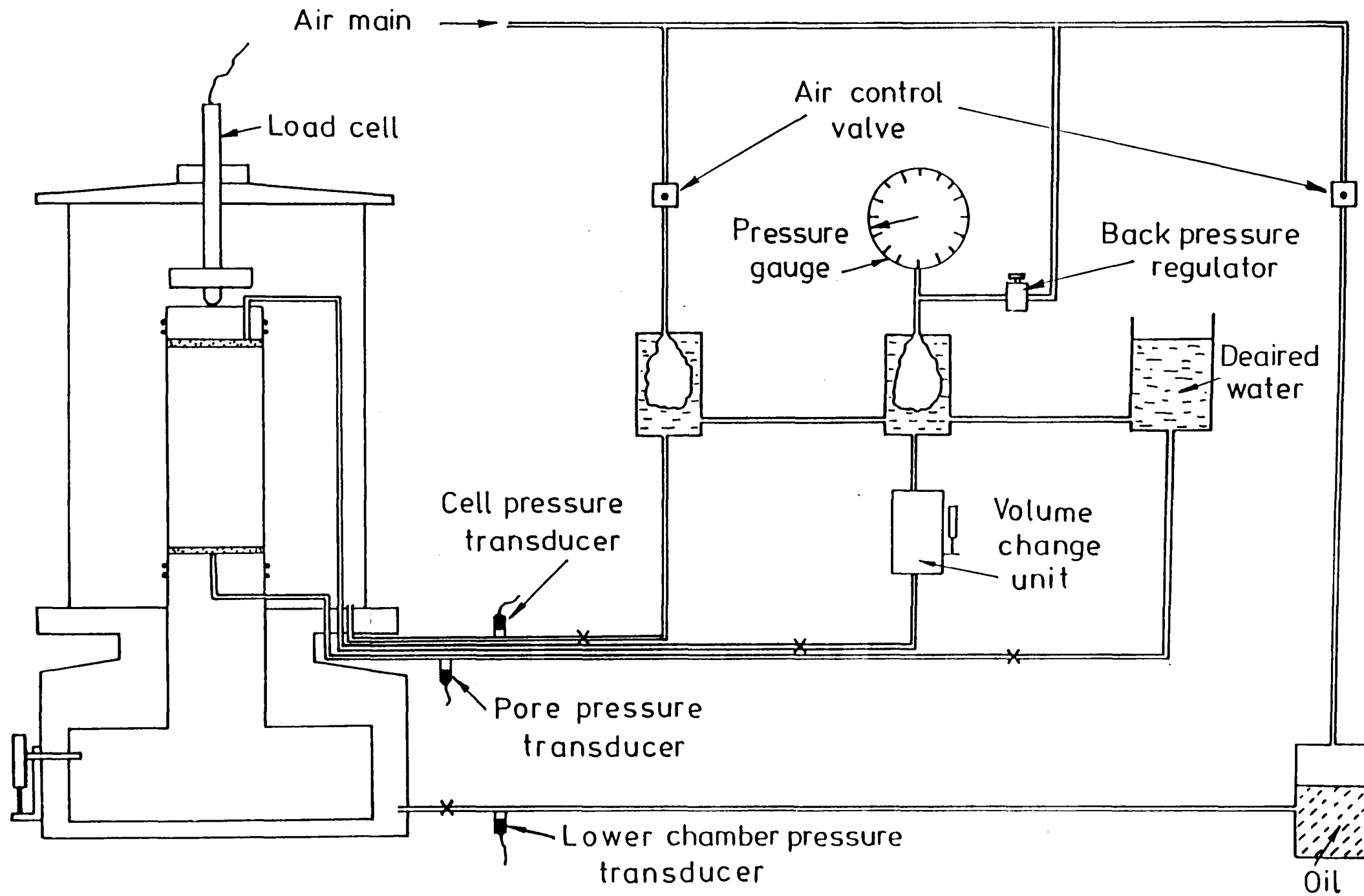
FIG. 3·2   GENERAL LAYOUT OF STRESS PATH CELL

Original design

After modification
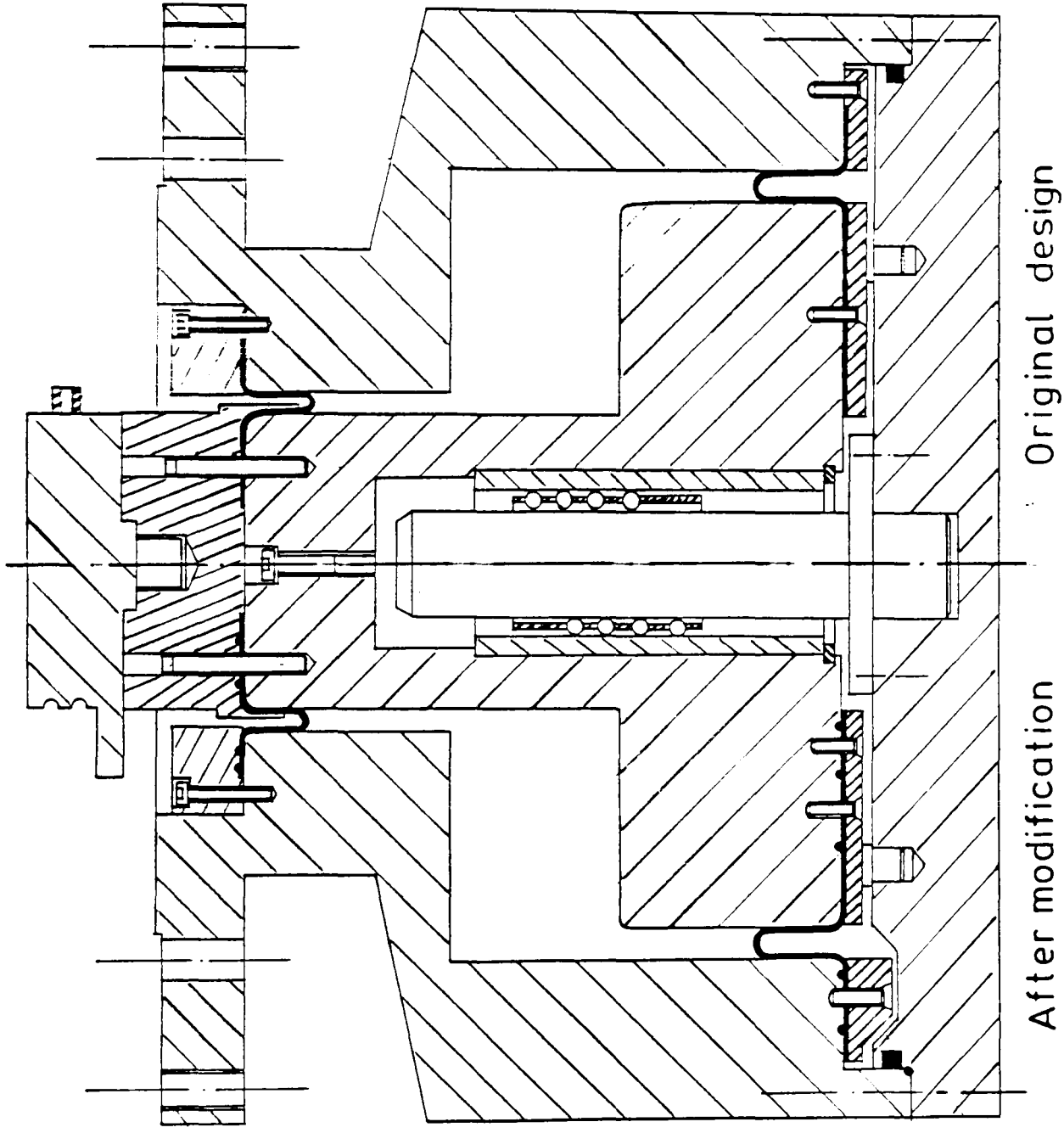
FIG. 3·3   MAJOR   MODIFICATIONS   ON   STRESS PATH CELL
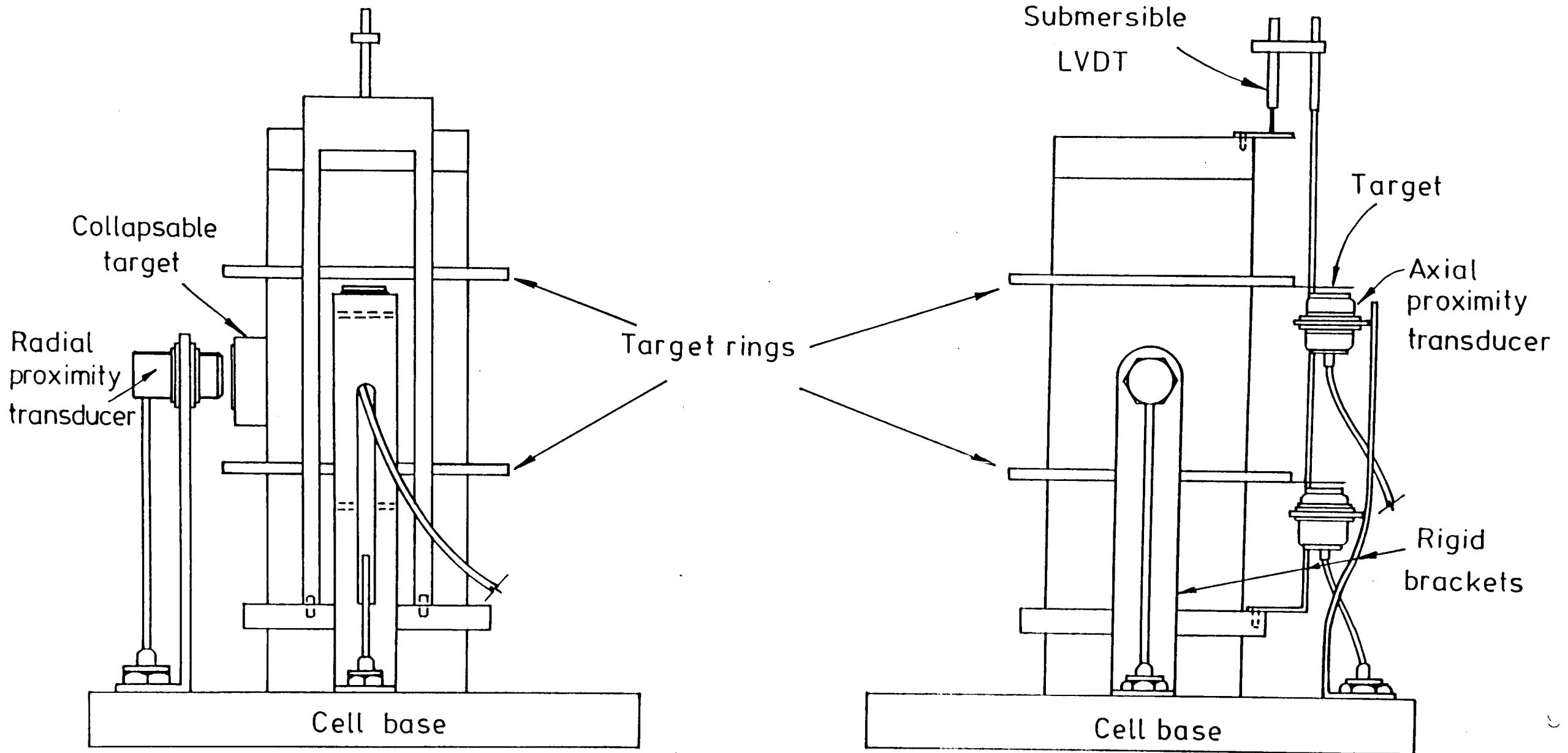
FIG. 3·4   GENERAL LAYOUT OF INSTRUMENTATION WITHIN STRESS PATH CELL

(ONLY HALF SHOWN BY REASON OF SYMMETRY)

Output signal (V) — vertical axis, values 0 to 5
Input displacement (mm) — horizontal axis, values 0 to 6·0

Note

Data points covered
by thickness of line
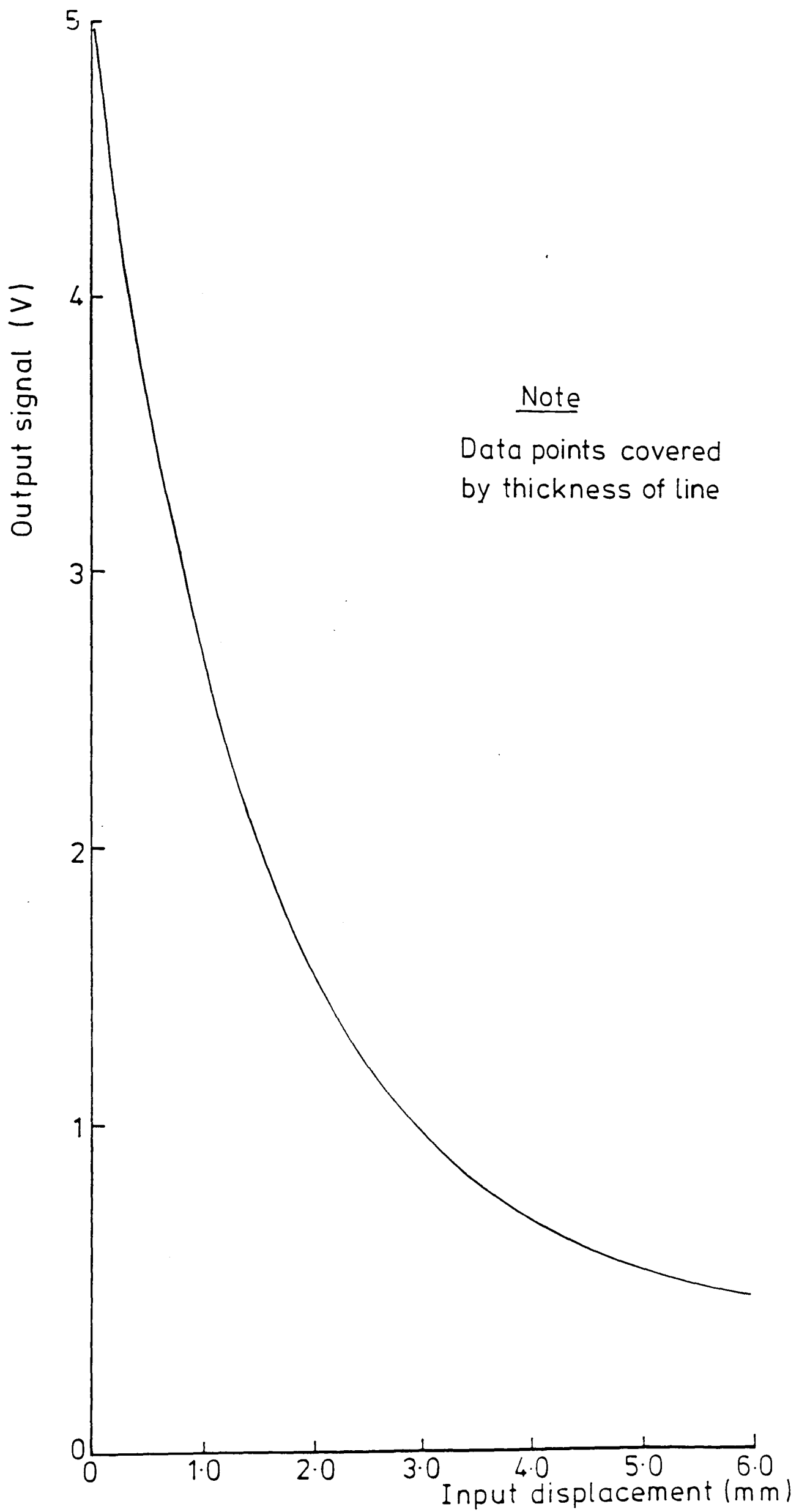
FIG. 3·5 TYPICAL CHARACTERISTICS OF PROXIMITY TRANSDUCER
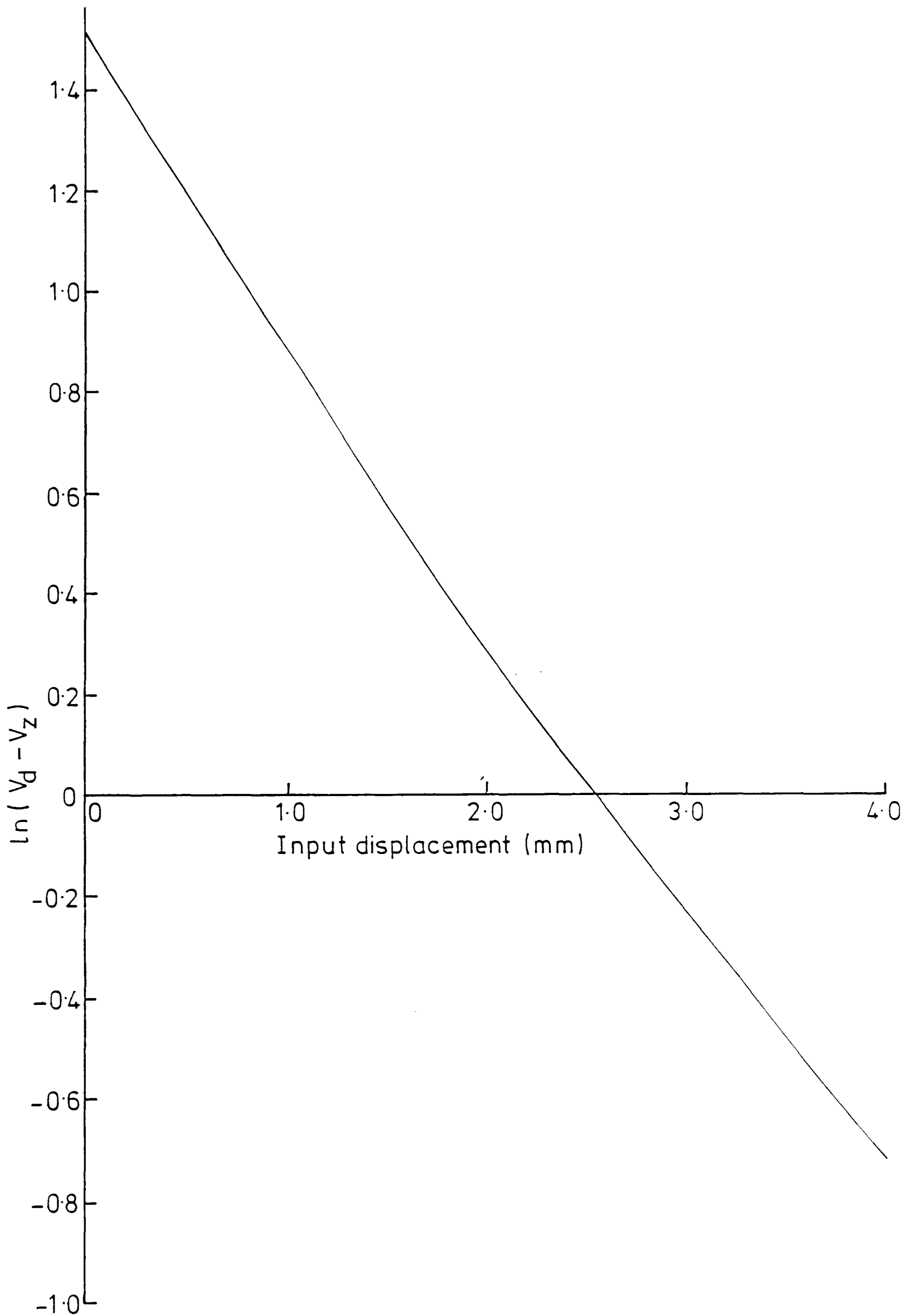
FIG 3·6   TYPICAL LINEARIZED CHARACTERISTICS OF PROXIMITY

TRANSDUCER

10
12
20
Rubber band
35
30
50
Target
30
45°
Glued on
75
65
Bushing
Dimensions in mm
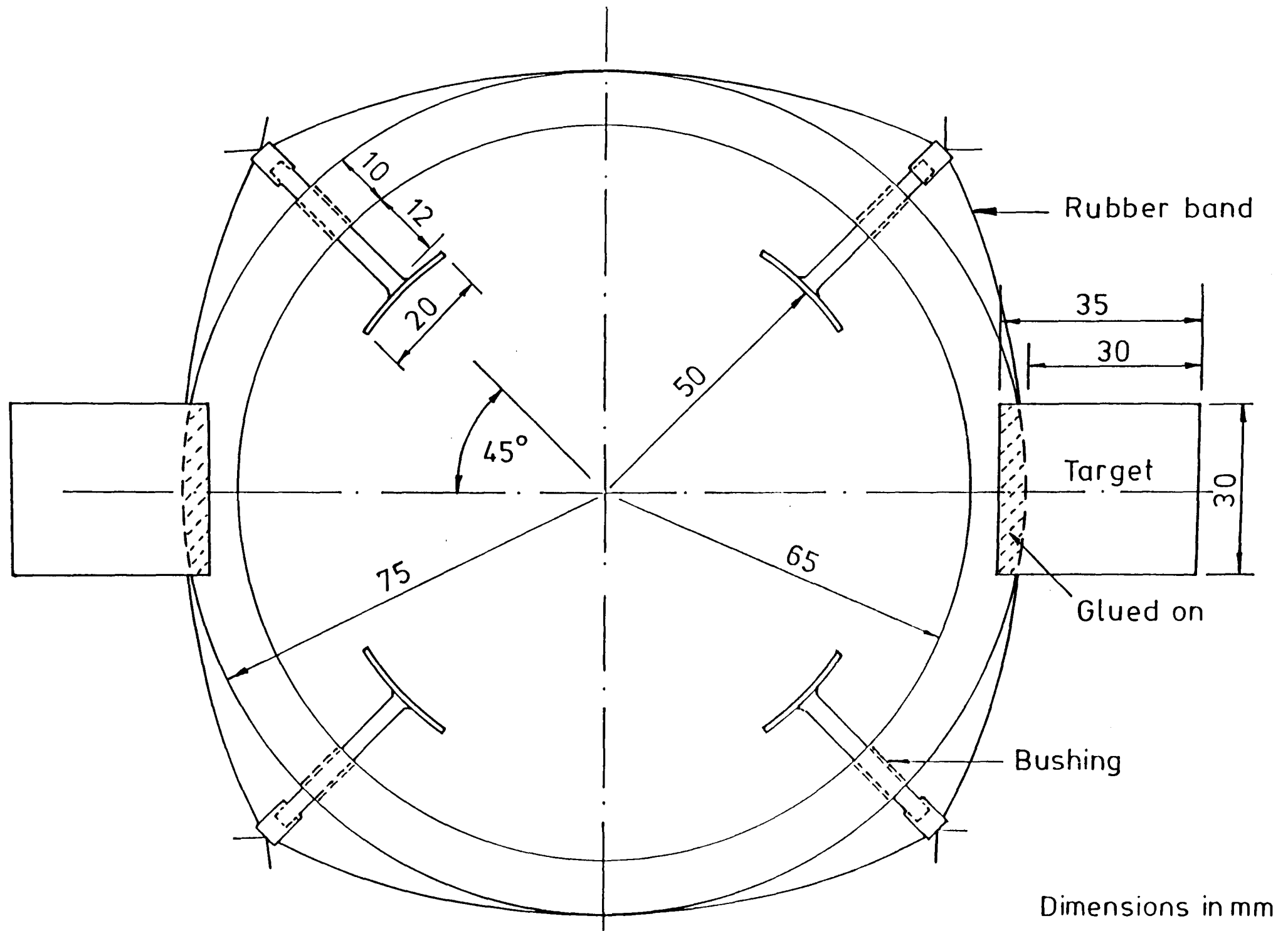
FIG. 3·7   TARGET RING FOR LOCAL AXIAL STRAIN MEASUREMENTS

Top crosshead

A

Specimen tube

Tie rods
(Four)

Screwed columns
(Two)

B

C
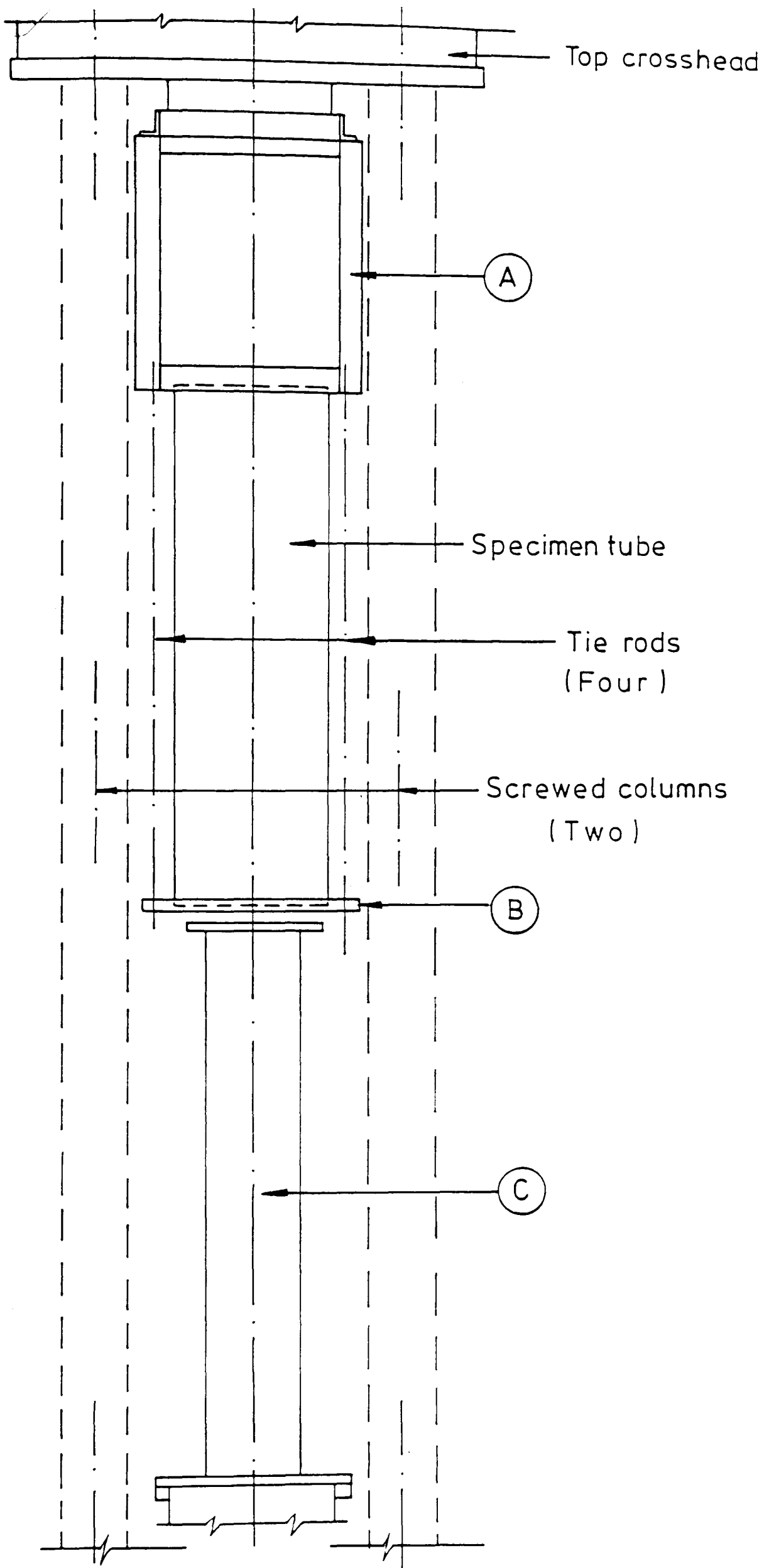
FIG. 3·8   EXTRUSION OF 250mm DIAMETER SAMPLES

CHAPTER 4

DEVELOPMENT OF A COMPUTERIZED CONTROL SYSTEM

4.1   INTRODUCTION

This chapter describes a computerized control system which is capable of applying specified sequences of stress to a soil specimen in the triaxial stress path cell described in the previous chapter, Section 3.2.   This is a closed-loop system which relies upon feedback from the instrumentation described in Section 3.4.1. The computer also serves as a data logger and processor. The development, operation and limitations of the system are discussed.

In recent years microcomputers have become widely employed for control and data acquisition purposes in commercial soil mechanics laboratories (Prince, 1986) and research institutions (Woods and Clinton, 1986). Computerized systems have a number of attractions as follows:-

i)   Flexibility and precision of control

Rates of change of stress or strain can be predetermined or related to the behaviour of a specimen (e.g. in respect of pore pressure equilibration or dissipation). Control can be based on feedback from many transducers and frequent comparisons can be made between existing and target quantities.

ii)   Accuracy of data

Certain measurement errors, such as those due to the compliance of transducers or a drift in their energization voltage, can be corrected by calculation providing sufficient information is made available to the computer.

iii)   Convenience of data processing

Data retrieved from transducers can be processed immediately, converted to engineering units and displayed to determine the

progress of a test. Large amounts of data can be stored conveniently (e.g. on magnetic media) and retrieved easily for subsequent analysis and plotting.

4.2 THE SYSTEM CONFIGURATION

The configuration of the control system developed for the present work is shown in Figure 4.1. The system is designed to monitor and control one stress path cell of the Bishop-Wesley type. Pressure is supplied to the system from a compressed air main at 700 kN/m^2. The back pressure in the specimen is controlled manually by means of a regulator. The lower chamber pressure and the cell pressure are regulated by manostat valves driven by stepper motors. The stepper motors are controlled by the computer via a suitable interface. Two analogue to digital converters enable information to be transferred to the computer from the transducers which monitor the applied pressures and the response of the soil specimen.

4.2.1 The Computer and Peripherals

The control system is based on an Apple II microcomputer with a memory capacity of 48K words. The computer has a floppy disc driver and a black/white video display unit (VDU).

Two different analogue to digital converters are needed because some of the transducers (proximity transducers and submersible LVDTs) are energized by alternating current (AC) whereas the remainder are energized by direct durrent (DC). An "Analogue Input Unit" manufactured by the Micro Consultants Group, Surrey, England, is used for the DC transducers and a "System 16" unit, made by Sangamo, West Sussex, England, is used for the AC ones. These converters are of 12 bit resolution and are connected to the computer by standard IEEE bus cables in a daisy chain configuration. Signals sampled by the computer from the DC transducers and the submersible LVDTs are immediately converted into engineering units

by means of calibration factors stored in the computer, whereas those from the proximity transducers are not. To have converted the latter readings would have used a significant proportion of the computer's memory capacity, due to the complexity of the calibrations (see Section 3.4.2).

The disc driver permits data to be stored on and retrieved from floppy discs. As a particular stress path is being followed, all the transducers (14 in total) are scanned by the computer at particular time intervals which must be specified in advance. The readings obtained during these "data scans" are stored in the computer until 35 such scans have been made. Because of the limited memory capacity of the computer, the readings are then transferred into a file on a floppy disc. As the test continues this process is repeated, a new file being created each time information is transferred to the disc. After nine files have been created, the storage of the disc is exhausted and a new disc has to be provided. For each test an ultimate limit of 100 files is imposed, corresponding to a maximum of 3500 data scans, and this has been found to be more than enough for the present research. Data stored on floppy discs are easily transferred to other computers for analysis and plotting.

4.2.2 Load/Pressure Control System

The control of the lower chamber and cell pressures was achieved using two manostat pressure regulators (type EMC-101, manufactured by John Watson & Smith Ltd., Leeds, England). The similarly automatic control of back pressure was not considered essential since, if the back pressure is kept constant and full drainage is allowed, the effective stress path can be fully controlled by varying the total stress path. Therefore, in order to save computer memory for other purposes, the back pressure was controlled manually by a simple regulator. The manostat pressure regulators are operated by electric stepper motors which can be commanded to open or close the control valves in a number of discrete

steps. Each valve operates over a pressure range from 14 kN/m^2 to
840 kN/m^2. However, the maximum supply pressure presently available
is 700 kN/m^2. Altogether the stepper motors can be driven through
2000 ±200 steps, each step corresponding to a pressure change of about
0.4 kN/m^2. In order that the stepper motors could be commanded from
the computer, an interface card had to be made within the Department.

The main air pressure supply was shared by many other pieces of
equipment and, as a result of varying demand, significant pressure
fluctuations upstream, and also downstream of the manostat valves were
occasionally experienced. An additional control (pressure reducing)
valve was therefore introduced on the upstream side of each manostat
valve to smooth out the fluctuations and the downstream pressure could
then be controlled with a precision of ±1.0 kN/m^2. These additional
valves also permitted limits to be set to the cell pressure and deviator
stress which could not be exceeded, even if the manostat valves were to
misfunction. An upper limit was set such that, even if no cell pressure
was applied, the axial load could not exceed the load cell capacity
(13 kN). The upper limit for cell pressure was set at 550 kN/m^2.

4.3   CONTROL ALGORITHM

A control algorithm was developed to permit a specific linear
stress path, or a set of linear stress paths, to be followed in the
(p', q) plane. The logic of the algorithm is shown in Figure 4.2 in
the form of a flow chart. With the present version of the algorithm,
only compressive (positive q) stress paths may be followed in order to
conserve computer memory.

The programme was designed to allow stress paths with a constant
deviator stress to be followed, but this capability has not been
commissioned. For all other stress paths the control was based on a

constant rate of change of deviator stress. While strains remain small, this control mode is considered to be more suitable than the axial strain rate control used in conventional tests. This is because the soil is relatively stiff initially and, should a constant rate of strain be imposed, an excessive rate of change of stress may result, see Figure 4.3. On the other hand, at large strains tending towards failure, the soil becomes relatively soft and under stress control the strain rate may become excessive. Atkinson et al. (1985) have described a hybrid control system with which the test is initially stress-controlled but becomes strain-controlled as the strains increase. However, in the present work, where the emphasis was placed on measuring the behaviour of the soil at small strains, stress control was used throughout. A method of preventing uncontrolled collapse of the specimen had to be devised and will be discussed later in this section.

The deviator stresses measured by the load cell were used by the control algorithm to determine the actual rate of loading. It would not have been sensible to base the control upon the measured lower chamber pressure for two reasons. Firstly, because of the multiplier effect referred to in Section 3.3, the control would have been too insensitive. Secondly, the friction losses in the rolling Bellofram seals would have required corrections to be made.

For a given linear total stress path the deviator stress at the start and finish of the stress path, the rate of change of deviator stress and the scan interval for data scans must be specified. A set of up to 20 such stress paths can be specified to run consecutively. After this set of stress paths has been executed, another set can be specified provided that the test has not been terminated by the control algorithm (see below) and that the limit of 100 data files has not been exceeded. Making use of equations (3.3) and (3.4), the target deviator stress and cell pressure after a certain time are calculated and compared with the

existing values, obtained by implementing a "control scan". After each control scan, if the differences between existing and target values exceed a certain limit, the stepper motors are instructed to make the necessary adjustments. In order to calculate the existing deviator stress, the axial strain of the specimen has to be known (see equation (2.3)). Where possible the average of the two submersible LVDT readings (end cap axial strain measurements) is taken. When either of these has gone out of the calibrated range, the external displacement transducer reading is used instead. The current strain readings are sampled during the control scan referred to above, but no readings are taken from the proximity transducers (local strain measurements) for control purposes.

As failure is approached under stress-controlled conditions, the strain rate increases and, eventually, the specimen collapses. In these circumstances (i.e. at very large strains) there is a possibility of damaging the local strain instrumentation. The perspex rings bearing the targets for axial strain measurement (see Section 3.4.2) are especially vulnerable. In order to prevent this, upper limits were set on both the axial strain and the rate of axial strain. Typical values of these control limits in the tests on Cowden Till were 5% and 20%/hour respectively. If either of these limits was exceeded, the lower chamber pressure was released as quickly as possible. However, it was found that a false impression of strain rate could be gained from an individual transducer (end cap measurement) if significant inhomogenous deformation existed during shearing and the test could be terminated prematurely. Therefore the programme was modified so that the strain rate limit was applied to the average end cap measurement and only became effective when the axial strain exceeded a certain value (typically 2%).

It would have been possible to arrange for different loading rates to be specified over different axial strain ranges instead of over different deviator stress ranges, as chosen. However, two problems would have arisen

Firstly, the selection of a suitable loading rate during unload-reload cycles would have been more difficult, as the recovery of axial strain during unloading is unknown. Secondly, because of bedding errors, the actual axial strain could have been less than that measured and used in the specification of loading rates.

Control scans were made at time intervals which depended on whether the specimen was being loaded for the first time, unloaded, or reloaded. Loading was interpreted for this purpose as an increase in deviator stress. For stress path involving loading, control scans were initiated at intervals of 15 seconds, but for unloading and reloading the corresponding intervals were 60 seconds and 30 seconds respectively. The larger intervals during unloading and reloading were found to be necessary to allow previously commanded pressure changes to take effect. Whenever the loading direction was reversed, it was found that there was some slackness ("backlash") of the stepper motor drive system. This meant that some of the pressure commands were ineffective or delayed.

The control limit for cell pressure was simply set at ± 1 kN/m^2. For deviator stress it was more difficult to specify suitable control limits for two reasons. Firstly, the friction existing in the bearings of the loading ram and the Bellofram seals was variable, particularly when the loading direction changed. Secondly, the flow of oil into or out of the lower chamber had a damping effect so that more time was required for pressures to be adjusted. During unloading, air must also bleed from the manostat valve (at a rate not exceeding 3×10^{-3} m^3/minute) and this imposed a further damping effect. For loading and reloading paths the stepper motor will increase the lower chamber pressure by a single step if the existing deviator stress is more than 1.5 kN/m^2 below the target value and will reduce the pressure by a single step if the existing stress is more than 10.0 kN/m^2 above the target value. For unloading paths the

pressure will be reduced by a single step if the existing deviator stress is more than 5.0 kN/m^2 above the target value and will be increased by a single step if the deviator stress is more than 10.0 kN/m^2 below the target value. These limits have been arrived at by trial and error so as to obtain acceptable control, although they do not necessarily represent the optimum values. It may be noted that Atkinson et al. (1985) experienced a friction variation equivalent to ±10 kN/m^2 in deviator stress when using a 38mm stress path cell and concluded that, since the friction depends on the rate and direction of loading, it is difficult to deal with in control algorithms. In the present work a deviator stress fluctuation of ±20 kN/m^2 was experienced during unloading and reloading when the control limits were set at ±1.5 kN/m^2 and control scans were conducted every 15 seconds. In order to avoid this type of instability it was necessary to set different control limits and control scan intervals for different loading directions, as indicated above.

The control algorithm described above is intended to operate automatically. However, a manual over-ride facility exists which permits the automatic control to be interrupted and the stepper motor positions to be controlled directly from the keyboard. Subsequent stress paths may also be respecified before automatic control is restored. This facility is particularly useful if the initial loading rate proves unsuitable.

On the VDU of the computer current values of the deviator stress, cell pressure, pore pressure, axial strain, and volumetric strain are displayed after each control scan, together with the target values of deviator stress and cell pressure. Data obtained during data scans are not displayed but the scan number and file number in which the data are being stored are shown. Due to the limited computer capacity, graphical output was not possible. Nevertheless, the information displayed is

sufficient for an experienced operator to assess the progress of the test. It is also possible for a subroutine of the programme to be used simply to display the readings from certain (AC) transducers as specimens are being set up.

Computer programmes for data processing were also developed. This permitted the readings from the proximity transducers to be converted to engineering units. Averages of the data collected for each position of the stepper motor controlling the lower chamber pressure were also computed. Any data collected when the measuring deviator stress differed from the target value by more than 5.0 kN/m^2 were rejected, but this only occurred upon reversal of the loading direction and was extremely rare.

Air supplies

Stepper motors & valves

A

B

Computer & Disc driver

Displacement

Deviator load

Analogue input unit

System 16

Submersible LVDTs

Proximity transducers

Air/water interface

Air supply

Pressure regulator

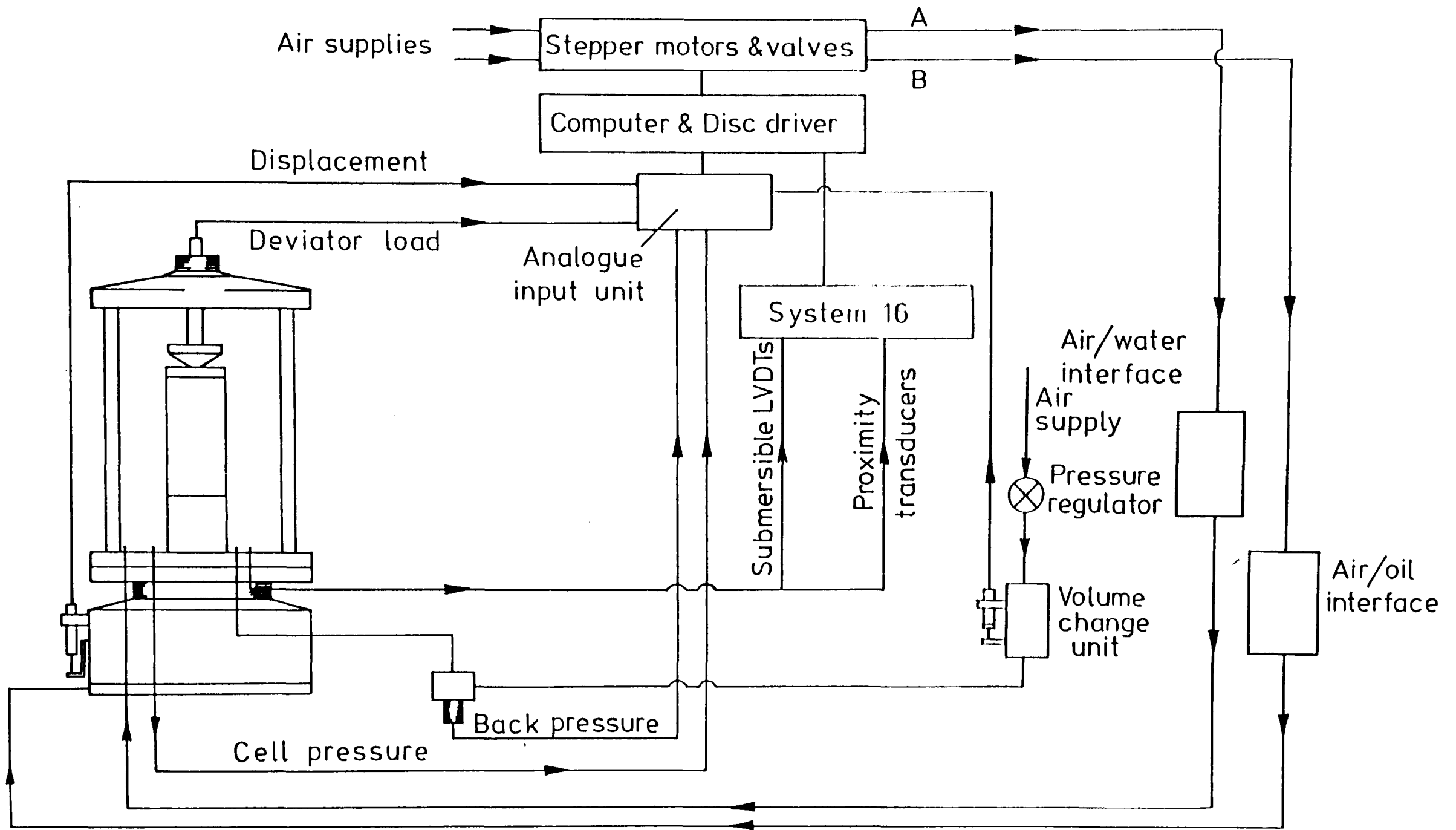Volume change unit

Air/oil interface

Back pressure
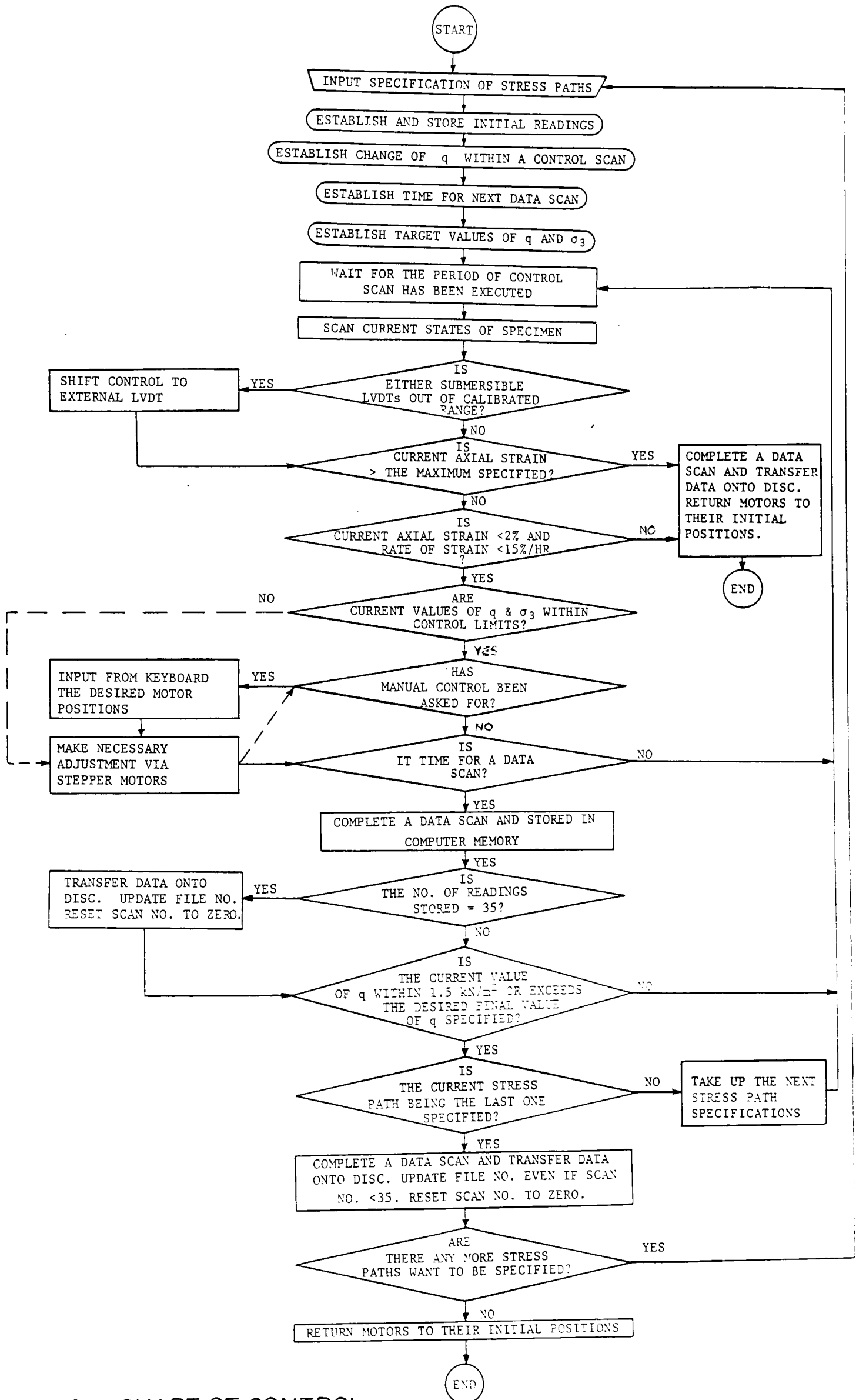
Cell pressure

FIG. 4·1   SYSTEM   CONFIGURATION
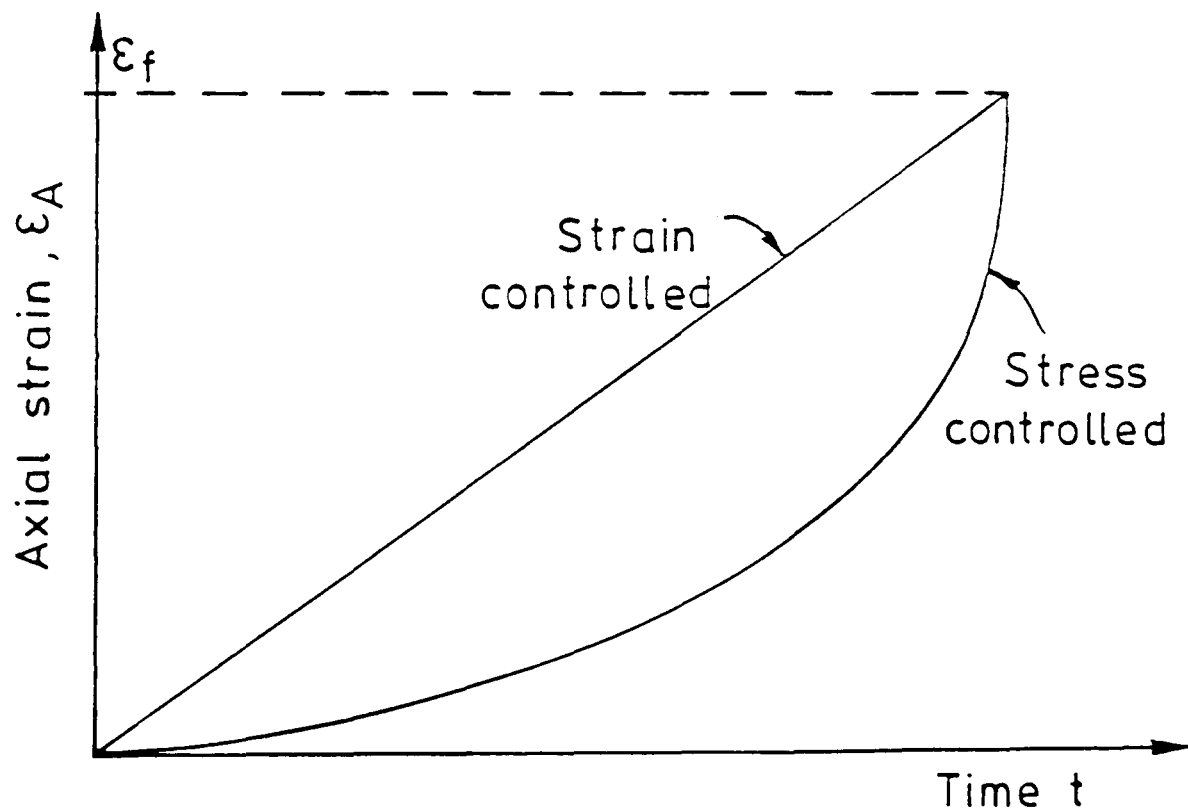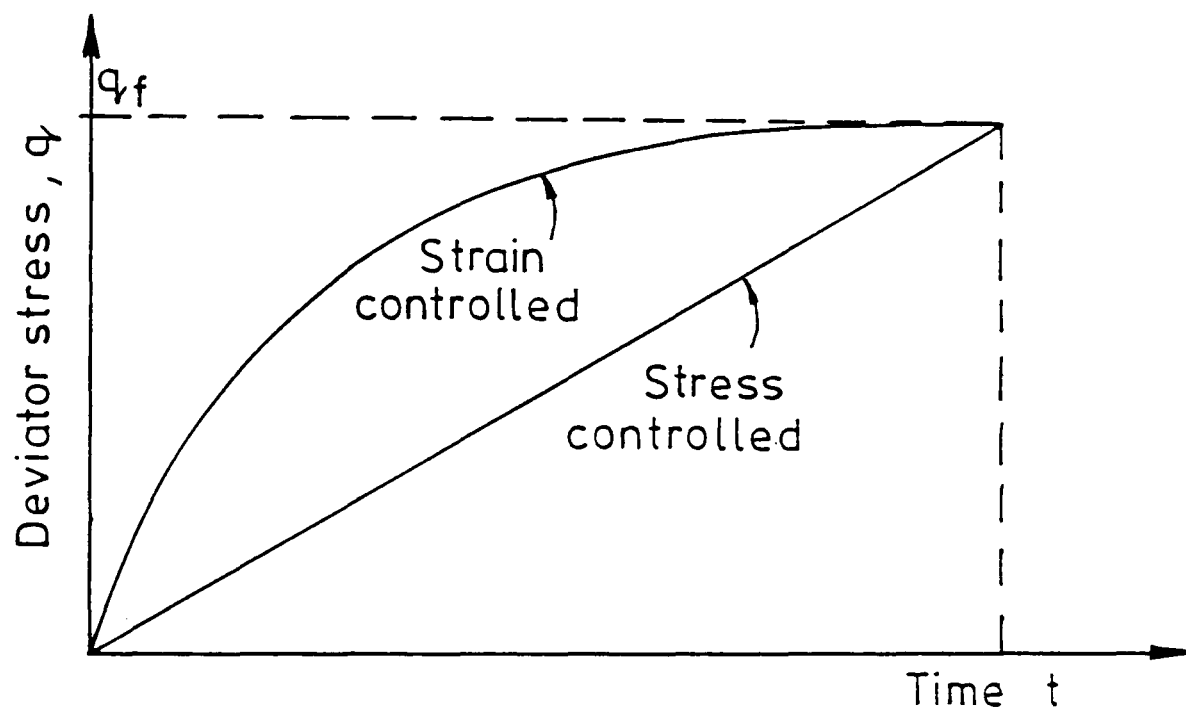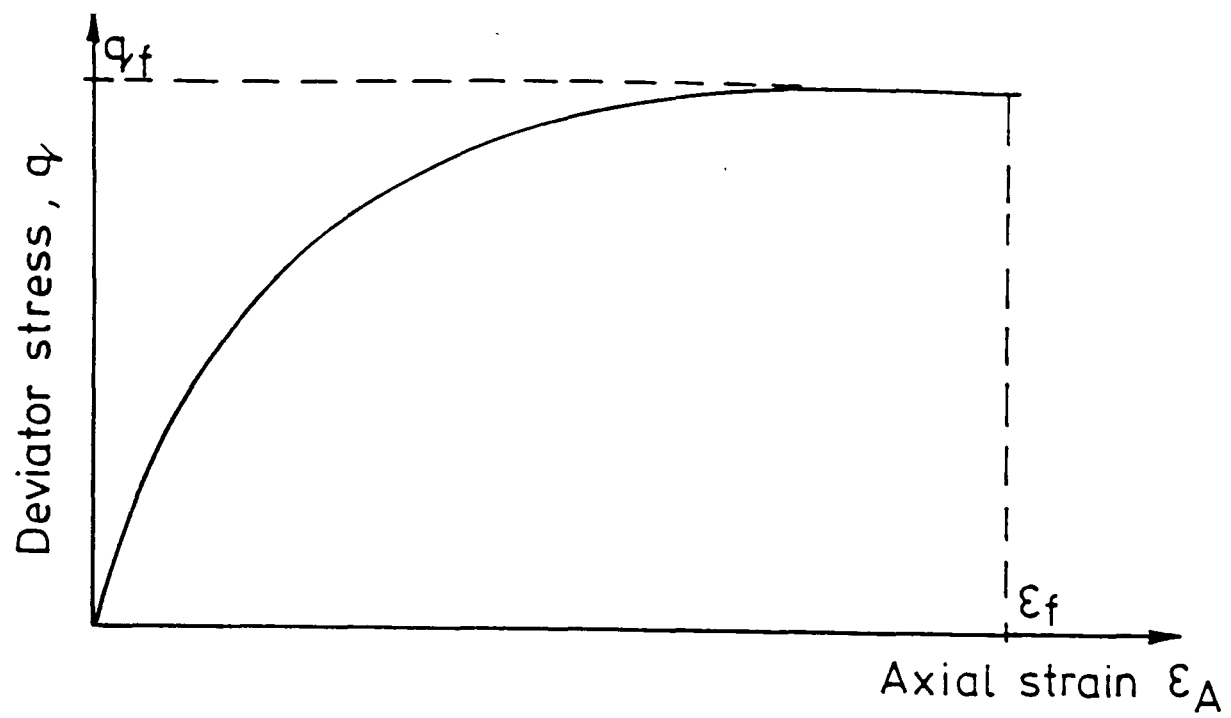
FIG.4-2 FLOW CHART OF CONTROL
ALOGRITHM

FIG.4·3 VARIATION OF STRESS AND STRAIN WITH TIME IN STRESS AND STRAIN CONTROLLED TRIAXIAL TESTS ON,1984)

CHAPTER 5

TEST RESULTS

5.1 INITIAL REMARKS

In this chapter the results of a series of proving tests are discussed before those of the main tests on Cowden Till are reported. The main objectives of the proving tests were, firstly, to evaluate the performance of the instrumentation and computer programmes and, secondly, to gain practical experience in dealing with specimens of the Cowden material. It was also possible to assess a suitable rate of loading prior to the main tests.

In presenting the results emphasis is placed on the stress-strain behaviour at small strain levels as the specimens were sheared. For the sake of clarity, unless otherwise stated, on all stress-strain graphs each data point corresponds to the average of the readings taken for a particular position of the stepper motor controlling the deviator stress, each strain reading usually being the average of measurements made on opposite sides of the specimen. Although external axial strain measurements were made (see Section 3.4.1), they could not be used for the determination of stiffness parameters over the first 0.1% of axial strain due to the lack of precision of the transducer (see Table 3.1). In addition the external strain measurement was one-sided and at small strains was significantly affected by slight tilting of the loading ram. Therefore, except for the typical results shown in Figure 5.8, no such data are presented at small strain levels. However, for higher strain levels the external strain data are presented so that cross checks on other measurements can be made. For specimens tested to larger strain levels the maximum deviator stress has been taken as the last individual reading (rather than the average of measurements made for the last load step).

5.2 STRESS AND STRAIN COMPUTATION

The average dimensions of the specimen at the start of shearing were calculated from the dimensions measured initially, taking account of changes measured during saturation and consolidation by the submersible LVDTs (for the length) and proximity transducers (for the diameter). These dimensions were required as input information for the control algorithm.

The assumption that the specimen deforms as a right cylinder was used for the computation of the axial stress (see equation (2.3)). As discussed in Section 2.2.2, this assumption was unlikely to introduce an error of more than 5% into the values of the stresses in the central part of the specimen. The deviator loads were obtained from the load cell readings. No correction was applied to the deviator stress for membrane stiffness in view of the relatively high stiffness of the soil. Also, no correction was made for the restraint of the filter paper drains due to their spiral configuration.

Strains were computed from the displacements measured during each test as shown in Figure 5.1. The following strains were calculated: the average end cap axial strain measured by the two submersible LVDTs mounted across the end caps, ε_E; the average local axial strain, ε_L, obtained from the relative displacements of the two pairs of proximity transducers; and the local radial strain, ε_R, measured by one pair of proximity transducers. In addition, axial strains determined from measurements on left and right hand sides of the specimen were calculated, these being denoted by ε_{LL}, ε_{LR} and ε_{EL}, ε_{ER} for the local and end cap measurements respectively.

Typically the precision of the proximity transducers can be taken with not less than 95% confidence as $\pm 2\mu m$ over the first millimeter, as shown in Table 3.2. The overall uncertainty in a single measurement

(average of 10 readings) of the displacement is therefore not more than ±2.2μm, since the slip gauges used in the calibration have an accuracy of ±0.2μm, British Standards Institution (1950). With reference to Figure 5.1, the vertical distance between each pair of transducers, l_1, is determined by means of a vernier height gauge with an accuracy of ±20μm, British Standards Institution (1983). When used to measure l_1, this instrument has a precision (with 95% confidence) of ±100μm. The overall uncertainty in l_1 is thus not more than ±120μm. In order to compute the gauge length, L_g, it is necessary to add to or subtract from l_1 the small distances l_2 and l_3, as measured by the transducers. Theoretically the total uncertainty in the gauge length measurement does not exceed ±124.4μm (= ±(120 + 2.2 + 2.2)μm) but because of misalignment of the targets the true uncertainty may be somewhat higher.

The compressive axial strain, ε_A, determined from a local measurement over one side of the specimen is given by :-

$$\varepsilon_A = \frac{x - y}{L_g} \qquad (5.1)$$

where x and y are the increases in l_2 and l_3 respectively.
An upper bound for the error in the strain, $\delta\varepsilon_A$, is therefore

$$\delta\varepsilon_A = \frac{\delta x + \delta y}{L_g} + \frac{|\varepsilon_A|}{L_g} \delta L_g \qquad (5.2)$$

where δx, δy and δL_g are the magnitudes of the small uncertainties in x, y and L_g respectively ($\delta x = \delta y = \pm(2.2 + 2.2) + \pm 4.4$μm, $\delta L_g = \pm 124.4$μm). The maximum error in a single measurement of local axial strain can now be computed, with not less than 95% confidence, for a typical gauge length, L_g = 100mm, as shown in Table 5.1. Any plausible increase in δL_g due to target misalignment would have little influence on the tabulated values.

The above analysis considered the inaccuracy resulting from both random and systematic errors and the uncertainties have been combined by taking an ordinary sum. However, if only independent random errors are considered, the uncertainties can be combined by taking the quadratic sum (i.e. the square root of the sum of the squares of the individual uncertainties), Taylor (1982). Thus in equation (5.2), $\delta x + \delta y$ would be replaced by $\sqrt{(\delta x)^2 + (\delta y)^2}$. Furthermore, for a single test the errors in the gauge length as well as the datum readings would become systematic. Equation (5.2) can therefore be re-written for the "largest probable error" (i.e. the random error which will not be exceeded at the 95% confidence level) in the strain, $\delta \varepsilon_A$, as:-

$$\delta \varepsilon_A = \frac{\sqrt{(\delta x)^2 + (\delta y)^2}}{L_g} \tag{5.3}$$

The (random) error in determining the change in displacement of the target using a proximity transducer (δx or δy) would be reduced to $\pm 2.0\mu m$. Table 5.2 shows the results of such an analysis.

It should be noted that the above calculations concern the measurements on one side of the specimen only, although the average of measurements on opposite sides was often used in the strain computations. If equal uncertainties are involved in a number of measurements, which are then averaged, it can be shown (Taylor, 1982), that the error in the average measurement is equal to the error of the individual measurements divided by the square root of the number of measurements being averaged. Taking both systematic and random errors into account, the maximum error in the averaged relative displacements from two sides ($\delta x + \delta y$) therefore becomes $\pm 6.2\mu m$ ($= \pm \dfrac{4.4 + 4.4}{\sqrt{2}} \mu m$); similarly, δL_g becomes $\pm 88.0\mu m$ ($= \pm \dfrac{120 + 2.2 + 2.2}{\sqrt{2}} \mu m$). If only random errors are considered, the largest probable error in the relative displacement ($\sqrt{(\delta x)^2 + (\delta y)^2}$)

would be ±2.0μm (= ± $\frac{\sqrt{2^2 + 2^2}}{\sqrt{2}}$ μm). Tables 5.3 and 5.4 show the

maximum and largest probable errors obtained by applying equations (5.2)

and (5.3) to the average local axial strain measurements.

Similar reasoning can be applied to the end cap axial strain

measurement. Equation (5.1) can be applied with x and y now representing

the current and datum readings respectively of the submersible LVDT at

one side of the specimen, and L_g the length of the specimen prior to

shearing. The typical precision of the LVDTs is ±70μm (Table 3.1) and

the accuracy of a single reading following calibration against slip

gauges is therefore ±70.2μm (= ±(70.0 + 0.2)μm). Allowing for both

random and systematic errors, the combined uncertainty (δx + δy)

becomes ±140.4μm. The length of the specimen after trimming was deter-

mined by the vernier height gauge and is therefore subject to a maximum

error of ±120.0μm for a single measurement. However, the mean of six

readings was taken and the corresponding uncertainty is therefore

±49.0μm (= ± $\frac{120}{\sqrt{6}}$ μm). During saturation and consolidation, the change

in the length L_g was determined from the change in the submersible LVDT

readings and a further error of ±140.4μm may have occurred. The maximum

uncertainty in determining the length of the specimen prior to shearing,

δL_g, is thus ±189.4μm with not less than 95% confidence. For a typical

specimen of length 200mm, the results of applying equation (5.2) to

obtain the maximum errors are shown in Table 5.5. For independent random

errors only, the largest probable error in the relative displacement

across the end caps becomes ±70.0μm (= ±$\sqrt{70^2 + 0^2}$ μm) since the uncer-

tainty in the datum reading (y) is considered systematic. Table 5.6

shows the largest probable error in the end cap axial strain measurement.

For the average of the measurements on opposite sides of the specimen,

the maximum error (δx + δy) becomes ±99.3μm (= ± $\frac{140.4}{\sqrt{2}}$ μm) and δL_g is

± 148.3 m ($= \pm (49 + \dfrac{140.4}{\sqrt{2}})\mu m$). Similarly the largest probable error $\sqrt{(\delta x)^2 + (\delta y)^2}$ equals $\pm 49.5 \mu m$ ($= \pm \dfrac{70.0}{\sqrt{2}} \mu m$). Tables 5.7 and 5.8 show respectively the maximum and largest probable errors in the average end cap axial strain measurements.

The local radial strain, ε_R, is given by:-

$$\varepsilon_R = \frac{a + b}{2R} \qquad (5.4)$$

where a and b are the outward movements recorded by the transducers on opposite sides of the specimen and R denotes the radius. The diameter of the specimen was determined after trimming by averaging six readings from an external micrometer with an accuracy of $\pm 3.0\mu m$, British Standards Institution (1950), and a precision of $\pm 20.0\mu m$. Consequently, the initial diameter was subject to an error with not less than 95% confidence of $\pm 11.2\mu m$ ($= \pm (\dfrac{20}{\sqrt{6}} + 3)\mu m$). The initial uncertainty in the radius was therefore 5.6μm. After saturation and consolidation, the new radius was determined from the change in the sum of the transducer readings and therefore a further error of $\pm 4.4\mu m$ may have occurred. The maximum error in the radius, prior to shearing is therefore $\pm 10.0\mu m$ ($= \pm (5.6 + 4.4)\mu m$). The maximum error in the radial strain, $\delta \varepsilon_R$, is:-

$$\delta \varepsilon_R = \frac{\delta a + \delta b}{2R} + \frac{|\varepsilon_R|}{R} \delta R \qquad (5.5)$$

where δa, δb and δR are the uncertainties in a, b and R respectively ($\delta a = \delta b = \pm 4.4\mu m$; $\delta R = \pm 10.0\mu m$). Similarly the largest probable error is:-

$$\delta \varepsilon_R = \frac{\sqrt{(\delta a)^2 + (\delta b)^2}}{2R} \qquad (5.6)$$

with $\delta a = \delta b = \pm 2.0\mu m$. Tables 5.9 and 5.10 show the maximum error and

the largest probable error respectively for a typical specimen radius of 50 mm.

The uncertainties contained in Tables 5.1 to 5.10 are compared at the 0.1% strain level in Table 5.11. For the average local axial strain and the local radial strain measurements, the largest probable errors do not exceed ±0.002% and ±0.003% respectively. The superiority of the local axial strain measurements over the end cap measurements is also seen.

Following the computation of the local axial and radial strains, Poisson's ratio, ν, could be calculated (by definition $\nu = \frac{\varepsilon_R}{\varepsilon_L}$). Alternative, indirect methods of calculating ν, involving the use of externally measured volume changes, were not adopted. The fractional error in determining the Poisson's ratio is equal to the sum of the fractional errors of the local strain measurements. For example, for a material with $\nu = 0.5$ at 0.1% axial strain (0.05% radial strain), from Tables 5.3 and 5.9, the maximum fractional error would be 0.239 (= 0.063 + 0.176) and the value of ν would therefore be determined as 0.50±0.12.

5.3 PROVING TESTS

5.3.1 Description and Objectives

Altogether three sets of proving tests were conducted. The first set consisted of 3 tests (YR1, YR2 and YR3) on a rubber block with a hardness degree (British Standards Institution, 1957) of about 55. In order to evaluate the operation of the control system described in Section 4.3 it was more convenient to conduct tests with a dummy specimen of this type since simpler procedures could be adopted in setting up the instrumentation. Moreover, bearing in mind that no two soil samples are the same, by testing a material of known elastic properties

a better evaluation of the measurement system could be achieved, including a check on the repeatibility of the measurements.

It will be seen in the next section that the rubber block chosen was unfortunately too soft for small strain data to be gathered. Also, the tests on the rubber block did not involve any measurement of pore water pressure and therefore experience of the early procedural stages (equilibrium of pore pressure, saturation and isotropic consolidation) could not be gained. It was therefore necessary to perform some tests on soil specimens but these had to be reasonably uniform and reproducible. Two remoulded specimens of compacted Cowden material were prepared. Only soil particles passing through a 425 μm sieve were used. These were compacted by a 2.5 kg rammer falling through a height of 300 mm as described in Test 12 of British Standards Institution (1975) except that six layers were formed with 30 blows per layer. The tests on these specimens (RS1, RS2) were consolidated undrained tests.

The last set of proving tests consisted of two tests on intact specimens similar to those used in the main test series (see Section 5.4). Experience in the trimming of specimens from the 250mm diameter blocks was thereby gained. Another objective was to assess a suitable rate of loading and the time required for saturation and consolidation. The performance of the measuring system could also be evaluated under more realistic conditions. The tests on these intact specimens (TR1, TR2) were consolidated drained tests. The samples from which the specimens were obtained were supplied in advance of the main investigation. After extrusion from the 250mm diameter tube sampler, one specimen (TR2) was wrapped in polythene cling film and aluminium foil and placed in a polythene bag before being transferred to a high humidity room. The other specimen (TR1) was subjected to storage conditions identical to those of the main specimens (see Section 3.5.2) for two months before being stored in the humidity room for a further three months.

It should be noted that during these proving tests the setting up procedures described in Section 3.5.3 were adopted throughout except for the method of gluing on the radial strain targets. In the proving tests, and the first of the main tests, each target was glued onto a thin-walled tube, as described in Section 3.5.3, but the tube was then glued not to the membrane but to a separate piece of rubber (30mm wide x 50mm high). Afterwards the whole target assembly was bonded onto the membrane with silicon rubber. This procedure was later thought to introduce an unnecessary restraint to the specimen. The rubber mounting piece was therefore omitted and the target assembly attached directly to the membrane with Araldite glue along the line of contact of the thin-walled tube. The result of this change will be discussed in Section 5.4.4 where the main test results are presented.

The details of the proving tests are summarized in Table 5.12.

5.3.2 Results of Proving Tests

As mentioned above, one of the objectives of the proving tests was to evaluate the performance of the control system. Based on the control algorithm described in Section 4.3, a typical relationship between deviator stress and time for a loading path (i.e. monotonic increase of deviator stress) is shown in Figure 5.2. At zero time the deviator stress is slightly greater than zero because a small amount of load had to be applied to ensure that the specimen and the load cell were in contact. Whilst the results of Figure 5.2 were being obtained the cell pressure was kept constant to within ± 1.0 kN/m^2. With a load cell precision of ± 6N (Table 3.1), the expected scatter in the deviator stress at constant load would be about 0.7 kN/m^2 for a 100mm diameter specimen. It will be remembered that the load cell reading is used to ascertain whether another load step is required. As mentioned in Section 4.2.2,

each load step corresponds to a change of about $0.4 \, kN/m^2$ in air pressure which is approximately equal to $2.8 \, kN/m^2$ in the deviator stress for a 100m diameter specimen. Against this background, the choice of a lower control limit on deviator stress of $-1.5 \, kN/m^2$ is seen to lead to an acceptable limitation of departures from the target line. In Figure 5.2 readings were being taken at one minute intervals and it is seen that the time for a load step to be fully implemented was about four minutes at low deviator stresses. As the test proceeds and the specimen diameter increases, the increment of deviator stress corresponding to a load step becomes smaller and hence better control is achieved. Also as more strain occurs in the specimen, more load steps are required simply to maintain the current deviator stress.

In the presentation of stress-strain data, the datum for the measurements will be taken as the point at which the load cell has just been brought into contact with the specimen (i.e. the small amount of deviator stress present at this stage, and the associated strain, will be discounted.

Results from tests on the rubber block are presented in Figures 5.3 to 5.5 and summarized in Table 5.13. The Poisson's ratio determined from the local strain measurements was found to be close to 0.5. This compares with a range of values of 0.46 to 0.49 quoted by Kaye and Laby (1973). According to Allen (1966) the Young's modulus of rubber at a hardness degree of 55 ± 2 is $3220\pm644 \, kN/m^2$; the values shown in Table 5.13 are within this range. In Figures 5.3 to 5.5 the agreement between the average local and end cap measurements is generally good, although there is a slight tendency for the local strain to exceed the end cap strain in test YR3. Although this could be attributed to the effect of end restraint, discussed in Section 2.2.2, misalignment of the submersible LVDTs could also have been responsible. A more detailed discussion of the latter aspect will be given in Section 5.4.4.

Typical local and end cap axial strain measurements on opposite sides of the specimen (test YR2) are shown in Figures 5.6 and 5.7 respectively. In these figures individual readings rather than load step averages are shown. The fact that the data are scattered unevenly around the lines of equality suggests that some non-uniform straining of the specimen was occurring, possibly due to variations of its material properties. For this reason the width of the scatter band could not readily be analysed.

As can be seen in Figures 5.3 to 5.5, very few measurements in the small strain range ($\leqslant$0.1%) were possible for the rubber block due to its low stiffness coupled with an inability of the apparatus to apply deviator stress increments of less than about $2.8 \, kN/m^2$. Two tests (RS1, RS2) on remoulded soil from Cowden were therefore carried out. The stress-strain curves from these specimens are presented in Figure 5.8. The external axial strain measurements are clearly unreliable in the small strain range, as noted in Section 5.1. There exists close agreement between the other two types of axial strain measurement and this implies that a negligible bedding error existed for these specimens. Since the specimens were prepared by remoulding the soil close to its plastic limit (see Table 5.12 and Figure 2.8), and after removing the coarsest particles ($\geqslant$425μm), it is possible that during isotropic consolidation the bedding errors would have been reduced (see Section 6.2).

For an intact specimen, it is more likely that a bedding error would exist since there would be asperities protruding from the specimen. However these bedding effects would be of a random nature due to variations in the sample and in the process of trimming. Figures 5.9 and 5.10 show the stress-strain curves from the proving tests on intact specimens of Cowden Till (tests TR1 and TR2). By comparison with the

results for the remoulded specimens (Figure 5.8), the agreement between the local and end cap measurements is less good. The differences are attributed to the existence of bedding errors and variations of strain within the specimen. The apparent change in stiffness shown by the end cap measurement in test TR1 at a strain level of about 0.02% could indicate the yielding of an asperity at the end of the specimen (e.g. a protruding gravel size particle could be pushed into the relatively soft clay surrounding it).

In order to assess the scatter occurring in the two types of measurement, the individual data rather than load step averages from test TR1 were plotted in Figures 5.11 to 5.13. Also indicated in the figures are the data taken immediately before each load step (with upward arrows) and immediately after each load step (with downward arrows). Within each load step it should be noted that, as a result of variations in deviator stress and cell pressure, the last reading before the next load increment is not necessarily the one with the lowest deviator stress and largest strain. Likewise the first reading after a load increment does not necessarily involve the highest deviator stress and lowest strain. The change of axial strain as the load is maintained (i.e. creep strain) gradually increases as the specimen becomes less stiff on loading. Figure 5.11 shows a scatter band of about 0.014% strain (i.e. ±0.007%) at strains of up to 0.1%. In Table 5.4 the largest probable error in the average local axial strain was given as only ±0.002%. However in Figure 5.11 additional scatter is introduced as a result of the variations in cell pressure, variations in deviator stress and creep strain.

Similarly, Figure 5.12 shows that the scatter in the radial strain data, 0.008% (i.e. ±0.004%), is greater than that predicted on the basis of measurement errors only in Table 5.10, that is ±0.003%.

On the other hand, Figure 5.13 shows a scatter band is the end cap axial strain measurement of 0.028% (i.e. ±0.014%), which is less than that calculated in Table 5.8 as ±0.025%. This is understandable since during calibration the LVDT armature was positioned randomly in a lateral sense within the space available inside the transducer body as each reading was taken. This gave rise to the relatively large errors presented in Tables 5.5 to 5.8 but represents the worst possible situation. It should be noted that, although the armatures were mounted freely within the transducer, any lateral movement of the armature induced during a test as a result of specimen tilting or the formation of a shear plane would generally be gradual. The actual errors in the end cap strain measurements would therefore not be as large as indicated in the above tables.

An attempt was also made to assess a suitable rate of loading from these tests. As mentioned in Section 3.6, the choice of loading rate is a matter of judgement for the present work. Atkinson et al. (1985) suggested a rate of around $1 \, kN/m^2$/hour for all-round drainage conditions but a rate of $2 \, kN/m^2$/hour was adopted for these tests. Figure 5.14 shows the effective stress paths for tests TR1 and TR2 together with the applied total stresses. Note should be taken of the false origin and splitting of the horizontal axis in this figure. Also indicated in the figure are the ideal stress paths of slope 3 (shown dotted) and the local axial strains. It can be seen that the excess pore pressures were significantly larger in test TR2 than in test TR1. Assuming the specimen is of an isotropic nature and elastic up to the strain level shown, the effective stress path for an undrained test would be a vertical line (Schofield and Wroth, 1968; Atkinson and Bransby, 1985). The degree of pore pressure dissipation along a given stress path may thus be calculated by linear interpolation between the

undrained and ideal drained effective stress paths. On average the implied degree of dissipation of excess pore water pressure in test TR2 was only about 40%. Thus the rate of $2 kN/m^2/hour$ was clearly too fast for drained testing with the spiral drainage employed and a rate of $0.7 kN/m^2/hour$ was subsequently adopted. However, the $2 kN/m^2/hour$ rate was retained for undrained tests. The control of the total stress path, shown in Figure 5.14, was considered to be satisfactory.

In summary, the proving tests demonstrated that the instrument-ation and the control algorithm developed were adequate, that the measurement of the stress-strain behaviour of soil in the small strain range could be achieved, and that in favourable circumstances (i.e. with a uniform specimen, free from bedding errors and tilting) the local and end cap axial strain measurements were comparable.

5.4 MAIN TESTS

5.4.1 Description and Objectives

It was mentioned in Section 2.3.3 that the in-situ stress state of the specimens obtained from Cowden was close to isotropic (i.e. $K_o = 1$) and in Section 3.5.2 that the specimens were stored under iso-tropic stress conditions with an effective stress of $90 kN/m^2$. It was therefore logical to start the triaxial stress paths in the (p',q) plane from a point on the p' axis. Although any total stress path could have been followed (providing $q>0$) no attempt was made to perform complicated stress paths for the following reasons. Firstly, the fact that data had to be obtained from a limited number of specimens imposed severe restrictions on the checking of repeatability. Secondly, it was desirable that the data so obtained could be compared with conventional triaxial test data as well as with field test data. It was therefore

decided that the test programme should consist mainly of conventional consolidated drained and undrained tests with the applied total stress path having a slope of 3 in the (p',q) plane.

It was considered of interest also to compare the results with the predictions of existing constitutive models and the test programme was initially conceived in relation to an anisotropic elastic model developed for London Clay by Atkinson (1973). The evaluation of Atkinson's model required both drained and undrained tests on vertical and horizontal samples.

The details of the main test programme are summarized in Table 5.14. Within each test reference number the type of test and the orientation of the specimen are incorporated (i.e. the letter U or D for undrained or drained conditions and the letter V or H for a vertically or horizontally orientated specimen). In order to maximize the data obtained from each test, an unload-reload cycle was included as suggested by Wroth (1982). All tests were unloaded at a deviator stress of about 50 kN/m^2 and most were reloaded to failure without changing the slope of the applied total stress path. However in tests T7 and T8, which were intended to demonstrate the capability of the apparatus to control stress paths other than the conventional ones as well as to check the repeability of the previous tests, the specimens were reloaded along a different stress path. This had a slope in the (p',q) plane of -1 and +1 in tests T7 and T8 respectively (see Figures 5.15(b) and (c)). Two tests prefixed with the letter R (RT5 and RT6) were repeats of tests T1 and T4 respectively for reasons which will become clear in later sections.

In order to compare different stress-strain curves and, consequently, material stiffnesses, it is convenient to use some simple stiffness indicators. For the purpose of the present work secant

Young's moduli were chosen. The points at which the moduli were computed were arbitrarily selected and corresponded to axial strains of 0.01%, 0.05% and 0.1%. These secant moduli were evaluated for both drained and undrained tests and are denoted as (E') and (E_u) respectively, with the corresponding axial strain indicated as a subscript. For example, $(E_u)_{0.01}$ denotes the undrained secant Young's modulus at 0.01% axial strain. In addition, the secant modulus commonly referred to as E_{50} was calculated as:-

$$(E_u)_{50} \text{ or } (E')_{50} = \frac{\Delta q_{max}}{2(\varepsilon_A)_{50}}$$

where Δq_{max} is the maximum change in deviator stress observed during a conventional shear test following isotropic or anisotropic consolidation and $(\varepsilon_A)_{50}$ is the axial strain when half that change has been applied. In addition, the average modulus during the unloading and reloading cycle, denoted by $(E')_{ur}$ and $(E_u)_{ur}$, for drained and undrained tests respectively, was estimated using a least squares fitting technique. Only the local axial strain measurements were used in the above calculations. As will be discussed later in this section, the end cap axial strain measurements in these tests proved unreliable.

The test results will be presented in two groups, results from the undrained tests and results from the drained tests. The stress-strain results will be plotted over two axial strain ranges: firstly, 0 to 0.5% so as to adequately present the data at small strains ($\leqslant$0.1%) and the data from unloading and reloading and, secondly, 0-5.0% so as to present the subsequent data. In the second case, the external axial strain measurements are also included so that the consistency of different methods of measurement can be checked. However, for clarity and because of the acknowledged inaccuracies at low strains, only external measurements greater than 0.5% are shown.

5.4.2 Results of Undrained Tests

Stress-strain curves from the undrained tests (T1UV, T2UH and RT5UV) are presented in Figures 5.16 to 5.18 and again (with enlarged scales) in Figures 5.19 to 5.21. It can be seen that test T2UH was stopped prematurely (Figure 5.17). This was because the rate of strain derived from the end cap measurement exceeded 20% per hour, the prescribed limit in the control algorithm. The algorithm was subsequently modified as explained in Section 4.3.

In test T1UV bedding errors appeared to be small since there is a close agreement between the local and end cap measurements in Figures 5.16 and 5.19. It may be noted from Table 5.14 that the moisture content of this specimen was uncharacteristically high. It is thought that the material of specimen T1UV had been remoulded in the presence of water either before or during the sampling operation. As a result of this the material was relatively soft and bedding errors could have been reduced significantly during consolidation. A repeat test (RT5UV) was later conducted.

In test T2UH the departure of the end cap measurement from the local one at small strains (Figure 5.20) indicates the existence of bedding errors. The moisture content of this specimen is lower than that of T1UV (see Table 5.14) and is considered to be more representative. Bedding errors are therefore more likely to persist. The very small negative local axial strain measurement (-0.004%) in the early stages of shearing is thought to be due to unrepresentative movement of gravel-sized particles within the specimen near the mounting pads of either the upper or lower target rings.

In certain respects the results from test RT5UV were different from those of tests T1UV and T2UH but were more typical of those obtained from the drained tests discussed in the following section. At

small strain levels the end cap measurements showed erratic behaviour (Figure 5.21).

Effective stress paths for the small strain regions of these tests are shown in Figure 5.22 where the local axial strains are also indicated. The degree of equalization of pore pressure within the specimen cannot be assessed without a measurement of pore poressure in the central portion of the specimen (e.g. Hight, 1983).

5.4.3 Results of Drained Tests

The results of the drained tests (T3DV, T4DH, RT6DH, T7DV and T8DV) are presented in Figures 5.23 to 5.27 and again (with enlarged scales) in Figures 5.28 to 5.32. Incomplete data were retrieved from test T4DH because of a failure of the mains power supply. Although an attempt was made to use a cylinder of compressed air to maintain the pressures in the apparatus, the air was exhausted before power was restored and a loss of pressure resulted. As the pressure fell, the cell pressure reduced in advance of the lower chamber pressure and the deviator stress on the specimen actually increased. This resulted in the specimen being sheared without any more data being retrieved. Fortunately, this happened after the small strain data had been obtained. A repeat test (RT6DH) was designed to check repeatability in the small strain range and to obtain data for larger strains. As the time available for testing was limited, this test was terminated manually once the stress ratio $\frac{\sigma'_1}{\sigma'_3}$ was observed to fall. Test T8DV was terminated manually when the limit of the cell pressure supply was reached (see Section 4.2.2).

Several general observations can be made in respect of the stress-strain data. Firstly, there is no general agreement between local and end cap axial strain data at either small or large strains.

In the small strain range, the end cap measurements sometimes indicate a stiffer response (tests T7DV and T8DV) and sometimes a less stiff one (tests T3DV, T4DH and RT6DH). Secondly, in the small strain range the end cap data are less self-consistent than the local data. For example, during the unloading and reloading stage the end cap measurements in tests T3DV and RT6DH (see Figures 5.28 and 5.30) did not conform to the usual pattern, i.e. approximately reversible behaviour with a hysteresis loop lying below the initial loading curve (a similarly erratic pattern of results was obtained in test RT5UV). Thirdly, at large strains the end cap measurement appears to be up to 50% smaller than the local one in several tests (notably T3DV, RT6DH and T7DV - also RT5UV). However, in all cases the local measurements show good agreement with the external measurements despite inaccuracies in the latter, already acknowledged, and inaccuracies in the former due to target misalignment at large strains.

The erratic end cap strain data obtained at small strains, especially during unloading and reloading, are thought to be due to a form of bedding error, namely a rocking motion of the end caps arising from the local deformation of irregularities protruding from the end surfaces of the specimen. This is further discussed with the help of a simple model in Section 6.2. An explanation for the discrepancies between the local and end cap measurements at large strains is given in the following section.

The early stages of the effective stress paths from these tests are shown in Figures 5.33 to 5.37 where the false origins and split horizontal scales should be noted. Local axial strain levels of the order of 0.01% and 0.1% are also indicated. The degree of dissipation of excess pore pressure was calculated in the fashion discussed in Section 5.3.2 for the proving tests and the results are tabulated for a

strain level of about 0.1% in Table 5.15. In tests T3DV, T4DH and RT6DH the degree of pore water pressure dissipation was acceptable (though barely so in test RT6DH) and justified the choice of the loading rate (see section 5.3.2). However, in tests T7DV and T8DV the degree of pore water pressure dissipation was unsatisfactory showing that the shearing was conducted too quickly. The complete stress paths for tests T7DV and T8DV are shown in Figures 5.38 and 5.39 where it can be seen that the control system was capable of controlling the total stress path in non-standard directions. However in test T7DV the effective stress path diverged rapidly from the intended one during the final stages of the test (labelled AB in Figure 5.38). Again, the rate of change of deviator stress was apparently too fast to allow full drainage under the applied loading. No attempt was made to lower the loading rate during the test, although this would have been possible, as the time available for completing the test was limited. It might be noted that the time taken to complete the stress path shown in Figure 5.38 was about 2 weeks.

5.4.4 Evaluation of Elastic Parameters

Before attempting to evaluate elastic parameters for the Cowden Till it is appropriate to consider the reliability of the axial strain data. As noted in the previous sections the end cap measurement was clearly suspect. In many cases much larger strains were measured locally than between the end caps, the differences becoming more apparent at larger strains. These differences are too large to be explained by end restraint or non-uniformity of strain in the specimen, but can be explained in terms of tilting of the specimen as a result of eccentric loading. The principal reason for suspecting the end cap measurement to be erroneous, rather than the local measurement, is the

good agreement between the local and external measurements at large
strains in all tests. This agreement implies that in making the local
measurements there is no slipping of the target mounting pads relative
to the membrane and also no relative movement between the membrane and
the specimen.

In order to explain some of the errors occurring in the end cap
measurements, the result of test T3DV will be examined in some detail,
the greatest discrepancies between the end cap and local strains being
seen in this test. Figure 5.40 shows the displacements of various
points of the specimen in test T3DV at a local axial strain of 2%.
The displacement measured by the external transducer is indicated at
the bottom of the specimen and those measured by the proximity trans-
ducers are shown at the sides. The relative displacements between the
end caps measured by the submersible LVDTs are also indicated and com-
pared with values expected on the assumption that the top of the speci-
men does not move. It can be seen that relative movements of 1.837 mm
and 3.160 mm were apparently not detected by the submersible LVDTs.
This could only be explained if both the corresponding target points
were being moved upwards relative to the average level of the top cap.

In many tests (including test T3DV), because of the difficulty
of trimming the specimen accurately, the loading was slightly eccentric
and tilting of the top cap was observed. It was noted in Section 3.2
that some eccentricity of loading was to be tolerated. Unfortunately
the submersible LVDTs were aligned with the centre of the top cap rather
than with the loading ram. Figure 5.41 shows a plan view of the top
cap with the LVDTs sited at positions L and R, each about 60 mm from
the centre of the top cap, 0. Assuming the axis of tilting of the top
cap, denoted by the dotted line T-T, to be offset from 0 by a distance

d and to make an angle θ with the line LR, the following equations may be derived:—

$$x = (d + 60 \sin \theta) \tan \gamma$$
$$y = (d - 60 \sin \theta) \tan \gamma$$

(5.7)

where x and y are the upward movements of the LVDT targets at R and L respectively (i.e. x = 3.160 mm; y = 1.837 mm and γ is the angle of tilting). It was observed whilst setting up the specimens that the maximum eccentricity of the loading ram (d) was about 5 mm but, as tilting of the top cap occurred, the contact between the top cap and the load cell could have allowed sliding as well as rotation (see Plate 3.3) and therefore it is possible that the eccentricity increased. In addition, insufficient care in lining up the LVDTs with the centre of the top cap could have increased the value of d. If the largest plausible value, d = 10 mm, is substituted into equation (5.7), the values of θ and γ are 2.5° and 14.0° respectively. A tilt of this order was observed towards the ends of test T3DV.

In view of the difficulty of interpreting the end cap axial strain measurements due to the effect of either eccentric loading (discussed above) or of bedding errors at small strain levels (see also Section 6.2), the end cap data were rejected for the purpose of evaluating stiffness parameters. In contrast, it was felt that confidence could be placed in the local strain results. It should be noted that in the event of the specimen tilting, the average of the two local axial strain measurements would still represent the average axial strain, although the measuring points (centre lines of transducer and target) were about 90 mm away from the centre-line of the specimen. Figure 5.42 illustrates a situation where the specimen is tilted with small angles of α and β at the upper and low target rings respectively. The target rings are attached to the specimen at points A, B, C and D, moving to A', B', C' and D'.

The actual displacement at the boundary of the specimen (a, b, c and d) is either underestimated or overestimated when the displacement is measured away from the boundary. However, by inspection of Figure 5.42, the underestimations and overestimations of displacement cancel out when the average relative displacement is computed. As already mentioned in Section 5.3.2, the external strain data were judged to be of no value in the small strain range. Although the external strain data could have provided stiffness parameters at larger strains (i.e. E_{50}), for consistency it was decided to base the evaluation of all stiffness parameters on the local measurements. A summary of the Young's moduli derived from the main tests and two of the proving tests is given in Table 5.16. It can be seen from the stress-strain data presented in previous sections that the data from the unload-reload cycle were relatively few in number compared with those from initial loading. This is attributed to the difficulty of controlling the unload-reload stage (see Section 4.3).

Values of Poisson's ratio may be derived from the plots of local axial strain versus local radial strain. The symbols ν_u and ν' will be taken to refer to undrained and drained tests respectively. The values of ν_u for the undrained tests (T1UV, T2UH and RT5UV) are shown in Figure 5.43. In test T1UV (Figure 5.43(a)) the result was close to the expected value, $\nu_u = 0.5$. Unfortunately, the results of tests T2UH and RT5UV were clearly erroneous (Figures 5.43(b) and (c)). As mentioned in Section 5.3.1, the technique of attaching the radial strain target to the specimen was modified after test T1UV (see Figure 5.44(b)). Unfortunately, because processing of the test data was delayed, the adverse effect of the change was not noticed until several more tests (T2UH to RT6DH) had been completed. Values of ν' from the drained tests T3DV, T4DH and RT6DH are therefore not presented as they were

also erroneous. It appears that the connection of the target to the membrane could not accommodate local deformations (such as the movement of a gravel particle beneath the membrane) and therefore the target started to become detached (see Figure 5.44(b)). In this case the tendency would have been for a higher radial strain to be recorded. The method of attaching the targets was again modified in the subsequent tests (T7DV and T8DV) in which the area of contact between the membrane and the thin-walled tube was increased by adding silicon rubber (see Figure 5.44(c)). This connection proved satisfactory and reasonable values of ν' were again obtained, as shown in Figure 5.45. Results from the proving tests TR1 and TR2, where the original technique of target attachment was used (see Section 5.3.1) are also presented in Figure 5.46. Poisson's ratios are included in the summary of elastic parameters in Table 5.16.

5.4.5 Uniformity of Strains

The uniformity of strain in the specimens at small strains can be examined by referring to Figures 5.47 and 5.48 where local axial strains are plotted on each side of the specimen in tests T1UV and T3DV. In test T1UV the specimen showed uncharacteristic, relatively uniform behaviour which may be connected with its probable remoulding in the base of the borehole (see Section 5.4.2). In test T3DV significant tilting of the specimen developed as discussed in the previous section. The non-uniform behaviour was considered to be more typical as it occurred in five out of eight main tests, although not to the same extent as in test T3DV. In assessing the extent of the non-uniformity it has to be remembered that the measurements were taken some distance away from the specimen boundary. However, this can be corrected for as indicated in Figure 5.42. The corrected values of ε_{LL} and ε_{LR} are also

shown in Figure 5.48. In Figures 5.49 and 5.50 the local radial displacements on each side of the specimen are compared. If it were to be assumed that no translation of the specimen occurs, these measurements would indicate the degree of non-uniformity of radial strain. However, it is probably more realistic to assume that the radial strains were reasonably uniform and that the measurements indicate the degree of translation of the specimens. The measurements then suggest that the centre of the specimen translated far more in test T3DV than in test T1UV. Suggested deformation modes are indicated in the figures.

An attempt was made to examine the fabric of the specimens after testing. After oven-drying the specimens were cut into halves. Specimen T1UV was cut by an electrically driven disc-saw tipped with a diamond cutting edge. This was a difficult operation and unfortunately the specimen split into several pieces during cutting. For Specimen T3DV, a hack-saw blade made of tungsten carbide was used to cut the specimen by hand with greater success. Plate 5.1 shows the resulting cross-sections in which the coarsest particles have been coloured according to their nature (white = chalk , black = coal or limestone, red = other rock types).

Particle size distributions of the specimens were also obtained in general accordance with the procedures of tests 12 and 7 (D) of British Standards Institution (1975). After being dried, cut and photographed, the whole specimen was soaked in a large beaker of dispersing agent of the concentration recommended in the above standard for a week. It was then sieved under tap water through 2 mm and 425 μm sieves and all the material passing through was collected. Materials retained on these sieves were then oven-dried and dry sieved through a nest of sieves sized from 6.3 mm to 63 μm. Materials passing the 425 μm sieve during wet sieving were oven-dried and sieved through a 63 μm sieve.

About 40 gm of material passing the 63 μm sieve was subjected to sedimentation analysis. The range of particle sizes so obtained is shown in Figure 5.51 and the average result is compared with published data in Figure 5.52. It can be seen that on average these eight specimens were slightly finer than the published data would have predicted. The proportion of coarse gravel particles was small. However, such particles are believed to have affected the strain measurements adversely in two ways. Firstly, bedding errors in the end cap axial strain measurements were almost unavoidable due to the difficulty of trimming a flat end surface without intersecting such particles and, secondly, the unrepresentative movement of these particles beneath the target mountings occasionally caused errors in the local strain measurements.

T 1 UV Specimen

T 3 DV Specimen

PLATE 5·1 SECTIONS OF COWDEN MATERIAL

Local axial strain ε_A (%)	Maximum error in ε_A $\delta\varepsilon_A$ (%)	Maximum fractional error $\dfrac{\delta\varepsilon_A}{\varepsilon_A}$
0.01	8.81×10^{-3}	0.881
0.05	8.86×10^{-3}	0.177
0.10	8.92×10^{-3}	0.089

TABLE 5.1   Maximum error with not less than 95% confidence in local axial strain over one side of specimen

Local axial strain ε_A (%)	Largest probable error in ε_A $\delta\varepsilon_A$ (%)	Largest probable fractional error $\dfrac{\delta\varepsilon_A}{\varepsilon_A}$
0.01	2.83×10^{-3}	0.283
0.05	2.83×10^{-3}	0.056
0.10	2.83×10^{-3}	0.028

TABLE 5.2   Largest probable error with 95% confidence in local axial strain over one side of specimen

Local axial strain ε_A (%)	Maximum error in ε_A $\delta\varepsilon_A$ (%)	Maximum fractional error $\dfrac{\delta\varepsilon_A}{\varepsilon_A}$
0.01	6.21×10^{-3}	0.621
0.05	6.24×10^{-3}	0.125
0.10	6.29×10^{-3}	0.063

TABLE 5.3   Maximum error with not less than 95% confidence in local axial strain over two sides of specimen

Local axial strain ε_A (%)	Largest probable error in ε_A $\delta\varepsilon_A$ (%)	Largest probable fractional error $\dfrac{\delta\varepsilon_A}{\varepsilon_A}$
0.01	2.00×10^{-3}	0.200
0.05	2.00×10^{-3}	0.040
0.10	2.00×10^{-3}	0.020

TABLE 5.4   Largest probable error with 95% confidence in local axial strain over two sides of specimen

End cap axial strain ε_A (%)	Maximum error in ε_A $\delta\varepsilon_A$ (%)	Maximum fractional error $\dfrac{\delta\varepsilon_A}{\varepsilon_A}$
0.01	0.070	7.022
0.05	0.070	1.405
0.10	0.070	0.703

TABLE 5.5   Maximum error with not less than 95% confidence in end cap axial strain over one side of specimen

End cap axial strain ε_A (%)	Largest probable error in ε_A $\delta\varepsilon_A$ (%)	Largest probable fractional error $\dfrac{\delta\varepsilon_A}{\varepsilon_A}$
0.01	0.035	3.500
0.05	0.035	0.700
0.10	0.035	0.350

TABLE 5.6   Largest probable error with 95% confidence in end cap strain over one side of specimen

End cap axial strain ε_A(%)	Maximum error in ε_A $\delta\varepsilon_A$(%)	Maximum fractional error $\dfrac{\delta\varepsilon_A}{\varepsilon_A}$
0.01	0.049	4.966
0.05	0.049	0.994
0.10	0.049	0.497

TABLE 5.7   Maximum error with not less than 95% confidence in end cap axial strain over two sides of specimen

End cap axial strain ε_A(%)	Largest probable error in ε_A $\delta\varepsilon_A$(%)	Largest probable fractional error $\dfrac{\delta\varepsilon_A}{\varepsilon_A}$
0.01	0.025	2.475
0.05	0.025	0.495
0.10	0.025	0.248

TABLE 5.8   Largest probable error with 95% confidence in end cap axial strain over two sides of specimen

Local radial strain ε_R(%)	Maximum error in ε_R $\delta\varepsilon_R$(%)	Largest fractional error $\dfrac{\delta\varepsilon_R}{\varepsilon_R}$
0.01	8.80×10^{-3}	0.880
0.05	8.81×10^{-3}	0.176
0.10	8.82×10^{-3}	0.088

TABLE 5.9   Maximum error with not less than 95% confidence in local radial strain

Local radial strain $\varepsilon_R(\%)$	Largest probable error in ε_R $\delta\varepsilon_R(\%)$	Largest probable fractional error $\dfrac{\delta\varepsilon_R}{\varepsilon_R}$
0.01	2.83×10^{-3}	0.283
0.05	2.83×10^{-3}	0.057
0.10	2.83×10^{-3}	0.028

TABLE 5.10   Largest probable error with 95% confidence in local radial strain

	Maximum Error (%) x 10^{-3}	Largest Probable Error (%) x 10^{-3}
Local axial strain (one-sided)	8.92	2.83
Local axial strain (two-sided)	6.29	2.00
Local radial strain	8.82	2.83
End cap axial strain (one-sided)	70.00	35.00
End cap axial strain (two-sided)	49.00	25.00

TABLE 5.11   Comparison of accuracy from instrumentation within stress path cell at 0.1% strain level

Test no.	Material	Cell Pressure (kN/m^2)	Back Pressure (kN/m^2)	Moisture Content (%)	Loading Rate $(kN/m^2/hr)$	Remark
YR1	Rubber	250	NIL	NIL	30	
YR2	Rubber	250	NIL	NIL	30	
YR3	Rubber	250	NIL	NIL	30	
RS1	Recompacted Soil	290	255	19.40	30	Consolidated undrained test
RS2	Recompacted Soil	300	215	18.44	30	Consolidated undrained test
TR1	Intact Soil	300	245	16.10	2	Consolidated drained test Horizontally orientated
TR2	Intact Soil	315	245	16.37	2	Consolidated drained test Vertically orientated

TABLE 5.12   Details of proving test

Test no.	Young's modulus from local measurement (kN/m^2)	Young's modulus from end cap measurements (kN/m^2)	Poisson's ratio ν_u
YR1	3077	3158	0.50
YR2	3000	3077	0.50
YR3	2941	3030	0.49
Average	3006	3088	0.50

TABLE 5.13   Young's modulus from proving tests on rubber block

Test no.	Moisture content (%)				Specific volume v	p'_o (kN/m^2)
	Before trimming*	After trimming*	Whole specimen (before test)	Whole specimen (after test)		
T1UV	16.98	16.41	15.62	15.65	1.422	89
T2UH	15.22	14.56	14.65	14.72	1.396	84
T3DV	14.92	14.04	14.50	15.62	1.392	89
T4DH	15.64	14.22	14.47	14.15	1.391	84
RT5UV	15.37	14.50	15.01	14.62	1.405	86
RT6DH	15.47	13.94	14.40	13.99	1.389	80
T7DV	15.66	15.10	15.40	16.07	1.416	79
T8DV	15.59	14.84	14.90	14.56	1.402	80
Average	15.61	14.70	14.87	14.95	1.402	84

Note: (1) *Average of six measurements from adjacent material removed from specimen
(2) Specific volume from moisture content from whole specimen before test assuming a specific gravity of 2.7

TABLE 5.14 Details of main tests

Test no.	Degree of dissipation of excess pore water pressure at $\varepsilon_L \approx 0.1\%$ (%)
T3DV	99
T4DH	90
RT6DH	80
T7DV	54
T8DV	·48

TABLE 5.15 Degree of dissipation of excess
pore water pressure for drained
tests

Test no.	Test condition	Secant modulus (MN/m^2)				Unload-reload modulus (MN/m^2)	Tangent modulus (MN/m^2)			Poisson's ratio
		$E_{0.01}$	$E_{0.05}$	$E_{0.1}$	E_{50}	E_{ur}	$E_{0.01}$	$E_{0.05}$	$E_{0.1}$	ν
TR1	Drained	33.00	27.80	23.10	-	-	33.00	20.83	14.38	0.46
TR2	Drained	52.00	33.20	26.00	-	-	33.33	21.43	16.28	0.34
T1UV	Undrained	42.00	33.60	23.80	7.42	48.79	42.00	18.11	11.82	0.50
T2UH	Undrained	235.00	76.00	46.80	-	120.62	235.00	24.00	11.38	1.76
T3DV	Drained	60.00	55.00	43.20	21.15	92.15	60.00	40.00	19.03	0.60
T4DH	Drained	74.00	49.20	39.80	-	92.77	46.00	35.00	24.22	0.77
RT5UV	Undrained	66.00	62.00	50.00	18.57	135.35	66.00	38.23	25.00	1.16
RT6DH	Drained	100.00	70.80	51.00	22.25	207.50	100.00	35.56	32.40	0.83
T7DV	Drained	60.00	38.00	29.60	-	-	40.00	26.00	17.80	0.30
T8DV	Drained	50.00	39.20	30.00	-	-	46.67	26.71	19.02	0.37

TABLE 5.16   Summary of elastic parameters obtained from local strain measurements

Submersible
LVDT

Triaxial specimen

Proximity transducers

Loading ram

Target mounted on specimen

Mounted on rigid external support

l_3

l_1

l_2

$(\varepsilon_{LL}, \varepsilon_{LR})$ Local strain measurement

$(\varepsilon_{EL}, \varepsilon_{ER})$ End cap strain measurement
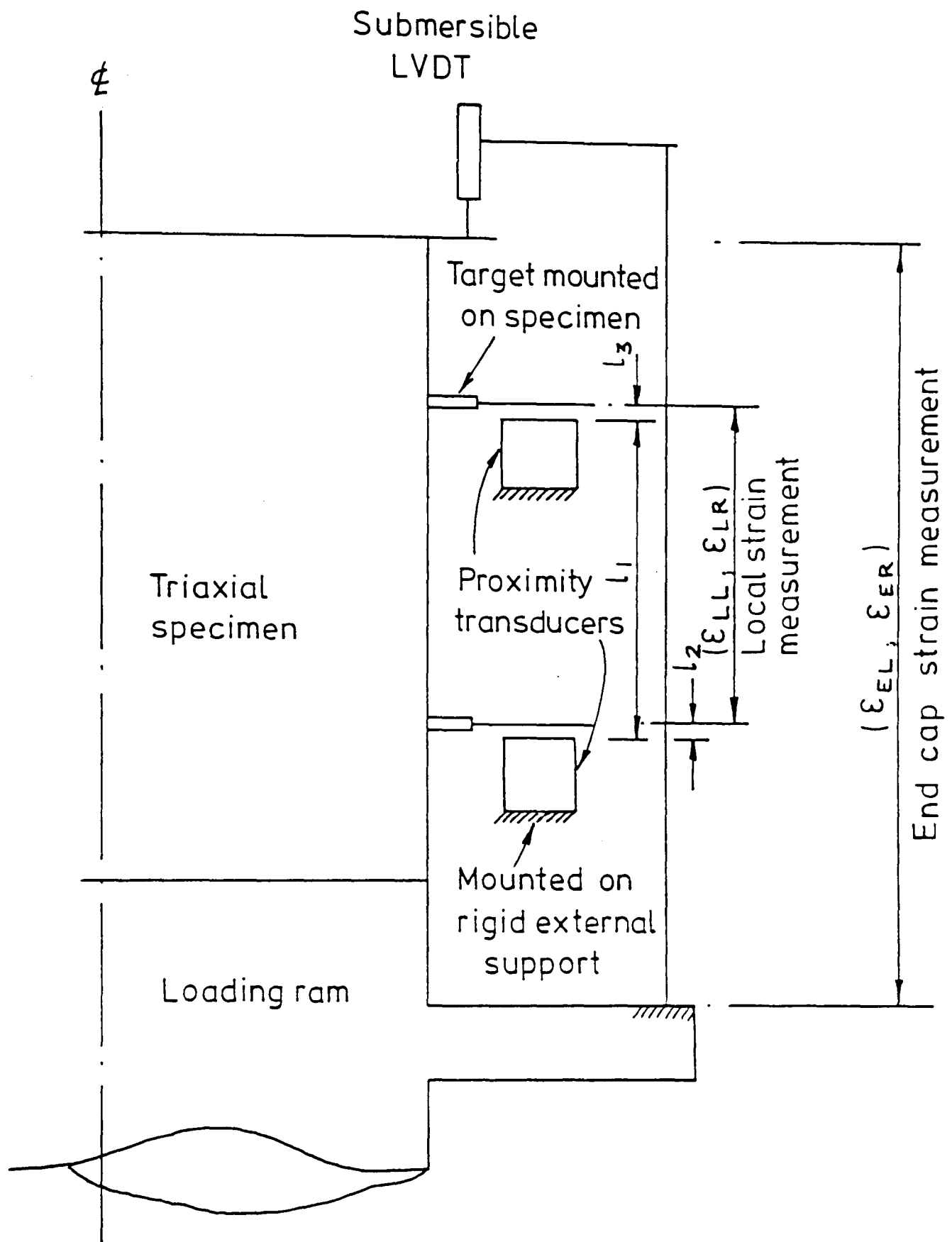
FIG. 5·1   DIAGRAMMATIC REPRESENTATION OF STRAIN
MEASUREMENTS WITHIN STRESS PATH CELL
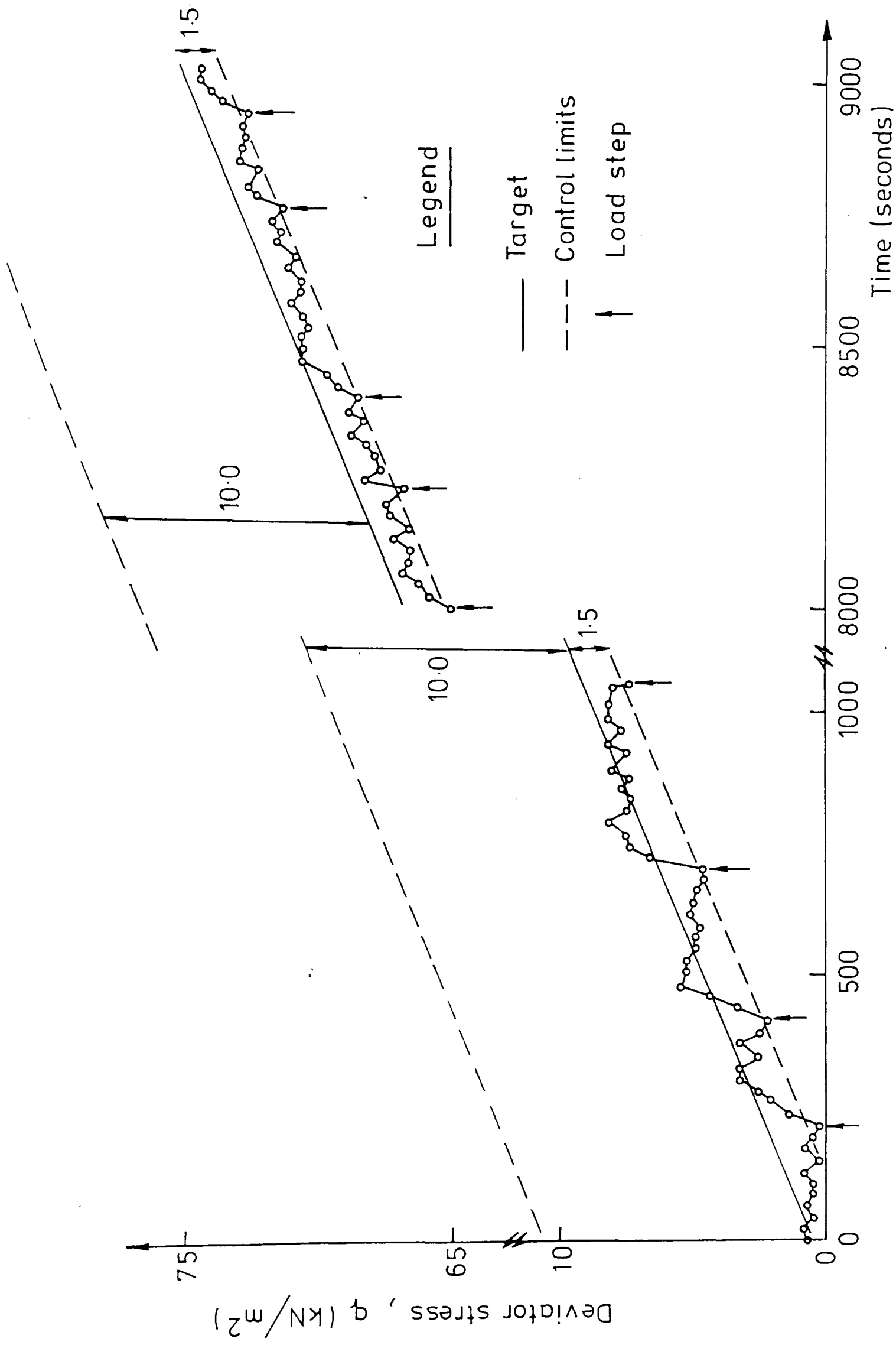
FIG. 5·2 TYPICAL VARIATION OF DEVIATOR STRESS WITH TIME (FROM PROVING TEST RS2)
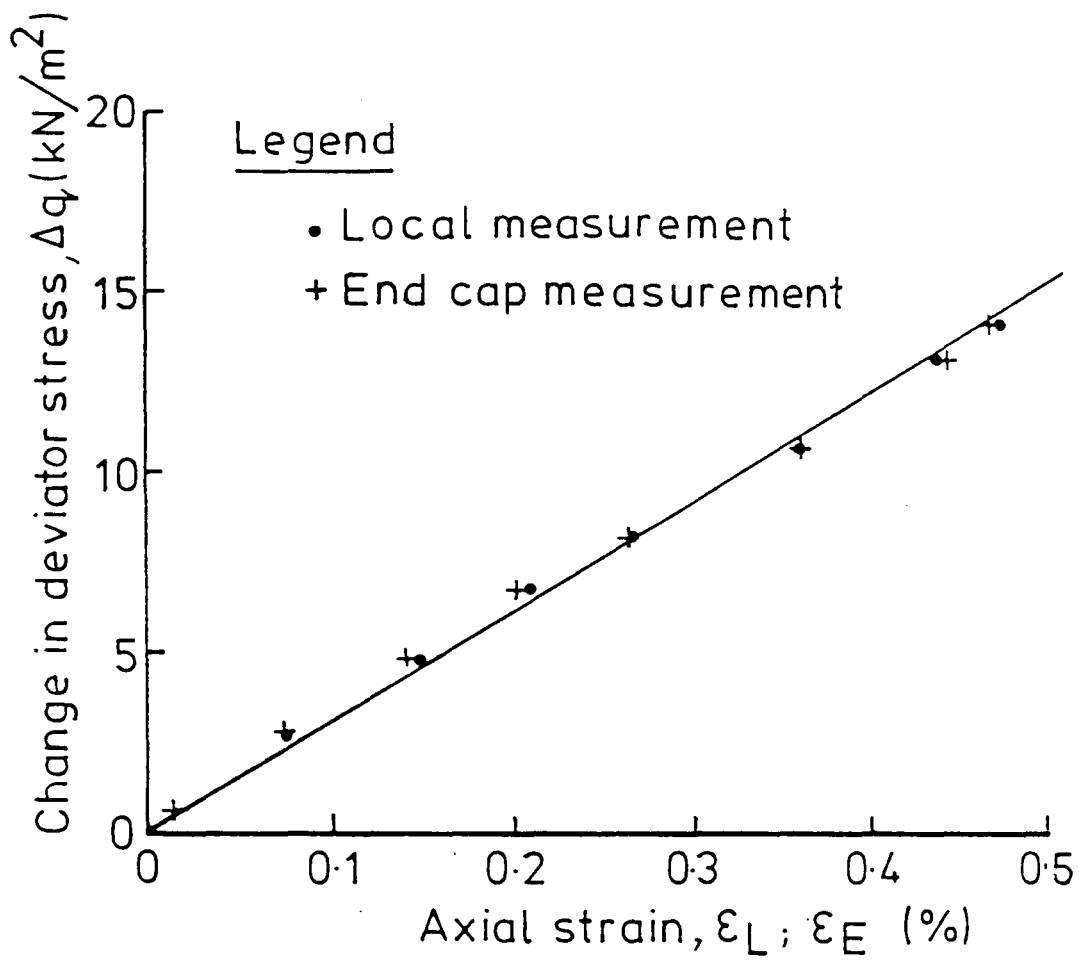
(a) Stress - Strain
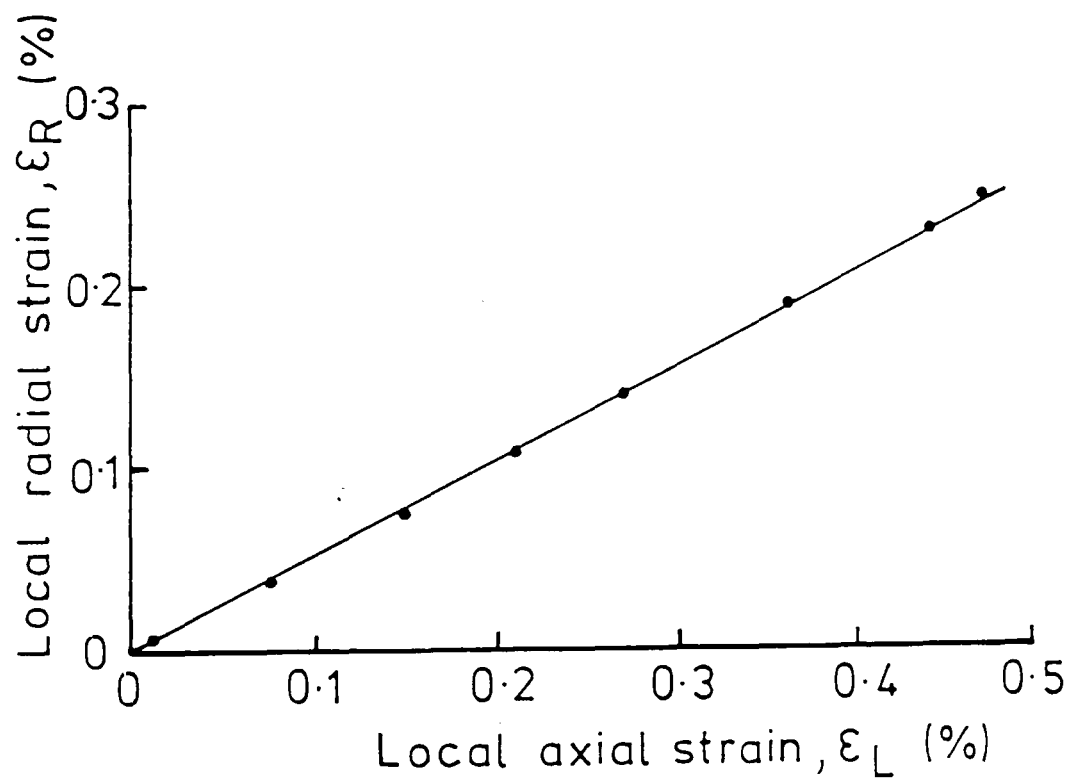
(b) Poisson's Ratio

FIG. 5·3 RESULTS OF PROVING TEST YR1

(a) Stress – strain
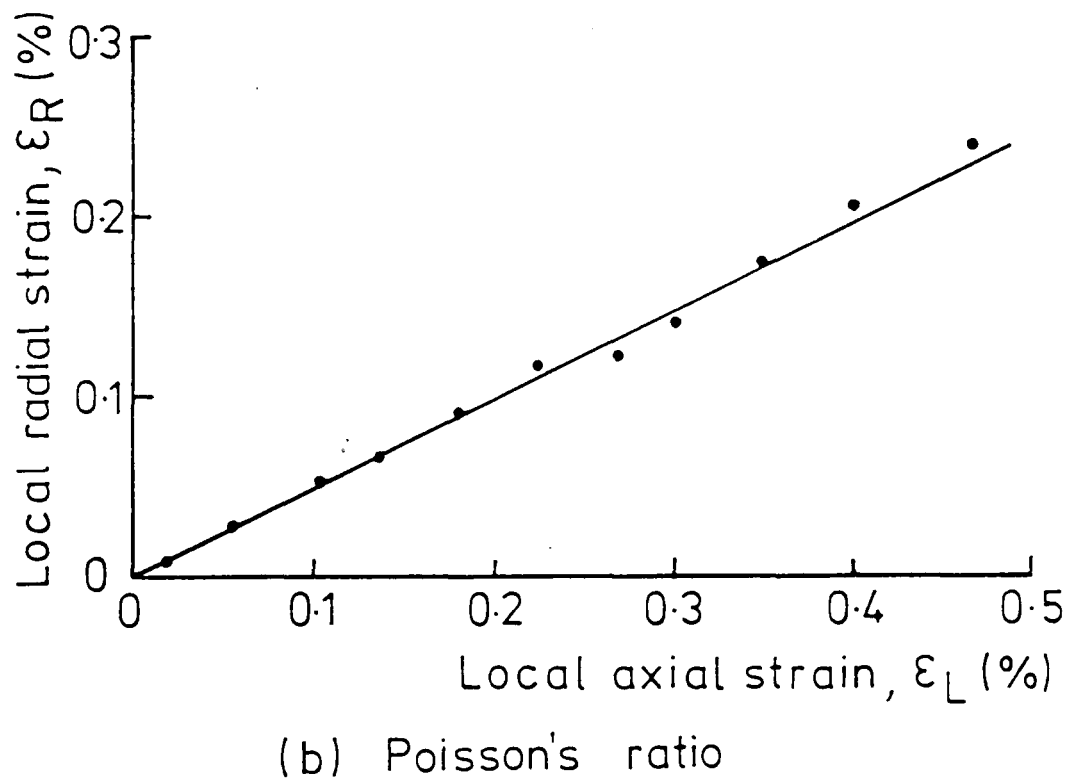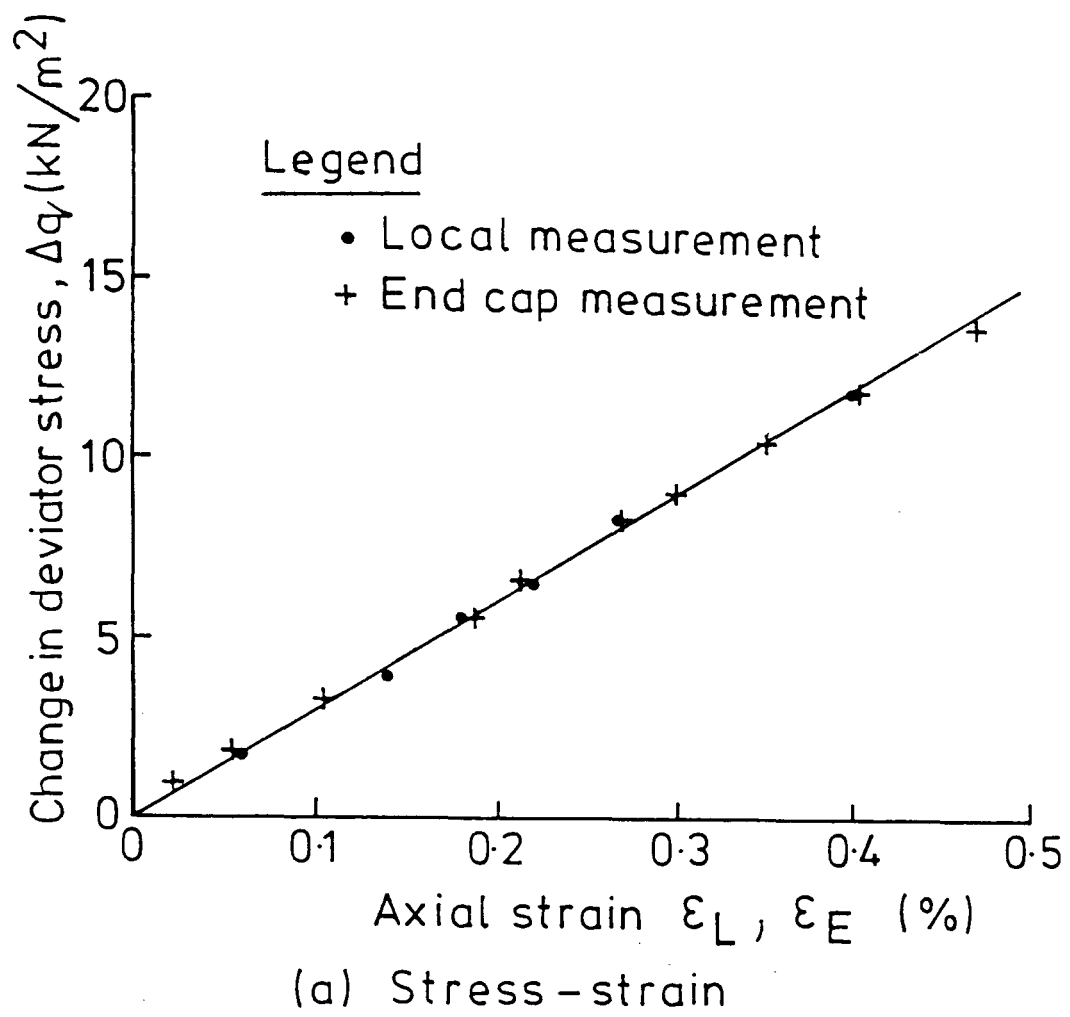
(b) Poisson's ratio

FIG. 5·4   RESULTS OF PROVING TEST YR2
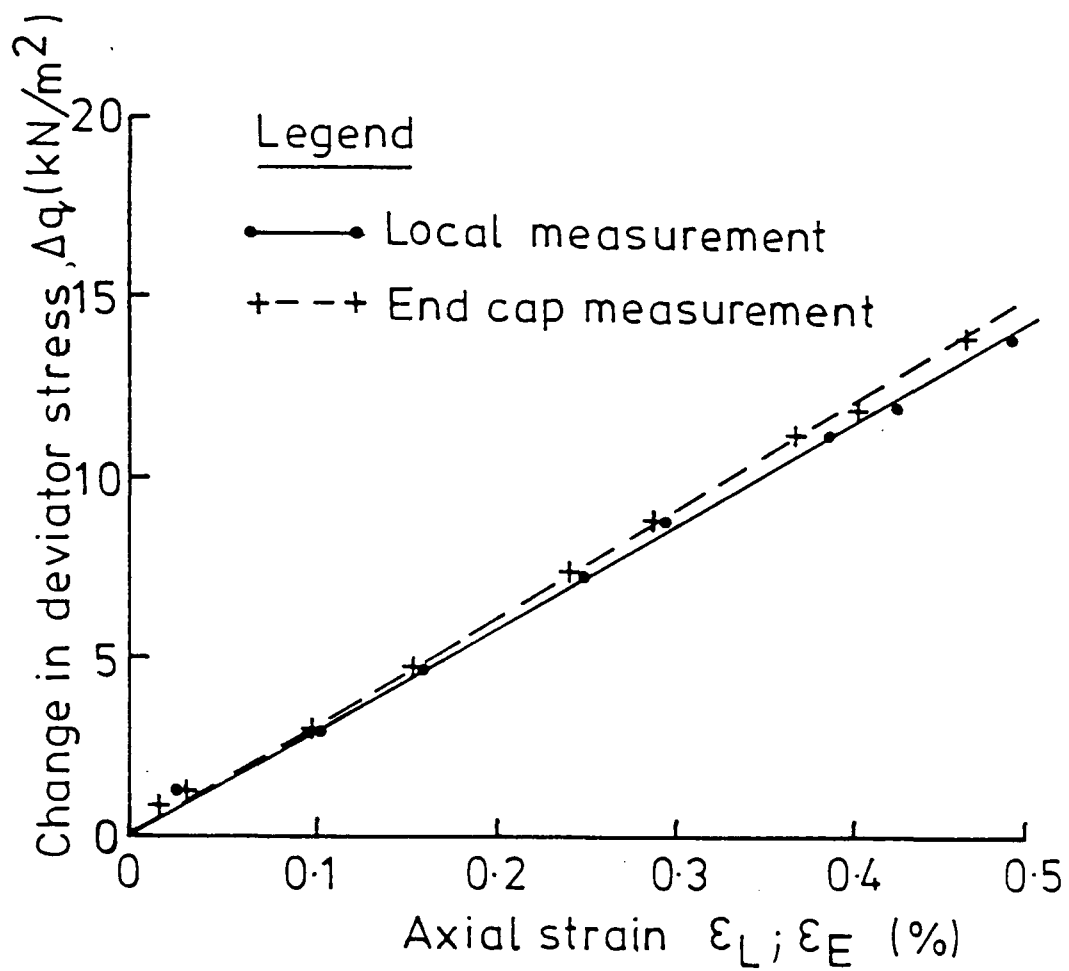
(a) Stress-strain
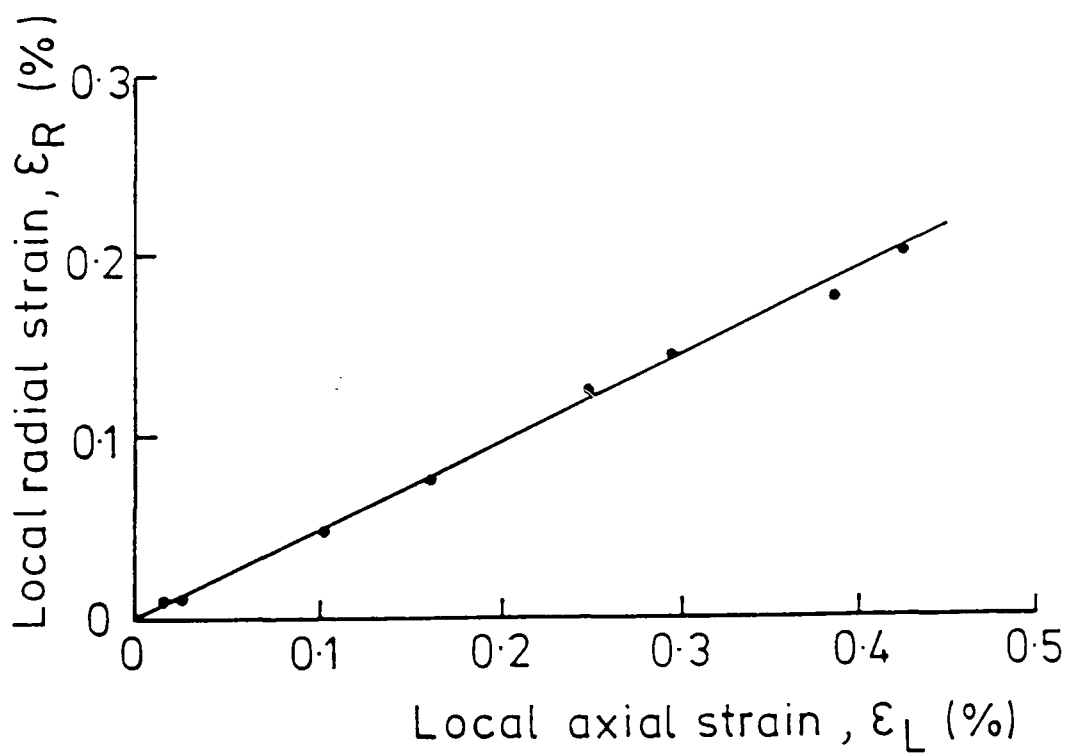
(b) Poisson's ratio

FIG.5·5   RESULTS OF PROVING TEST YR3
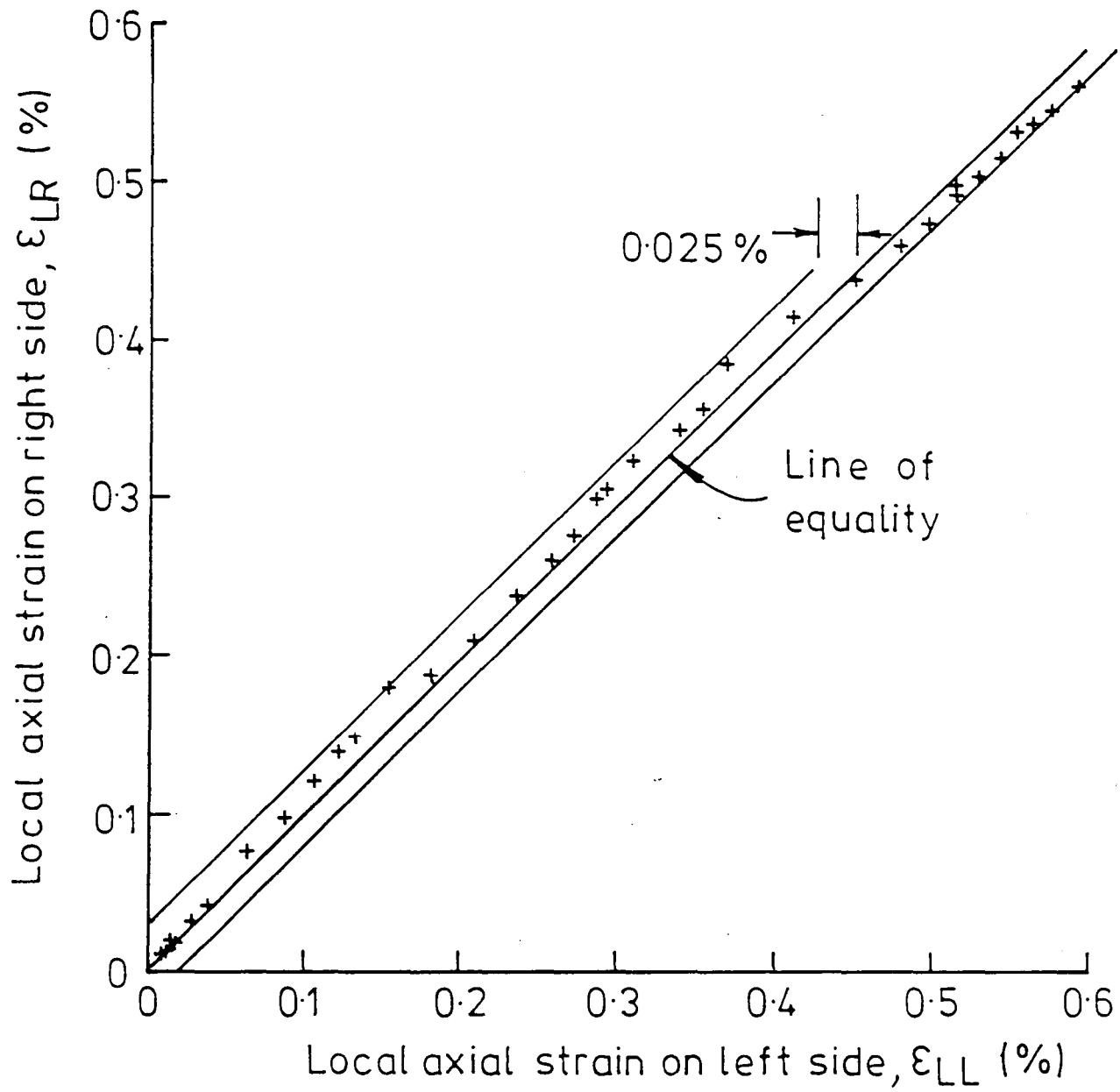
FIG. 5·6 TYPICAL DIFFERENCE BETWEEN INDIVIDUAL LOCAL
AXIAL STRAIN MEASUREMENTS (FROM PROVING TEST YR2)
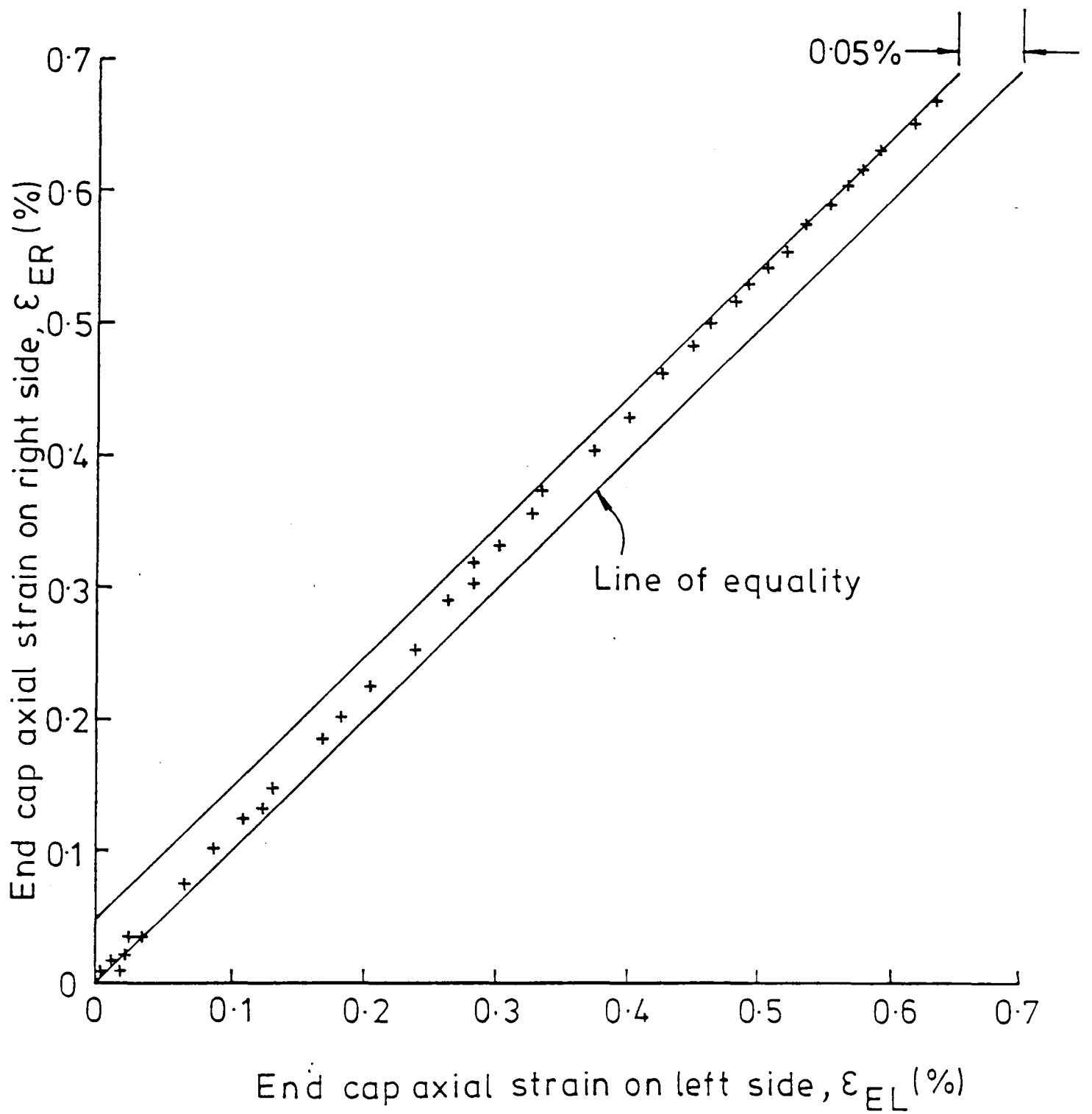
FIG. 5·7   TYPICAL DIFFERENCE BETWEEN INDIVIDUAL
          END CAP AXIAL STRAIN MEASUREMENTS
          (FROM PROVING TEST YR2)
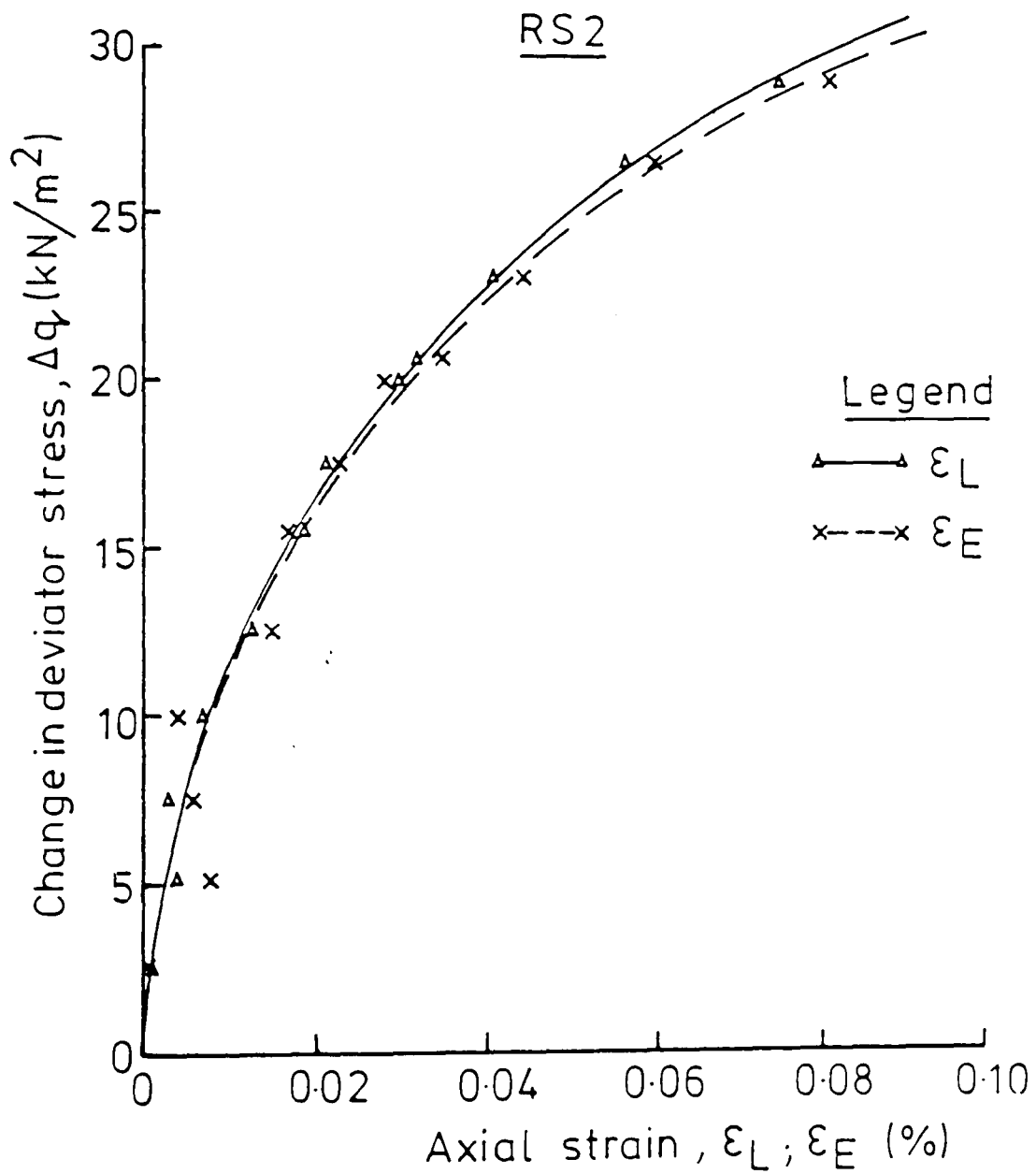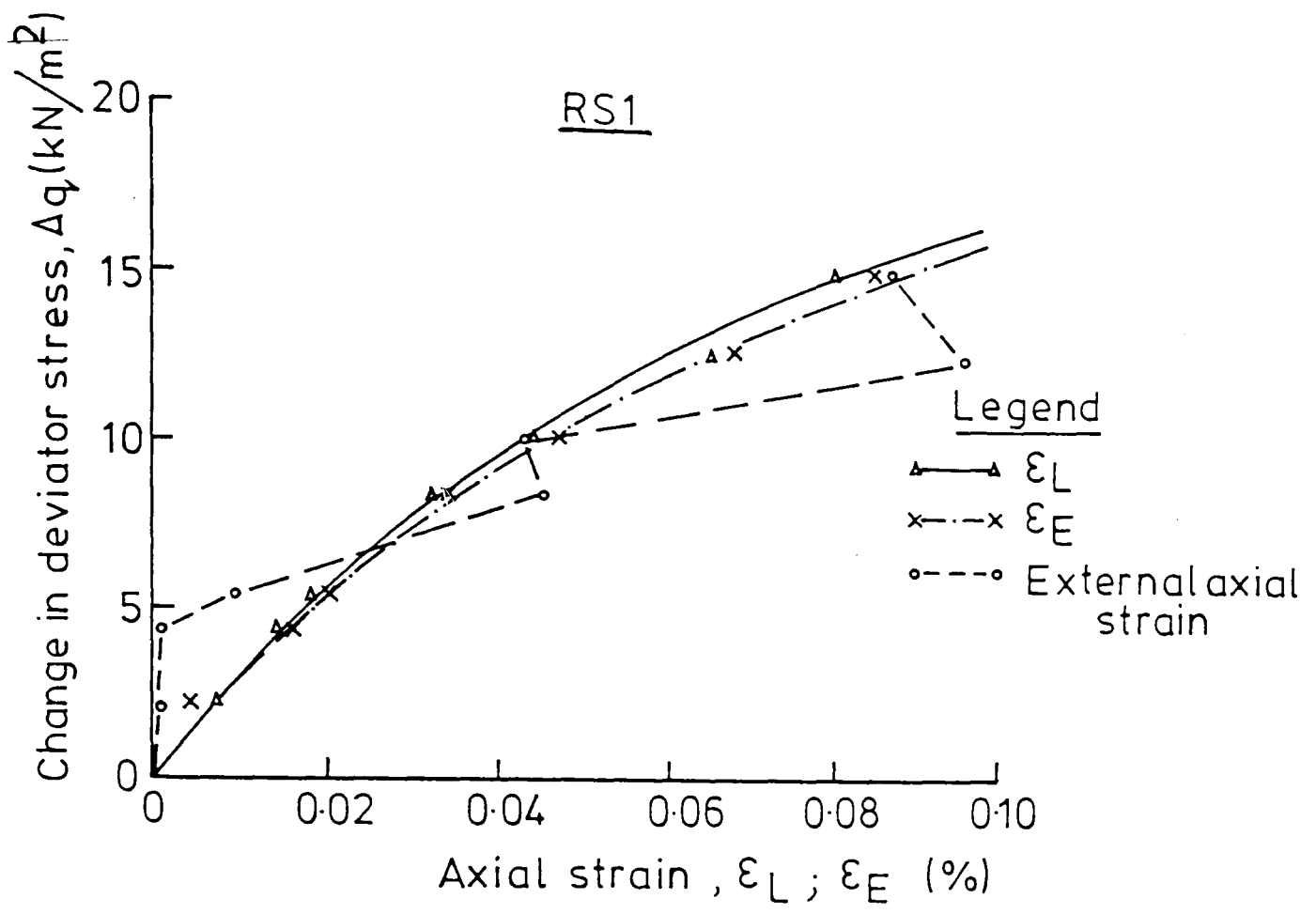
FIG. 5·8   RESULTS OF PROVING TESTS RS1 & RS2
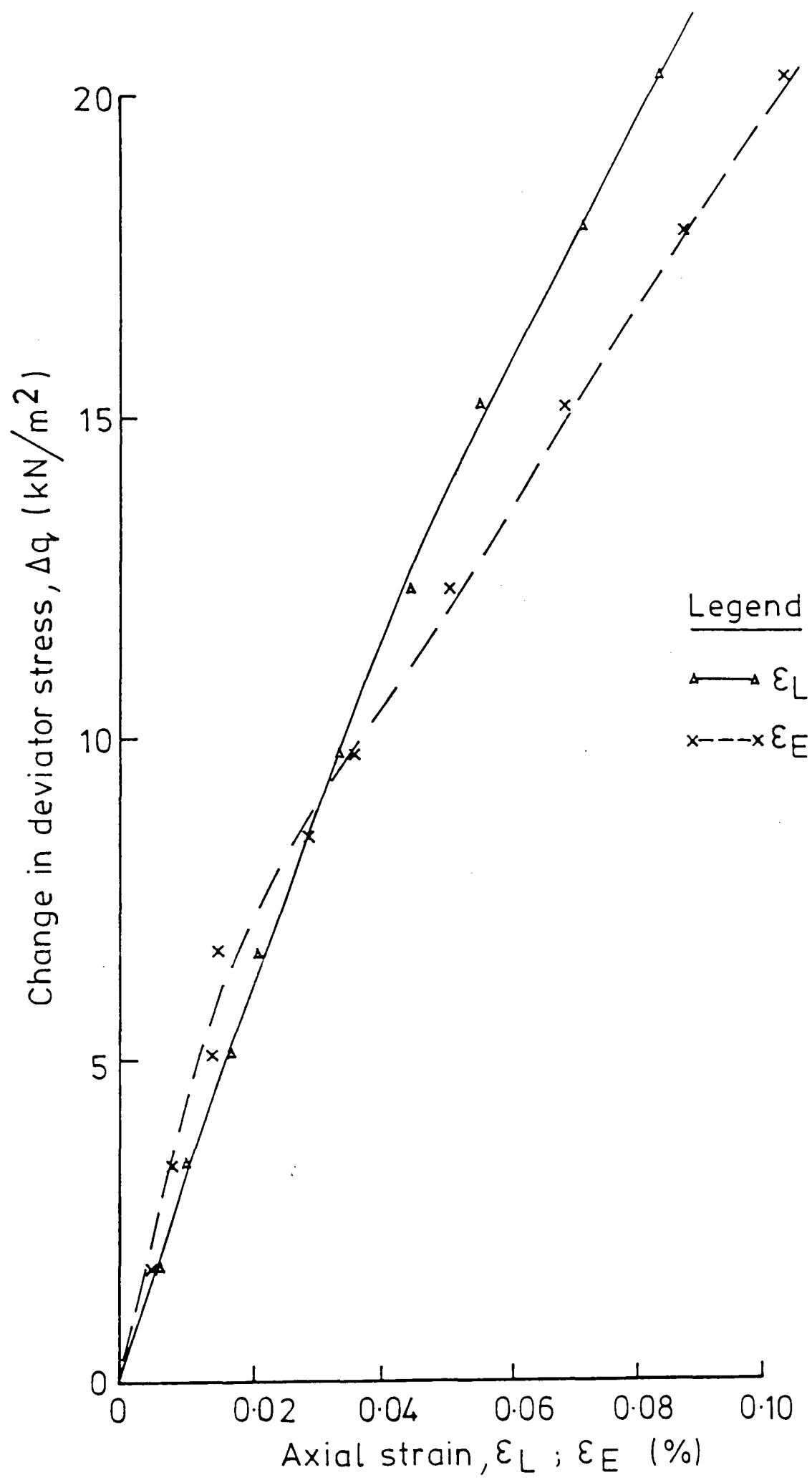
FIG. 5·9   RESULT OF PROVING TEST TR1
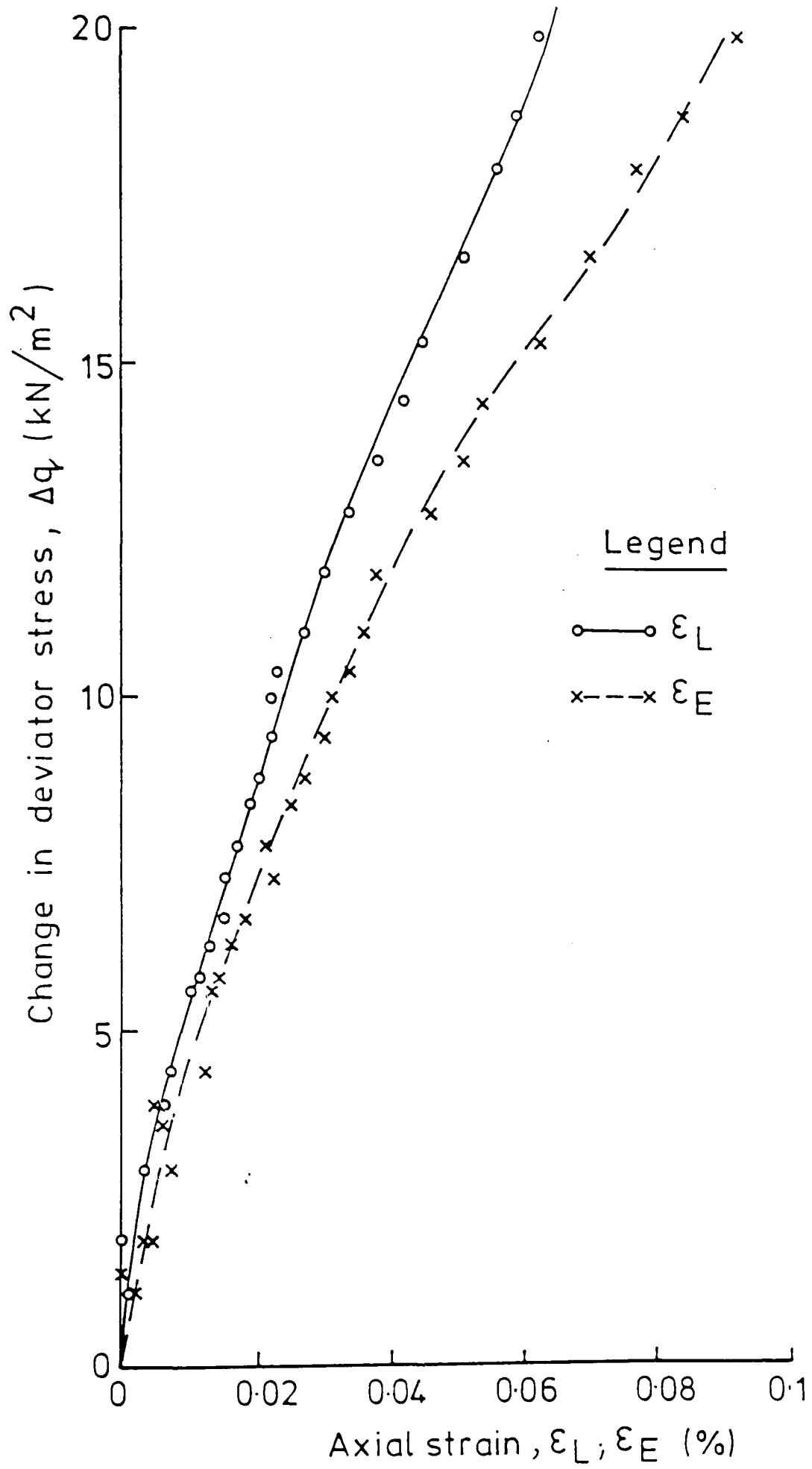
FIG. 5·10   RESULT OF PROVING TEST TR2
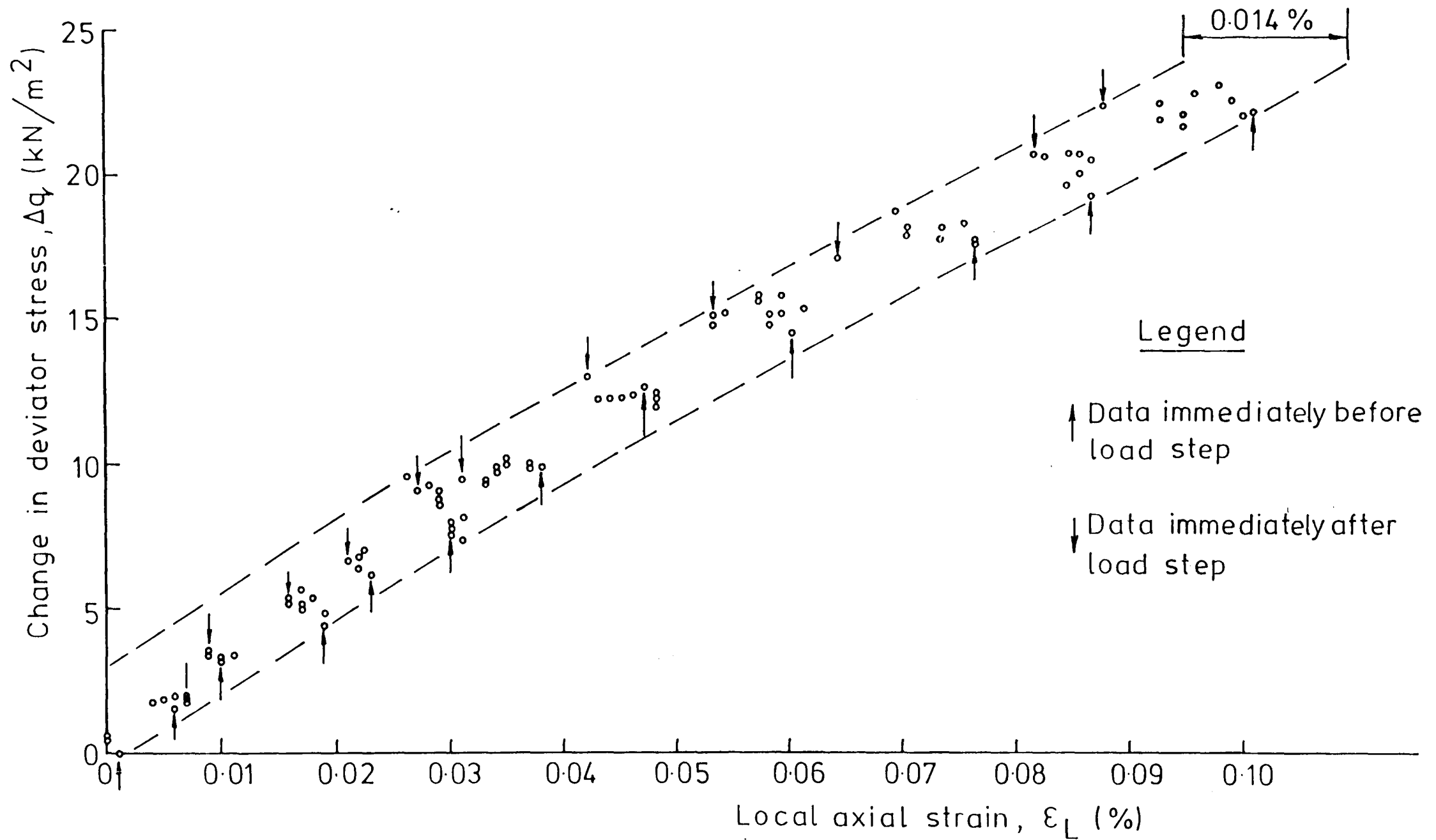
FIG. 5·11   SCATTER BAND OF LOCAL AXIAL STRAIN MEASUREMENT (FROM PROVING TEST TR1)
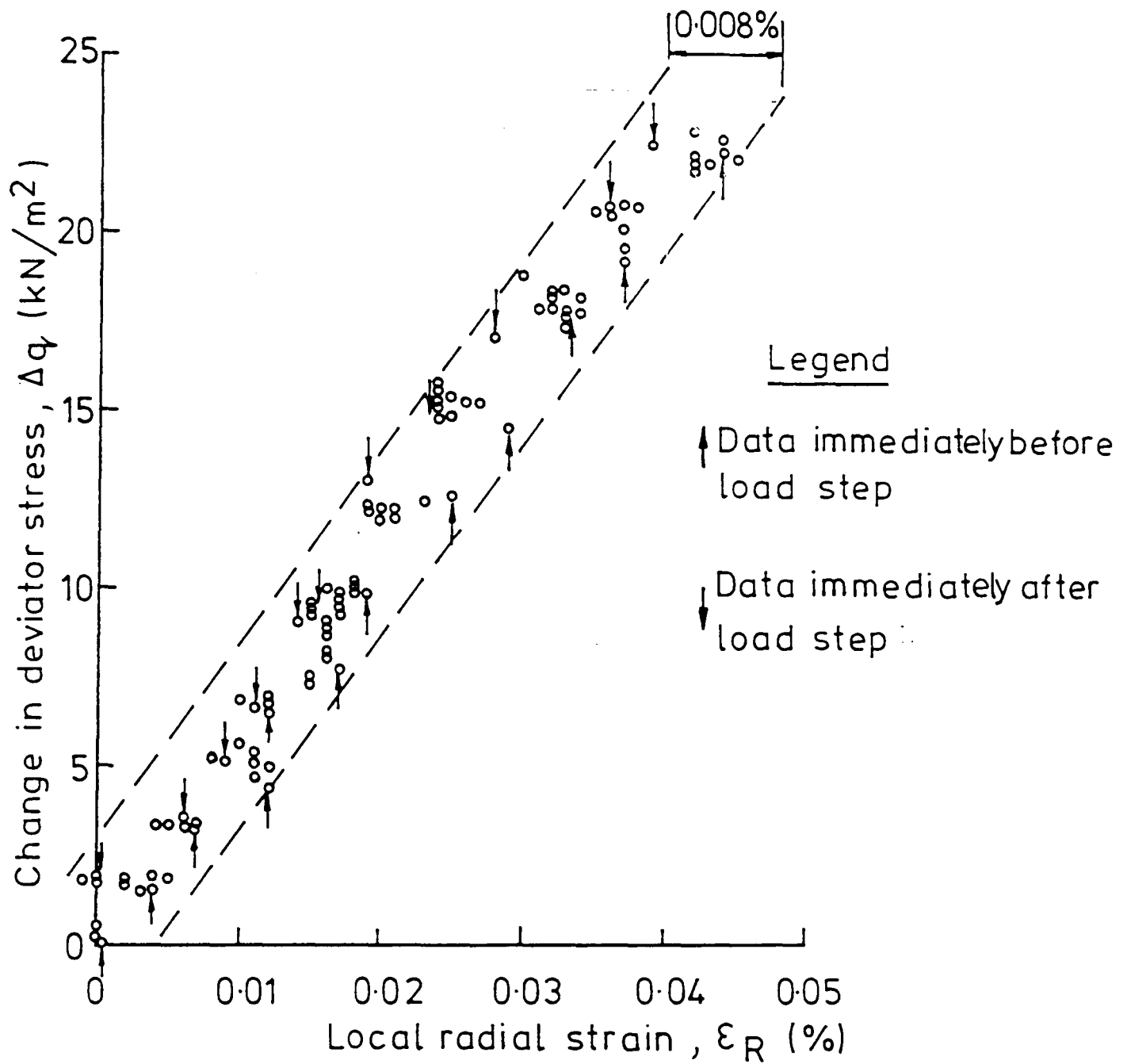
FIG. 5·12   SCATTER BAND OF LOCAL RADIAL

STRAIN MEASUREMENT (FROM PROVING TEST TR1)
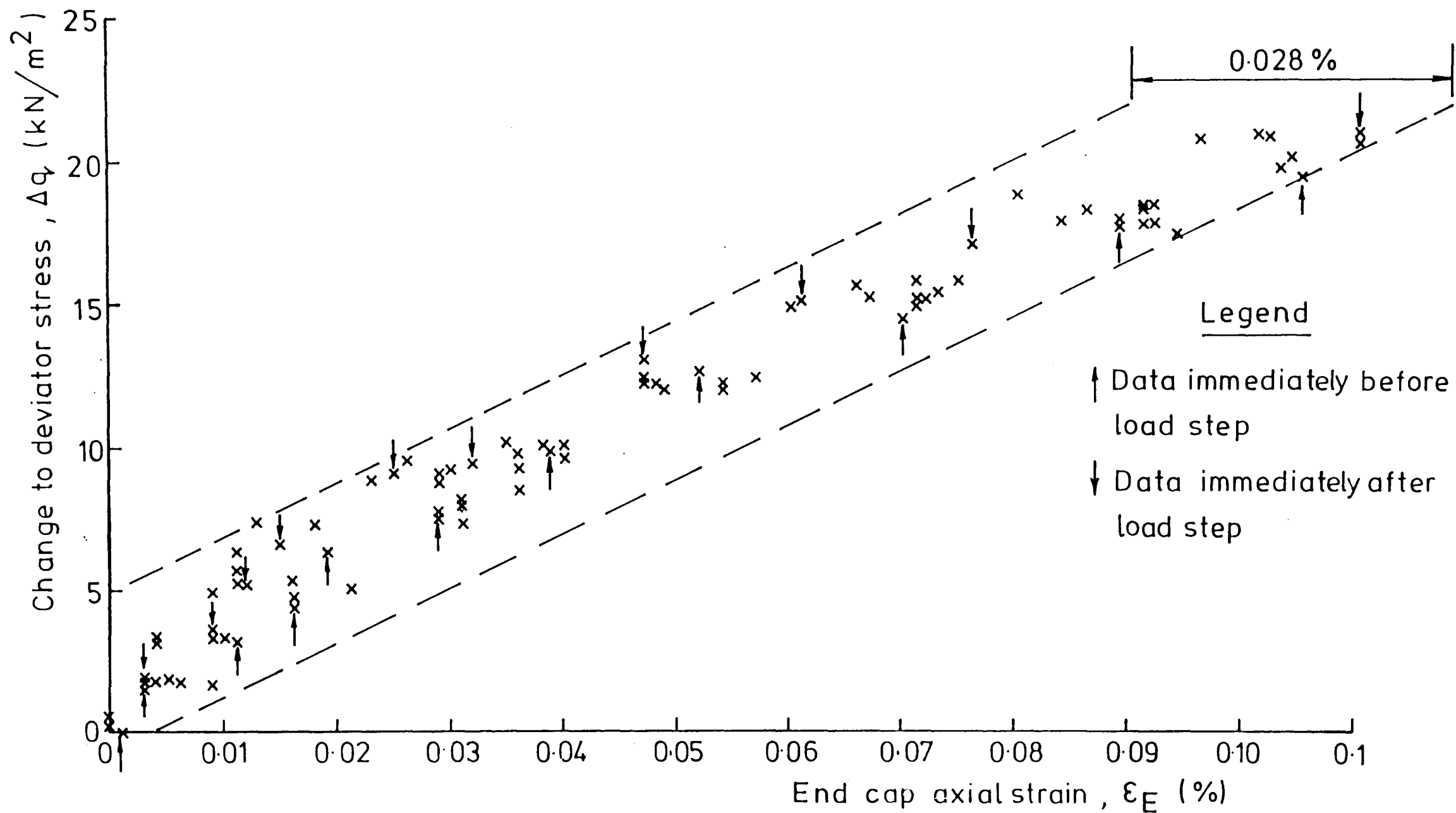
FIG. 5·13 SCATTER BAND OF END CAP AXIAL STRAIN MEASUREMENT
(FROM PROVING TEST TR1)
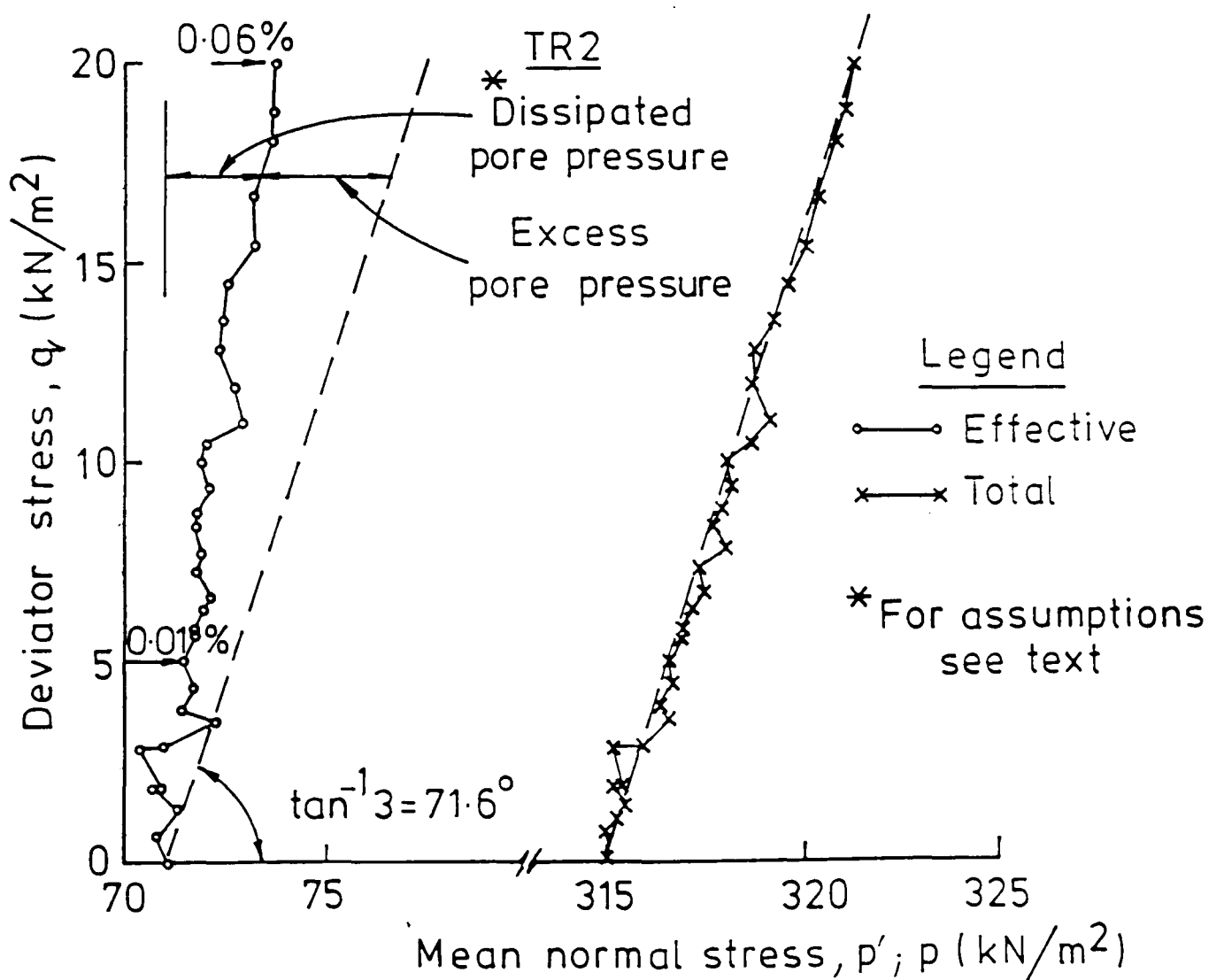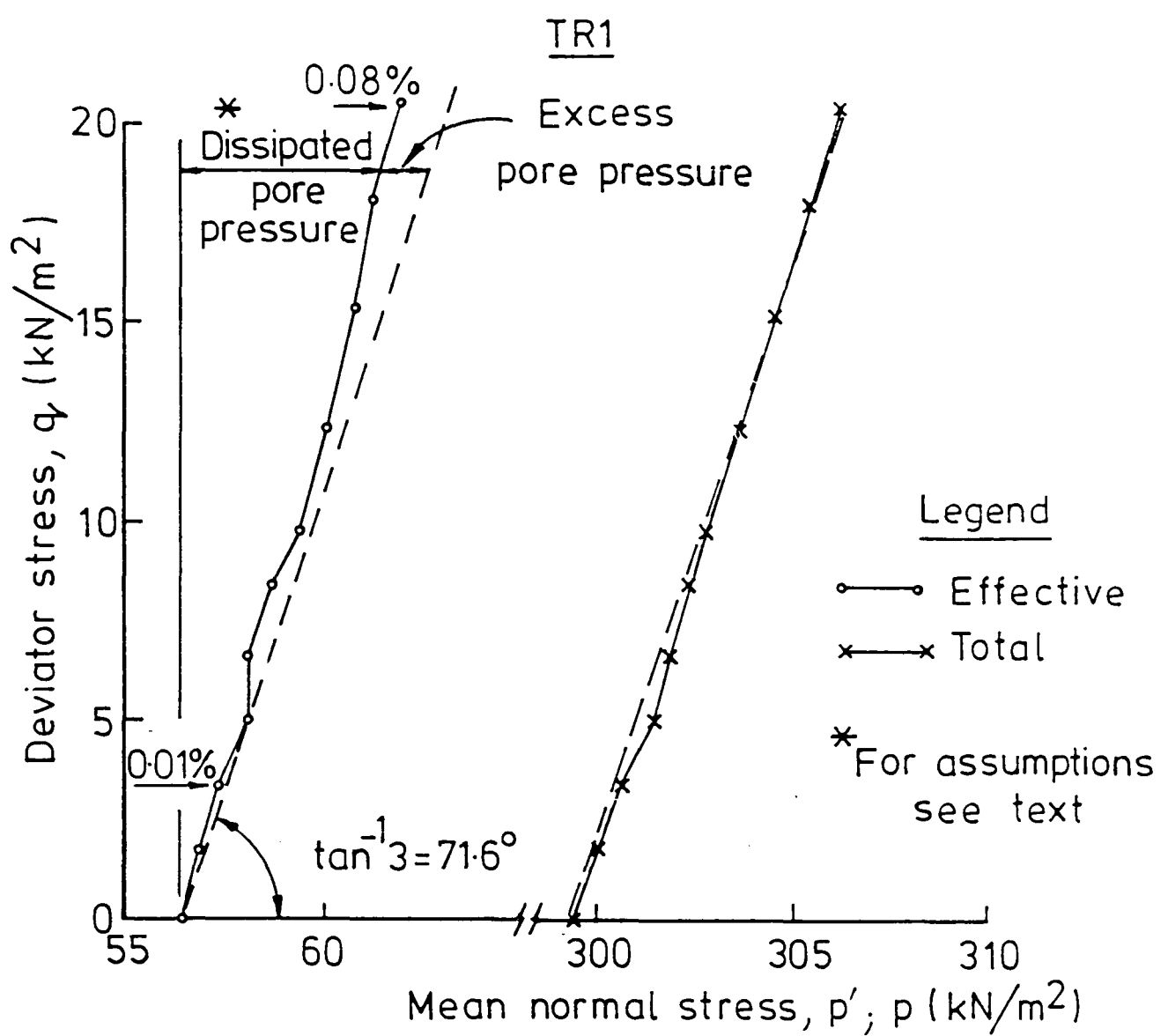
FIG 5.14   STRESS PATHS OF PROVING TESTS TR1 & TR2

(a) Tests T1UV, T2UH, T3DV, T4DH, RT5UV, RT6DH

(b) Test T7DV

(c) Test T8DV
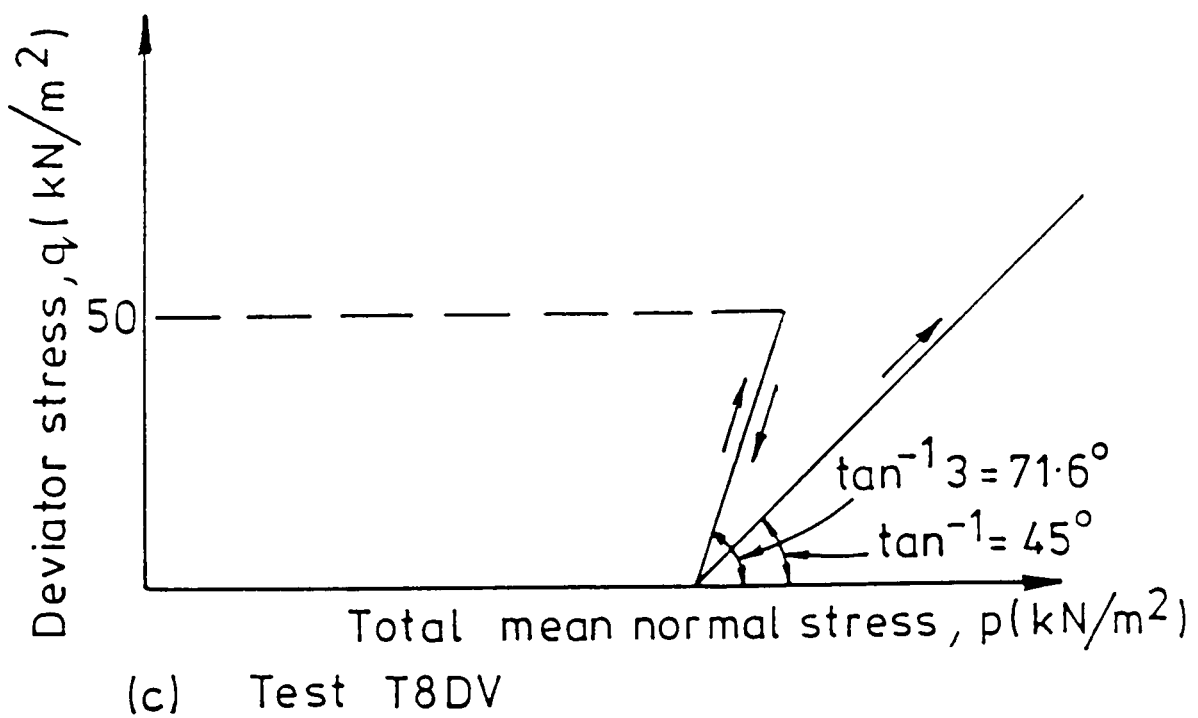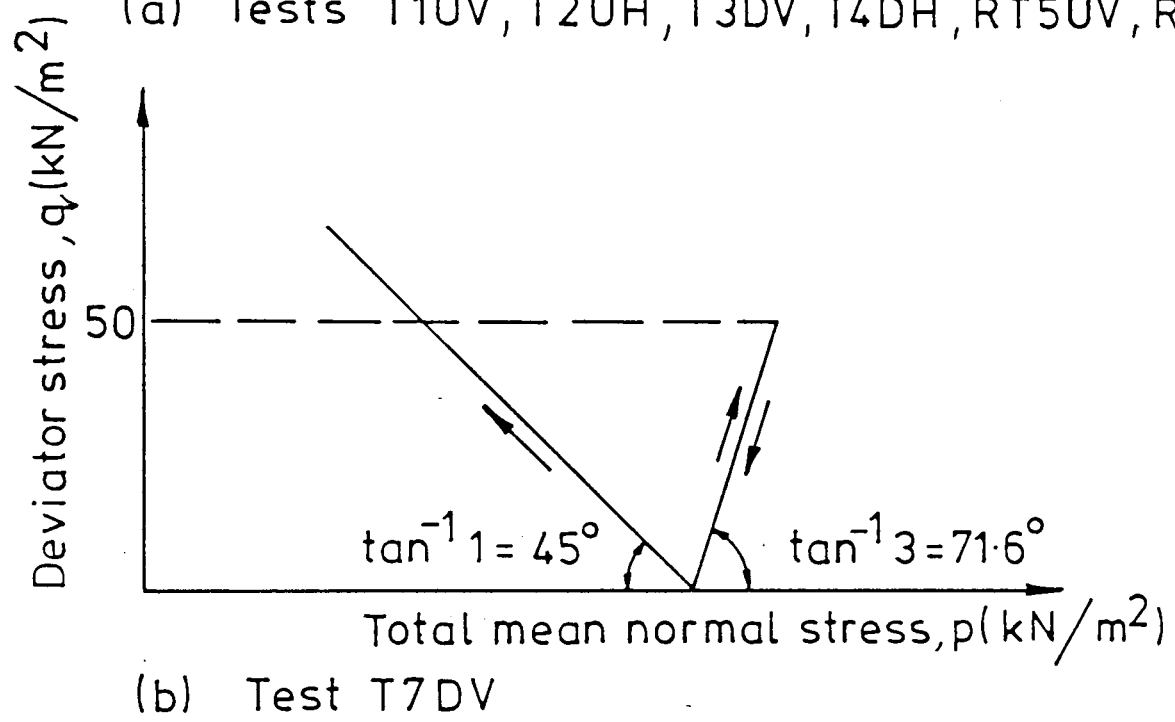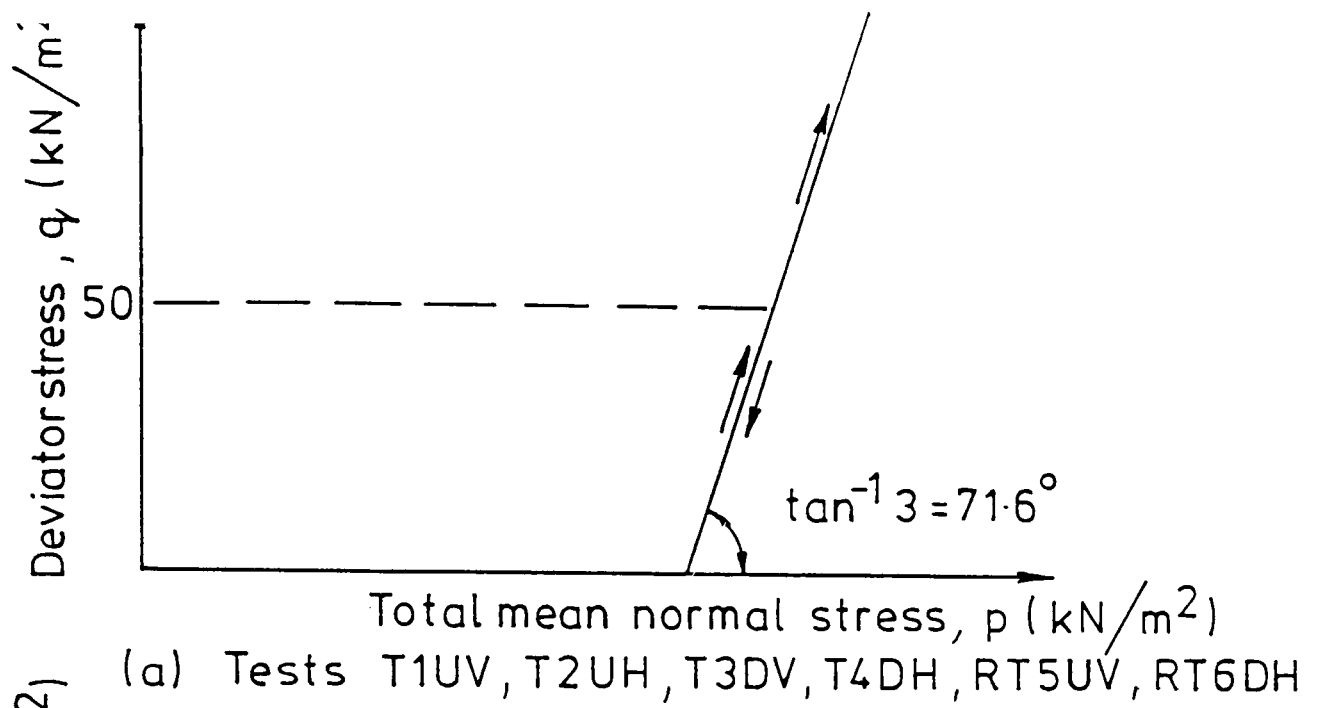
FIG. 5·15 SUMMARY OF TOTAL STRESS PATHS IN p−q
PLANE FOR MAIN TESTS
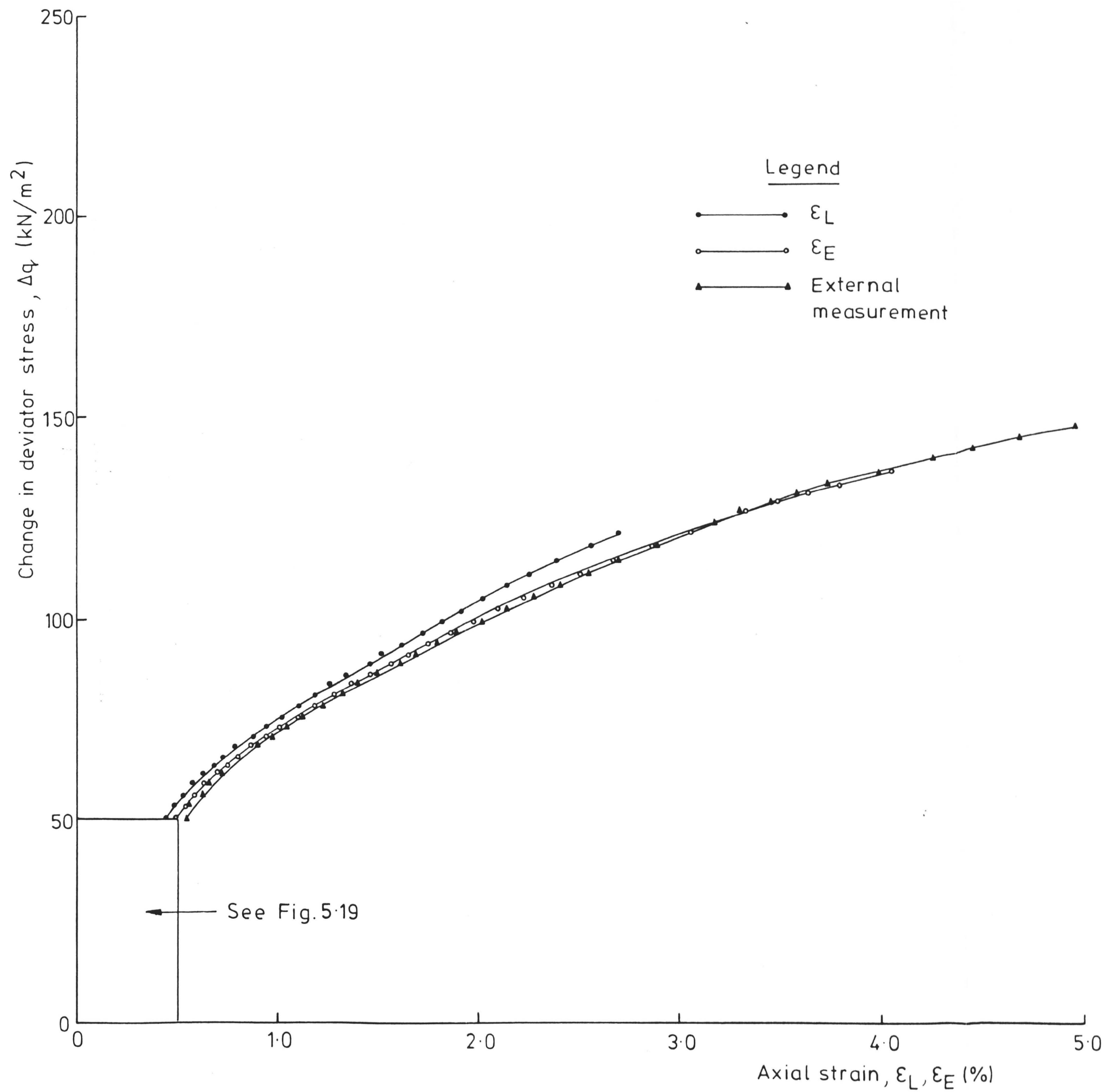
FIG. 5·16

FIG. 5·16   STRESS — STRAIN CURVES OF TEST T1UV
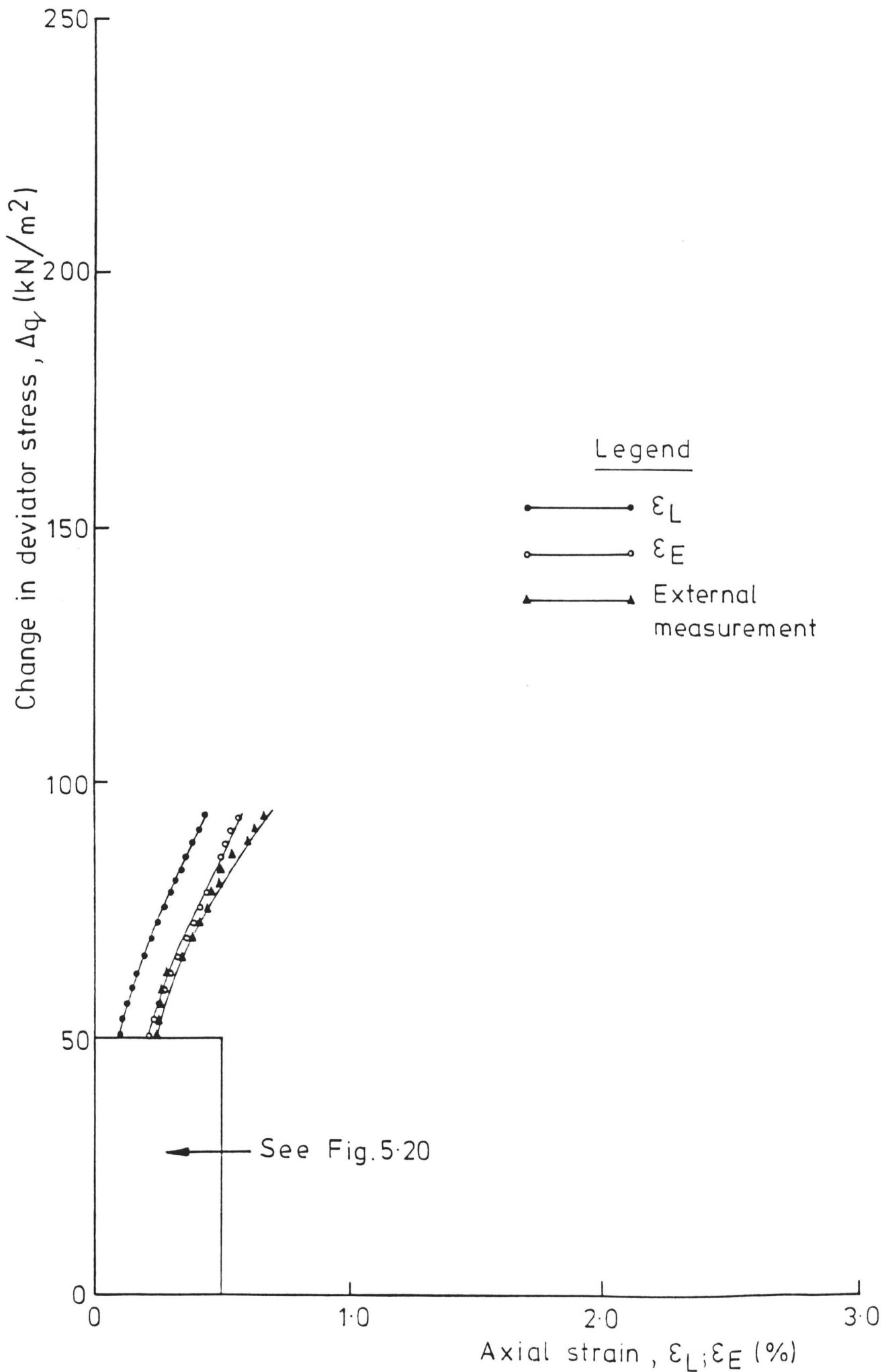
FIG.5·17   STRESS—STRAIN CURVES OF TEST T2UH
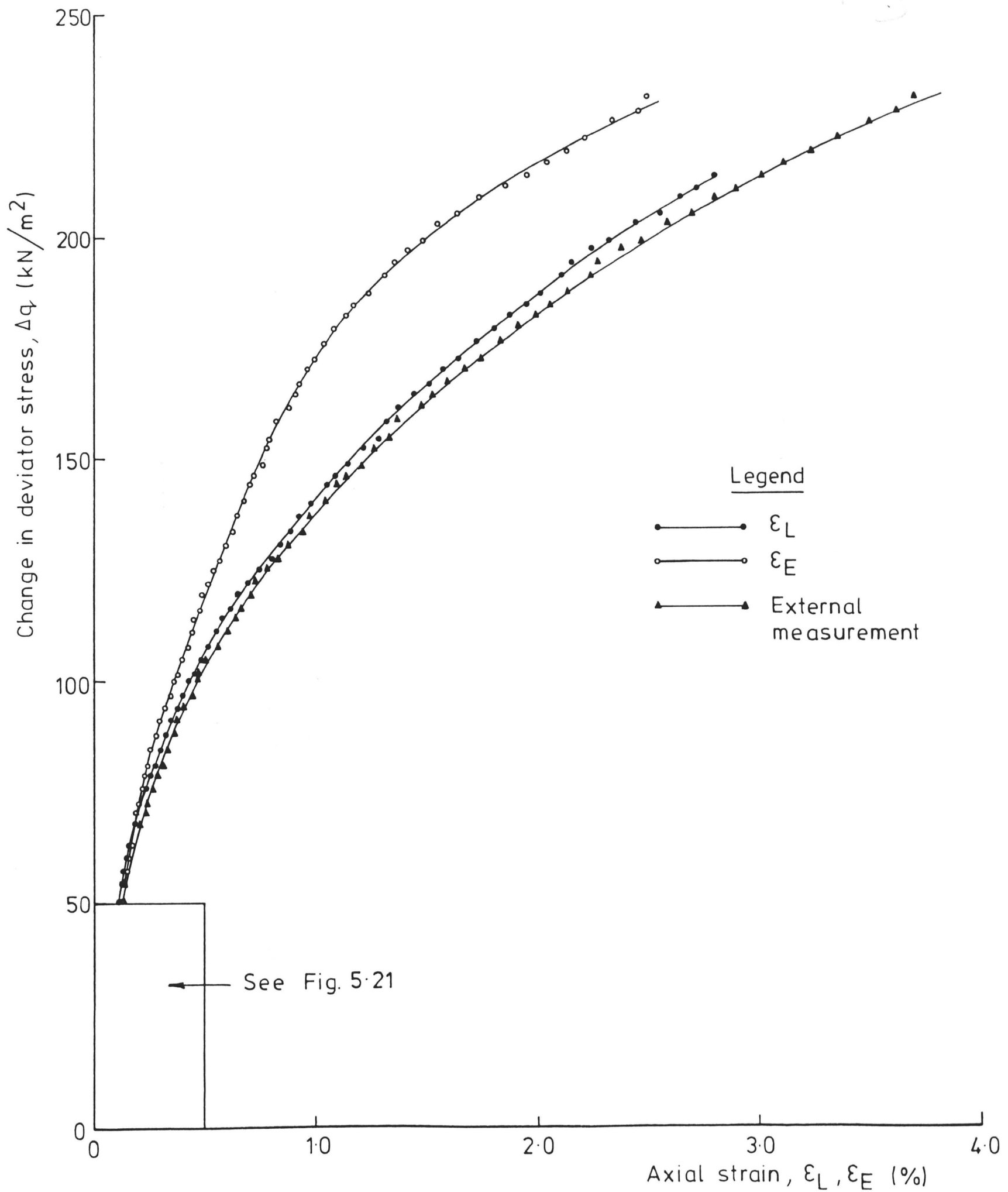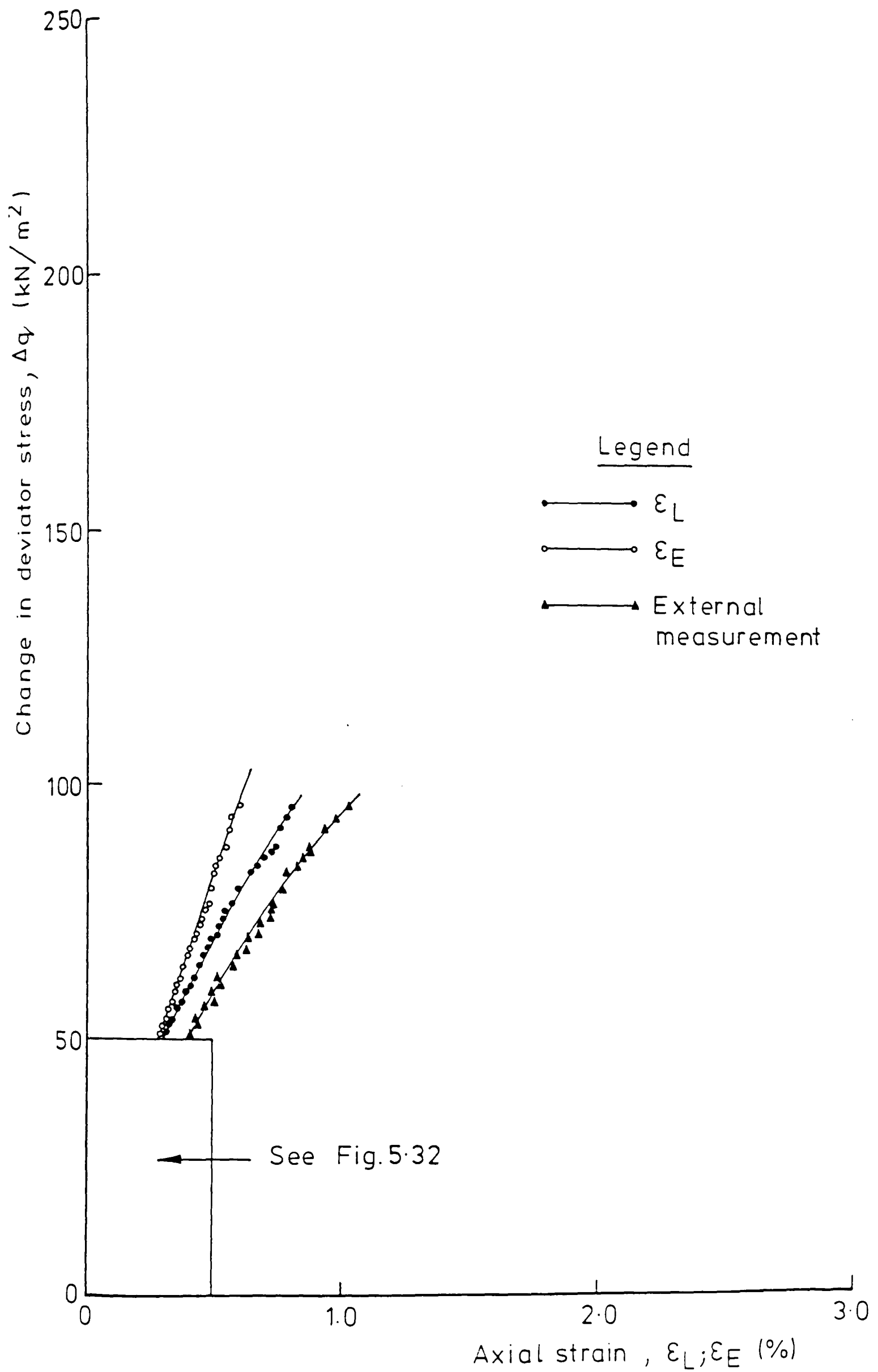
FIG.5·18

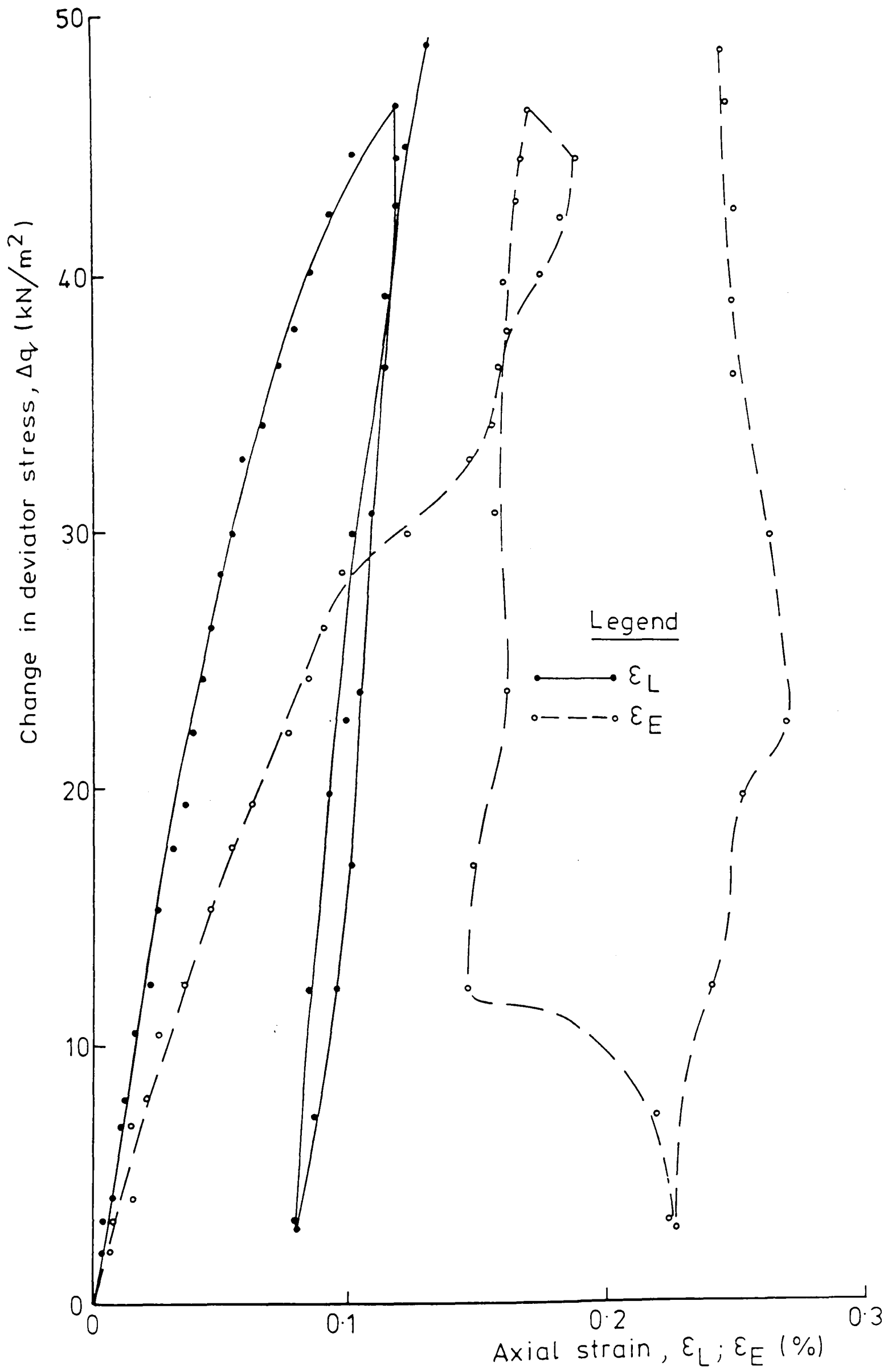FIG.5·18   STRESS — STRAIN CURVES OF TEST RT5UV
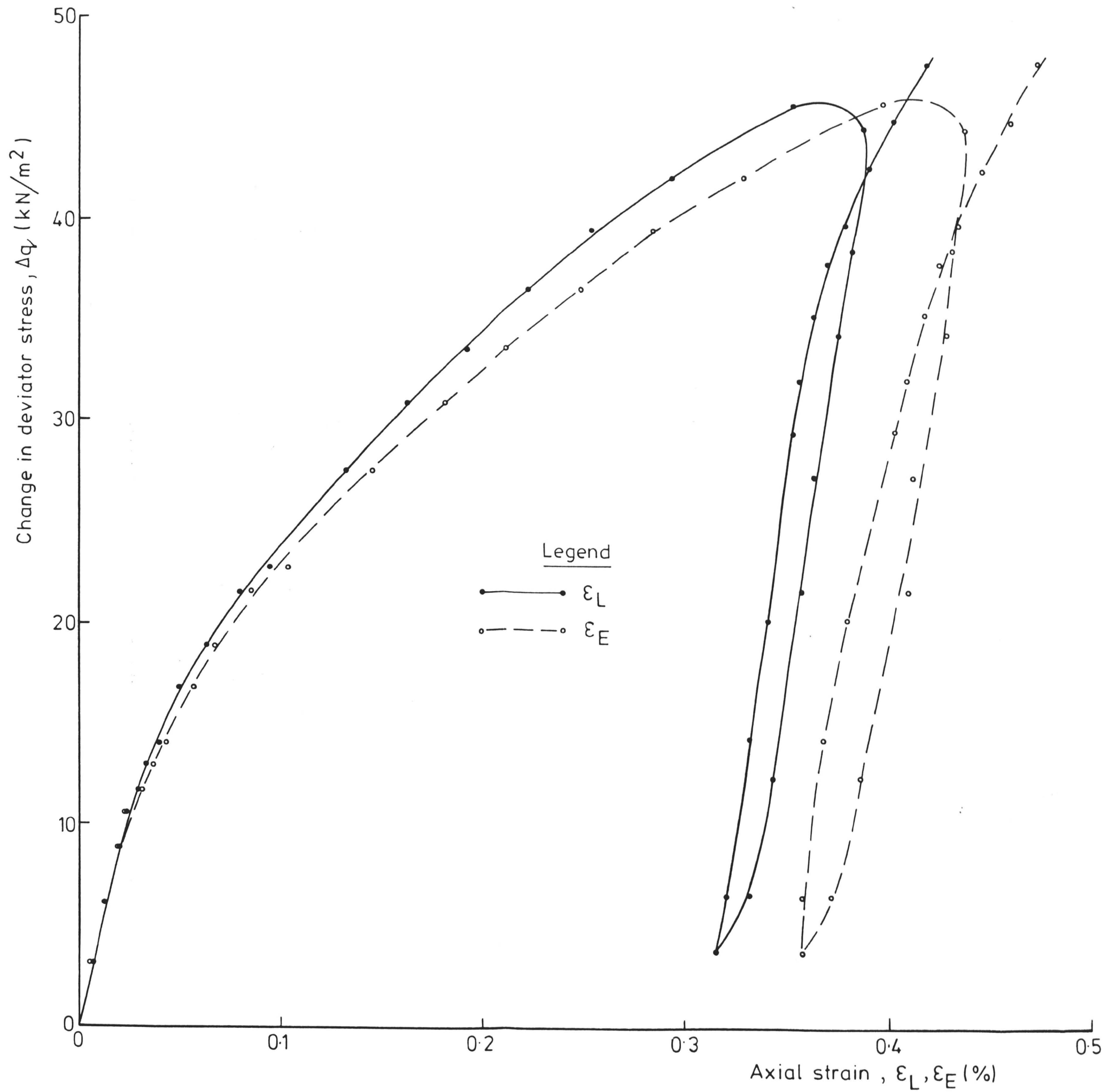
FIG. 5·19

FIG. 5·19   STRESS-STRAIN CURVES OF TEST T1UV AT SMALL STRAINS
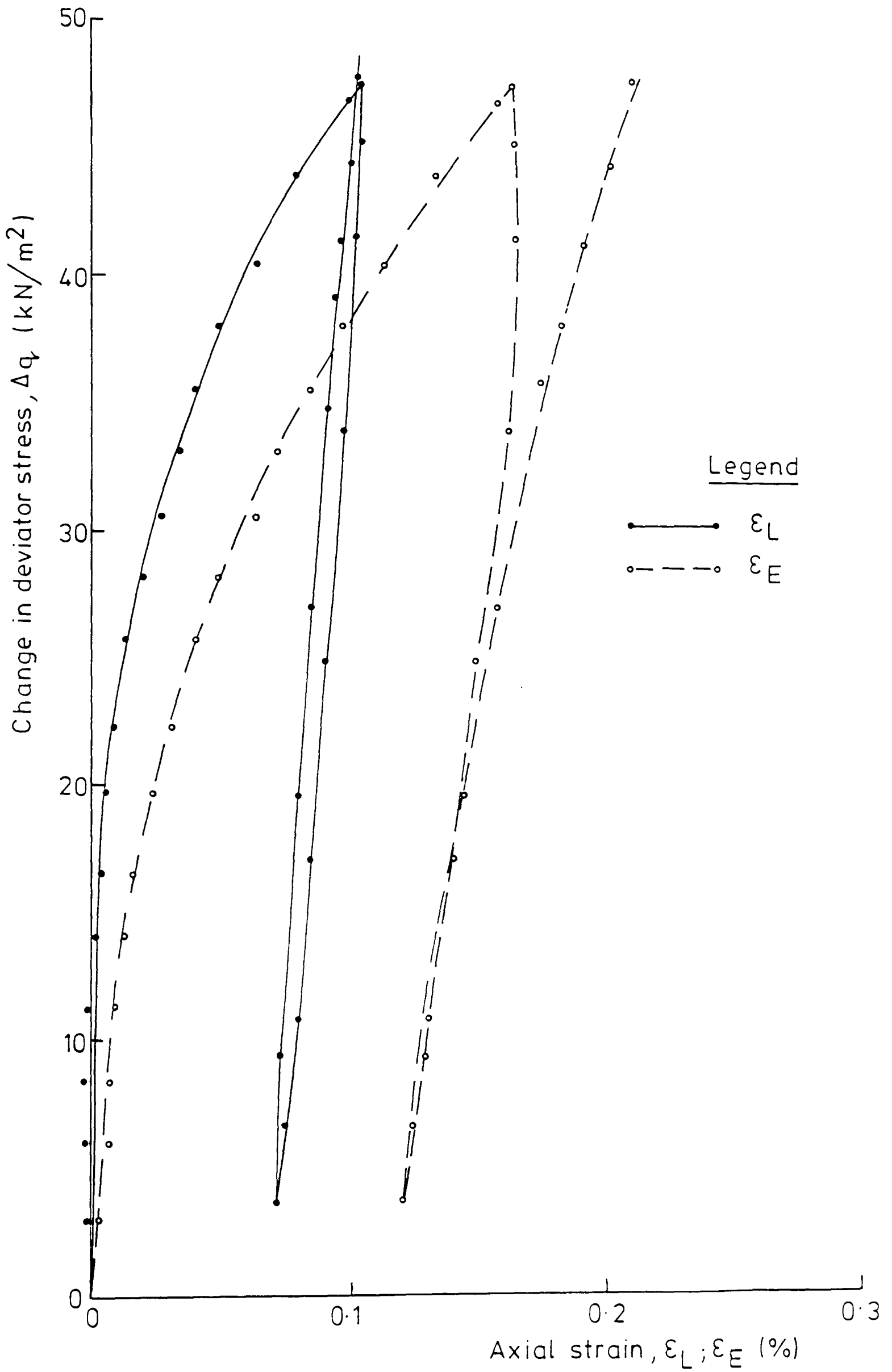
FIG. 5·20 STRESS-STRAIN CURVES OF TEST T2UH AT SMALL STRAINS
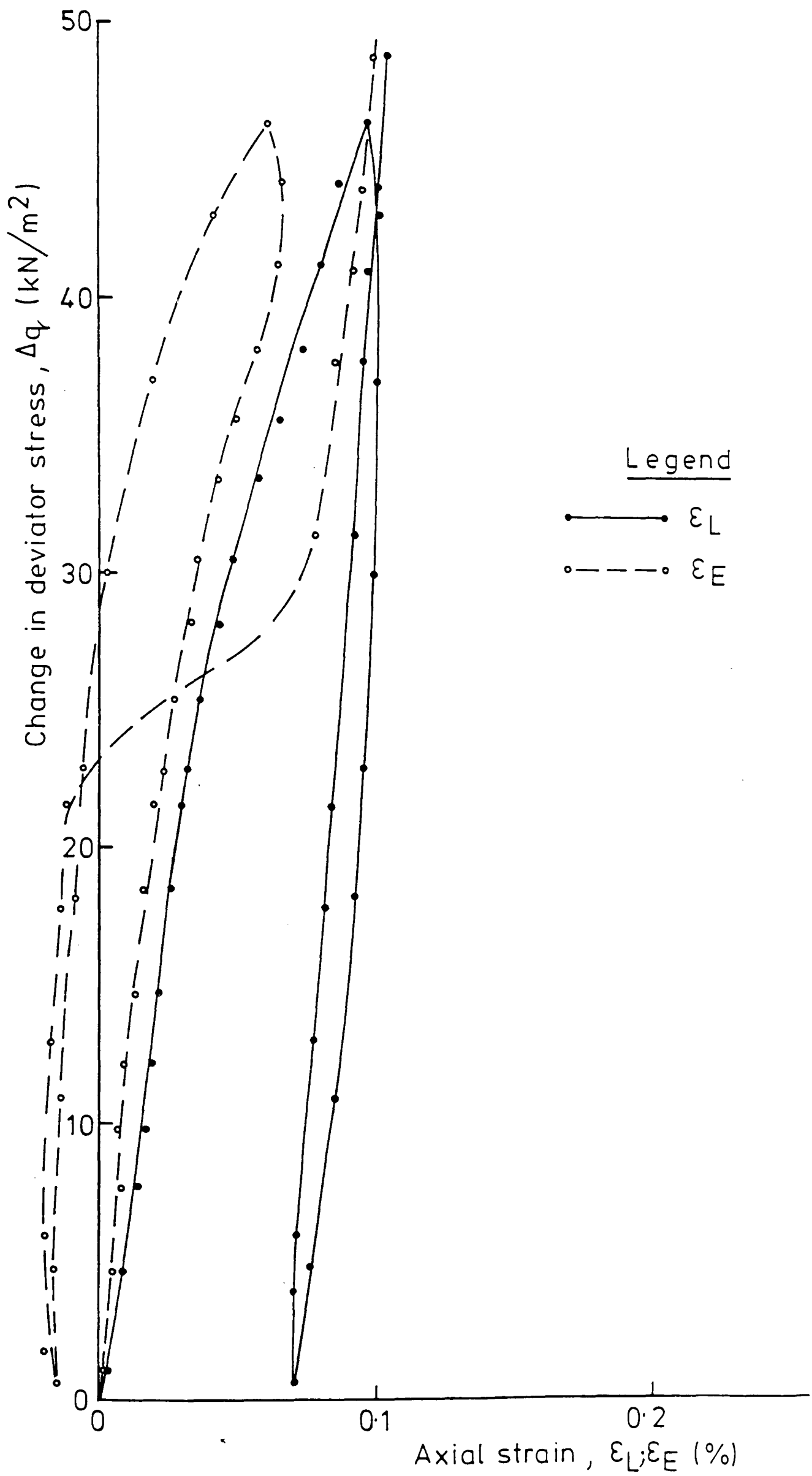
FIG.5·21   STRESS – STRAIN CURVES OF TEST RT5UV AT SMALL STRAINS
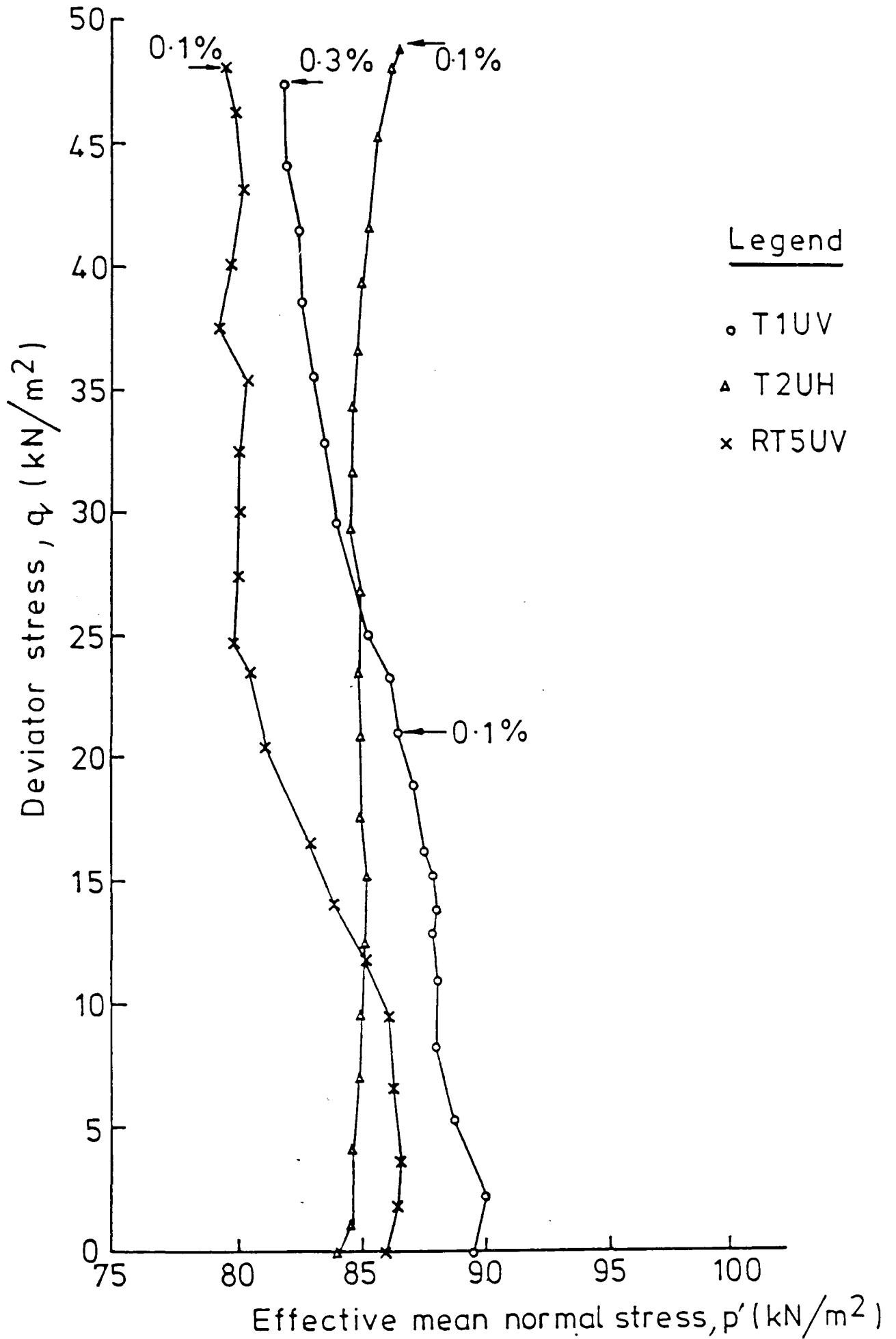
FIG. 5·22 EFFECTIVE STRESS PATHS OF
MAIN UNDRAINED TESTS
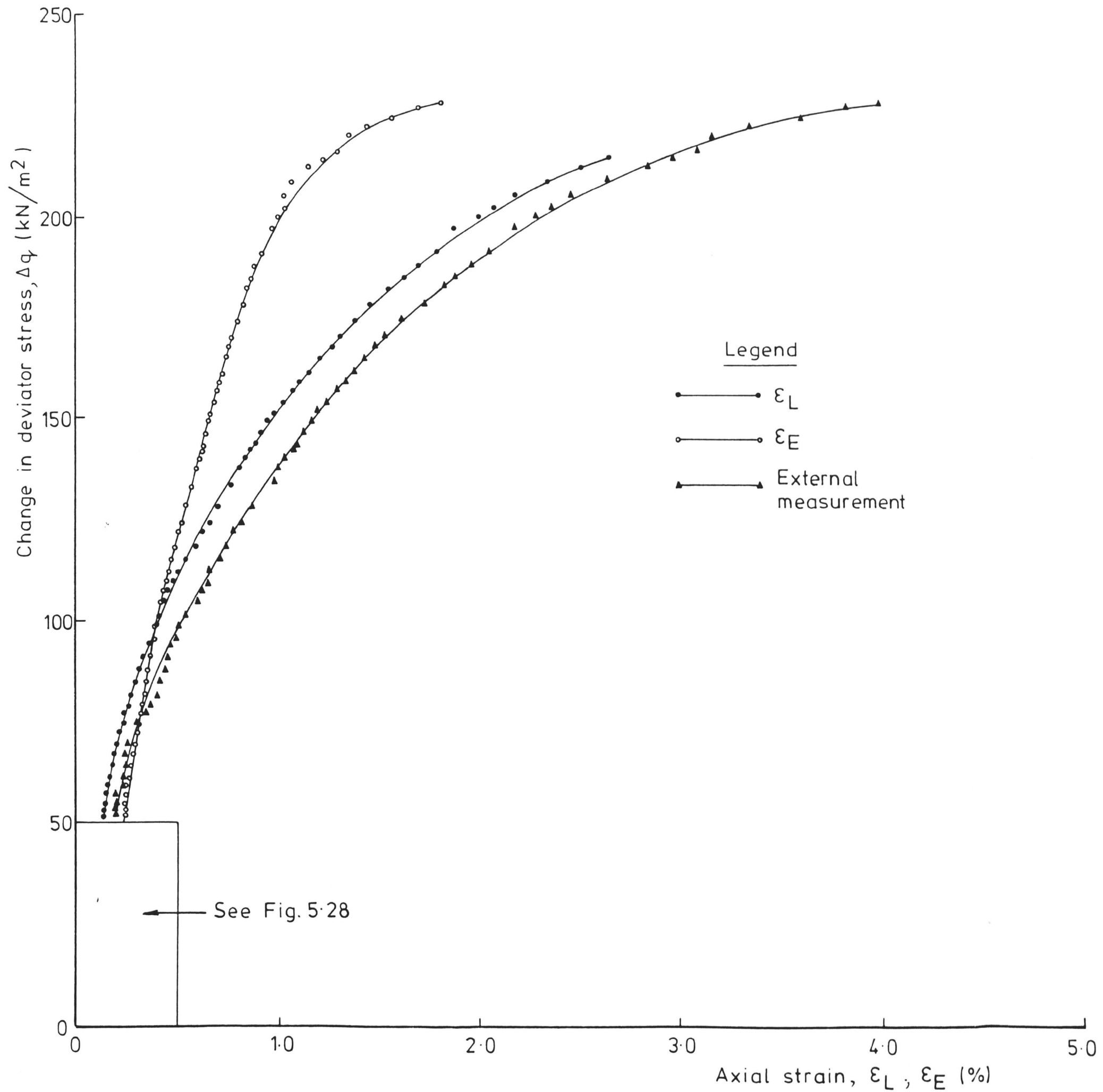
FIG. 5·23

STRESS — STRAIN CURVES OF TEST T3DV
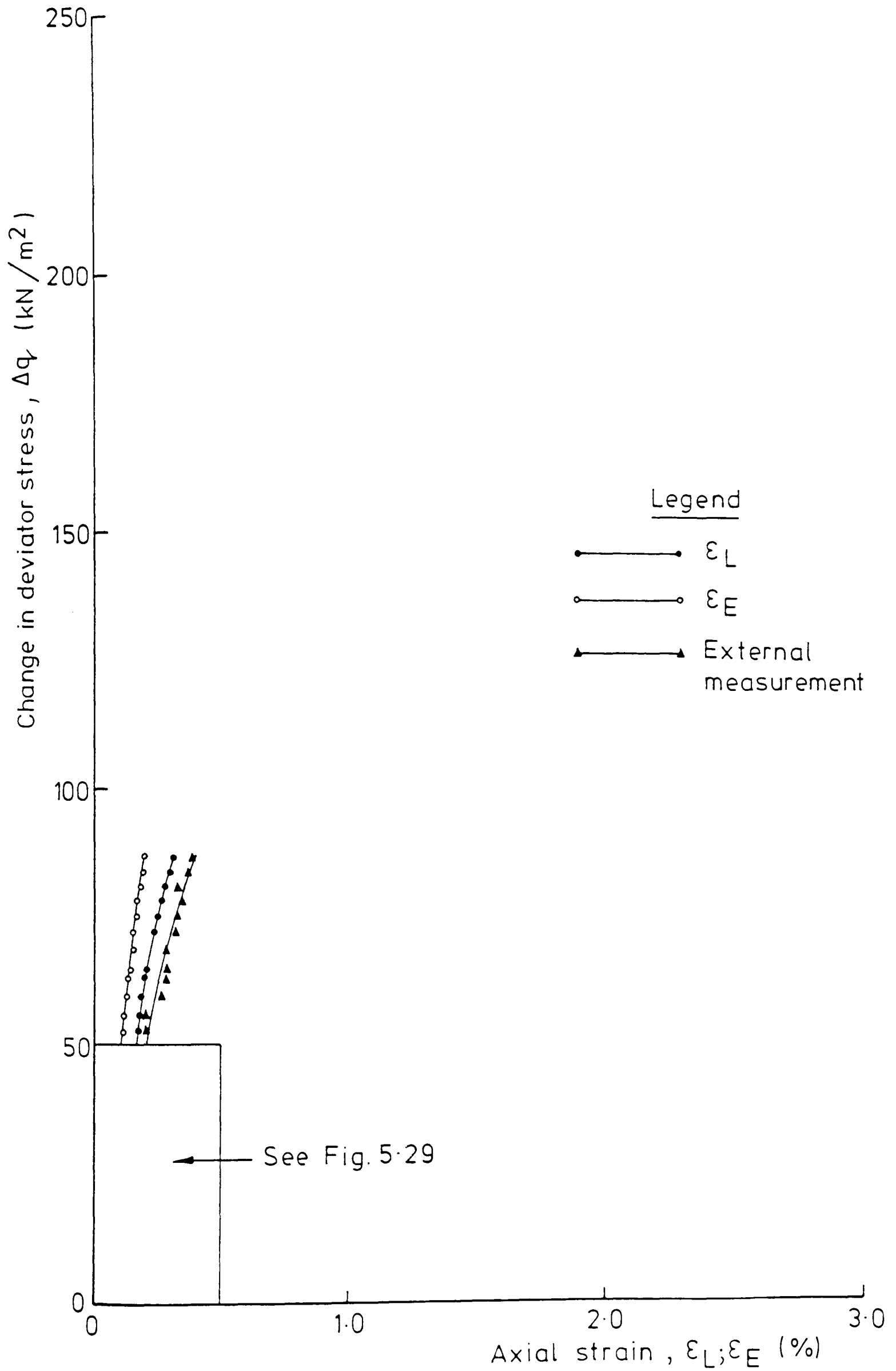
FIG.5·24 STRESS-STRAIN CURVES OF TEST T4DH
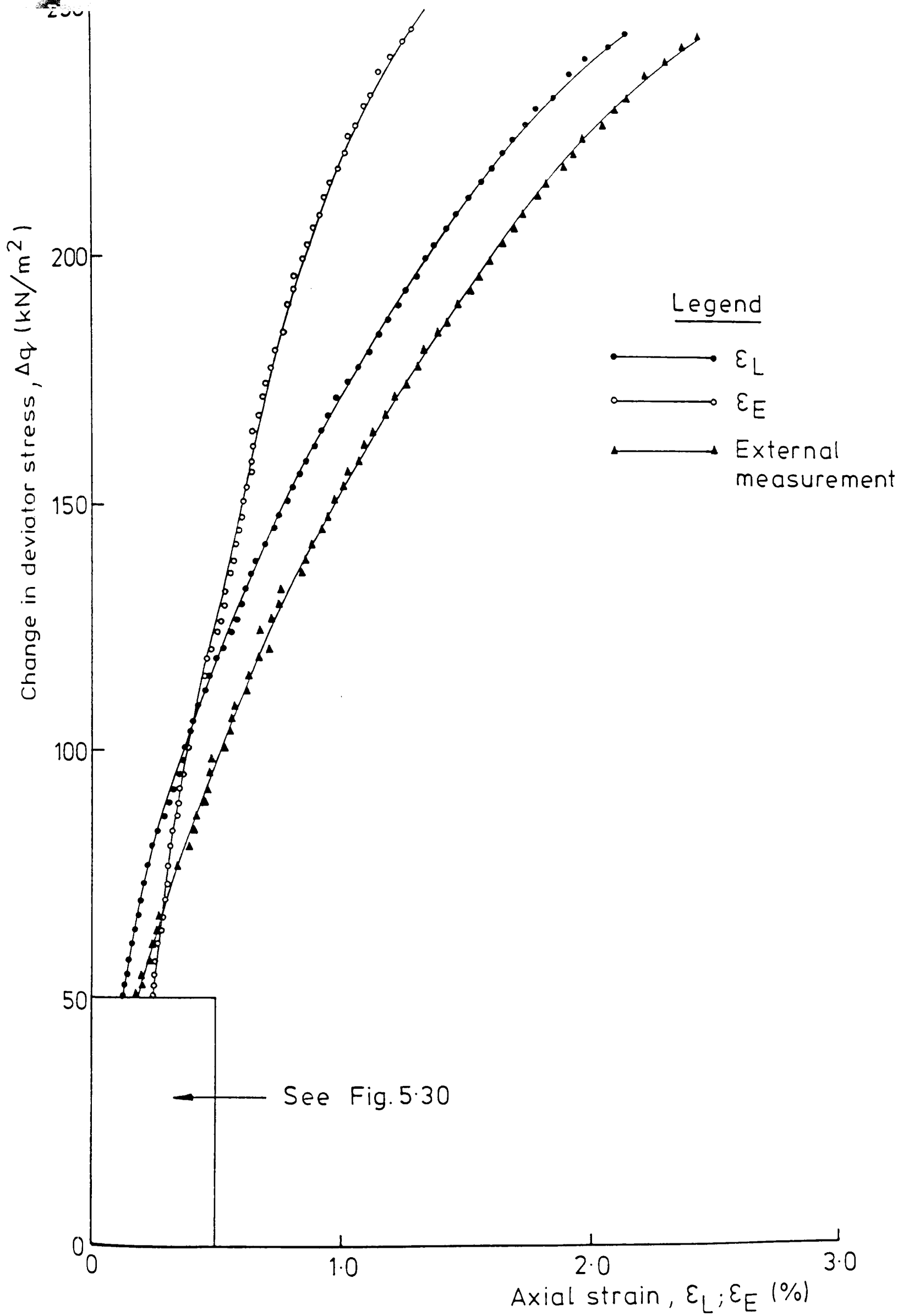
FIG. 5·25   STRESS—STRAIN CURVES OF TEST RT6DH
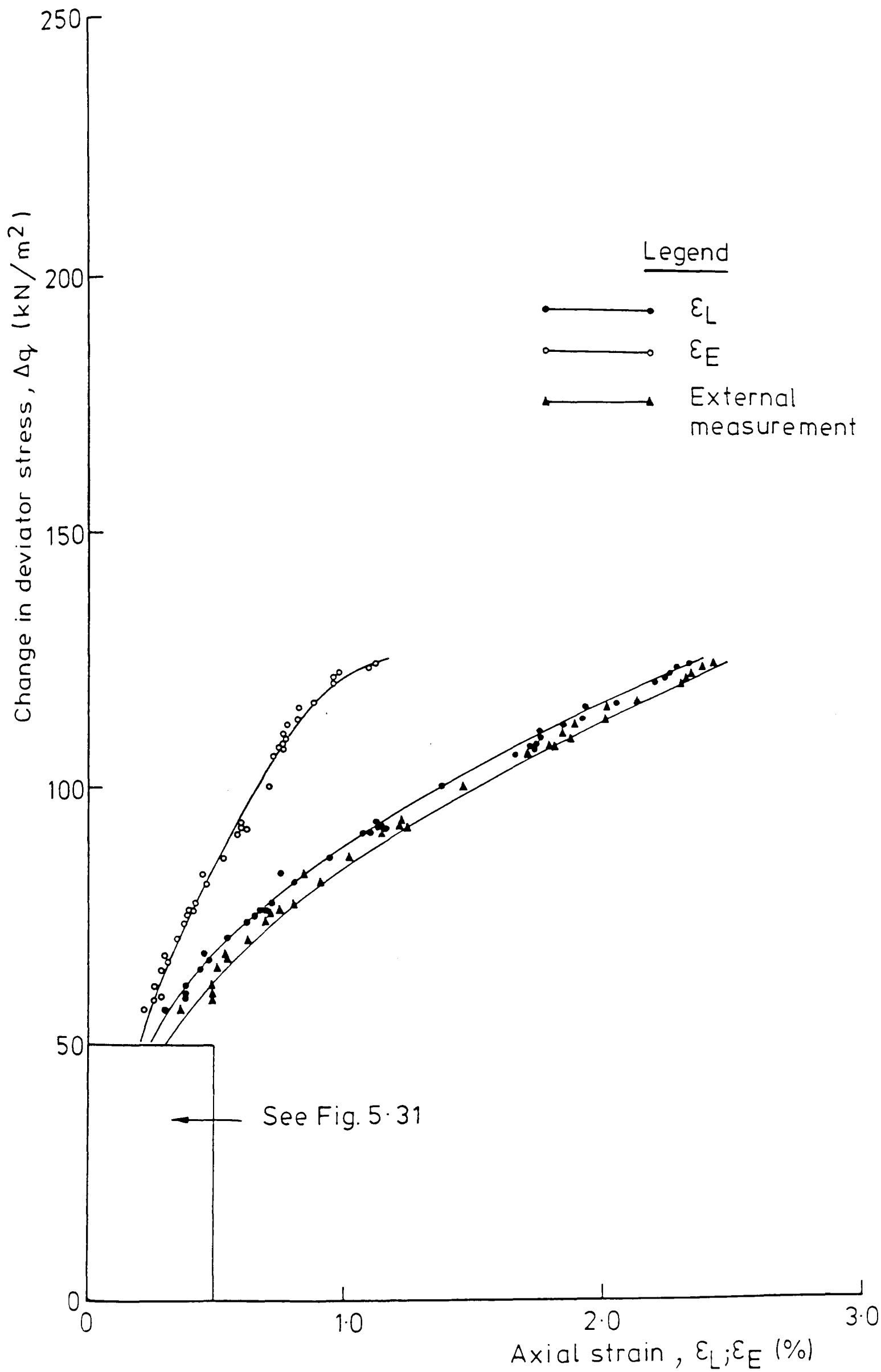
FIG. 5.26   STRESS – STRAIN CURVES OF TEST T7DV

FIG.5·27   STRESS – STRAIN CURVES OF TEST T8DV

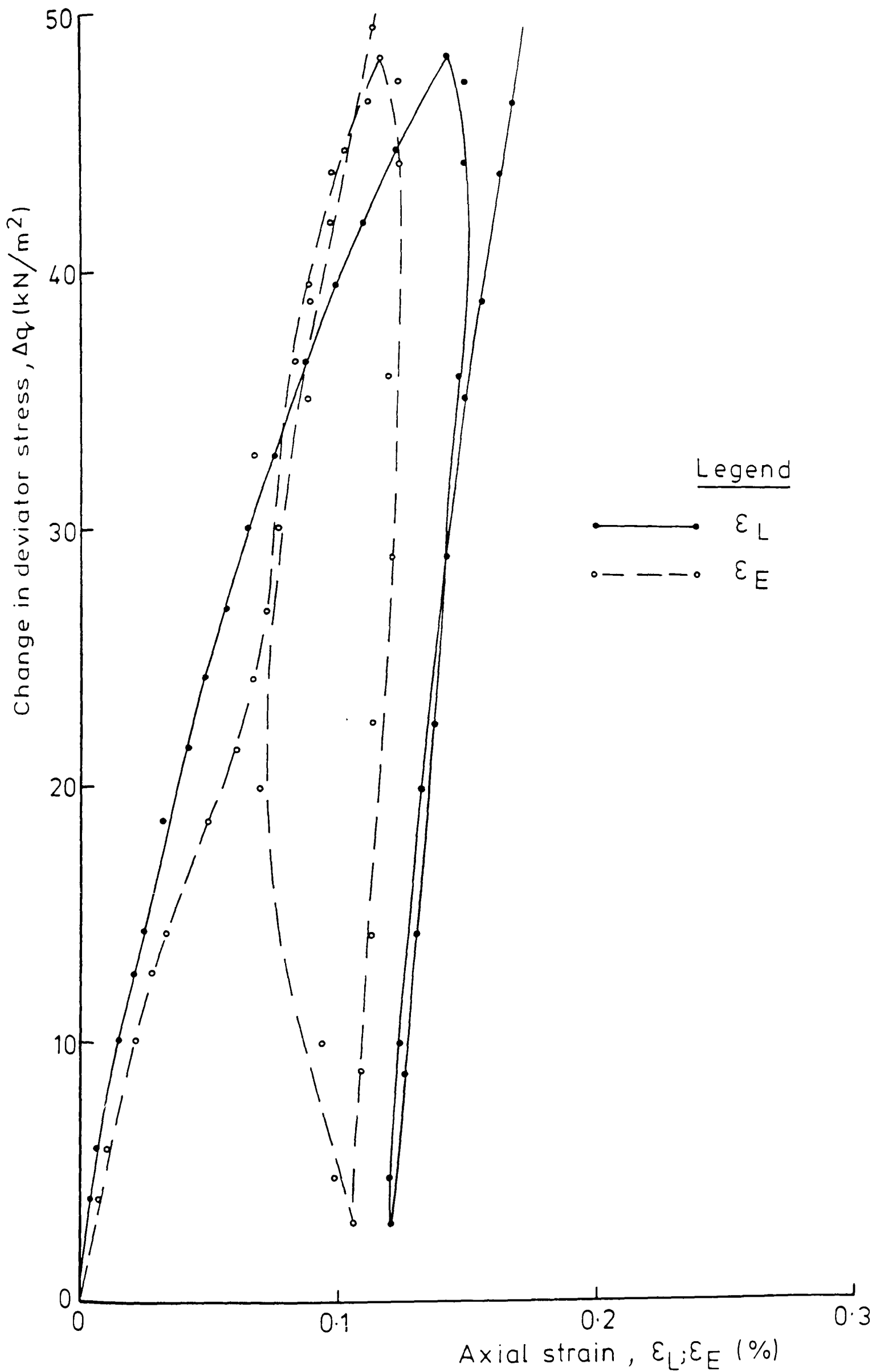FIG. 5·28 STRESS-STRAIN CURVES OF TEST T3DV AT SMALL STRAINS

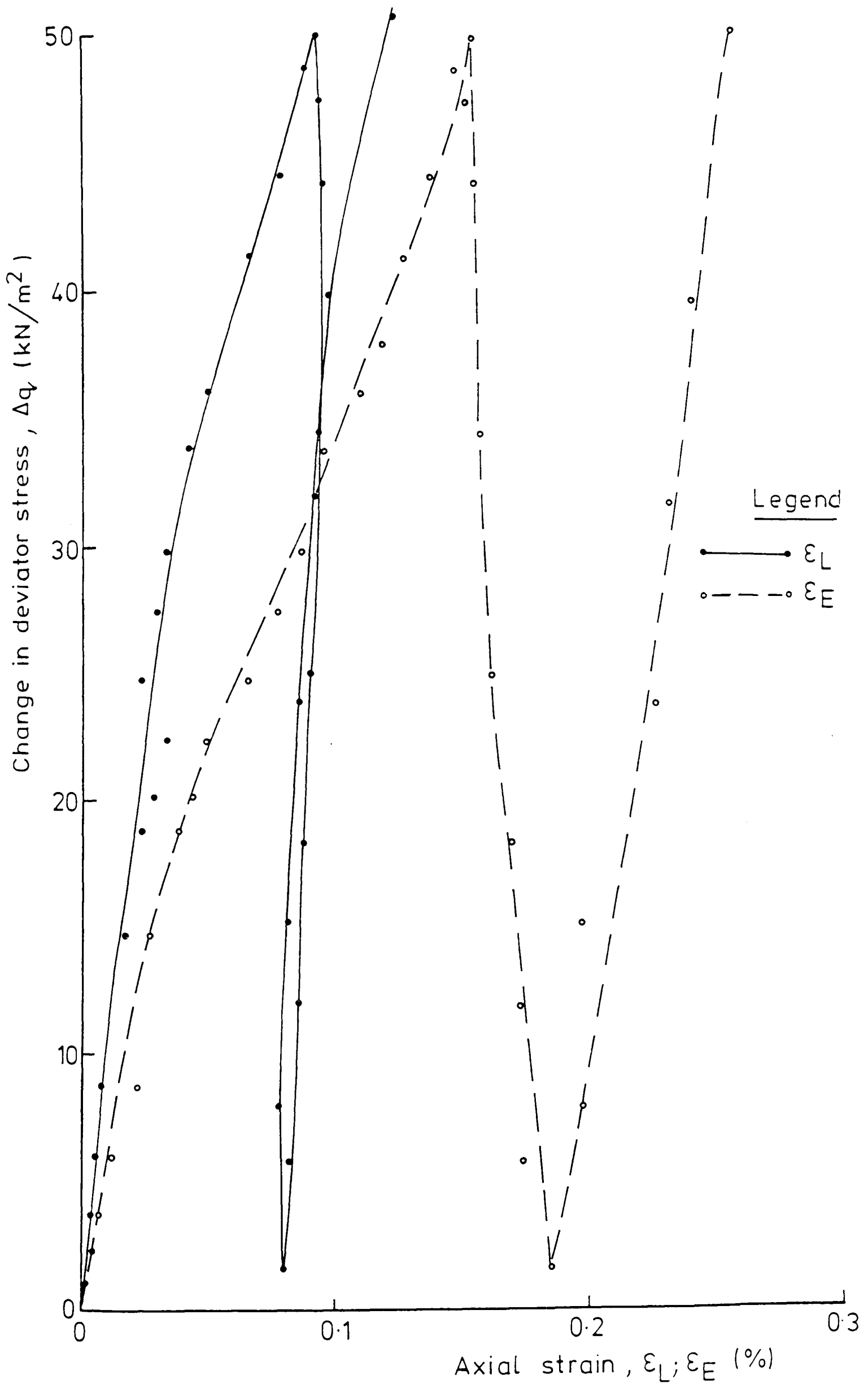FIG. 5·29   STRESS-STRAIN CURVES OF TEST T4DH AT SMALL STRAINS
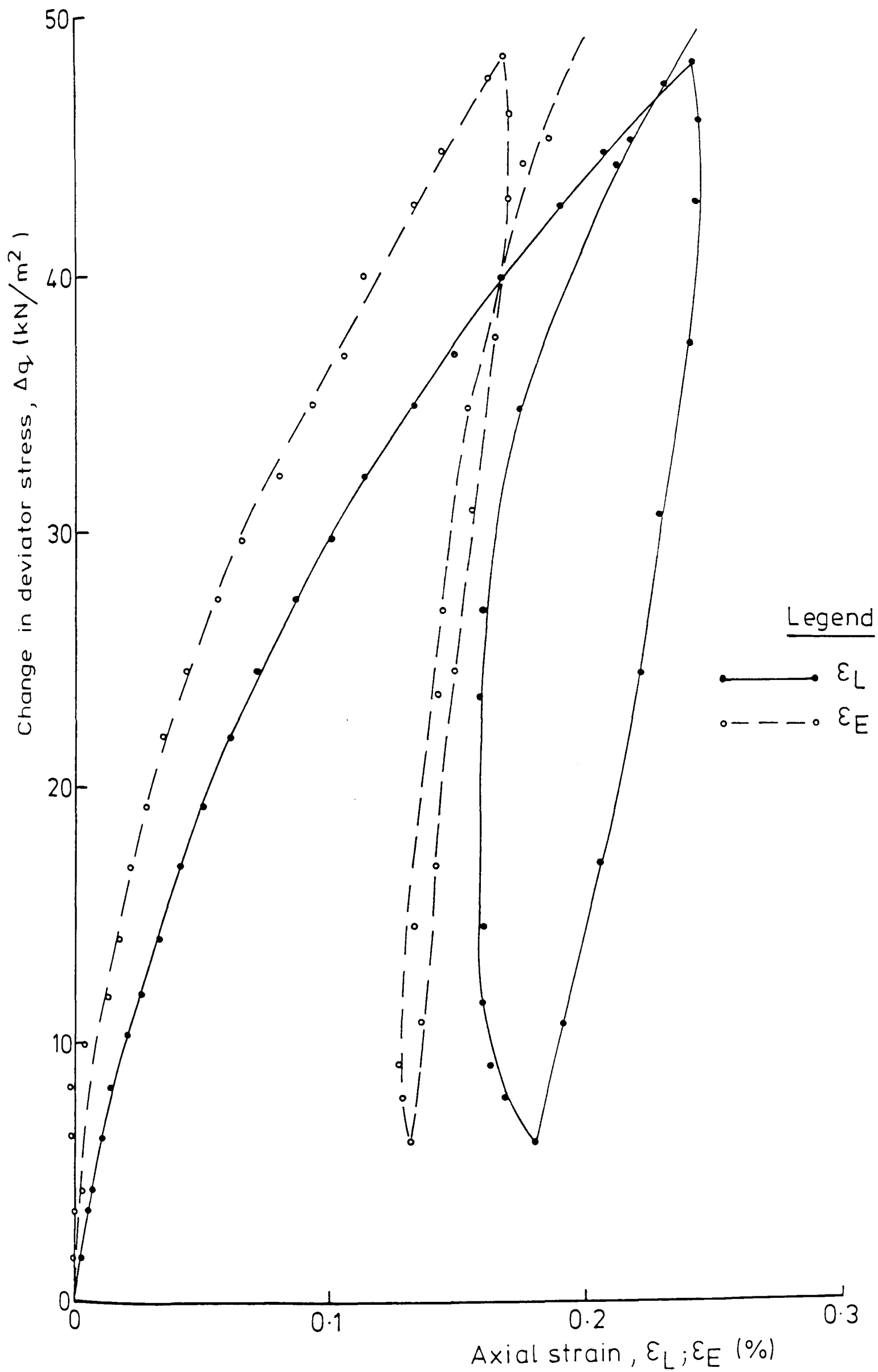
FIG.5·30 STRESS-STRAIN CURVES OF TEST RT6DH AT SMALL STRAINS

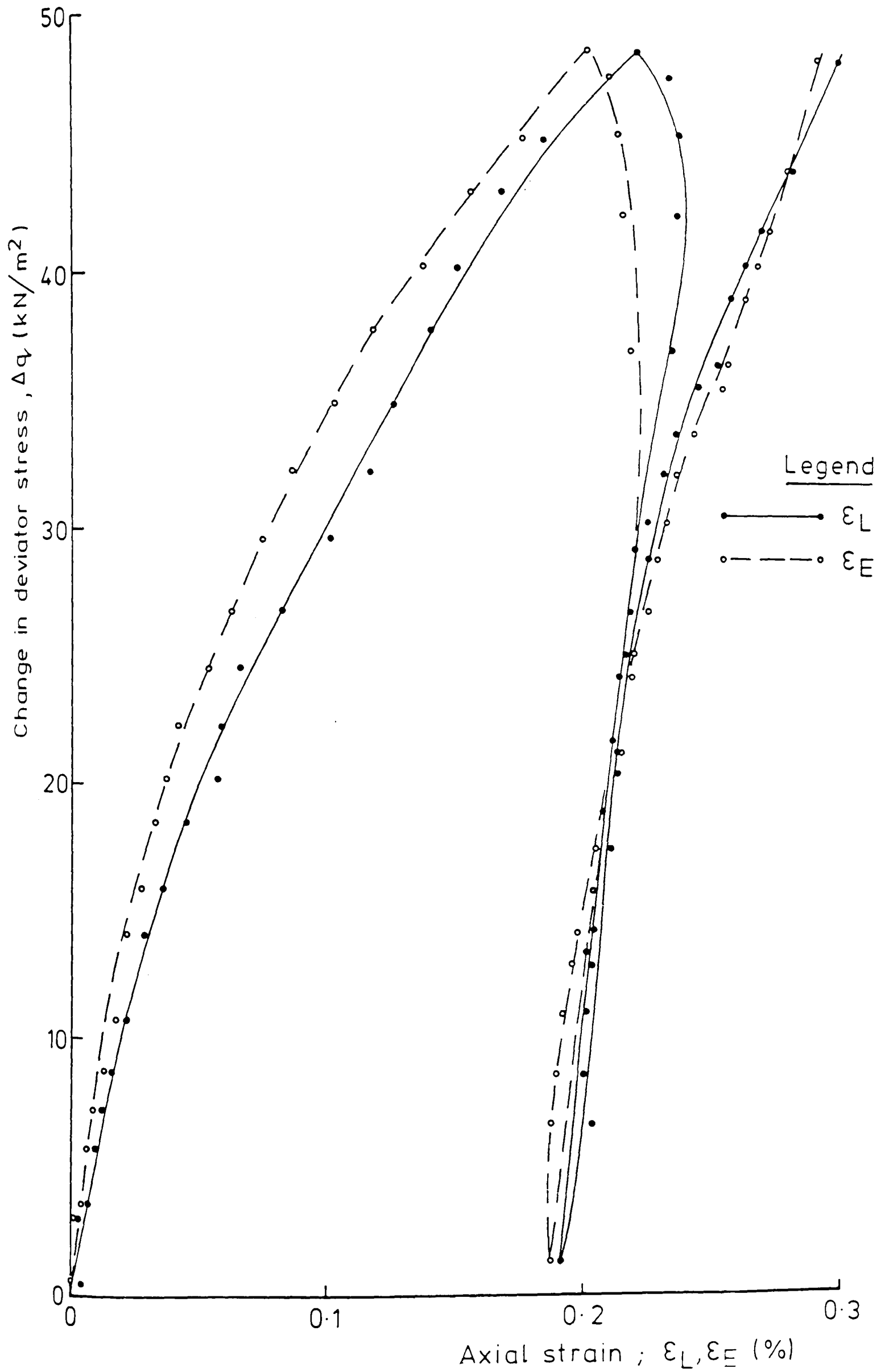IG.5·31 STRESS-STRAIN CURVES OF TEST T7DV AT SMALL STRAINS

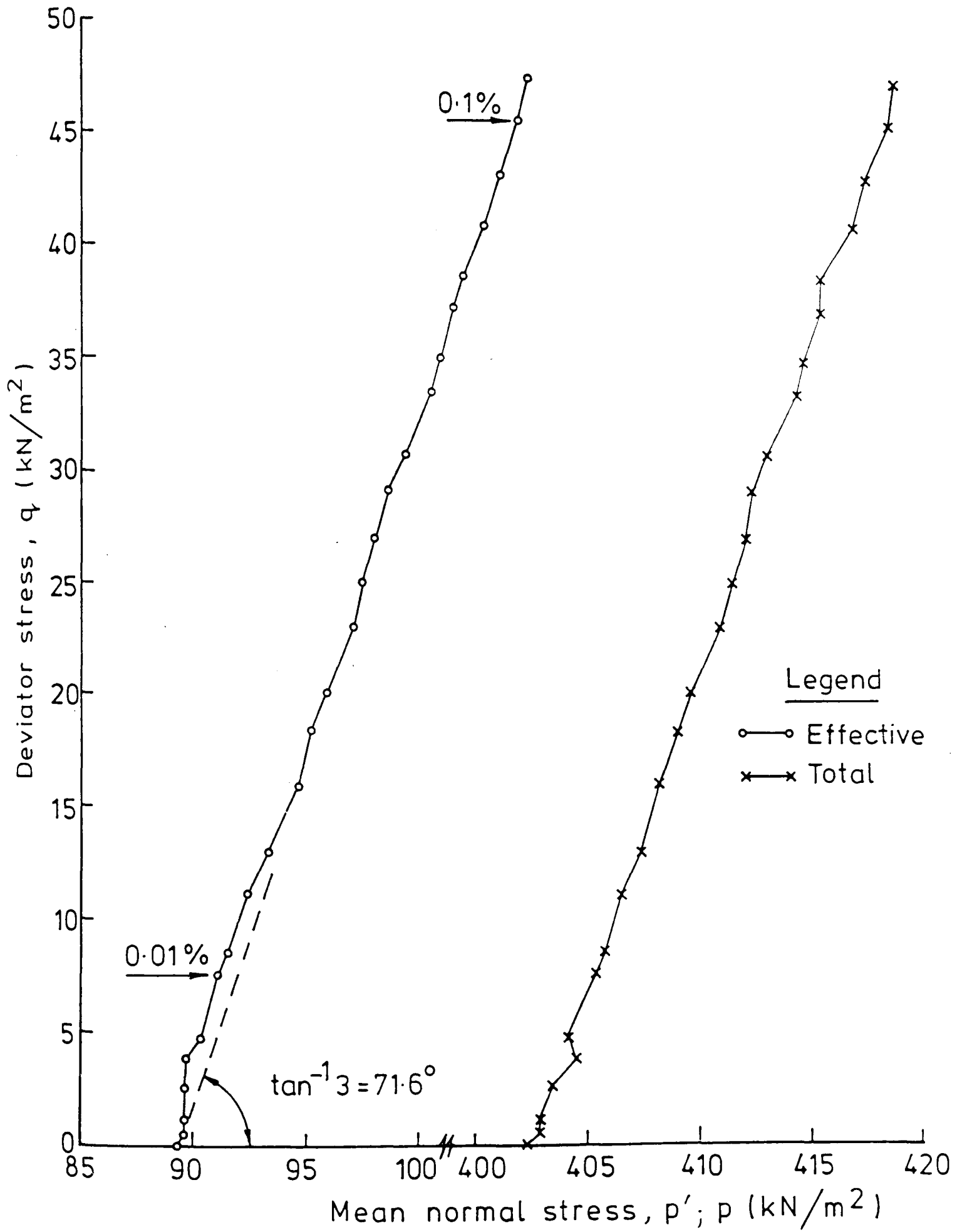FIG. 5·32   STRESS-STRAIN   CURVES OF TEST T8DV AT SMALL STRAINS
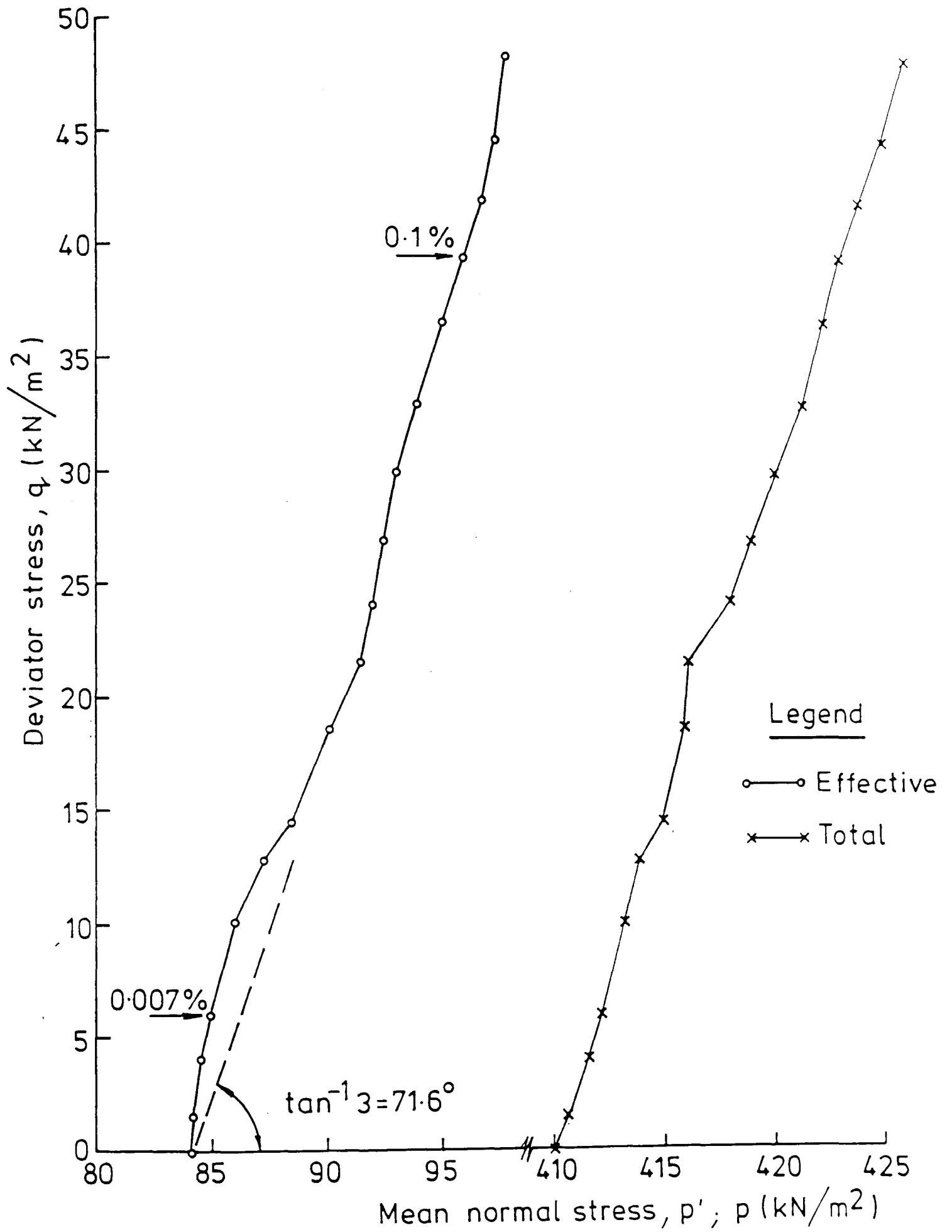
FIG. 5·33   STRESS PATHS OF TEST T3DV

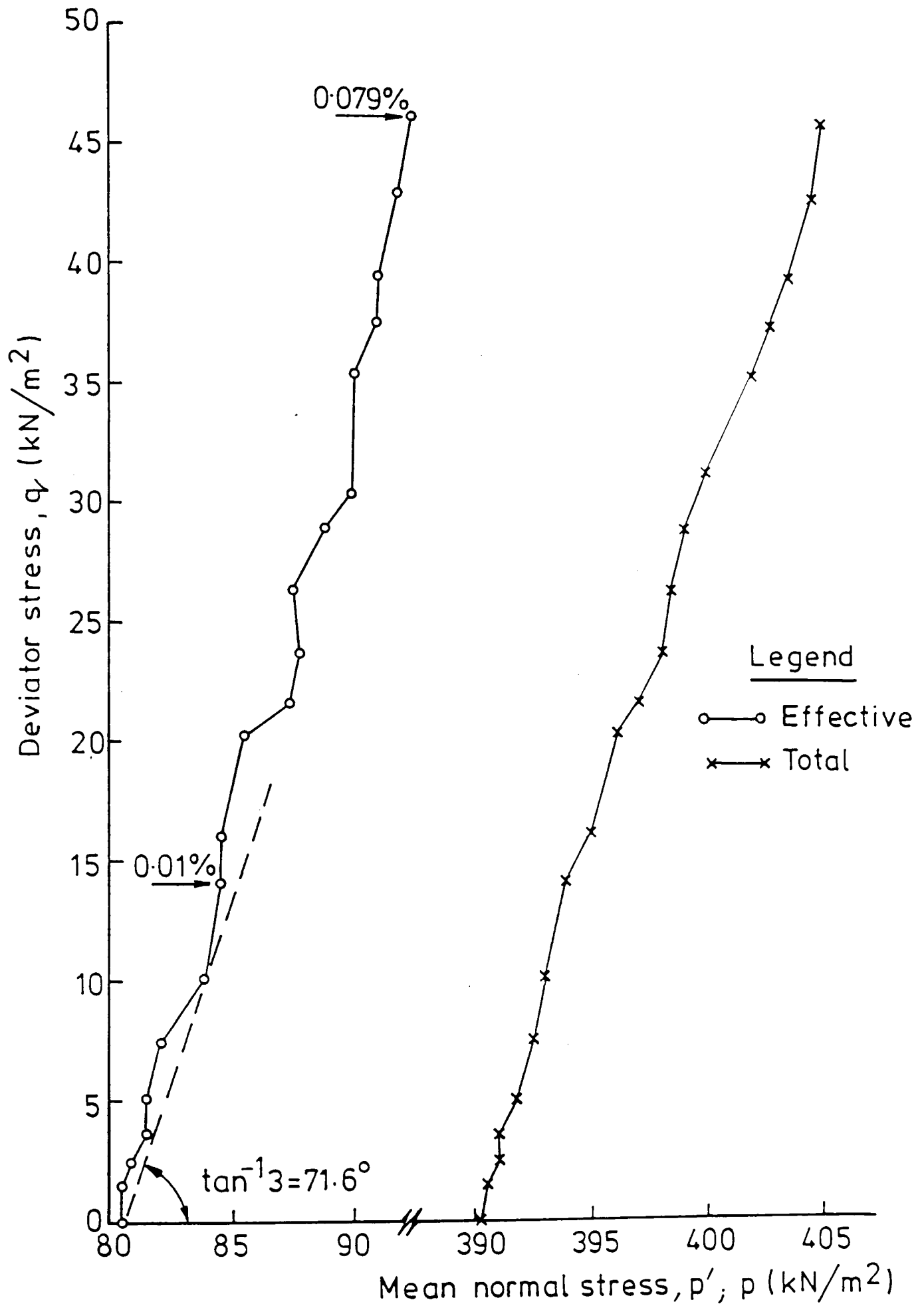FIG. 5·34 STRESS PATHS OF TEST T4DH

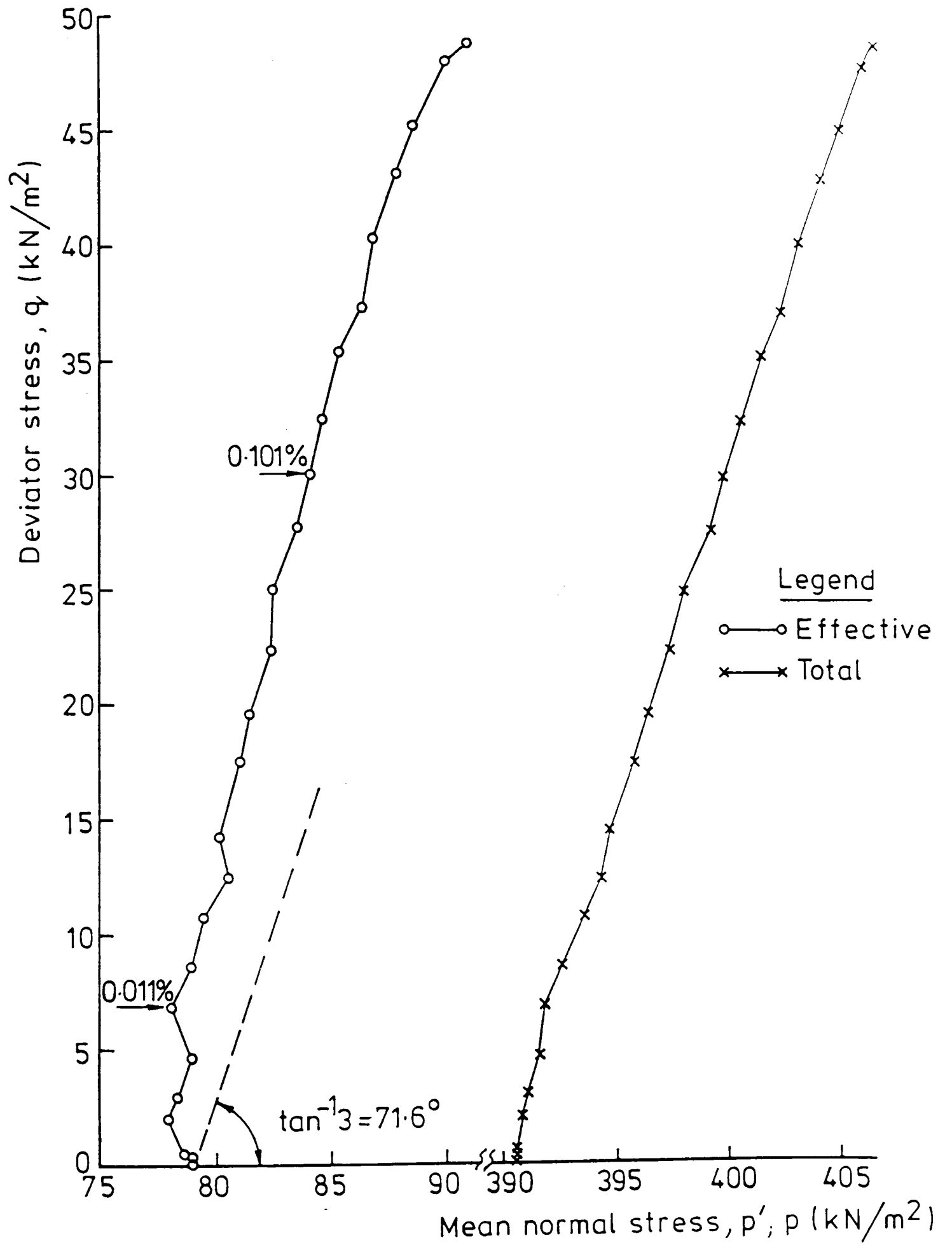FIG. 5·35   STRESS PATHS OF TEST RT6DH

FIG. 5·36   STRESS PATHS OF TEST T7DV
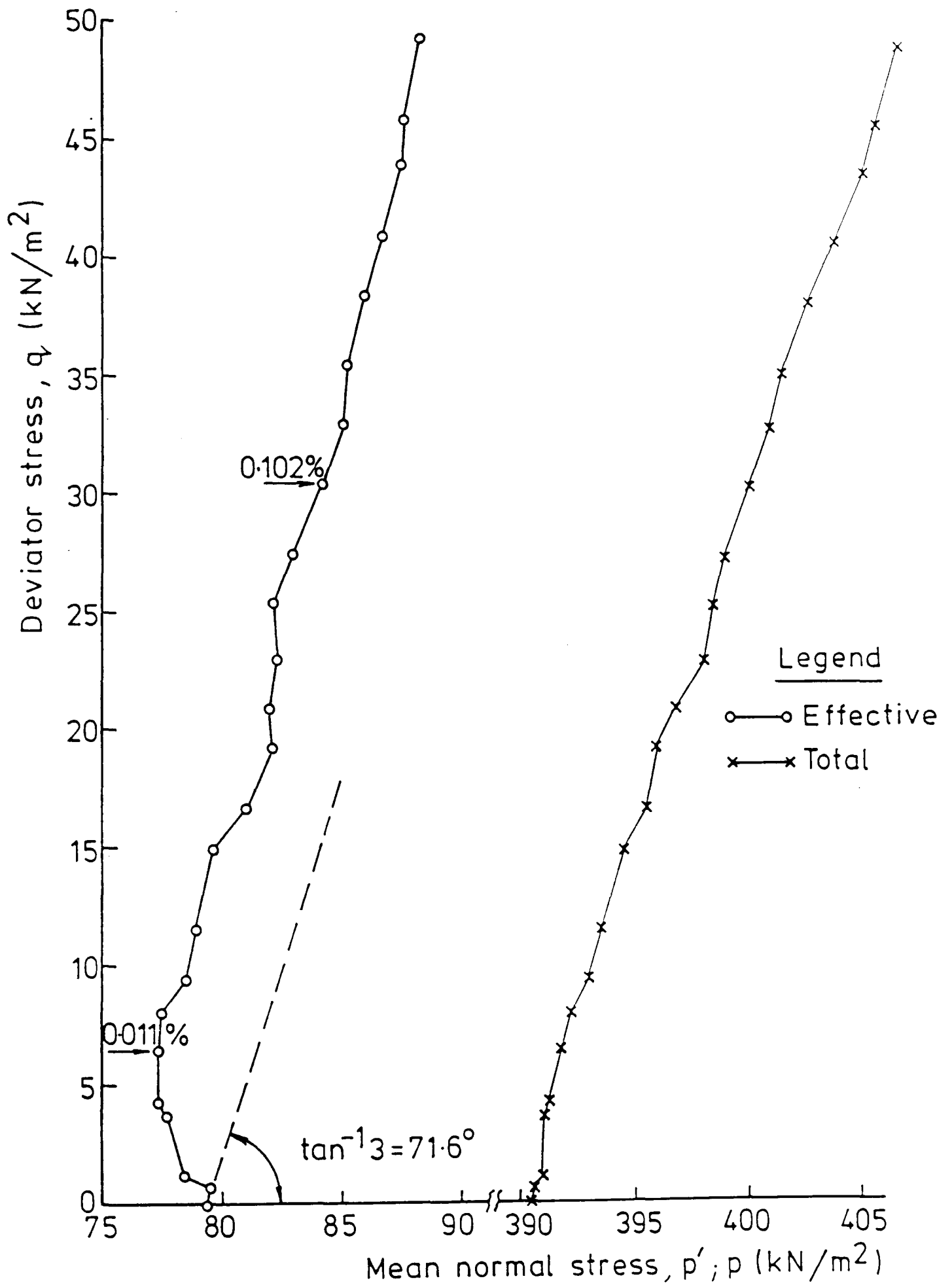
FIG. 5·37   STRESS PATHS OF TEST T8DV
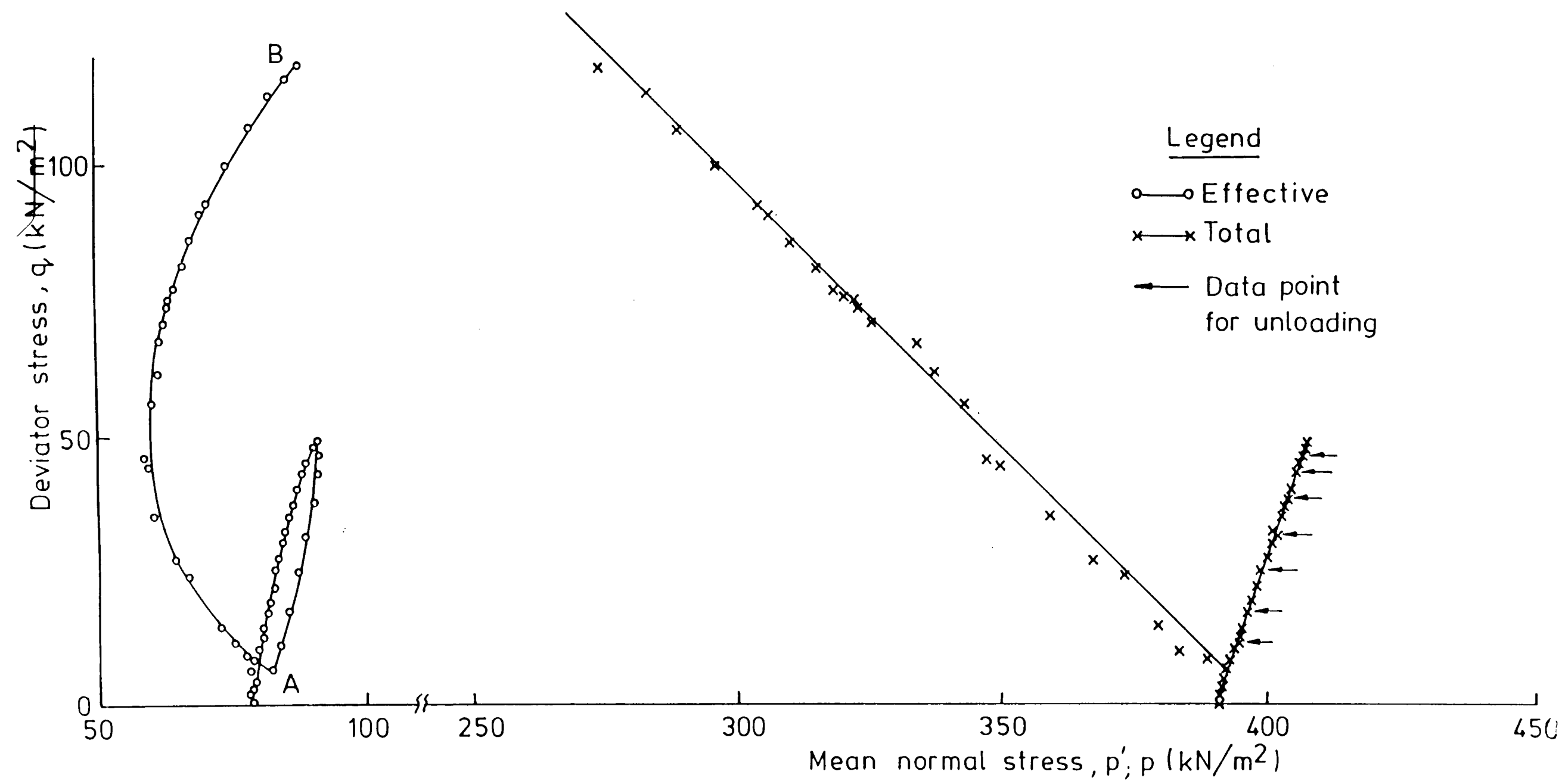
FIG. 5·38   COMPLETE STRESS PATHS OF TEST T7DV
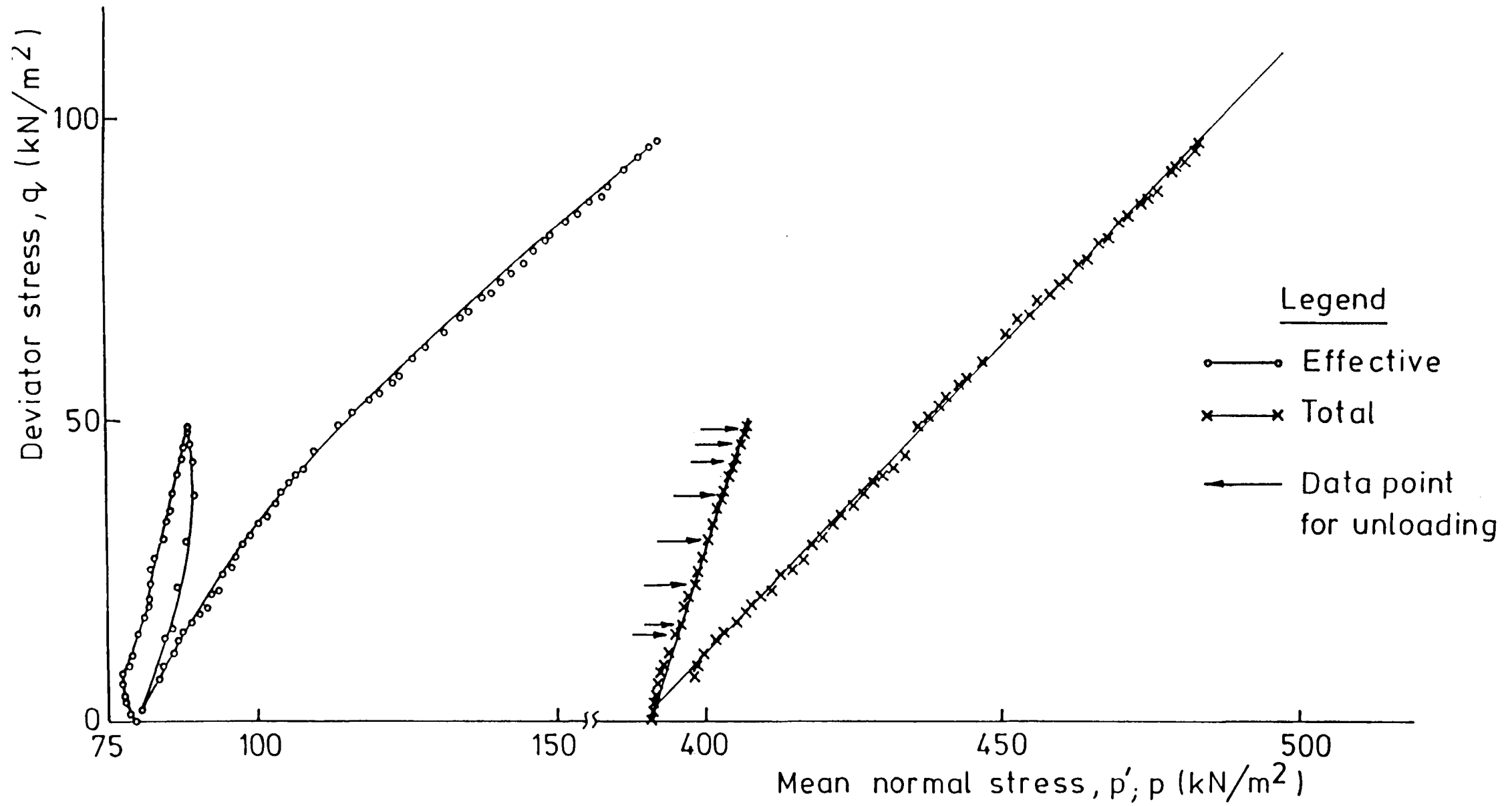
FIG.5·39   COMPLETE STRESS PATHS OF TEST T8DV
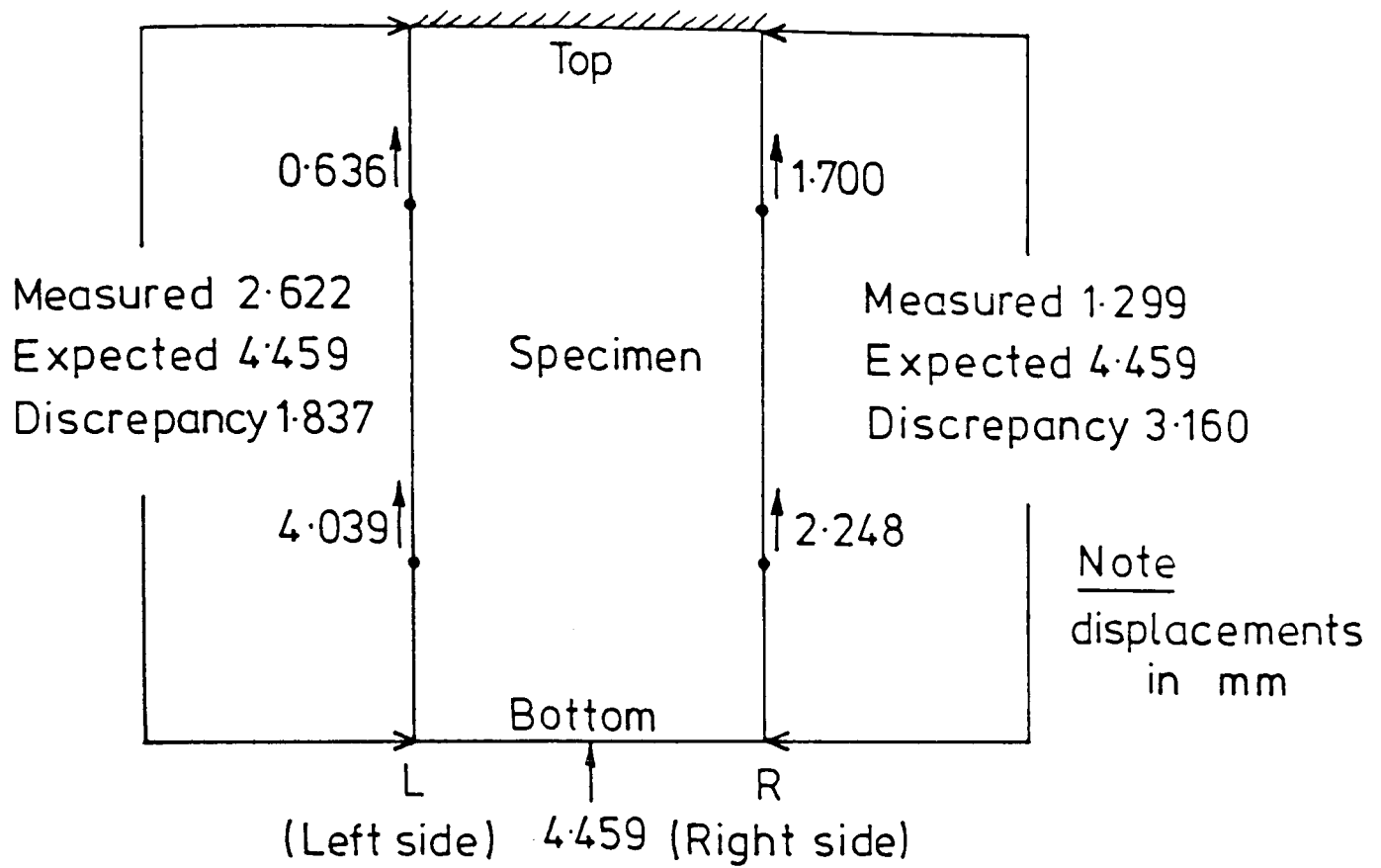
FIG.5·40 DISPLACEMENT DISTRIBUTION IN TEST T3DV AT ε_L=2%
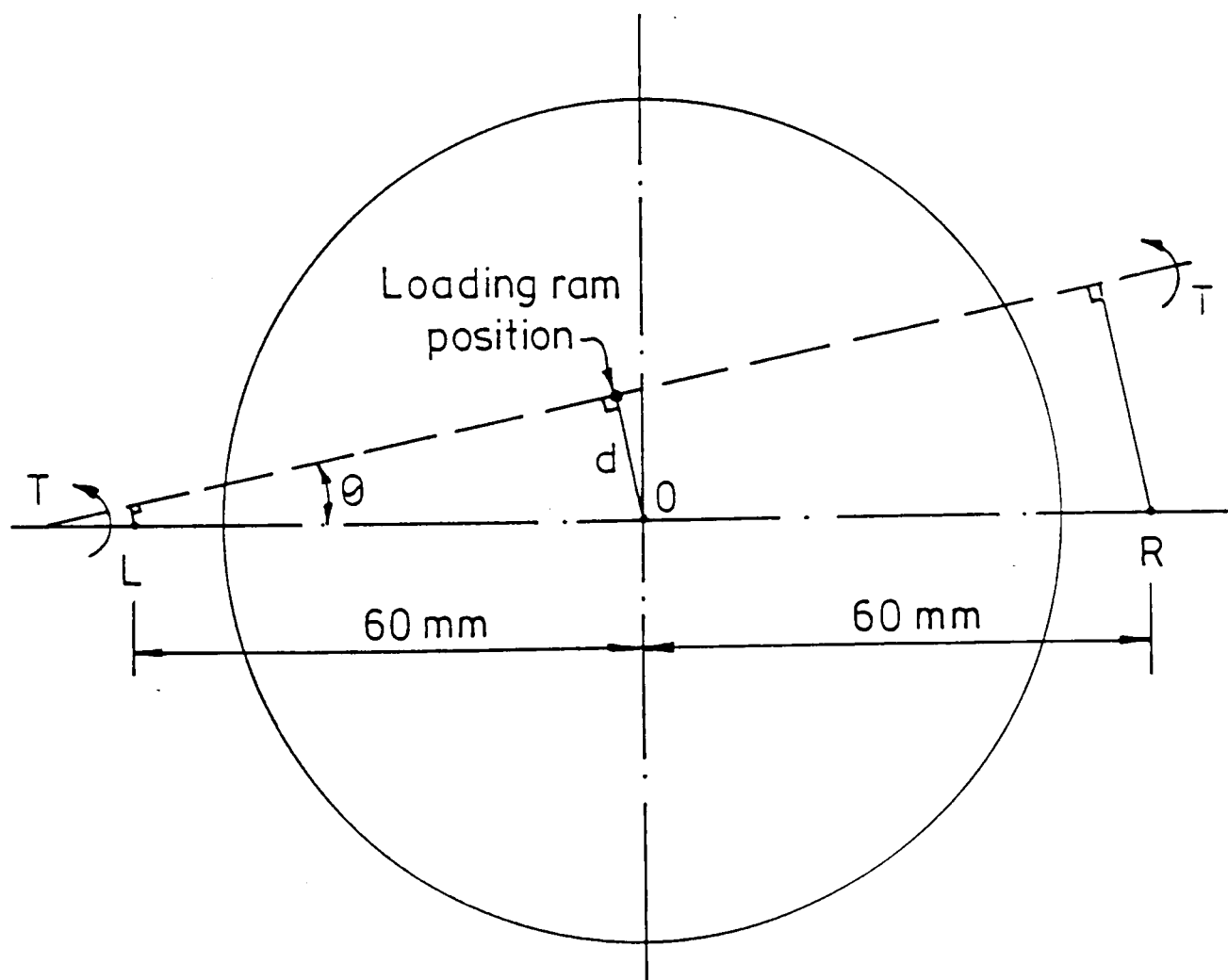
FIG.5·41 EFFECT OF TILTING ON END CAP MEASUREMENT

Centre lines of transducers

40 mm

40 mm

Upper target ring

Underestimated by 40 tan α mm

Overestimated by 40 tan α mm

α

A′

A

Actual displacement (a)

C′

C

Actual displacement (c)

Overestimated by 40 tan β mm

β

B′

B

Actual displacement (b)

D′

D

Underestimated by 40 tan β mm

Actual displacement (d)

Lower target ring
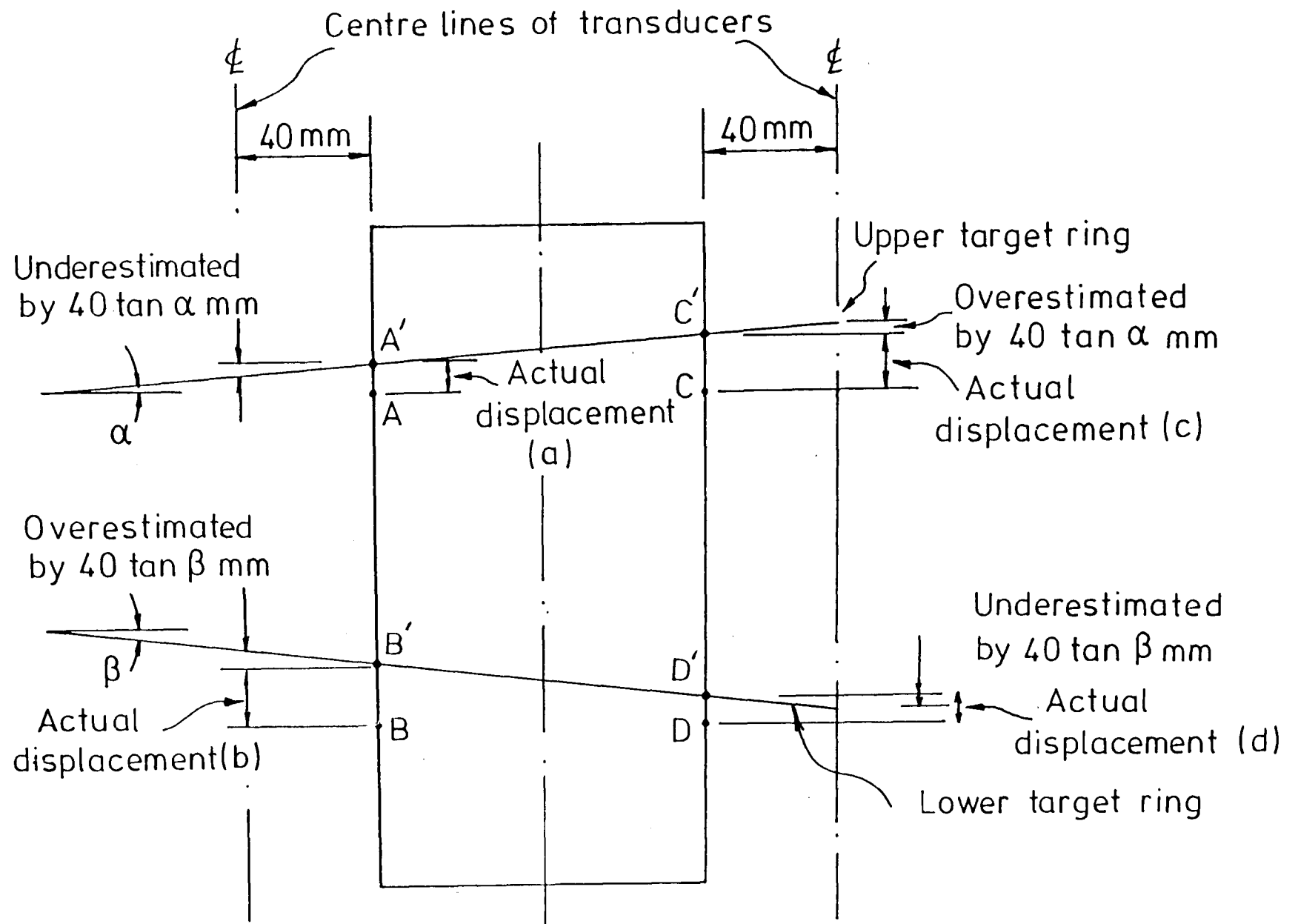
FIG. 5·42   EFFECT OF TILTING ON LOCAL AXIAL STRAIN
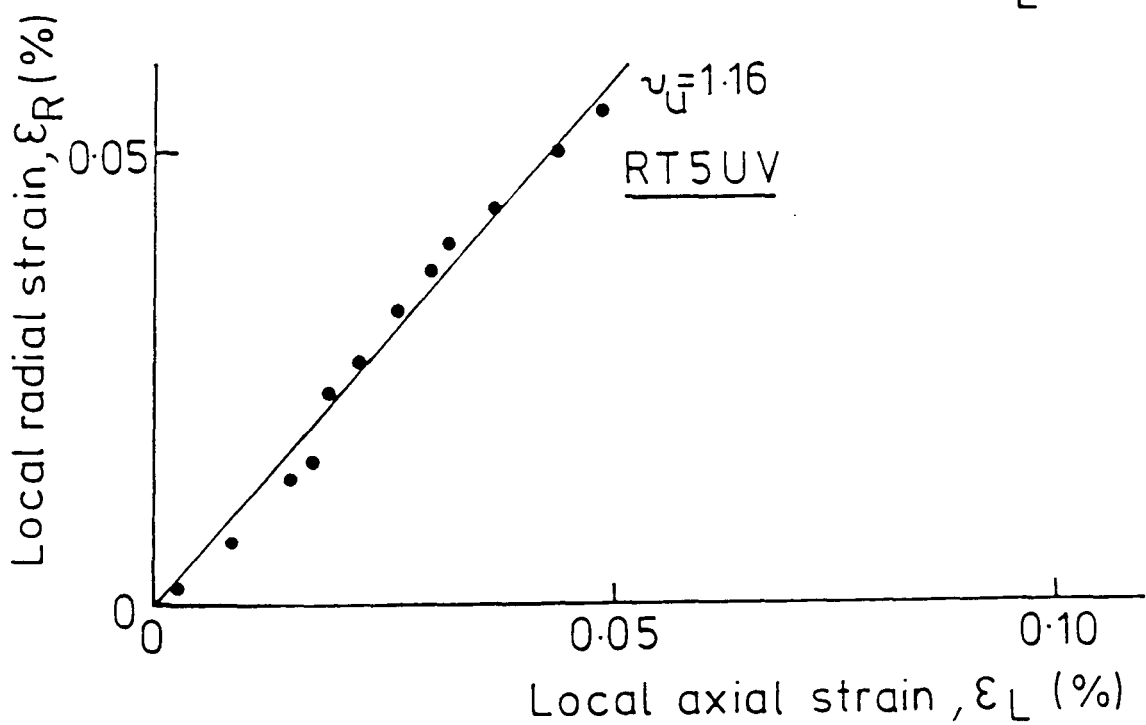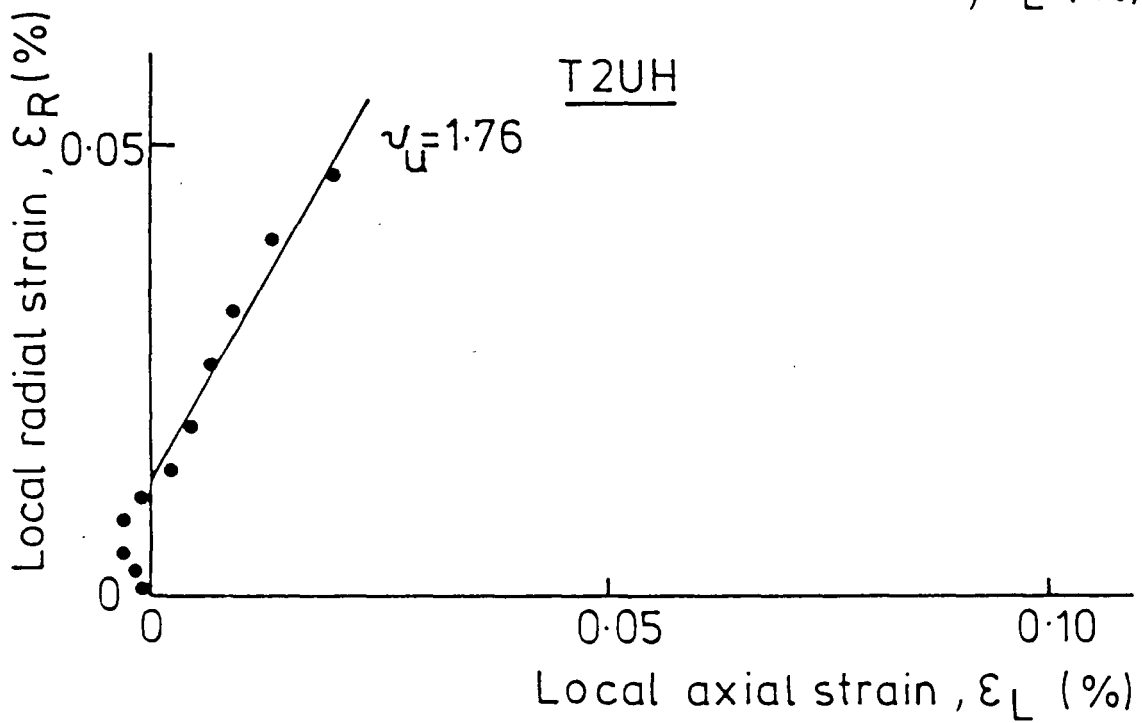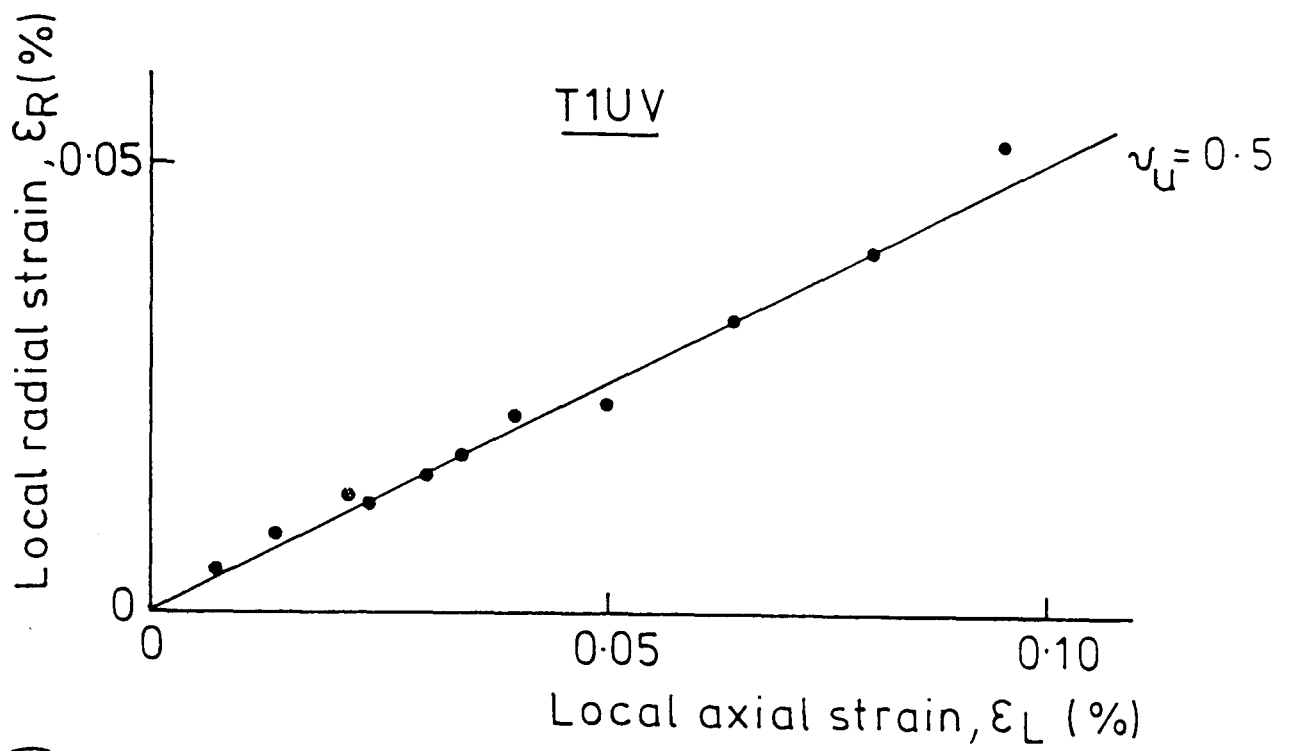
FIG.5·43 POISSON'S RATIO PLOT FOR TESTS
2UH AND RT5UV
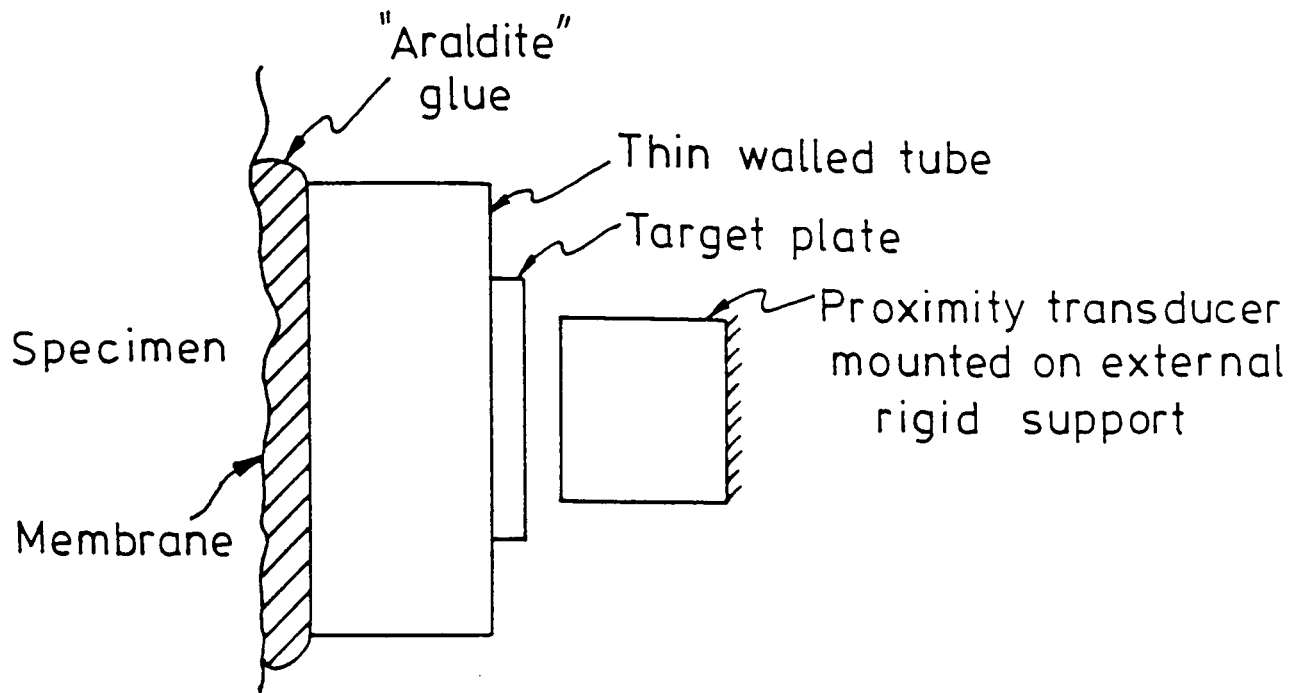
(a) SCHEMATIC ARRANGEMENT OF COLLAPSABLE
TARGET WITH A THIN LINE OF CONTACT GLUE
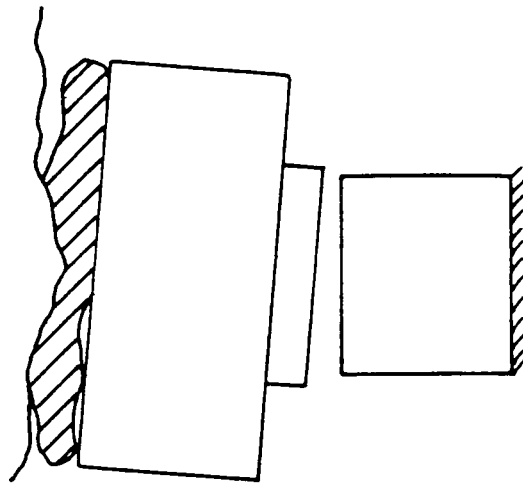
(b) EFFECT OF LOCAL DEFORMATION ON A THIN
LINE OF CONTACT GLUE
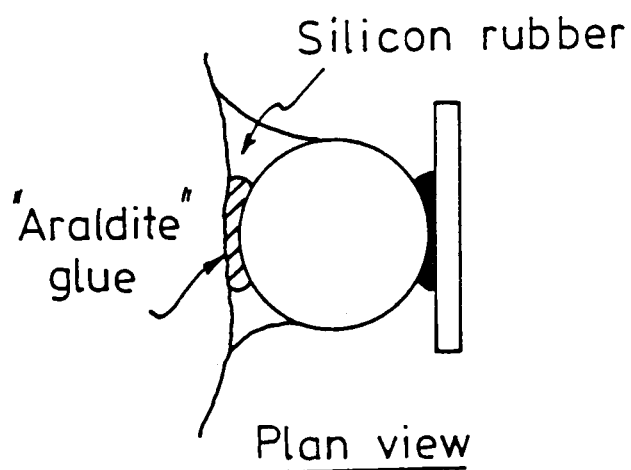
(c) FINAL ADOPTED METHOD OF ATTACHING
RADIAL TARGETS

FIG. 5·44 ARRANGEMENTS OF RADIAL STRAIN TARGETS
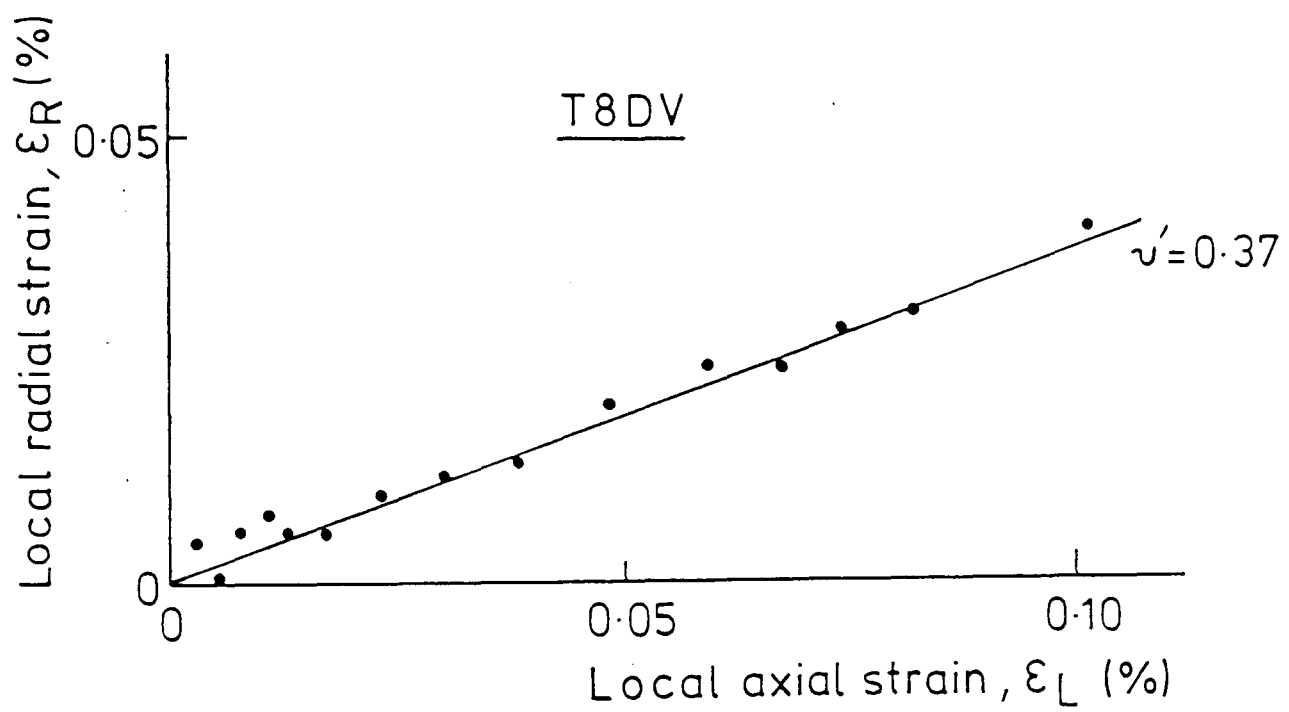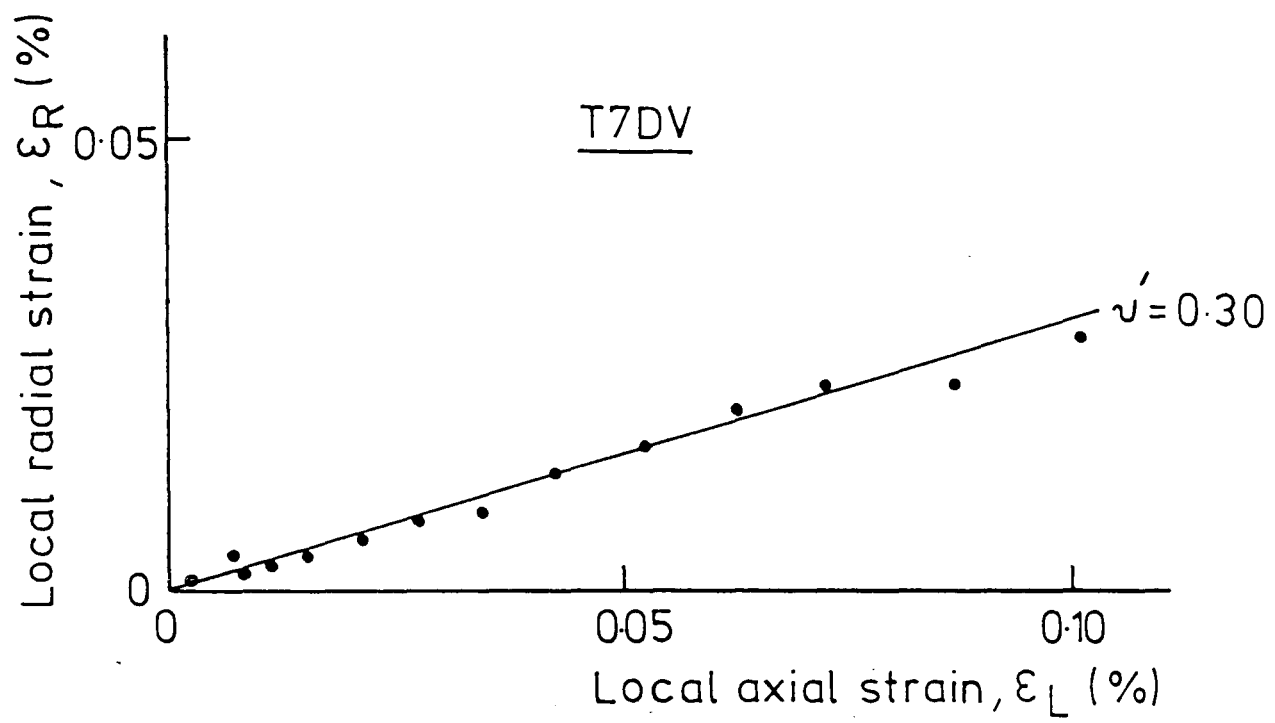
FIG. 5·45   POISSON'S RATIO FOR TESTS T7DV AND T8DV

TR1

Local radial strain, ε_R (%)

0.05

$\nu' = 0.46$

0

0   0.05   0.10

Local axial strain, ε_L (%)

TR2

Local radial strain, ε_R (%)

0.05

$\nu' = 0.34$

0

0   0.05   0.10

Local axial strain, ε_L (%)
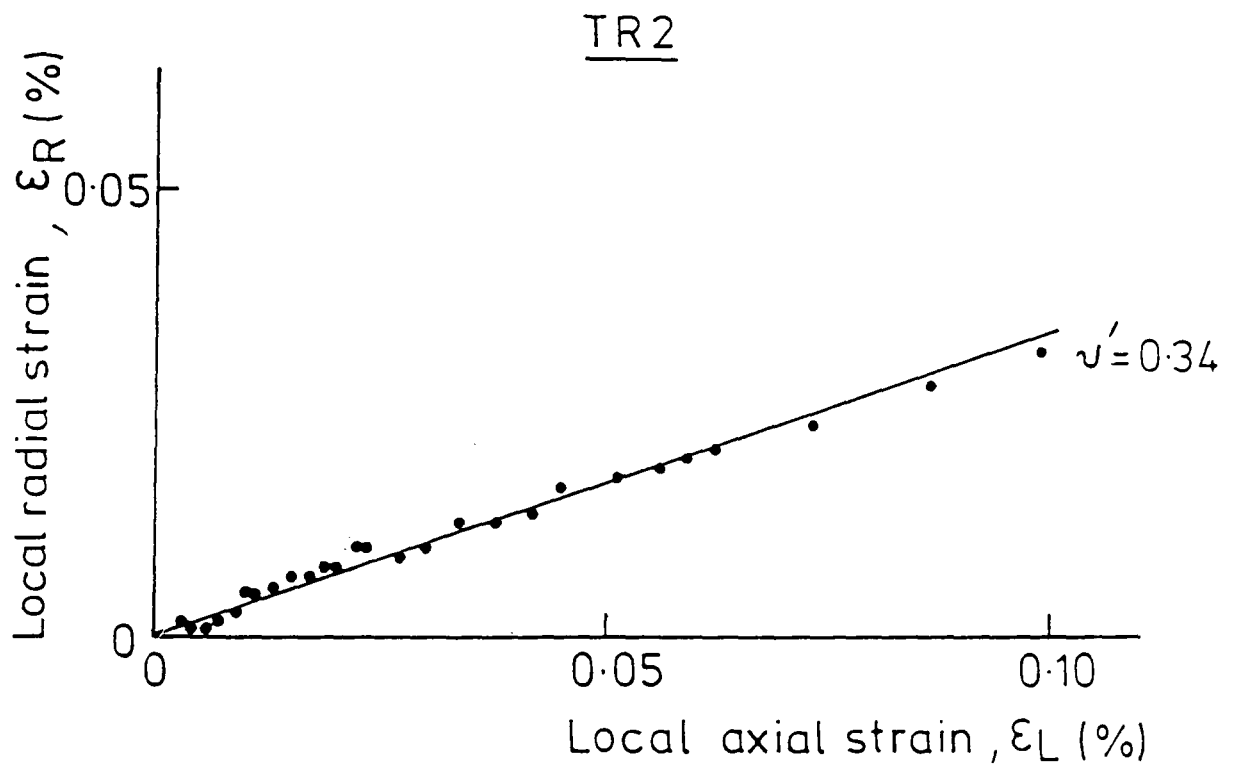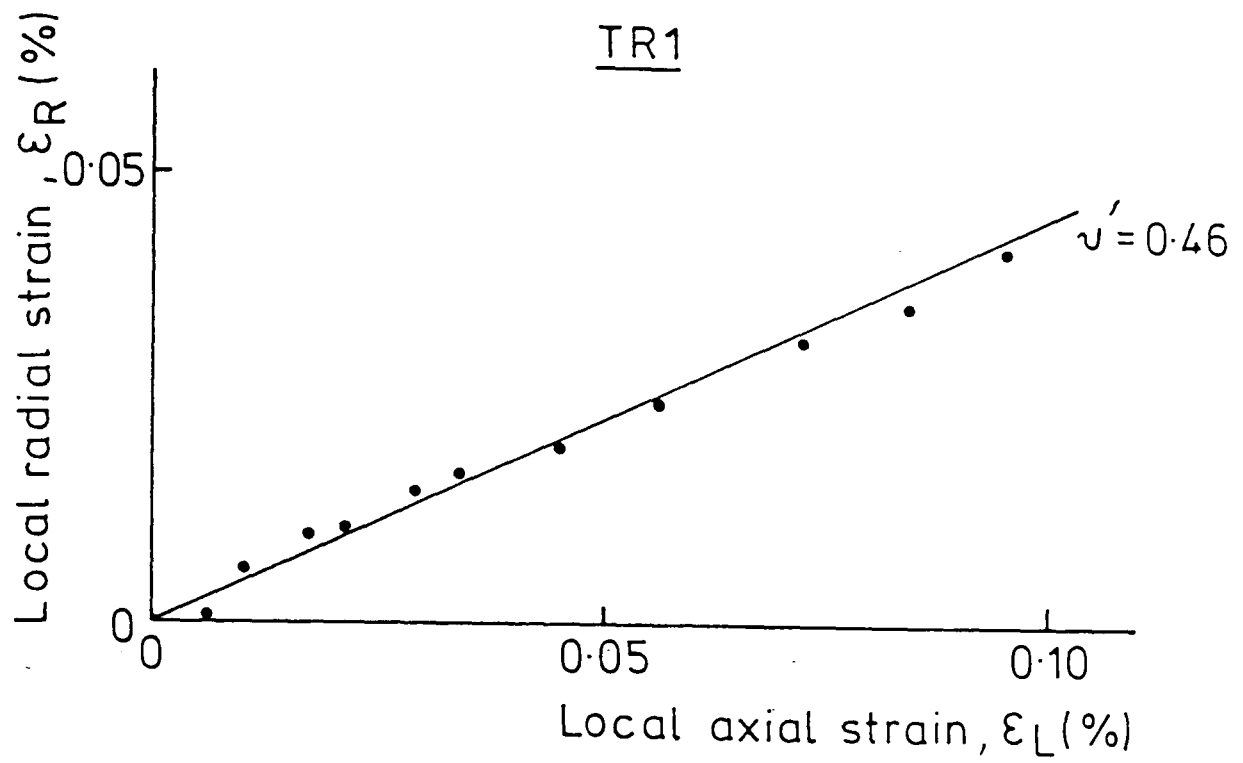
FIG. 5·46   POISSON'S RATIO PLOT FOR PROVING TESTS
TR1 AND TR2
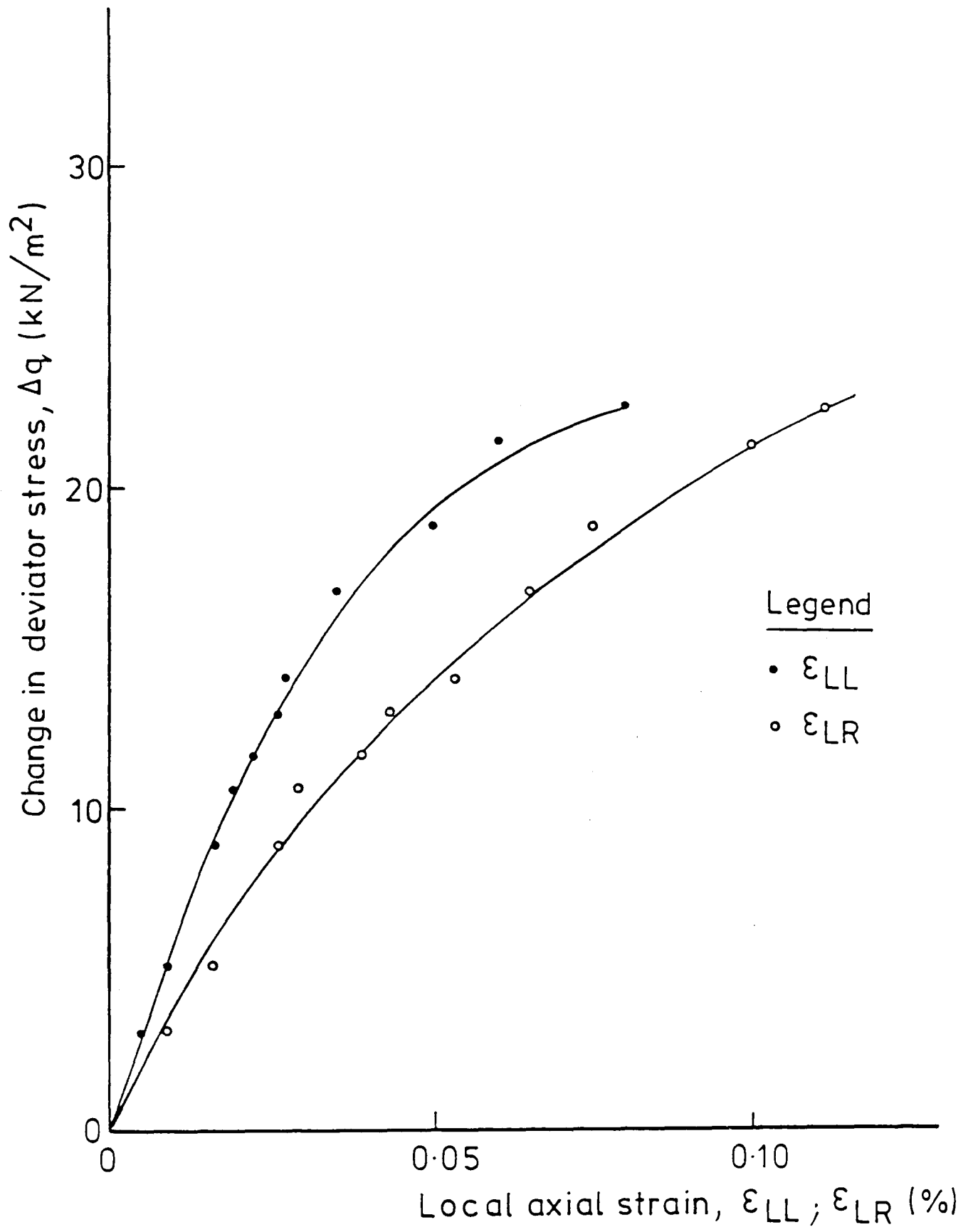
FIG. 5·47   NON−UNIFORMITY OF LOCAL AXIAL STRAIN IN TEST T1UV
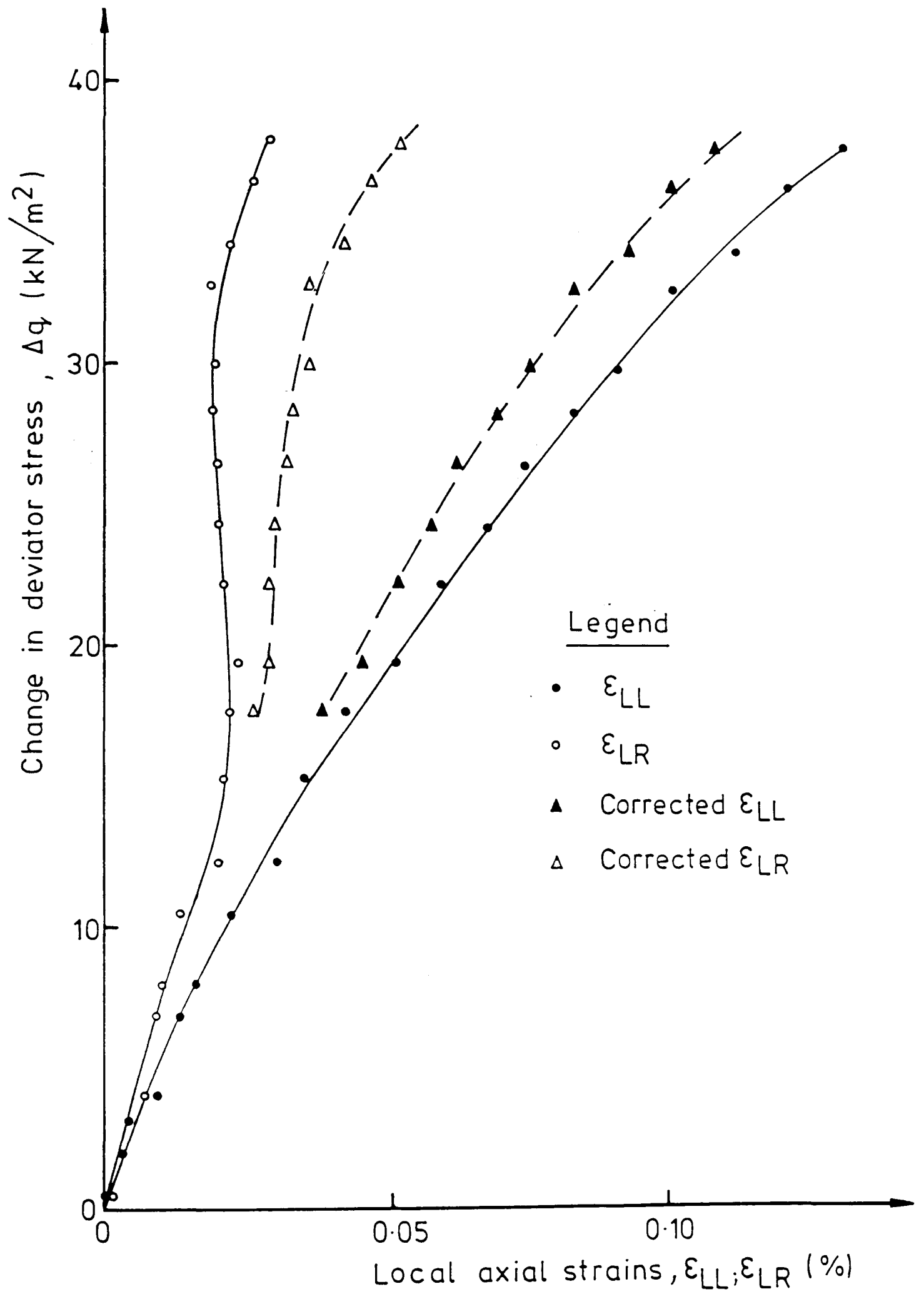
FIG.5·48 NON-UNIFORMITY OF LOCAL AXIAL STRAIN IN
TEST T3DV
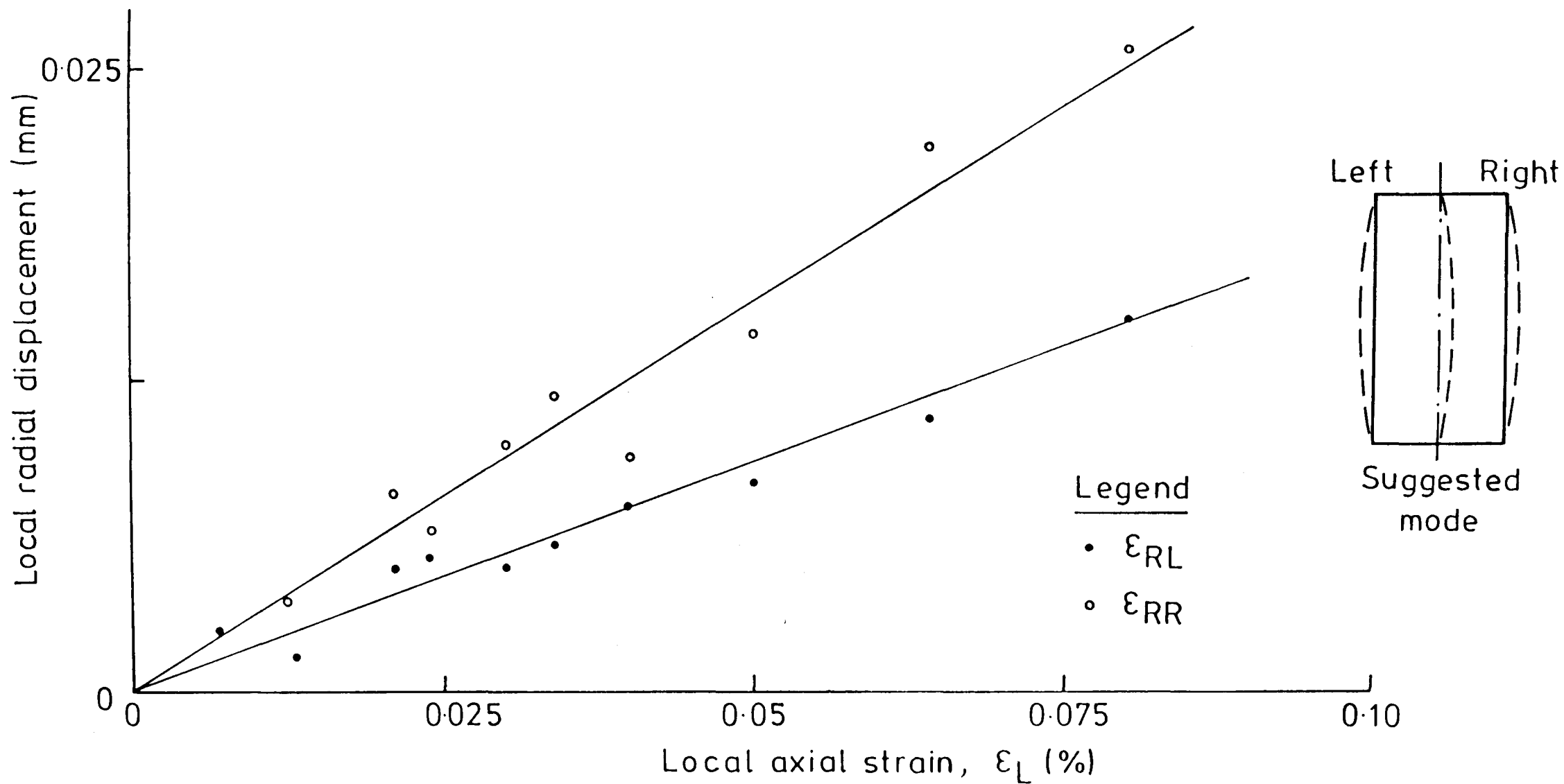
FIG. 5.49 NON-UNIFORMITY OF LOCAL RADIAL DISPLACEMENT IN TEST T1UV
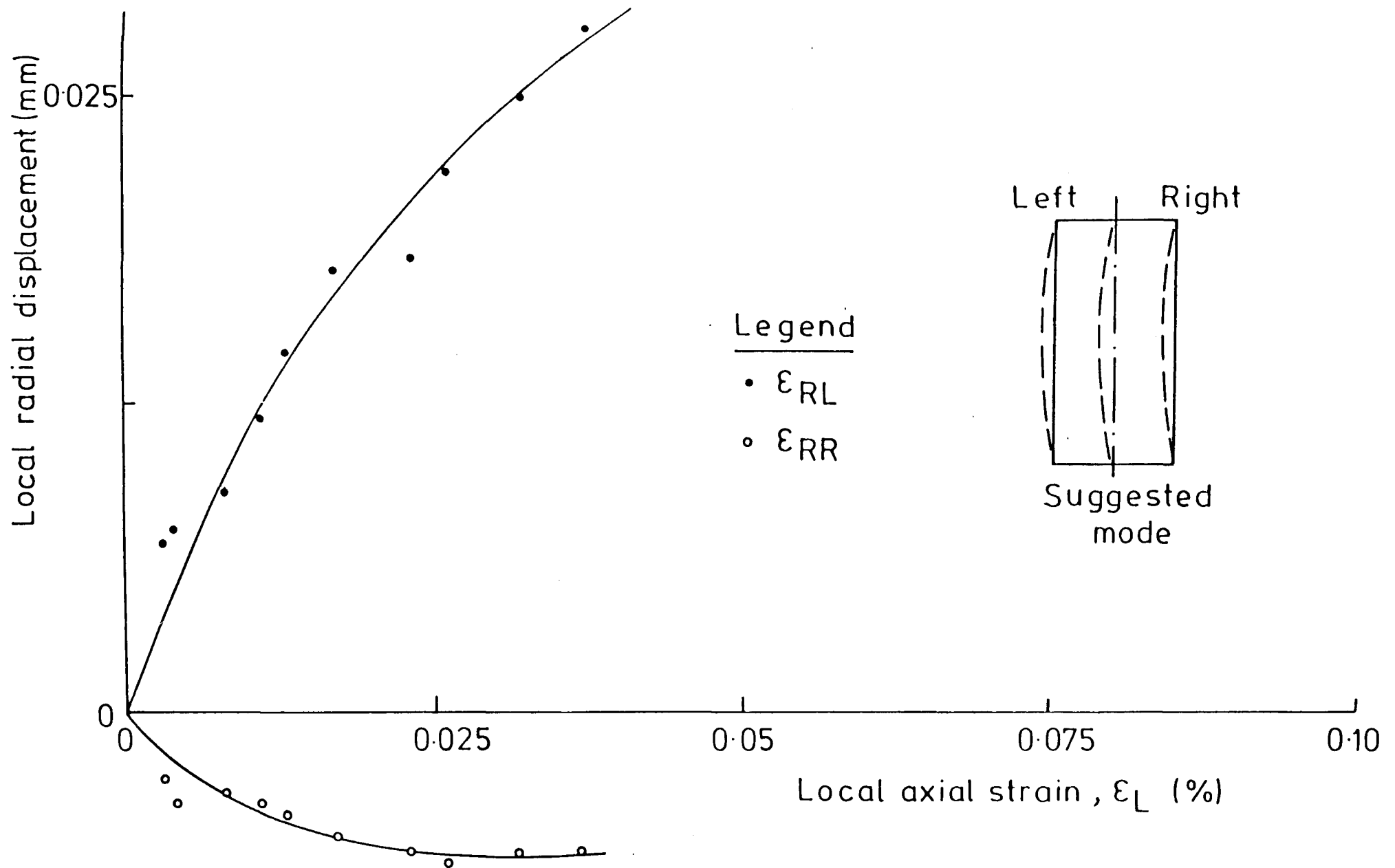
FIG. 5·50 NON-UNIFORMITY OF LOCAL RADIAL DISPLACEMENT IN TEST T3DV
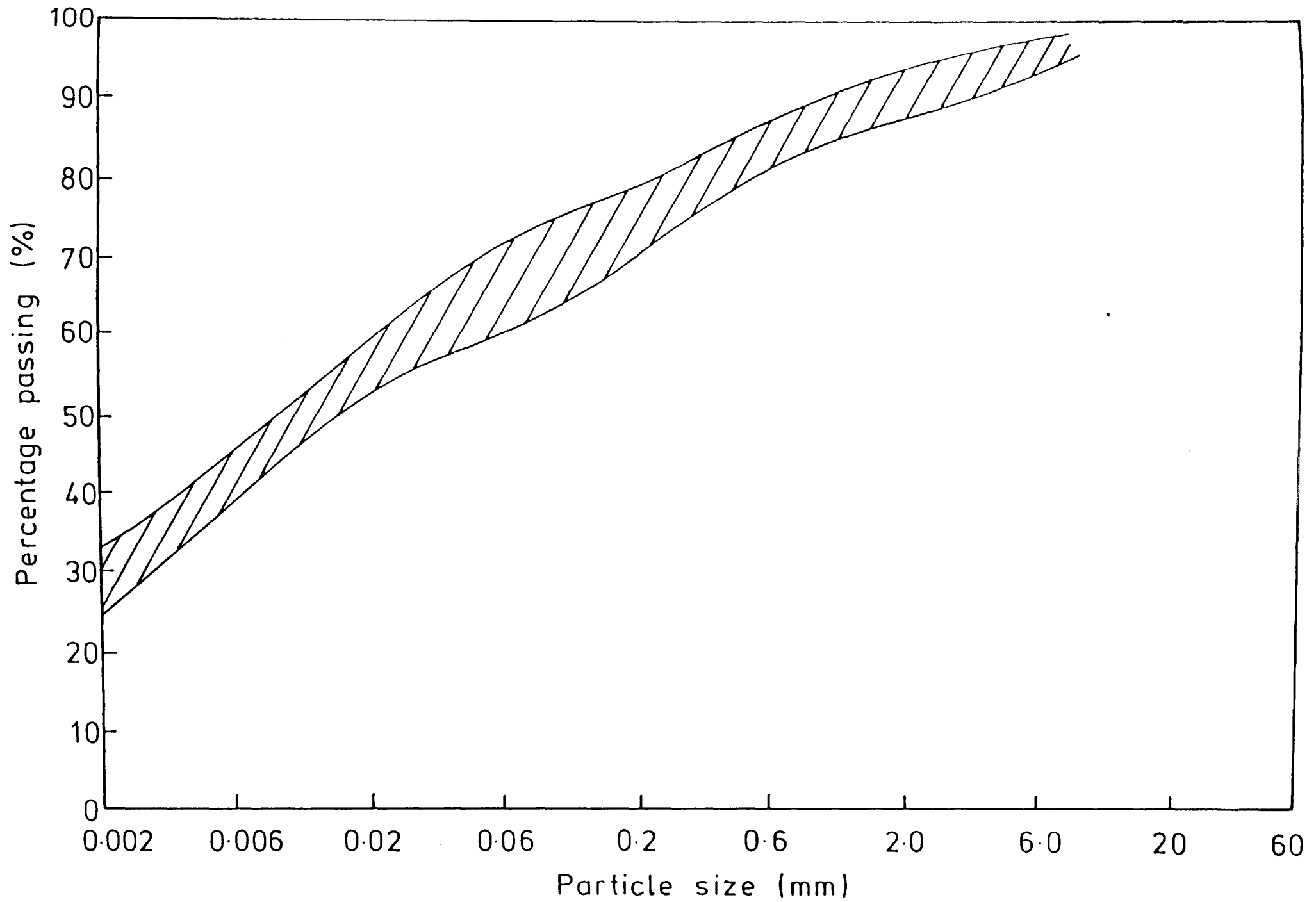
FIG. 5·51   PARTICLE SIZE DISTRIBUTION OF MAIN TEST SPECIMENS
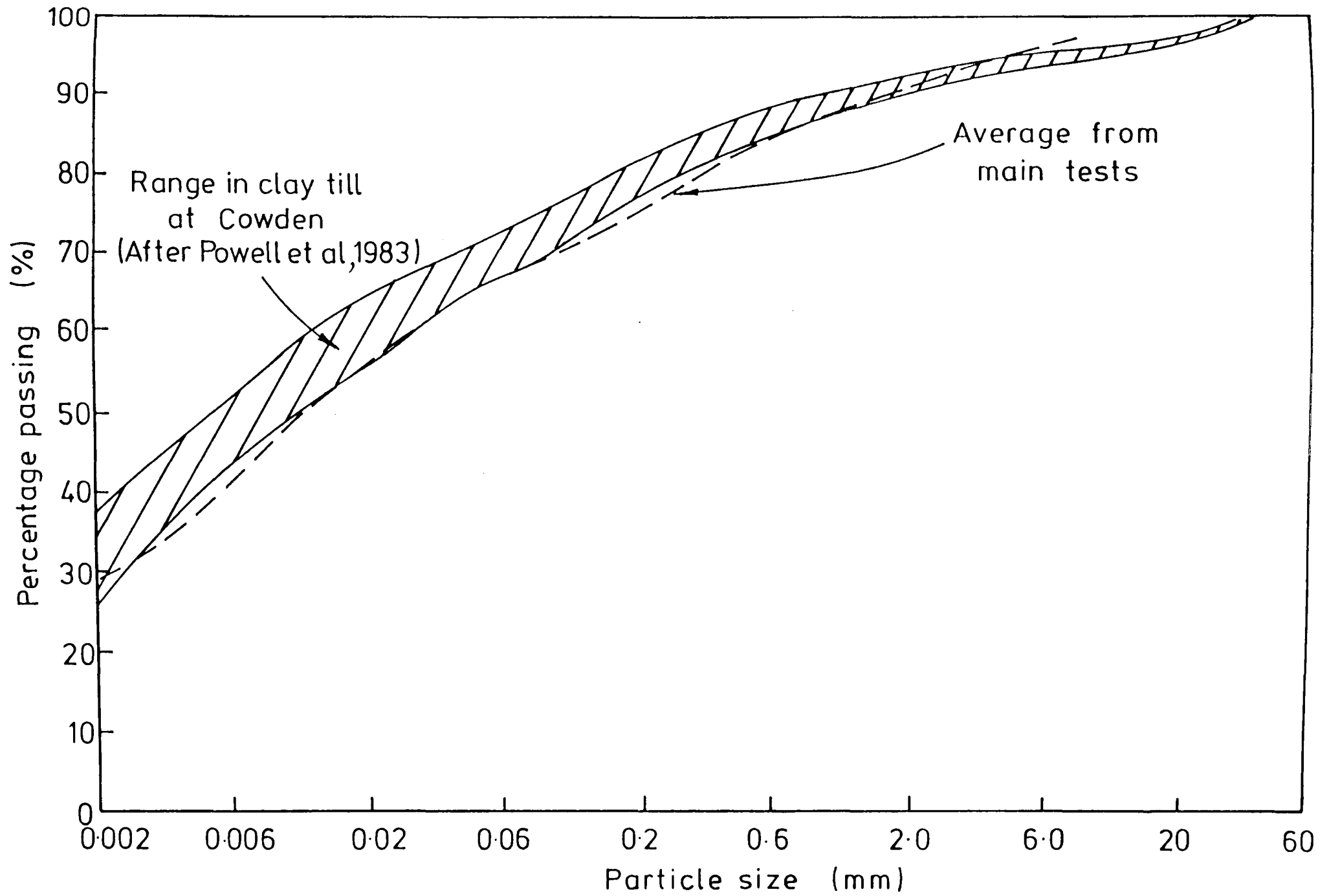
FIG. 5·52   COMPARISON OF PARTICLE SIZE DISTRIBUTIONS

CHAPTER 6

INTERPRETATION OF TEST RESULTS

6.1   INTRODUCTION

As mentioned in Section 3.4.1, the use of the end cap axial strain measurement was intended to permit the measurement of bedding errors originating at the ends of the specimen. These may be caused by a lack of flatness of the specimen's end surfaces, non-parallelism of the specimen end surfaces, and imperfect contact between the porous stones and the end caps.

Bedding errors can be reduced by careful trimming but cannot be completely eliminated. In view of their largely random nature, their magnitude is difficult to predict for a given test specimen. It is to be expected that they will be more severe for stiff clays, which generally present more difficulties as far as trimming of the ends is concerned, than for soft ones. The presence of heterogeneities, such as gravel particles left protruding from the end surfaces after trimming, can significantly increase the bedding errors. On the other hand it is also possible that, especially for softer materials, the application of an effective consolidation pressure will reduce the bedding errors during shearing significantly.

Bedding errors are conventionally associated with an initial concave shape of the stress-strain curve. The concave shape tends to disappear with increasing deviator stress and the stress-strain curve is generally corrected by extrapolating the more reliable portion backwards in order to define a new origin. Marsland (1971c) suggested that the zero correction in tests on London Clay would be due to the closing up of fissures, just as in the testing of rocks there is closure of cracks

and joints. However, the Imperial College type of load cell can similarly affect the initial portion of a stress-strain curve derived from externally measured displacements (Costa Filho, 1980).

In the remainder of this chapter an attempt is made to explain the form of the end cap strain measurements reported in the previous chapter and to estimate the bedding errors associated with the present series of tests. A comparison is also made between results based on the local strain measurements and the predictions of a model developed for overconsolidated clay by Pender (1978). The stiffness data assembled in Section 5.4.4 are also compared with the available field data.

6.2   THE EFFECT OF BEDDING ERRORS ON END CAP AXIAL STRAIN MEASUREMENT

In order to analyse the bedding errors, it is necessary to make simplifying assumptions regarding the form of the irregularities present on the end surfaces of the specimen. Consider, first, an extreme simplification in which the top cap is supported by three identical asperities protruding from the specimen and there is perfect contact at the bottom end of the specimen. The asperities are assumed to behave elastically and possess a stiffness k_b. It is assumed that the top cap is loaded at its centre, O, by a unit vertical load. Figure 6.1 shows such a situation with three alternative sets of asperities ($A_1B_1C_1$, $A_2B_2C_2$ and $A_2B_1C_1$), these cases being chosen for the sake of argument. The vertical load distribution for each case is found by firstly taking moments along the line BC to find the load on A, and then dividing the remaining load equally between B and C by reason of symmetry. The reactions may be divided by k_b to give the displacements of A, B and C. Points D_1 and D_2 correspond to the end cap strain measurement locations (assumed to be on the axis of symmetry and in the plane of the top cap) and their displacements are easily calculated. Figure 6.2 shows the corresponding motions

of the top cap (line D_1OD_2) as a result of eccentricity of the loading position relative to the asperities. It can be seen that a wide range of displacements is possible and that the average displacement (at point 0) also varies considerably. In reality the contacts would probably number more than three, would be randomly distributed, and would have different stiffnesses. As deformation proceeds new contacts would be made and, at a given instant, the displacements would be controlled by the dominant set of asperities. It is thus possible for rocking of the top cap to occur as one set of asperities takes over from another, with obvious adverse consequences for the end cap axial strain measurement.

During unloading, because different asperities may have different rebound characteristics, the dominant set of asperities could be quite different from that during the previous loading. This is thought to account for the complex and erratic pattern of behaviour seen in some of the end cap measurements (e.g. Figures 5.28 and 5.30).

In order to gain a better knowledge of the surface irregularities of Cowden Till specimens, five short, 100 mm diameter specimens were trimmed from blocks left over from the main tests. The end surfaces were trimmed in the usual way and coated with about a 5 mm thickness of epoxy resin. After it had set, the epoxy resin was detached and cut along a diameter. The surface profile of the trimmed surface of the Cowden Till was thus reflected in the epoxy resin cross-section which was then viewed under a stereo comparator of accuracy ±5μm (resolution ±1μm). Figures 6.3 and 6.4 show the smoothest and roughest profiles so obtained. These profiles have been corrected for curvature of the resin which occurred as it was cured. By inspection the surface roughnesses can perhaps be idealized as a sinusoidal variation with an amplitude, a_o, of 0.1 mm and wavelength, λ_b, of 10 mm at one extreme (Figure 6.3) and an amplitude of 1.0 mm and wavelength of 50 mm at the other (Figure 6.4).

The large amplitude of the latter is primarily attributed to the presence of sand and gravel particles.

The deformation of surface irregularities can be investigated using the methods given by Johnson (1985) for the contact mechanics of metals. The stress-strain behaviour of the material is assumed to be isotropic linear elastic or rigid-perfectly plastic. Consider an elastic medium, with Young's modulus E, under plain strain conditions subjected to a normal stress with sinusoidal variation, so that

$$p_n = p_o \cos \left(\frac{2\pi}{\lambda_b} x \right) \tag{6.1}$$

where p_n = normal pressure applied,

p_o = amplitude of applied pressure,

λ_b = wavelength of applied pressure, and

x = horizontal distance from an arbitrary chosen origin.

It may be shown that the resulting surface profile, $\bar{u}_z(x)$, has a sinusoidal variation of the same wavelength,

$$\bar{u}_z(x) = \frac{(1-\nu^2)\lambda_b}{\pi E} p_o \cos \left(\frac{2\pi x}{\lambda_b} \right) = a_o \cos \left(\frac{2\pi x}{\lambda_b} \right) \tag{6.2}$$

where the datum is at the mid-height of the surface variation. Conversely, if such a wavy surface exists initially in the absence of normal stress, the pressure required to flatten it is given by equation (6.1) with $p_o = \frac{\pi E a_o}{(1-\nu^2)\lambda_b}$. If the surface is just brought into contact with a second elastic body with a smooth flat surface, Figure 6.5(a), the gap between the surfaces, h(x), may be expressed by ;-

$$h(x) = a_o \left\{ 1 - \cos \left(\frac{2\pi x}{\lambda_b} \right) \right\} \tag{6.3}$$

If, under a mean pressure $\bar{p}$, the solids are now pressed into contact, in the absence of deformation, their profiles would overlap each other by the amount shown by the dotted lines in Figure 6.5(b) with a relative displacement of $\delta_1 + \delta_2$, but due to the contact pressure the surface within the contact zone is displaced by an amount $\bar{u}_{z1}$ or $\bar{u}_{z2}$ such that

$$\overline{u}_{z1}(x) + \overline{u}_{z2}(x) = \delta_1 + \delta_2 - h(x) \qquad (6.4)$$

To make further progress it is necessary to find a pressure distribution satisfying equation (6.4). For continuous contact the pressure distribution may be expressed as:-

$$p(x) = \overline{p} + p_o \cos\left(\frac{2\pi x}{\lambda_b}\right) \qquad (6.5)$$

For contacting elastic bodies a composite Young's modulus E^* may be defined by :-

$$\frac{1}{E^*} = \frac{1-\nu_1^2}{E_1} + \frac{1-\nu_2^2}{E_2}$$

where E_1, ν_2, E_2, ν_2 are the Young's moduli and Poisson's ratios of the materials on each side of the contact and p_o becomes $\frac{\pi E^* a_o}{\lambda_b}$. If $\overline{p} < p_o$ only partial contact is maintained over parallel strips of width $2w$. Without proof, Johnson (1985) states that, for equations (6.4) and (6.5) to be satisfied, the mean pressure $\overline{p}$ is given by :-

$$\overline{p} = \left(\frac{\pi E^* a_o}{\lambda_b}\right) \sin^2\left(\frac{\pi w}{\lambda_b}\right) \qquad (6.6)$$

The ratio of the real area of contact to the total area, $\frac{2w}{\lambda_b}$, can therefore be expressed as:-

$$\frac{2w}{\lambda_b} = \left(\frac{2}{\pi}\right) \sin^{-1} \sqrt{\frac{\overline{p}}{p_o}} \qquad (6.7)$$

Figure 6.6 shows the graphical representation of equation (6.7).

In applying the above analysis to the contact between end caps and a soil specimen, the Young's modulus of the end caps can be assumed to be much higher than that of the soil and consequently $E^* = \frac{E}{1-\nu^2}$ where E and ν are the soil parameters. The roughness profile of the ends of the specimen having been idealized in a sinusoidal form, the compression (bedding error) under a mean pressure $\overline{p}$ can be evaluated approximately from equations (6.7) and (6.2) by neglecting the distortion of the asperity outside the contact zone, Figure 6.5(c). The amount of compression is:-

$$a_o\left\{1 - \cos\left(\frac{2\pi w}{\lambda_b}\right)\right\} \qquad (6.8)$$

The pressure $\bar{p}_T$, required for complete flattening (elimination of the bedding) is obtained by substituting $w = \dfrac{\lambda_b}{2}$ into equation (6.6) so that

$$\bar{p}_T = \frac{\pi E}{(1-\nu^2)} \cdot \frac{a_o}{\lambda_b} = \frac{2\pi G}{(1-\nu)} \cdot \frac{a_o}{\lambda_b} \tag{6.9}$$

An alternative theoretical approach to the elastic flattening of an initially wavy surface was proposed by Davis and Salt (1986). If the surface is partially flattened so that its profile is defined by a second sinusoid with the same wavelength as the original one but a different amplitude a_1, it may be shown that the average work per unit area, W, needed to cause the partial flattening is

$$W = \frac{\pi G(a_o - a_1)^2}{2\lambda_b} \tag{6.10}$$

If the material is assumed to be isotropic and linearly elastic, the work done by the mean applied normal pressure, $\bar{p}$, is

$$W = \frac{1}{2}\bar{p}(a_o - a_1) \tag{6.11}$$

By equating equations (6.10) and (6.11), the normal pressure for partial flattening is

$$\bar{p} = \frac{\pi E}{2(1+\nu)} \cdot \frac{(a_o - a_1)}{\lambda_b} \tag{6.12}$$

and the corresponding pressure, $\bar{p}_T$, for total flattening is

$$\bar{p}_T = \frac{\pi E}{2(1+\nu)} \cdot \frac{a_o}{\lambda_b} = \frac{\pi G a_o}{\lambda_b} \tag{6.13}$$

It is interesting to note that both equations (6.9) and (6.13) incorporate the ratio $\dfrac{a_o}{\lambda_b}$ but differ by a factor of $\dfrac{2}{(1-\nu)}$. This factor ranges from 2 to 4 for materials having a Poisson's ratio ranging from 0 to 0.5. The author attributes this difference to a difference in boundary conditions. In Davis and Salt's approach only vertical movement at the boundary is allowed and any shear stress present at the boundary does no work (see Figure 6.7). In the previous approach, lateral movements occur at the boundary which is assumed frictionless. Again no work is done by the shear stress but there is a different distribution of strain.

The above approaches, based on the theory of elasticity, permit a prediction of the bedding error to be made if the surface profile, appropriate soil properties and applied pressure are known. A third, and contrasting, approach is arrived at by considering the plastic deformation of a regular serrated surface pressed against a rigid flat surface as shown in Figure 6.8. The deformation of a single wedge-shaped asperity is shown in Figure 6.9 where φ is a function of the geometry of the asperity. Using the theory of plasticity, Johnson (1985) presented the solution for a serrated surface with a semi-angle (ξ) of 65° as shown in Figure 6.10 where s is the shear strength of the material and p_a, p_n are the asperity pressure and mean pressure applied to the surface respectively. With increasing load, the contact area increases and the zone of deformation shown in Figure 6.9 extends until point C reaches the trough between two serrations. This situation occurs when the ratio $\frac{2w}{\lambda_b}$ reaches 0.36. Further deformation is then constrained by the interference between adjacent serrations. When p_n reaches 5.14s overall indentation of the material occurs and no further deformation of the asperities will take place. For initially pointed asperities with $\xi = 65^{\circ}$ the amount of compression under a given normal pressure can be evaluated geometrically once the value of $\frac{2w}{\lambda_b}$ has been found from Figure 6.10. With reference to Figure 6.9, the compression is calculated by equating the areas OAB and BB'C assuming that B'C is approximately equal to BC ($= \sqrt{2}w$). For Cowden Till the initial geometry of the serrated surface has been calculated for the two extreme cases mentioned above by equating the area beneath the sinusoidal variation to the area beneath wedges having a semi-angle (ξ) of 65°. The resulting idealizations for the two extremes are shown in Figures 6.3 and 6.4 respectively.

As an illustration of what might be possible in applying the three analyses outlined above to the problem of bedding errors in triaxial tests, they have been used, together with the profile idealizations of Figures 6.3 and 6.4, to predict the end cap axial strain in test T2UH from the local measurements in the small strain region. In doing this, the effects of end restraint and of non-parallelism of the end surfaces have been ignored, and the secant Young's modulus obtained from the local measurements at 0.1% and 0.4% strain have been arbitrarily chosen to represent a linear elastic behaviour of the Cowden material. Since the test was terminated prematurely (see Section 5.4.2), for the plastic wedge approach the undrained shear strength has been taken as 100 kN/m^2 from the in-situ plate test results (see Figure 2.15).

Figures 6.11 to 6.13 show the predicted end cap strains together with the actual measurements and the local measurements. In making these predictions allowance was made for the deformation of the end surfaces due to the application of the isotropic consolidation pressure. The amount of bedding eliminated was assumed to be equal at each end of the specimen.

It is clear from Figures 6.11 to 6.13 that bedding errors may not be evident as a reversal of curvature of the stress-strain curve and therefore the conventional method of correction may not be applicable. The plastic approach shows an inadequate correction for the smoothest surface and over-correction for the roughest one. The limited results obtained from the elastic approaches suggest that the surface of specimen T2UH may have tended towards the roughest extreme, with the lower Young's modulus appearing to give more satisfactory results at strains approaching 0.1%.

The difficulties in applying these theoretical approaches, particularly the elastic ones, to the problem of bedding errors are serious.

Firstly, the wavelength of the surface irregularities (λ_b) must be small in comparison with the specimen diameter. Unfortunately, this was not the case for the roughest surface discussed above. Secondly, the elastic approaches only apply for a material with linear behaviour, whereas soil behaviour is generally non-linear. Thirdly, the choice of equivalent linear elastic parameters to represent non-linear behaviour is arbitrary as the strains associated with the elimination of the bedding are unknown.

Figure 6.14 shows the pressure required for complete flattening of an initially wavy surface as predicted by the two elastic approaches. As already mentioned, the pressures predicted by the two approaches for a given ratio of $\frac{a_o}{\lambda_b}$ differ by a factor of 4. The figure could potentially be used to assess the likelihood of eliminating bedding errors during consolidation. For a given mean applied pressure, the corresponding ratio $\frac{a_o}{\lambda_b}$ for which total elimination of the bedding error can be achieved is higher for a "soft" material (say $G = 5000$ kN/m^2) than for a stiff one (say $G = 15000$ kN/m^2). Likewise, for any given initial roughness of the surface $\frac{a_o}{\lambda_b}$ the pressure required for its complete flattening is higher for a stiff clay than a soft one. For a given soil, localized remoulding of the soil close to the end surfaces during trimming operations may effectively reduce the stiffness and so reduce the bedding error following consolidation.

6.3 COMPARISON WITH MATHEMATICAL MODELS

Mathematical soil models are needed for the prediction or interpretation of soil deformations. Numerous models have been developed in order to represent the widely varying behaviours of natural soils. These models have various degrees of generality, simplicity and accuracy, as discussed in Section 1.2. It is now well known, from laboratory

studies of both "undisturbed" and reconstituted soil specimens, that the
stress-strain behaviour of most soils is non-linear and anisotropic.
The soil itself is not likely to be homogeneous.

On the basis of the limited test results presented in Chapter 5,
in this section the stress-strain behaviour of isotropically consolid-
ated Cowden Till at small strains is compared with the predictions of
some well known models. One objective of the test programme was to
examine the anisotropy of the material by testing both vertically and
horizontally samples. For a cross-anisotropic elastic soil with a verti-
cal axis of symmetry, it can be shown (e.g. Jaeger and Cook, 1976) that
the material behaviour is governed by five independent elastic constants,
defined in terms of effective stress as:

E'_V = Young's modulus in the vertical direction,

E'_H = Young's modulus in the horizontal direction,

ν'_1 = Poisson's ratio for strain in any horizontal direction due
to a horizontal stress applied at right angles,

ν'_3 = Poisson's ratio for strain in the horizontal direction due
to a vertical stress, and

G'_V = shear modulus in any vertical plane.

Atkinson (1973) proposed the use of such a model to predict the behaviour
of undisturbed London Clay. The parameters E'_V, E'_H, ν'_1 and ν'_3 can be
obtained from two drained compression tests on vertical and horizontal
samples, if it assumed that the Poisson's ratios and the degree of aniso-
tropy n $(= \dfrac{E'_V}{E'_H})$ remain constant during loading. Atkinson also suggested
that a distinction between elastic and plastic behaviour could be made
by observing that in the elastic range the stress path in the undrained
tests should be linear $(\dfrac{d\sigma'_1}{d\sigma'_3}$ = constant) and in drained tests the
strain path should be linear $(1 - \dfrac{d\varepsilon_V}{d\varepsilon_A}$ = constant). The linearity of the
stress or strain path does not depend on the linearity of the stress-

strain curve and therefore the model is not limited to linear elastic behaviour. For non-linear behaviour tangent moduli are required and these have been measured directly from the stress-strain data presented in Chapter 5 (see Table 5.16).

For Cowden Till, Figures 5.45 and 5.46 show that ν' is essentially constant in the small strain range. From the results listed in Table 5.16 mean values of n may be evaluated at different strain levels for the drained tests including tests TR1 and TR2. The mean value of n is 0.75 at 0.01% strain, 0.94 at 0.05% strain and 0.76 at 0.1% strain. The mean value of n between 0.01 and 0.1% strain is about 0.82, so that the material behaviour may be considered as approximately isotropic.

Since the undrained stress paths in the (p', q) plane (Figure 5.22) are approximately linear, the stress paths in the (σ'_1, σ'_3) plane should also be linear. For four of the drained tests, the Poisson's ratio plot from local measurements (see Figures 5.45 and 5.46) was seen to be linear; thus the associated strain path should be linear. In Figure 6.15 strain paths are shown for the remaining drained tests, in which the radial strain measurements were considered unreliable. The externally measured volume changes have been plotted against the locally measured axial strains. Again, approximate linearity is evident. Some of the data are erratic, but this could be due to non-uniformity of the local strain.

From the evidence reviewed above, it appears that Cowden Till could be modelled as a non-linear elastic material. If it is now assumed that the material is isotropic, then n = 1 and $\nu'_1 = \nu'_3$. The best estimate of ν' may be obtained by taking the mean of the results from tests T7DV, T8DV and TR2 in Table 5.16 (the result from test TR1 being regarded as unrepresentative), so that $\nu' = 0.34$. A prediction of the undrained modulus at any given strain level may now be made as follows:-

$$E_u = E'_v \left[\frac{3(1 - 2\nu')}{2(1 - \nu - 2\nu^2)} \right] \qquad (6.14)$$

Thus $E_u = 1.12 \, E'_v$

Table 6.1 shows a comparison of these predictions with values measured in tests RT5UV and T2UH. At each strain level the value of E'_v was taken as the mean value obtained from tests TR2, T3DV, T7DV and T8DV. Clearly, the model appears to be more satisfactory for the specimens in test RT5UV. However, it may be remembered that the results obtained in test T2UH were questionable at small strains (see Section 5.4.2) and this may invalidate the comparison made in Table 6.1.

Since, as noted above, the behaviour of Cowden Till appears to be approximately isotropic, the question arises as to whether an interpretation can be based on the critical state soil models mentioned in Section 1.2.3. Critical state parameters have been evaluated by the Author on the basis of data from 14 oedometer tests and 8 consolidated undrained triaxial compression tests on intact material. These test data were reported by Gallagher (1983). The average values of λ, M and Γ were 0.071, 1.06 and 1.81 respectively. The value of M corresponds to $\phi' = 26.7^o$ (see Section 2.3.4). The average value of κ during unload-reload cycles in the oedometer tests was 0.015. However, at an effective stress of 90 kN/m^2, which is close to the average effective stress prior to shearing in the present investigation (p'_o = 84 kN/m^2), the mean values of κ during unloading and reloading were 0.017 and 0.009 respectively. The average of these two values is thus 0.013, slightly less than the value quoted above. All the above values may be compared with those for the remoulded material (see Section 2.3.4).

The plastic deformation of normally consolidated or lightly over-consolidated clays can be modelled reasonably well by the Cam Clay model. However, it is generally accepted that the Cam Clay model is

less successful in describing the yield behaviour of heavily over-
consolidated clays, for which a different state boundary surface applies
(Atkinson and Bransby, 1978). Also, the practical importance of the
small strain range has been discussed in Section 1.1 and it is therefore
essential to develop models that can predict behaviour well beneath the
state boundary surface.

In the critical state theories the soil behaviour beneath the
state boundary surface is considered to be elastic. It then follows
that the Young's moduli are given by:-

$$E' = \frac{3\nu p'(1 - 2\nu')}{\kappa} \qquad\qquad (6.15a)$$

$$\text{and} \qquad E_u = \frac{9\nu p'(1 - 2\nu')}{2\kappa(1 + \nu')} \qquad\qquad (6.15b)$$

Taking the value of κ as 0.015 together with the mean value of $v = 1.402$
from Table 5.14 and $\nu' = 0.34$, at the average effective stress prior to
shearing ($p' = 84$ kN/m^2) the initial drained and undrained stiffnesses
can be calculated as 7.57 MN/m^2 and 8.44 MN/m^2 respectively. Clearly,
these are much lower than the stiffnesses observed experimentally (see
Table 5.16), although if the value of κ during reloading ($\kappa = 0.009$) is
substituted into equation (6.15), the discrepancy reduces. The values
of E' and E_u then become 12.61 MN/m^2 and 14.10 MN/m^2 respectively.
Nevertheless, this simple approach to the estimation of stiffness is in-
adequate.

Pender (1978) has developed a model for overconsolidated clays
based on critical state concepts which allows for both distortional and
volumetric plastic strains beneath the state boundary surface. Elastic
shear strains are assumed to be zero. From the stress-strain data at
small strain levels presented in Chapter 5, it is evident that plastic
strains are predominant.

The undrained stress path is assumed to be parabolic and is of the form :—

$$\left(\frac{\eta}{M}\right)^2 = \frac{p'_{cs}}{p'}\left\{\frac{1 - \dfrac{p'_o}{p'}}{1 - \dfrac{p'_o}{p'_{cs}}}\right\} \tag{6.16}$$

where η is the stress ratio $\frac{q}{p'}$, and p'_{cs} the value of p' at the critical state. The plastic shear strain, ϵ^P, plastic volumetric strain, V^P, and elastic volumetric strain, V^e, are given by :—

$$d\epsilon^P = \frac{2\kappa\left(\dfrac{p'}{p'_{cs}}\right)\eta\ d\eta}{M^2 v\left(\dfrac{2p'_o}{p'} - 1\right)\left\{M - \left(\dfrac{p'}{p'_{cs}}\right)\eta\right\}} \tag{6.17a}$$

$$dV^P = \frac{2\kappa\left(\dfrac{p'_o}{p'_{cs}} - 1\right)\left(\dfrac{p'}{p'_{cs}}\right)\eta\ d\eta}{M^2 v\left(\dfrac{2p'_o}{p'} - 1\right)} \tag{6.17b}$$

and $\qquad dV^e = \dfrac{\kappa dp'}{p'v}$ $\qquad\qquad\qquad\qquad\qquad$ (6.17c)

For drained tests both p'_o and p'_{cs} vary and are determined by examining the hypothetical undrained stress path that passes through the current stress state. The accumulated strains can therefore be calculated by a numerical process, as described by Pender (1978), providing $d\eta$ is small. In order to compare the predictions of Pender's model with the stress-strain curves presented in Chapter 5, it has to be assumed that the difference between the natural (or logarithmic) strain and the linear strain is negligible. For drained tests the shear strain calculated from the model is converted into axial strain by adding one-third of the total volumetric strain onto the plastic shear strain.

Figures 6.16 and 6.17 show the comparisons between the predicted stress-strain curves with the present test results using the critical state parameters for the intact material and the average value of initial

specific volume, v = 1.402 (Table 5.14). It can be seen that for both the drained and undrained tests the predicted stress-strain curves lie in the middle of the measured range if the result of test T1UV is rejected. Pender's model is therefore reasonably successful in predicting the stress-strain response of Cowden Till at small strains.

6.4   COMPARISON WITH PUBLISHED DATA

As mentioned in Section 1.3.1, the primary objective of the research was to obtain data on the small strain behaviour of Cowden Till in the laboratory and subsequently to compare them with existing field data. It was hoped that the discrepancy in stiffness parameters between the laboratory and field measurements could be minimized. The comparison of stiffnesses presented here makes use of data from plate loading tests conducted by the BRE with under-plate instrumentation. However, as some of the specimens were tested to failure (as defined by the control algorithm of Section 4.3) their strength parameters can be compared, briefly, with those obtained previously.

Figure 6.18 shows the present undrained shear strengths in comparison with those measured in compressive triaxial tests on isotropically consolidated specimens from pushed tube samples, Marsland and Powell (1985). Unfortunately, one of the three present undrained tests was terminated prematurely (see Section 5.4.2), so that only two remaining data points can be plotted. It can be seen that the strength of specimen T1UV was uncharacteristically low but this specimen was thought to have been subjected to significant sampling disturbance, as mentioned in Section 5.4.2. However, the result from test RT5UV was consistent with the previous data, as also shown in Figure 6.19.

Figure 6.20 compares the effective stresses at failure from the present research with those published by Marsland and Powell (1985).

If c' is taken as zero, the mean angle of shearing resistance (ϕ') measured in the present tests (five results) is 35.2°. In general the present strengths lie at the upper end of the previously observed spectrum. In one case (test RT5UV) an anomalously high strength was recorded. Mechanical disturbance during sampling can induce a change in effective stress prior to shearing, as discussed in Section 2.2, and hence a change in undrained strength. On the other hand, effective strength parameters are relatively insensitive to disturbance unless there is loss of cementing or an appreciable change of density. Even so, it appears that changes of density have affected the results shown in Figure 6.20. In the present tests there was a significant reduction of moisture content during consolidation and storage, from 17% in-situ (see Figure 2.8) to about 15% (see Table 5.14). A reduction of moisture content was noted in the previous tests on Vibro specimens and must also have occurred when pushed samples were consolidated. Since the effective strength would be expected to increase as the moisture content reduces (density increase), this probably explains why the present results are more consistent with those from the Vibro specimens than the unconsolidated pushed specimens.

The pre-failure behaviour of a triaxial specimen (i.e. its stiffness) would be expected to be much more susceptible to changes of structure during sampling (see Section 2.2). The method of sampling for the 250 mm tube samples, described in Section 3.5.1, can be considered as a non-displacement method (i.e. the soil is subjected to negligible shear strain as it enters the sampling tube). On the other hand, the pushed samples obtained by Marsland and Powell (1985) probably suffered a significant shear strain. Since the diameter to wall thickness ratio was 60, it can be roughly estimated from Figure 2.1 that a shear strain of 0.2% occurred during sampling. The secant shear moduli at half of the

failure stress, $(G)_{50}$, from the present tests are compared with those from Marsland and Powell's pushed samples in Figure 6.21. Only the tests reaching failure with the same total stress path are included (four results). The present shear moduli have been obtained from the Young's moduli with

$$(G)_{50} = (G')_{50} = (G_u)_{50} = \frac{(E_u)_{50}}{2(1+\nu_u)} = \frac{(E')_{50}}{2(1+\nu')} \tag{6.18}$$

by assuming that ν' and ν_u are 0.34 and 0.50 respectively. From Figure 6.21 it can be seen that only the result of test T1UV compares well with the pushed sample data. In the other tests $(G)_{50}$ was about three times higher. This suggests that the 250 mm tube samples were significantly less disturbed than the pushed samples, sample T1UV being an exception, as discussed in Section 5.4.2.

Figures 6.22 and 6.23 summarize the effect of depth on the shear moduli evaluated by different techniques in previous and present investigations. Two relevant observations were made when reviewing previous data in Section 2.3.4. Firstly, there is not much change in stiffness with depth. Secondly, unless reference is made to strain levels, a comparison of moduli from different tests is difficult. Thus, the only directly comparable results are the values of $(G)_{50}$ from triaxial tests, discussed above. In the case of plate loading tests, a meaningful comparison with the present work can be made if data is available from under-plate instrumentation similar to that used by Marsland and Eason (1974). A comparison with such data will be made below. The difficulty of strain level may not arise to the same extent when comparing the moduli obtained during unloading and reloading, providing reasonably linear, reversible behaviour is exhibited. In that case the modulus would not depend upon the strain level. Unload-reload shear moduli are

compared in Figure 6.23, from which it can be seen that the present test results compare more favourably with those from the back analysis of in-situ model pile tests than with those from plate tests interpreted by equation (2.7). However this interpretation of the plate test is still being researched (Powell, 1987b) and it is possible that a better inter-pretation could have been made if under-plate data had been used.

To permit further comparison between the moduli obtained in the laboratory and in the field, the BRE has made available the unpublished results of a plate test conducted some years ago (Powell, 1987a). The test was conducted in a borehole at 5 m depth using a multi-point measur-ing system described by Marsland and Eason (1974) to measure displace-ments beneath the centre-line of the plate. The plate diameter was 865 mm and the borehole diameter was 900 mm. Table 6.2 lists the data supplied by BRE. The ratios of the settlements at the measuring points to those measured at the plate surface are tabulated in Table 6.3 and plotted in Figure 6.24 where the finite element prediction from Marsland and Eason (1974) is also shown. The interesting feature in Figure 6.24 is that whereas finite element analysis suggests that only 15% of the plate settlement is due to deformation of the clay within a depth of about half the plate diameter, the actual measurements indicate that a figure of between 25% and 35% is more appropriate. This could be due to deficiencies of the analysis or to a zone of disturbed material near the base of the borehole prior to installation of the plate. The latter is probably more likely (see below).

In order to interpret the data in terms of moduli at various strain levels, it is necessary to know the distribution of stress changes beneath the plate as it is loaded. A distribution of horizontal and vertical stress for this borehole plate test has been recommended by

Powell (1987b) on the basis of recent analysis conducted on behalf of the BRE at the City University. Changes on the centre-line are shown in Figure 6.25 together with the stress distribution for a plate loaded at the ground surface, as obtained by Poulos and Davis (1974). Lopes (1979) conducted a finite element analysis of a borehole plate test in London Clay and the resulting stress distribution is also included in Figure 6.25. It can be noted that in a borehole plate test, due to the restraint of material at the sides of the borehole above plate level, both the vertical and horizontal stresses are reduced considerably by comparison with those for a surface plate. Figure 6.26 shows the difference between the vertical and horizontal stresses due to the applied load and it is apparent that in Powell's distribution it is considerably less than in that of Poulos and Davis.

The soil between each pair of measuring points beneath the plate can be considered as a triaxial element under the above (axially symmetric) stresses and a stress-strain relationship can be derived as follows. Taking the start of loading of the plate as a datum, at any stage of the test the change of axial strain ($\Delta\varepsilon_A$) is computed from the change of relative displacement of the two ends of the element, and the average changes of applied stress ($\Delta\sigma_V$ and $\Delta\sigma_H$) over the height of the element are estimated by inspection of Figure 6.25. Following the procedure recommended by Powell (1987b) and assuming the soil to be undrained, the secant Young's modulus for the element at that stage of the test can then be calculated as:-

$$E_u = \frac{\Delta\sigma_V - 2\nu_u\Delta\sigma_H}{\Delta\varepsilon_A} = \frac{\Delta\sigma_V - \Delta\sigma_H}{\Delta\varepsilon_A} \qquad (6.19)$$

since $\nu_u = 0.5$ under undrained conditions.

The results of these calculations for two stages of the test in question are summarized in Table 6.4 and plotted as deviator stress $(\Delta\sigma_v - \Delta\sigma_H)$ versus axial strain in Figure 6.27. The uncharacteristic stress-strain relationship of the uppermost element (0-152 mm) is probably the result of disturbance near the base of the borehole. The next element may also have been subjected to a certain degree of disturbance. The lower two elements appear not to have suffered from disturbance and show almost identical behaviour. Another feature evident in Figure 6.27 is the non-linear nature of the behaviour at small strain levels, although the number of data is limited. Unfortunately data obtained at plate stresses below 170 kN/m^2 are insufficiently accurate to be included (Powell, 1987a).

As indicated by Wroth (1971) the undrained stiffness is dependent on the initial effective mean normal stress (p'_o) (see also equation (6.15b)). To permit a comparison between the moduli obtained in the present triaxial tests and those obtained in the plate tests, the moduli have been normalized by dividing by this parameter. For the triaxial tests, the values of p'_o were as tabulated in Table 5.14. For the plate test, which was conducted at 5 m depth, the effective vertical pressure p'_{vo} was 75 kN/m^2 (see Figure 2.10) and, since $\kappa_o \simeq 1$, p'_o was also taken as 75 kN/m^2. The normalized laboratory and field moduli at strain levels between 0.01% and 1.0% are compared in Figure 6.28 where acceptable agreement can be seen. The results for the uppermost element agree closely with the results for test T1UV and this supports the argument already made that the soil was disturbed in both cases. Consequently, these results differ from the rest. Below 0.1% strain the full extent of the stiffness variation observed in the tests becomes evident. Some of this has been caused by sampling disturbance and testing errors, especially in tests T1UV and T2UH. If these tests, and also RT6DH, are

rejected, the remaining results fall in a relatively narrow band. This may be more representative of the variation of stiffness in the field.

In making the comparison of laboratory and field data in Figure 6.28 it has been assumed that the soil is being subjected to initial loading from a given stress state. However when a borehole is prepared for a plate load test, the soil at the base of the borehole is subjected to stress relief. On subsequent loading by the plate, the measured deformation may well be influenced by the unload-reload characteristics of the soil. This aspect of the interpretation of plate load tests is still being investigated (Powell, 1987b) and the agreement evident in Figure 6.28 may prove to be misleading. (The range of unload-reload moduli in the triaxial tests is also indicated in the figure.) Nevertheless, the present evidence suggests that plate tests, though considerably more expensive and difficult to perform, would provide no better information about the stiffness of Cowden Till than triaxial tests of the type described in this thesis.

Figure 6.29 compares the normalized moduli of London Clay (Canons Park) from Jardine et al. (1985) with those obtained from the present triaxial tests on Cowden Till. If the results of tests T1UV, T2UH and RT6DH are excluded a remarkable degree of similarity is seen.

Axial strain (%)	Average tangent effective vertical modulus, E'_v (MN/m^2)	Tangent modulus (MN/m^2)					
		Vertical specimen (test RT5UV)			Horizontal specimen (test T2UH)		
		Measured	Predicted	$\dfrac{\text{Predicted}}{\text{Measured}}$	Measured	Predicted	$\dfrac{\text{Predicted}}{\text{Measured}}$
0.01	45.00	66.00	50.40	0.76	235.00	50.40	0.21
0.05	28.54	38.23	31.96	0.84	24.00	31.96	1.33
0.10	18.03	25.00	20.19	0.81	11.38	20.19	1.77

TABLE 6.1   Comparison of tangent Young's modulus with an anisotropic elastic model (Atkinson, 1973)

Depth beneath plate (mm)	Settlement (mm)	
	At Δq_p = 170 kN/m^2	At Δq_p = 330 kN/m^2
0	1.000	2.200
152	0.965	2.090
304	0.880	1.820
456	0.740	1.420
608	0.600	1.080

TABLE 6.2 Field measurement of a plate test at Cowden (courtesy of Powell, 1987a)

$\dfrac{\text{Depth of}}{\text{measuring point}}$ plate diameter	Settlement of ground at depth of measuring point / Settlement of plate at bottom of borehole	
	At Δq_p = 170 kN/m^2	At Δq_p = 330 kN/m^2
0.176	0.965	0.950
0.351	0.880	0.827
0.527	0.740	0.645
0.703	0.600	0.491

TABLE 6.3 Ratio of settlement of ground at measuring point to the settlement of plate

Triaxial specimen range beneath plate (mm)	At Δq_p = 170 kN/m^2			At Δq_p = 330 kN/m^2		
	Vertical strain (%)	Deviator stress $\Delta\sigma_v - \Delta\sigma_H$ (kN/m^2)	Secant Young's modulus (MN/m^2)	Vertical strain (%)	Deviator stress $\Delta\sigma_v - \Delta\sigma_H$ (kN/m^2)	Secant Young's modulus (MN/m^2)
0-152	0.023	8.33	36.22	0.072	16.17	22.46
152-304	0.056	26.44	47.21	0.178	51.32	28.83
304-456	0.092	39.61	43.05	0.263	76.89	29.24
456-608	0.092	37.15	40.38	0.224	72.11	32.19

TABLE 6.4 Stress-strain distribution beneath plate in a plate loading test (After Powell, 1987 a,b)
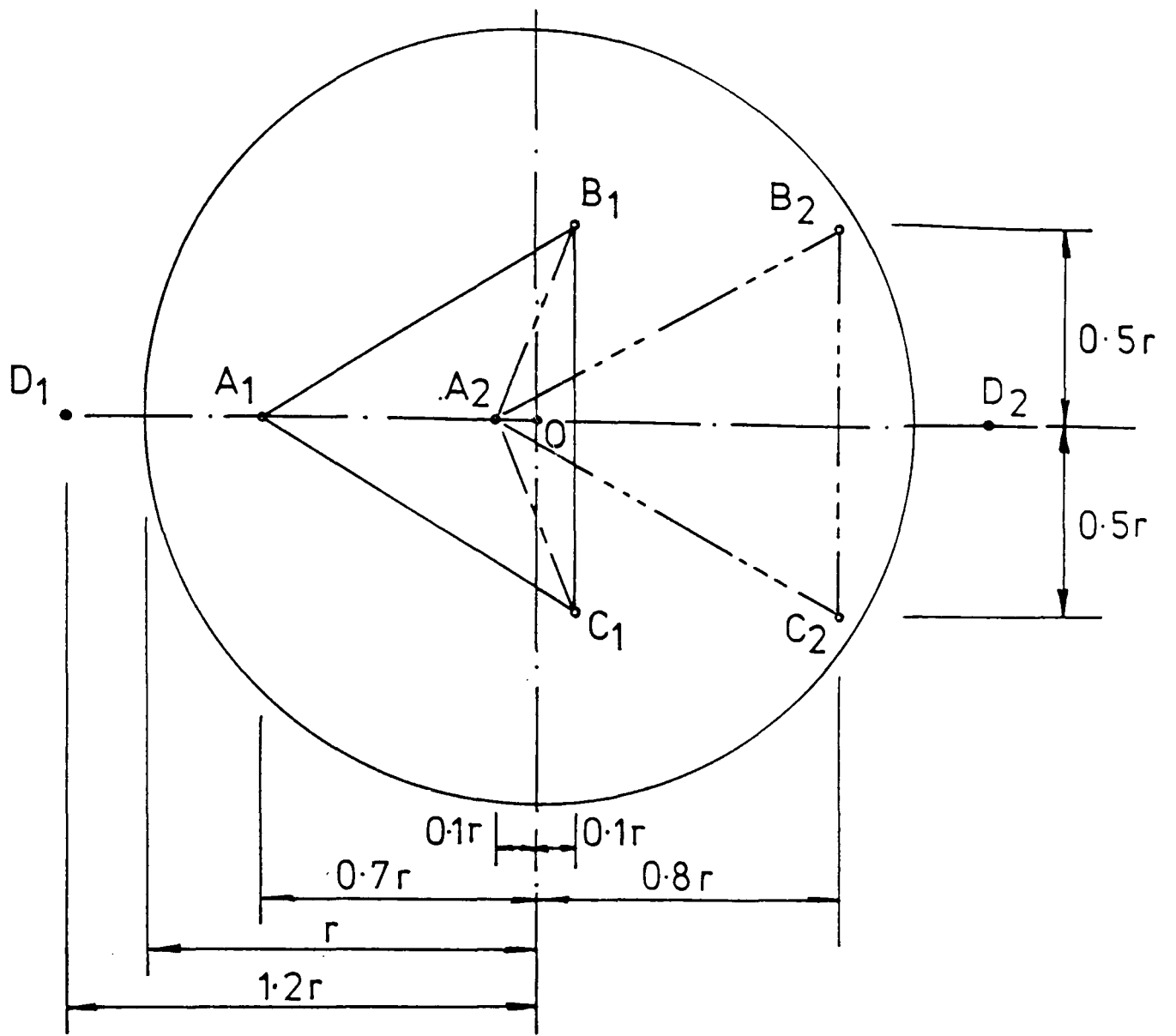
FIG. 6·1 - IDEALIZED BEDDING POSITIONS UNDER UNIT LOAD
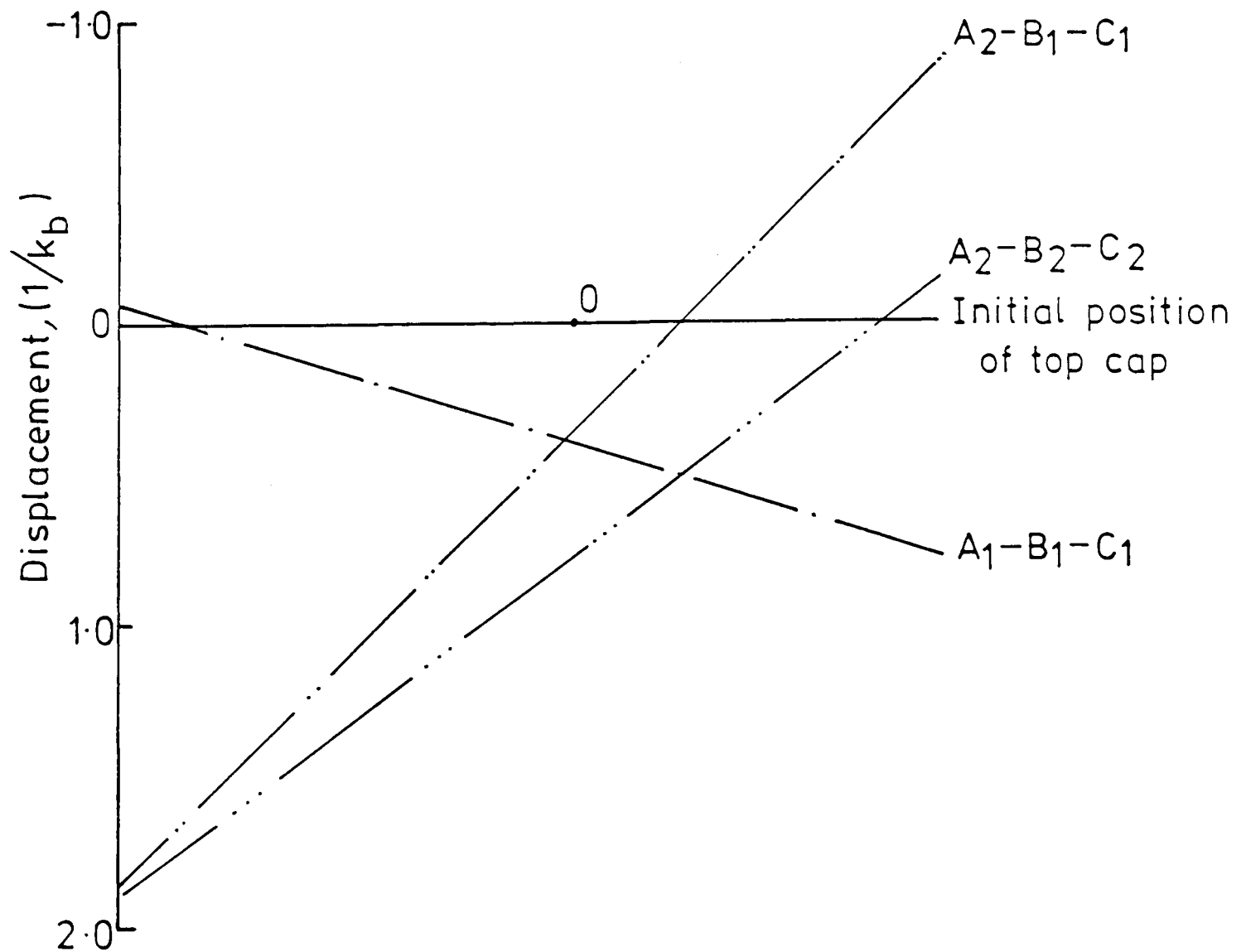
FIG.6·2 DISPLACEMENT PATTERNS OF TOP CAP CORRESPONDING TO FIG.6·1
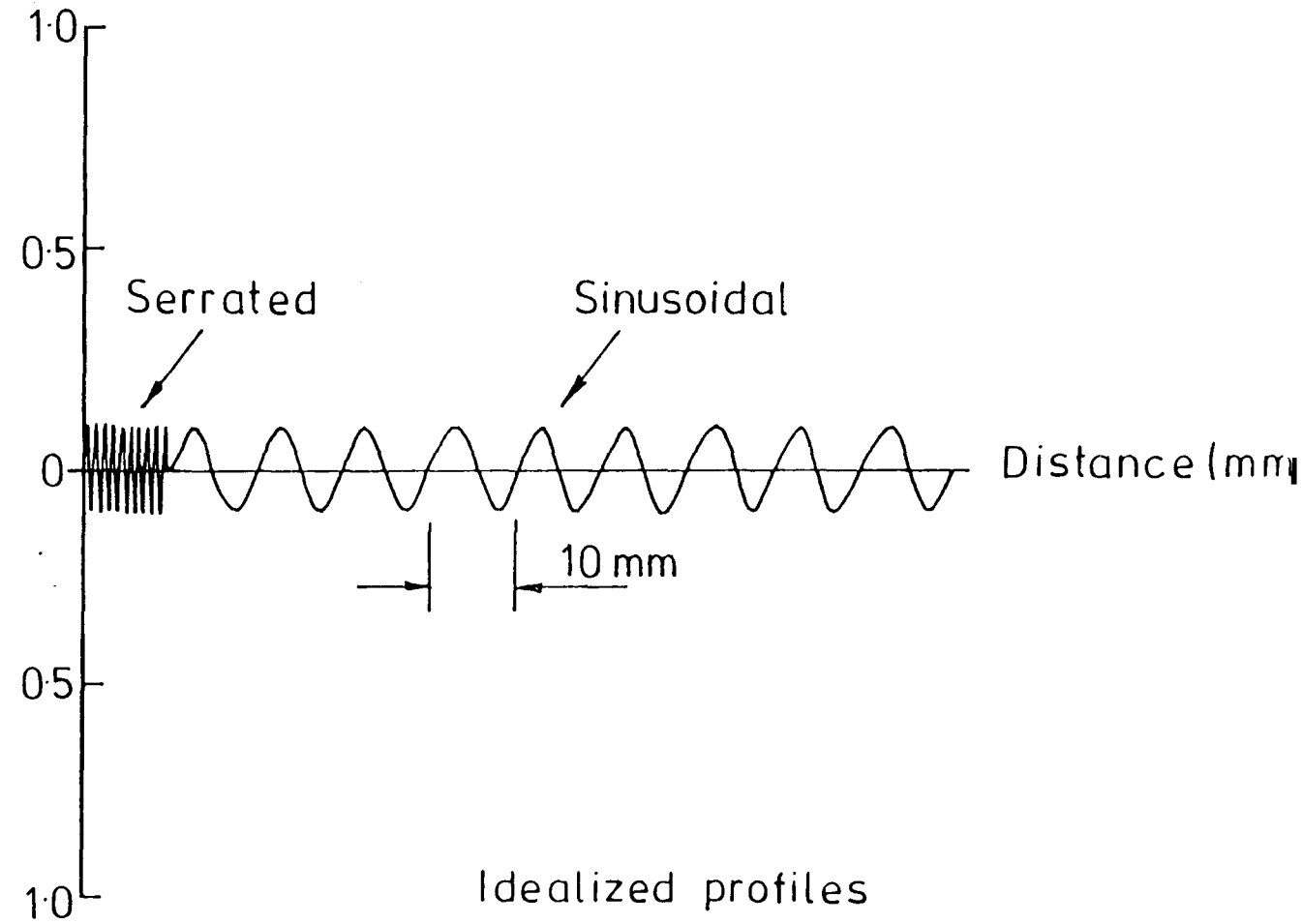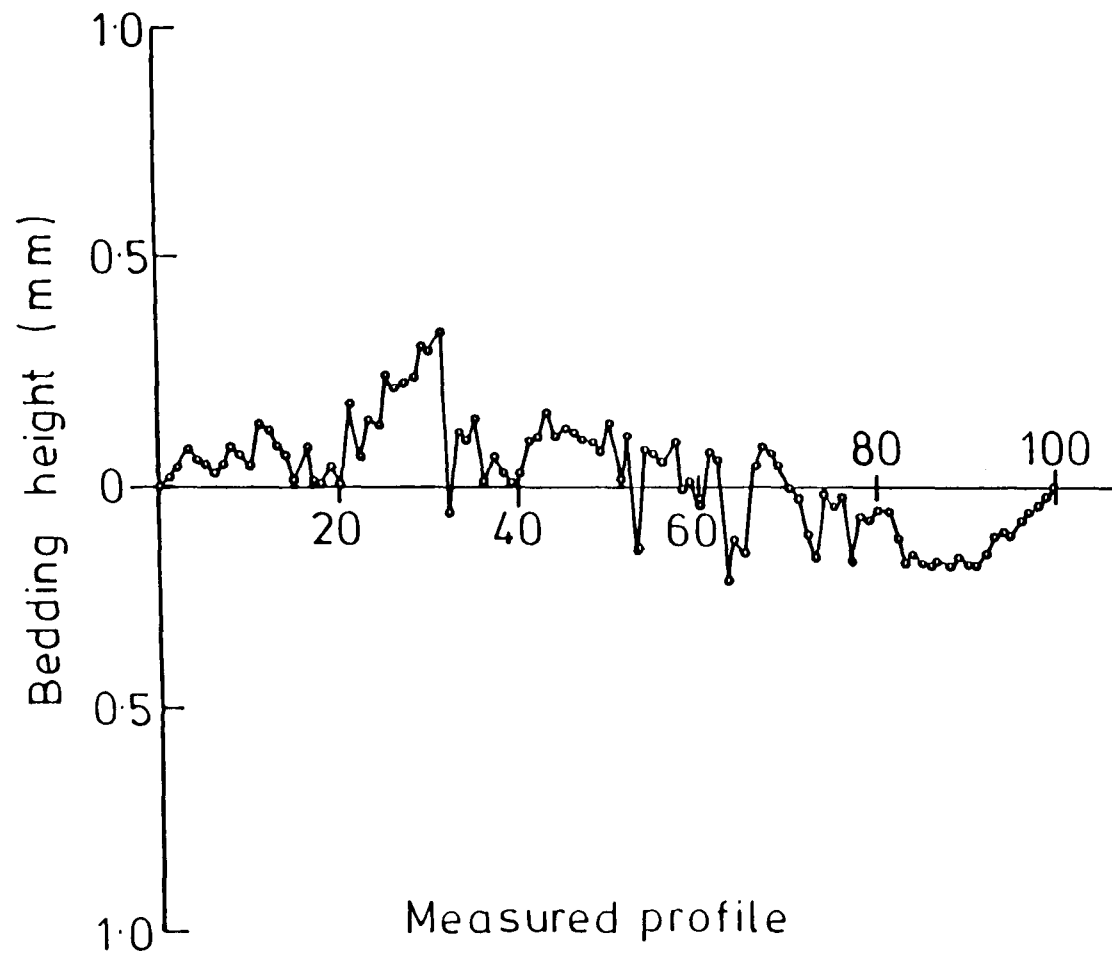
FIG. 6·3   SURFACE PROFILES OF TRIMMED SURFACE ON INTACT COWDEN MATERIAL

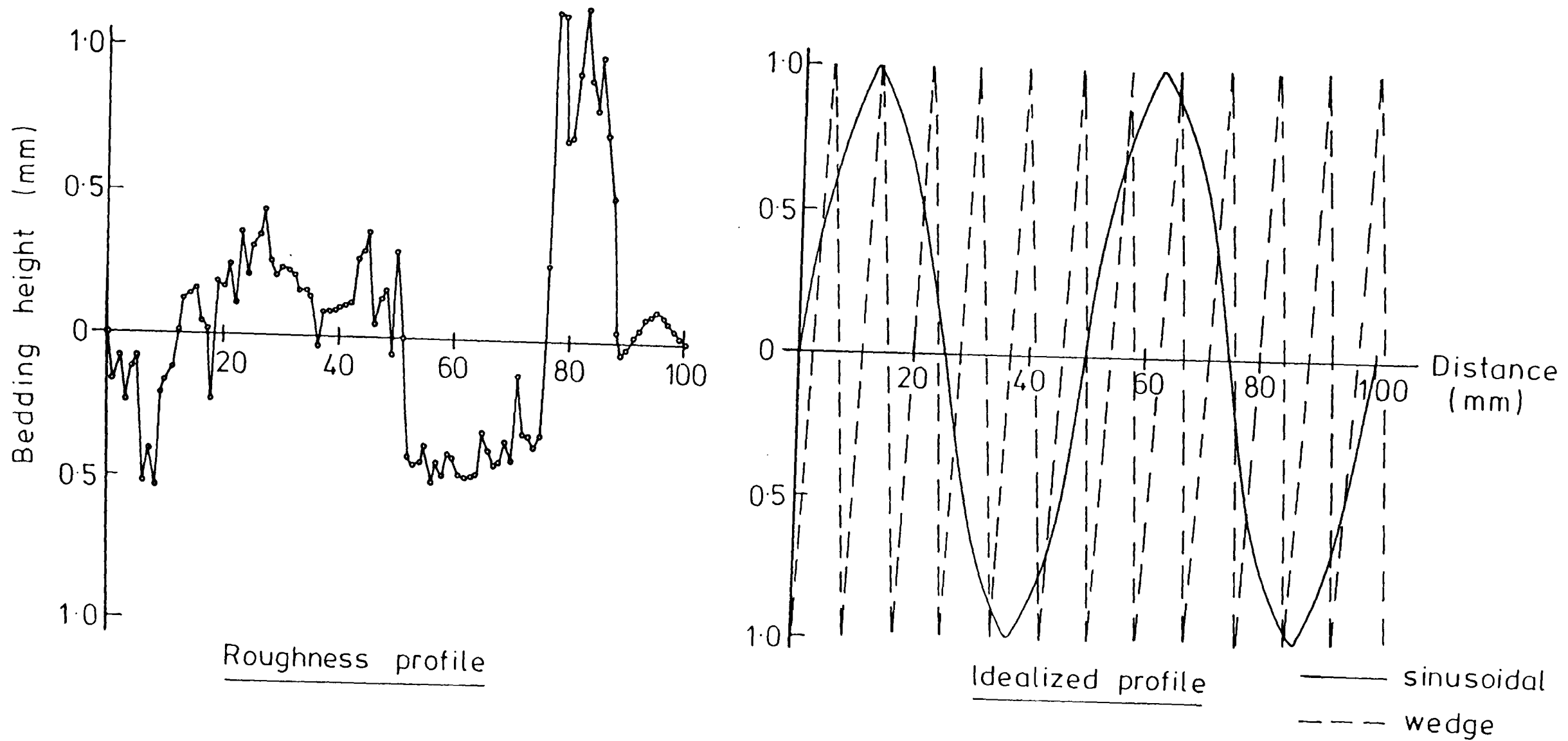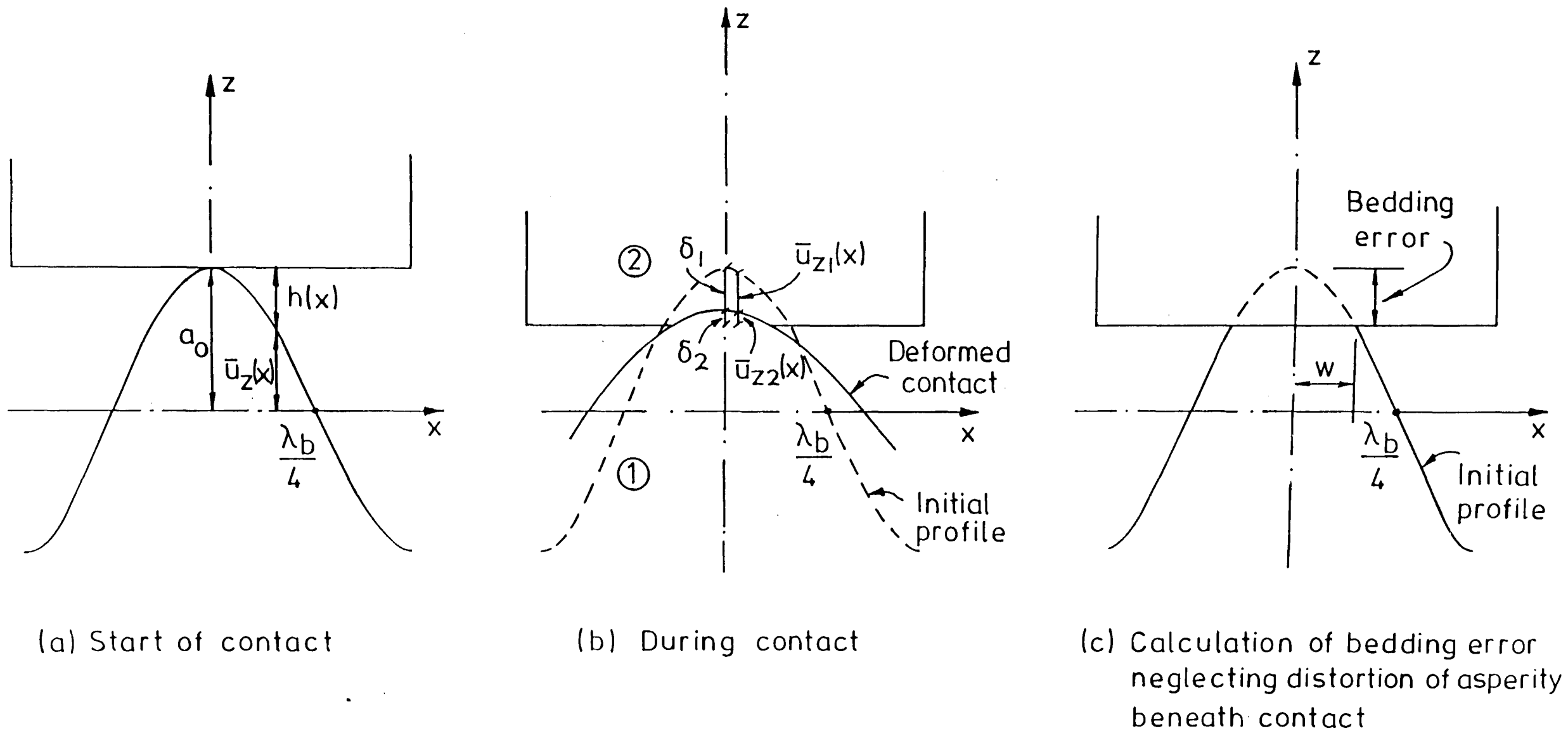FIG. 6·4   SURFACE PROFILES OF TRIMMED SURFACE ON INTACT COWDEN MATERIAL

(a) Start of contact   (b) During contact   (c) Calculation of bedding error neglecting distortion of asperity beneath contact

FIG. 6·5   IDEALIZED ELASTIC CONTACT PROFILE OF A SINUSOIDAL WAVY SURFACE WITH A FLAT SURFACE
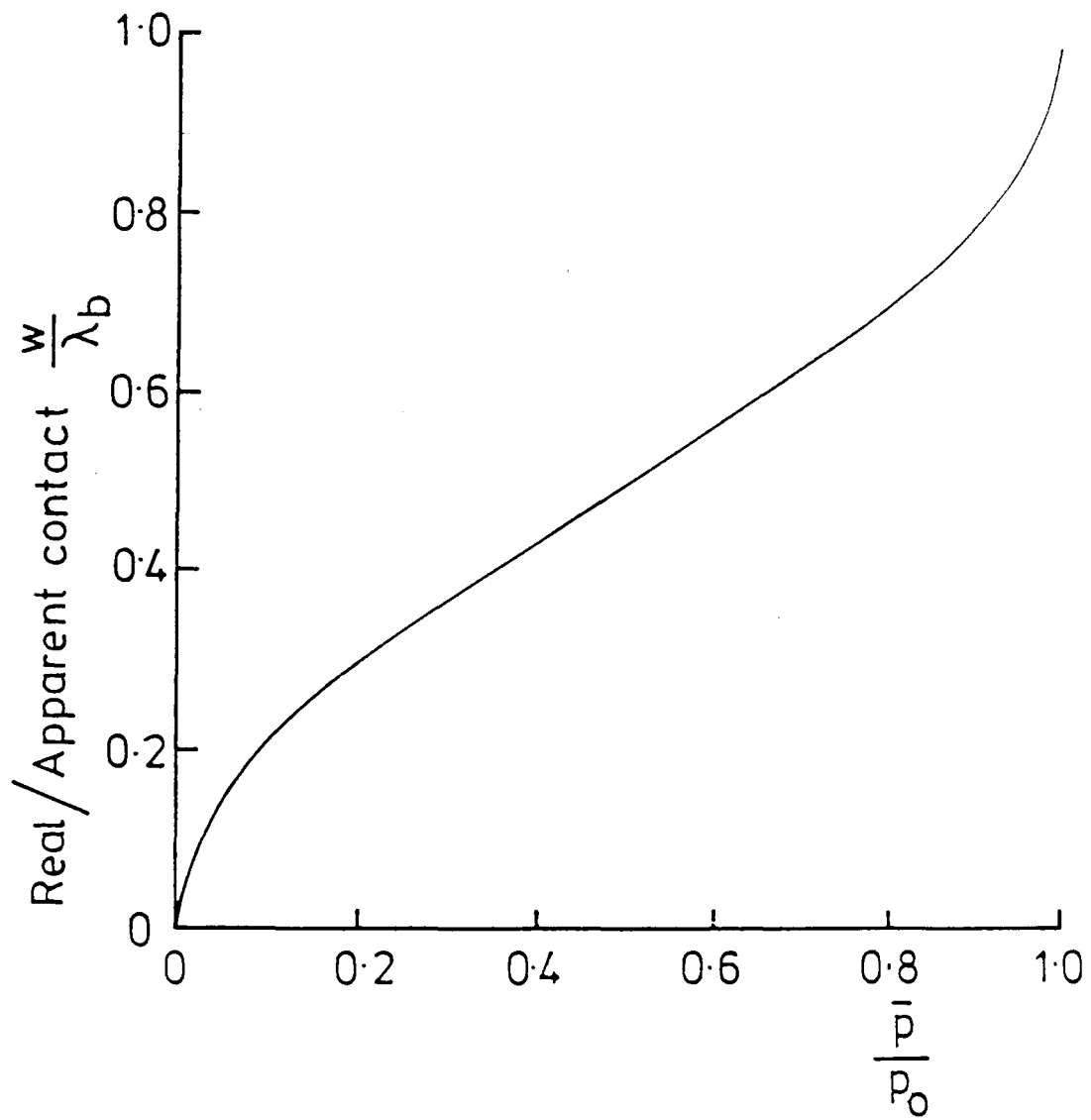
FIG.6·6   REAL AREA OF CONTACT BETWEEN ELASTIC
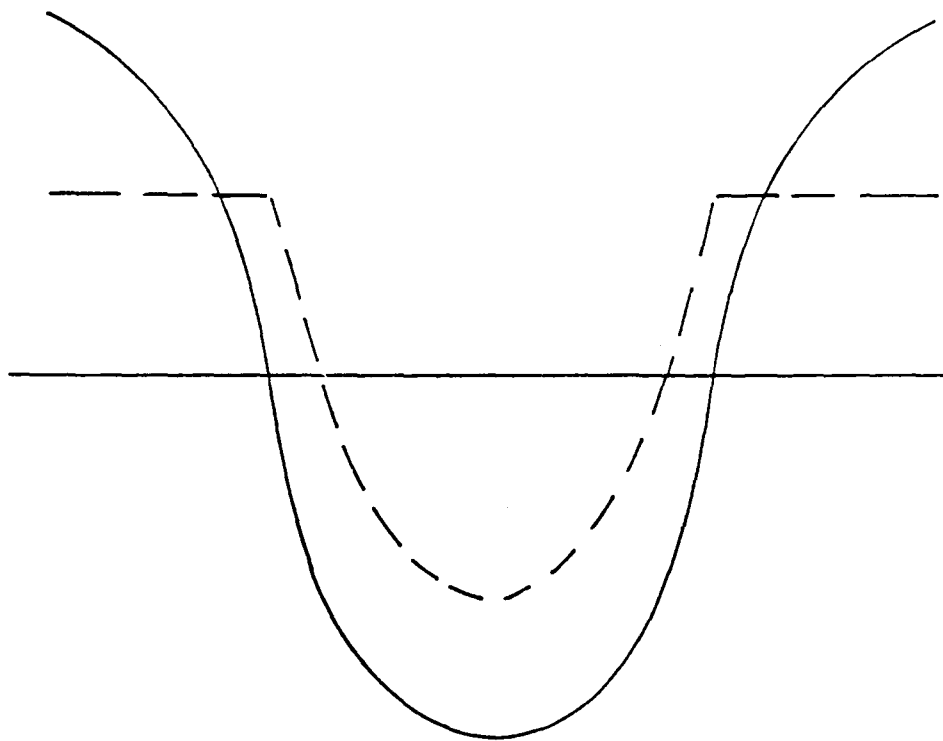BODIES UNDER A NORMAL PRESSURE (AFTER
JOHNSON, 1985)

Legend

————— Before applying normal stress
— — — After   „   „   „
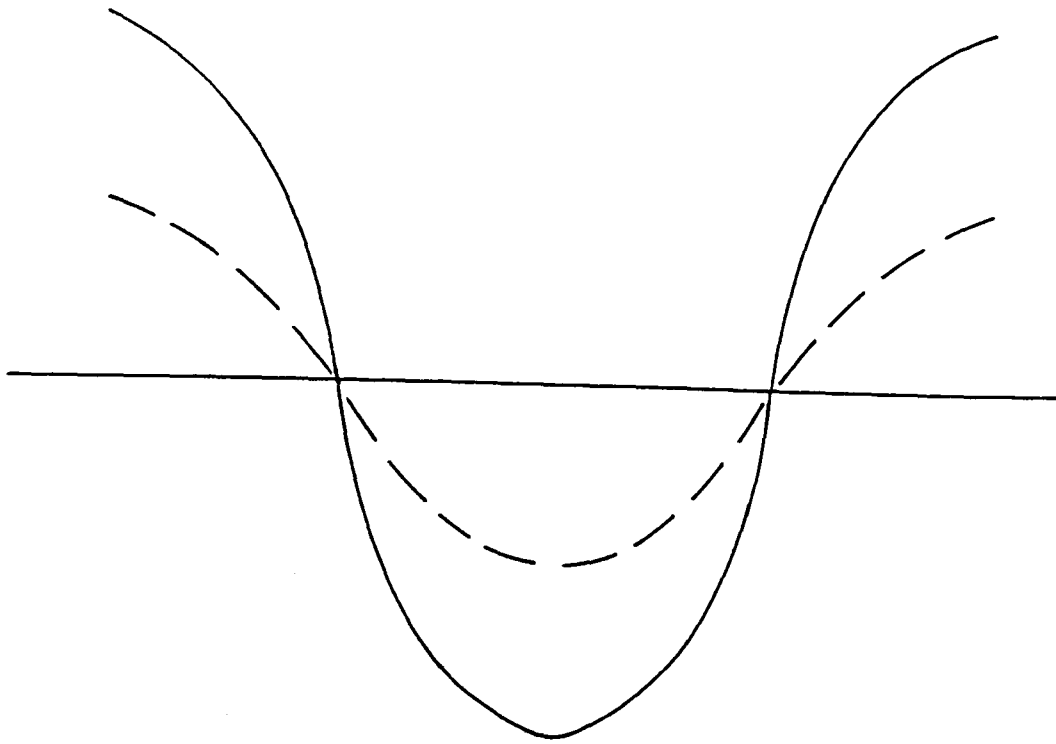
(a)

Davis & Salt (1986)

(b)

Johnson (1985)

FIG. 6·7   MECHANISMS OF DEFORMATION OF SINUSOIDAL
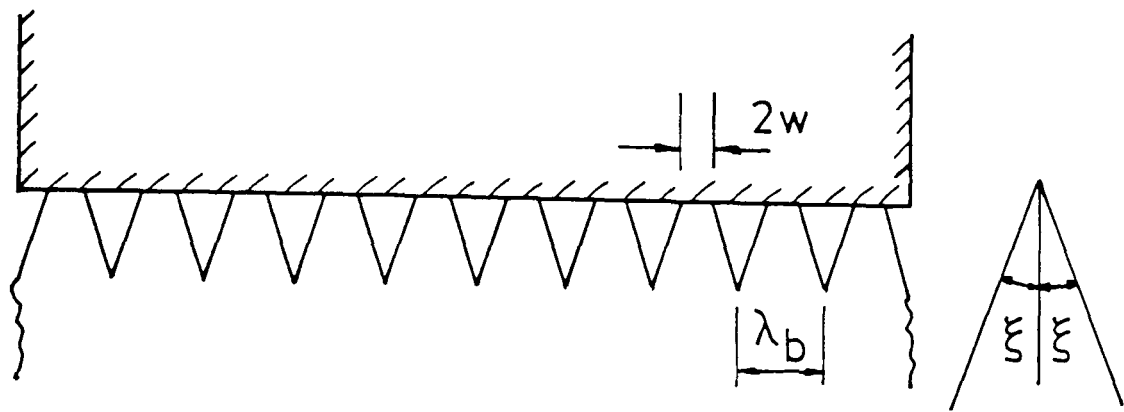WAVY SURFACE UNDER A UNIFORM PRESSURE

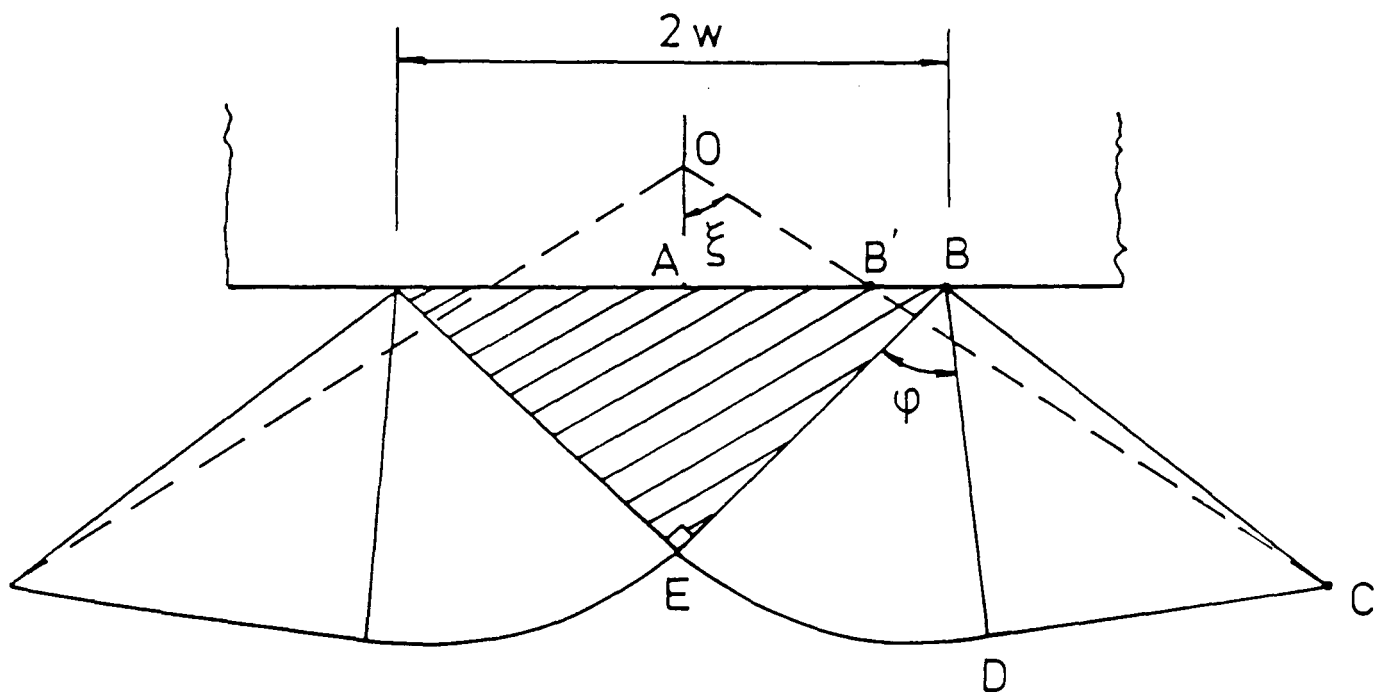FIG. 6·8 CRUSHING OF A REGULAR SERRATED PLASTIC
SURFACE BY A RIGID FLAT SURFACE

FIG. 6·9 CONTACT CONDITION BETWEEN A FLAT SURFACE
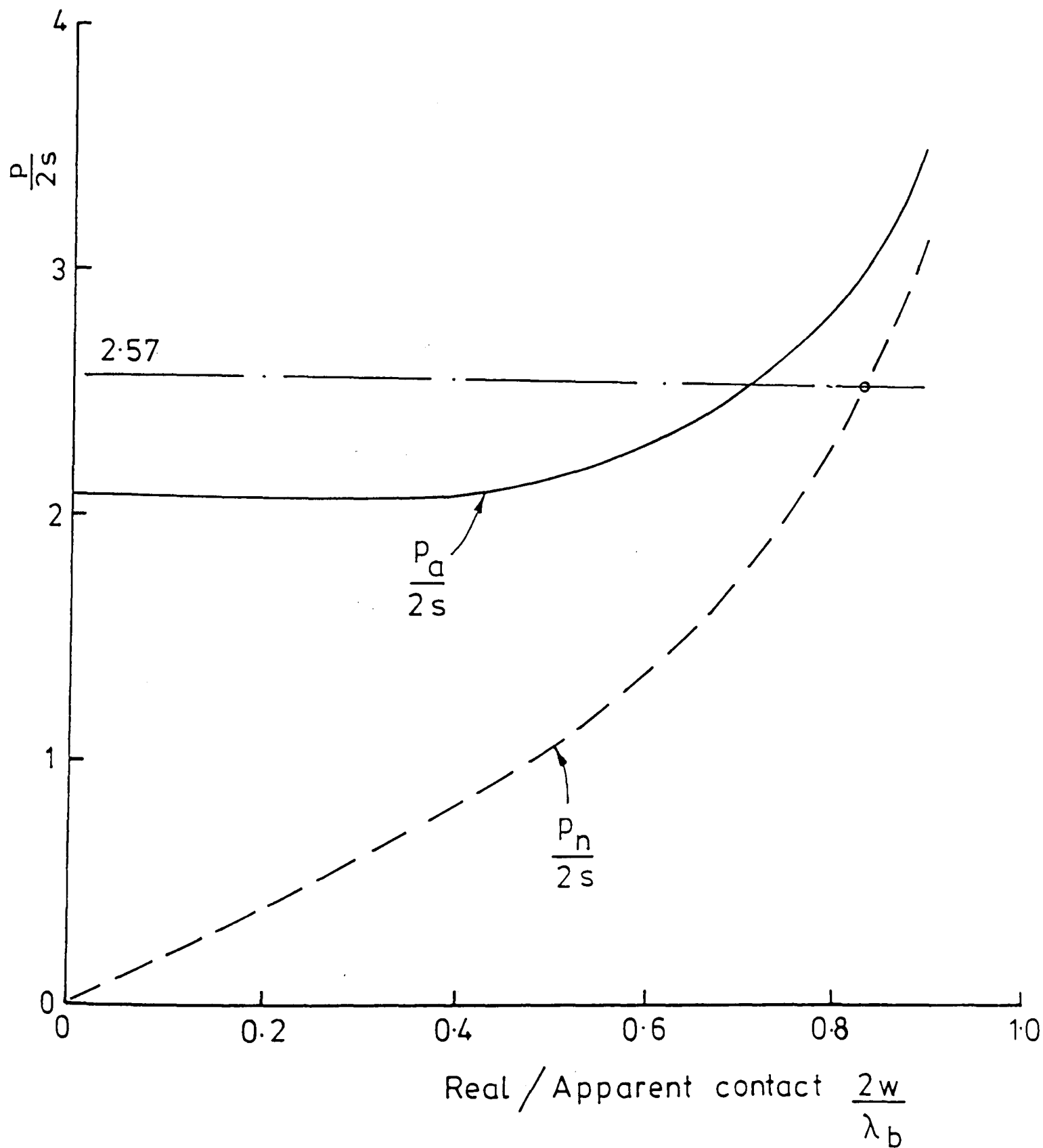AND A PLASTIC WEDGE (AFTER JOHNSON, 1985)

FIG. 6·10 REAL AREA OF CONTACT BETWEEN A RIGID FLAT
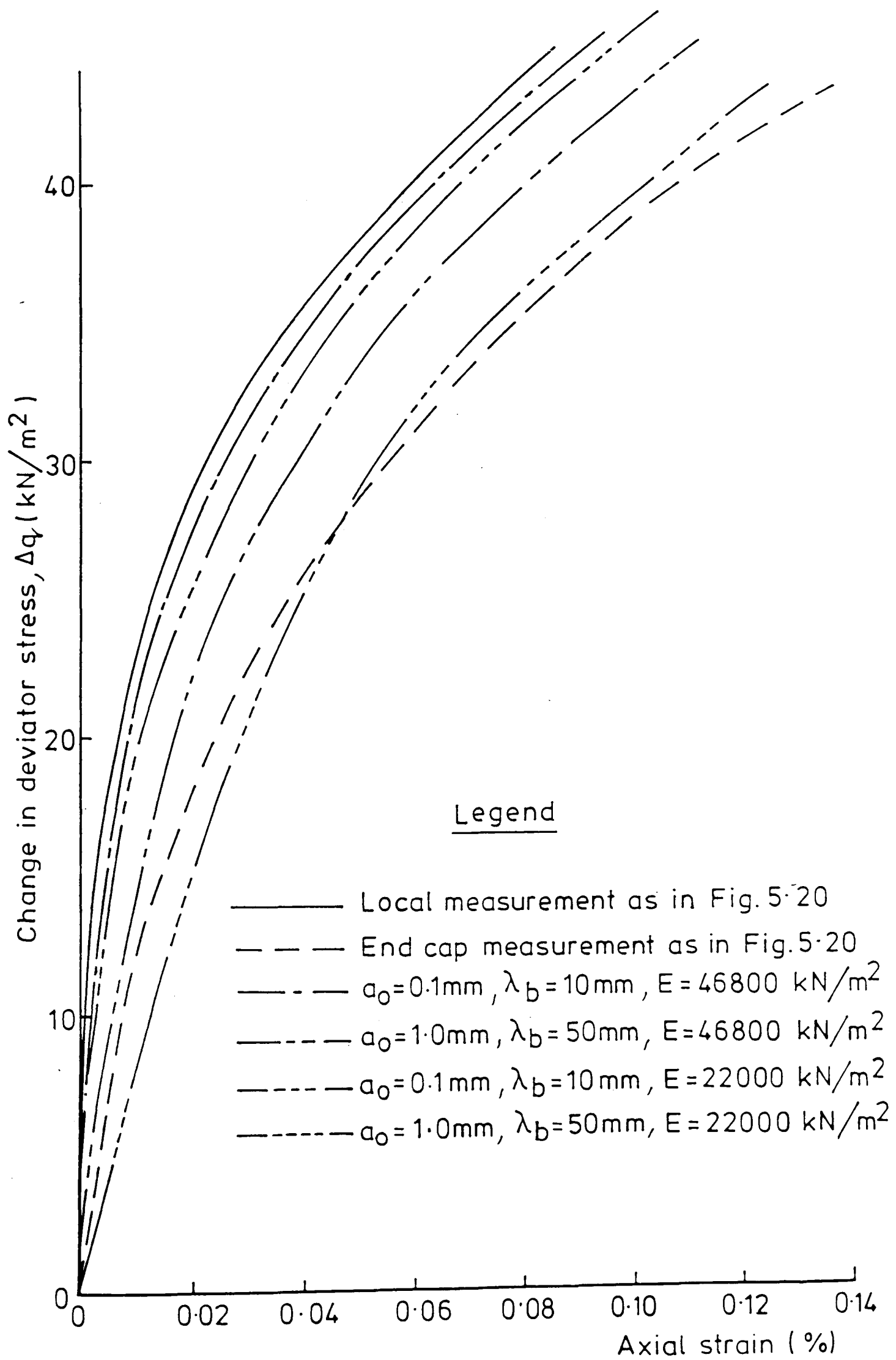SURFACE AND A PLASTIC SERRATED SURFACE (AFTER
JOHNSON, 1985)

FIG. 6·11 PREDICTION OF END CAP AXIAL STRAIN MEASUREMENT
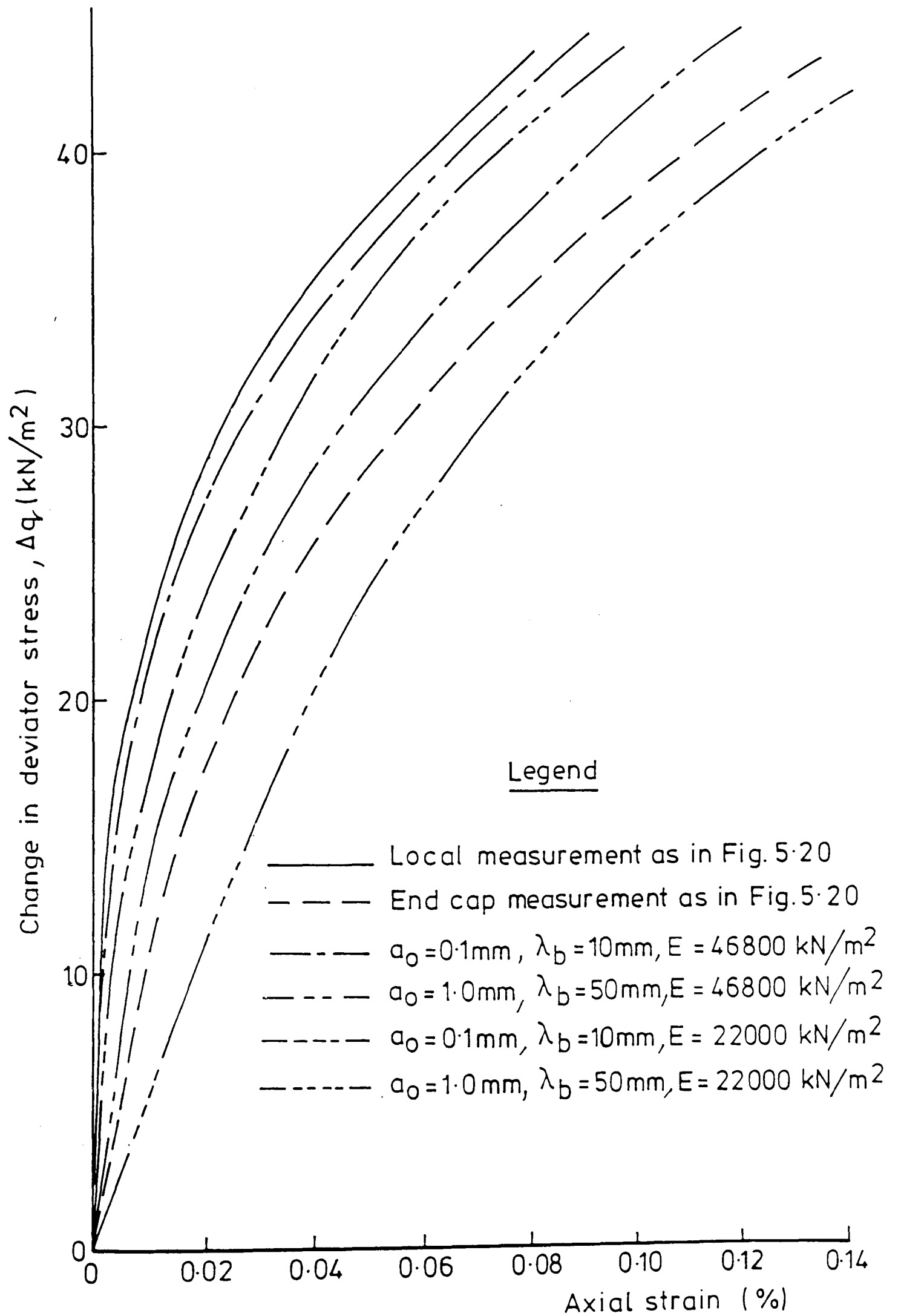BY JOHNSON'S APPROACH

Legend

——————— Local measurement as in Fig. 5·20

— — — End cap measurement as in Fig. 5·20

—·—·— $a_o = 0.1mm$, $\lambda_b = 10mm$, $E = 46800 \ kN/m^2$

— ·· — ·· — $a_o = 1.0mm$, $\lambda_b = 50mm$, $E = 46800 \ kN/m^2$

– – – – $a_o = 0.1mm$, $\lambda_b = 10mm$, $E = 22000 \ kN/m^2$

– ·· – ·· – $a_o = 1.0mm$, $\lambda_b = 50mm$, $E = 22000 \ kN/m^2$

Change in deviator stress, $\Delta q \ (kN/m^2)$

Axial strain (%)

FIG. 6·12   PREDICTION OF END CAP AXIAL STRAIN MEASUREMENT
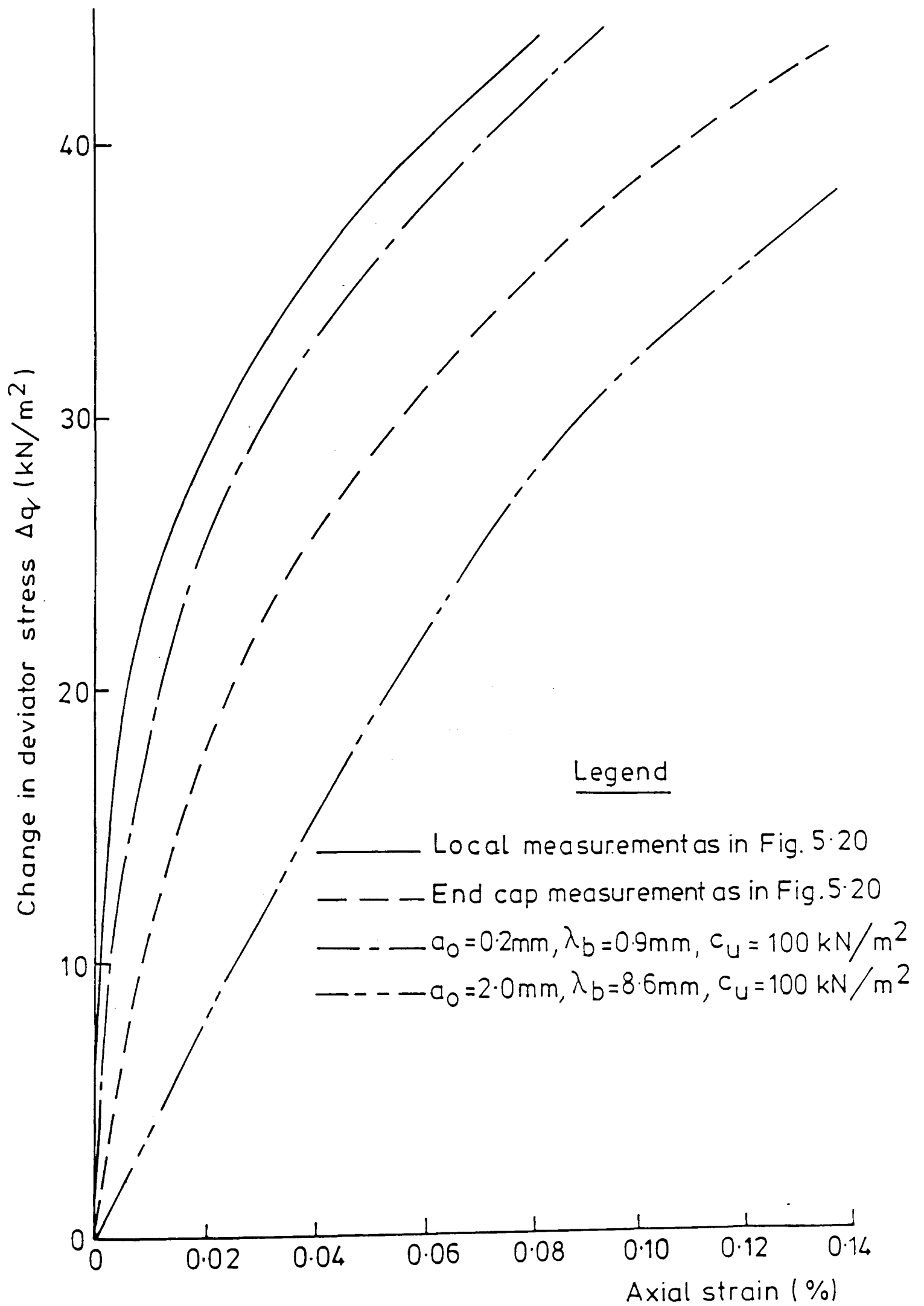BY DAVIS & SALT'S APPROACH

FIG. 6·13   PREDICTION OF END CAP AXIAL STRAIN MEASUREMENT
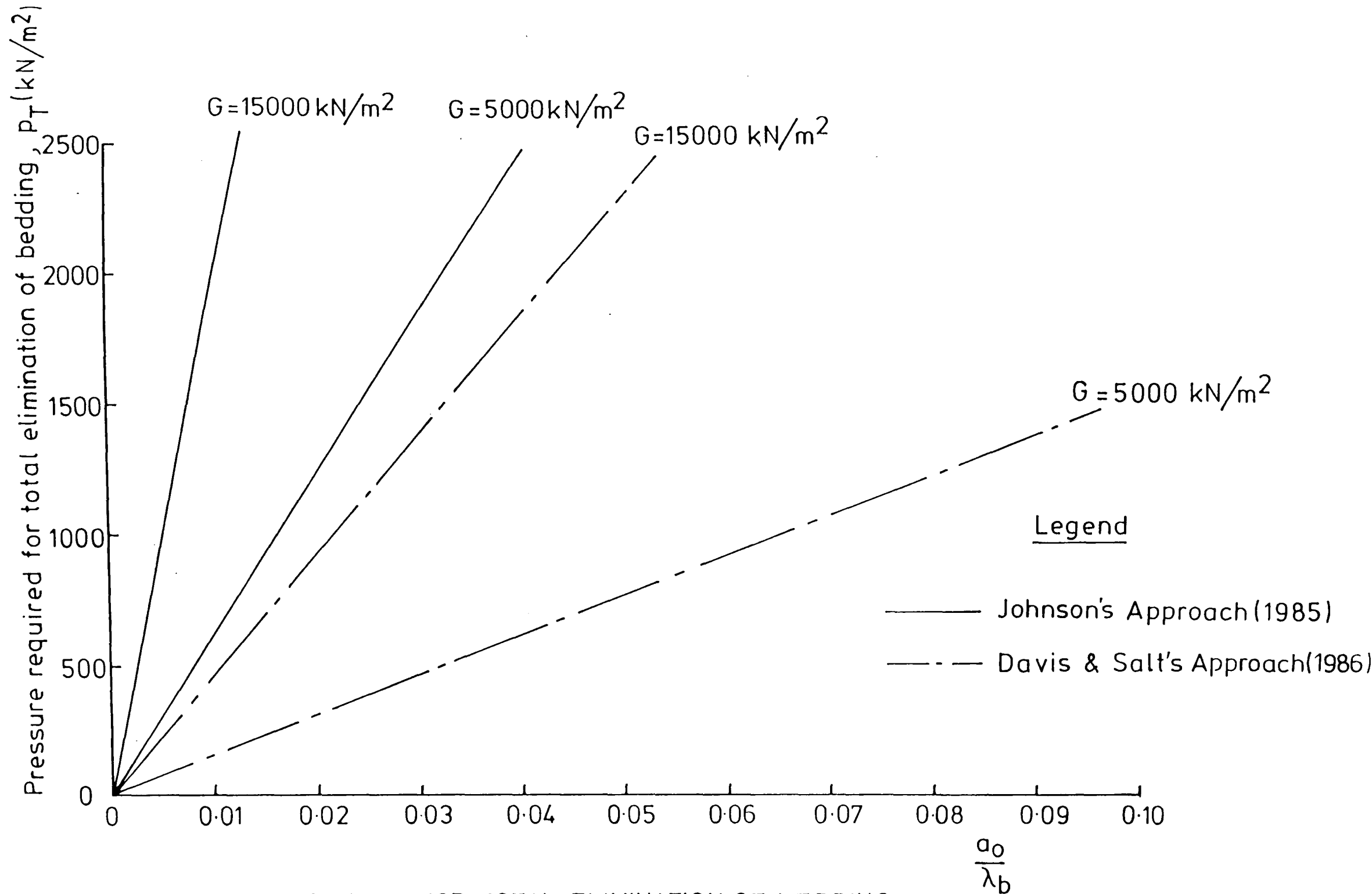BY RIGID WEDGE APPROACH

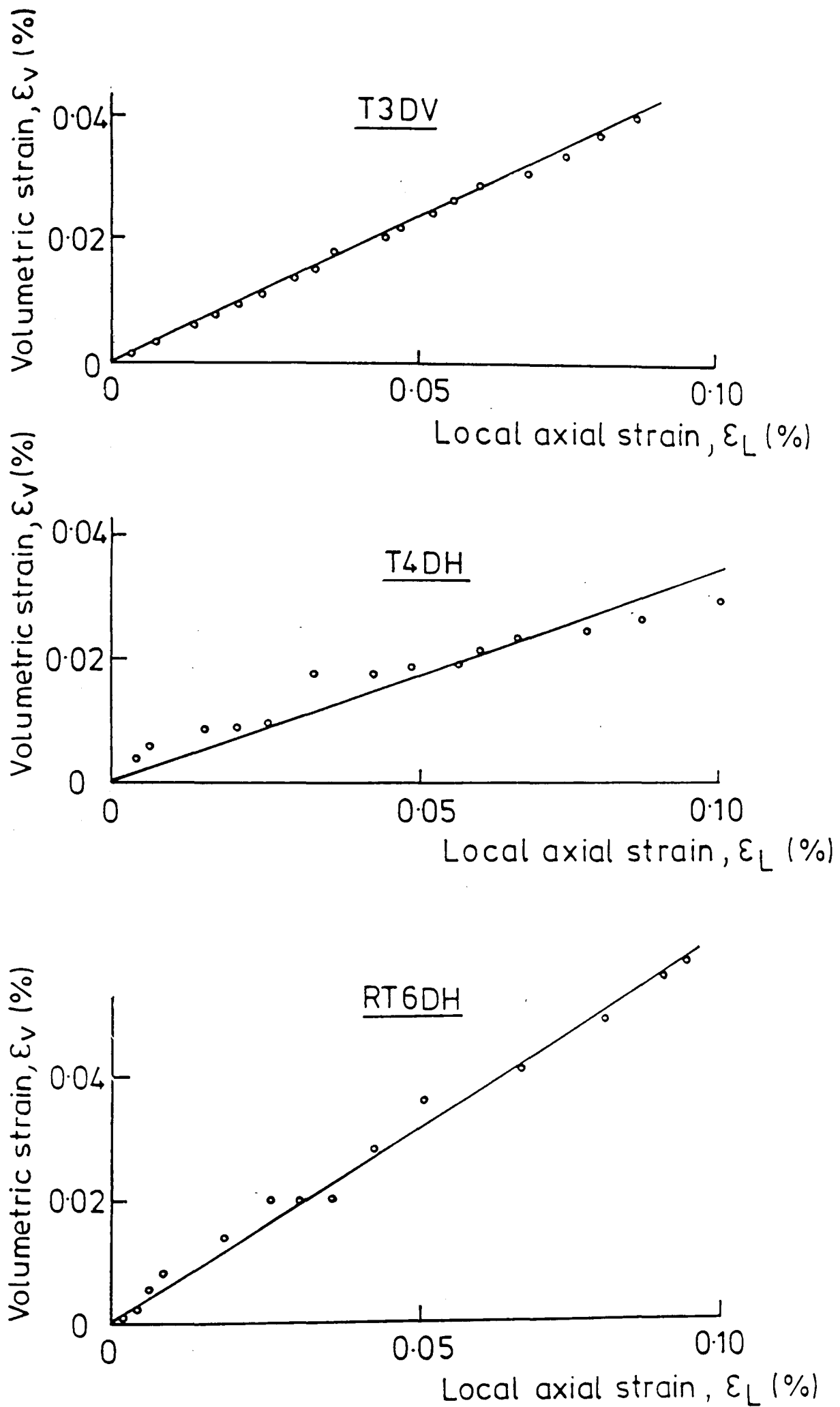FIG.6·14 PRESSURE REQUIRED FOR TOTAL ELIMINATION OF BEDDING

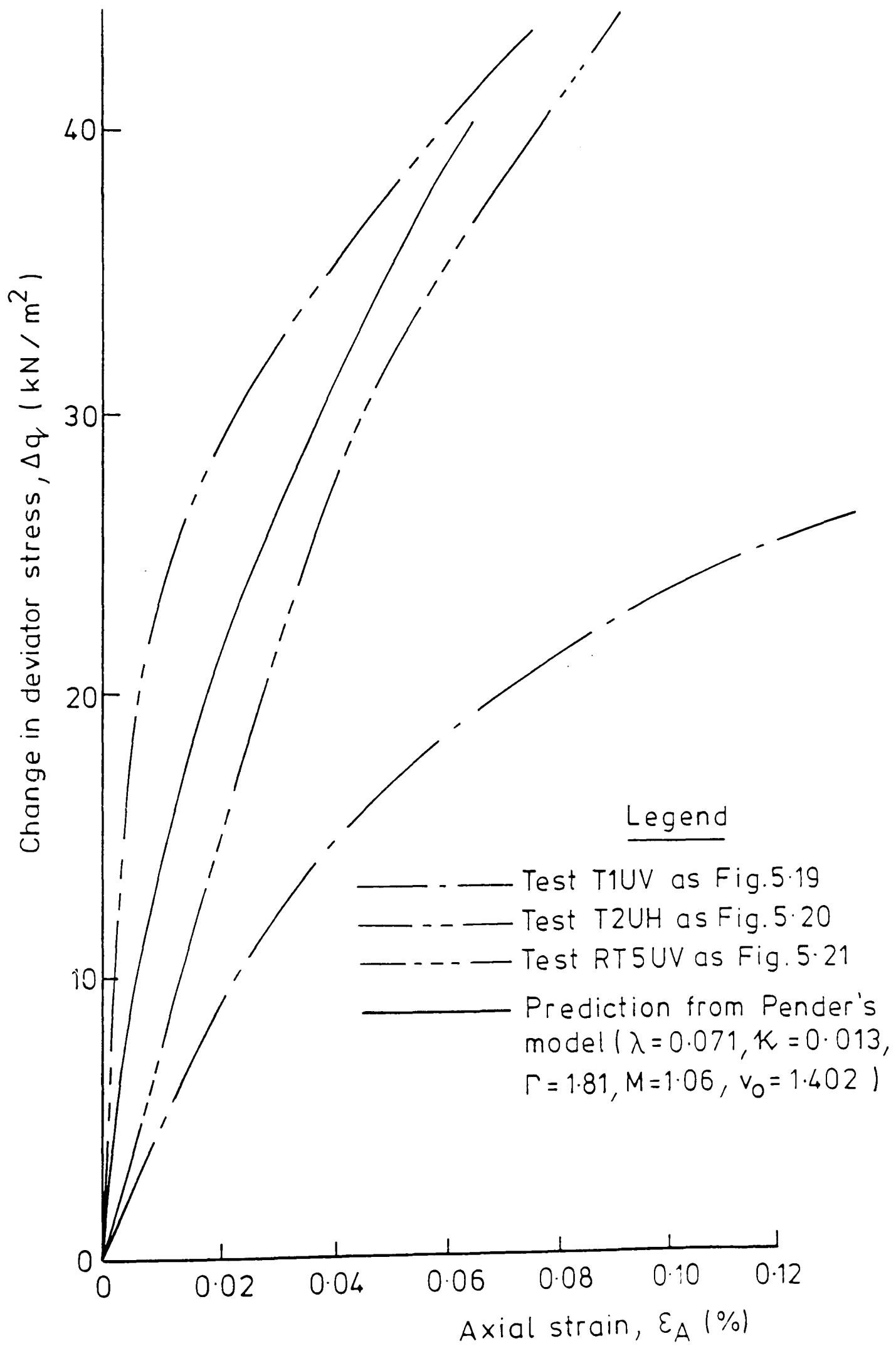FIG. 6·15   STRAIN PATHS FOR THREE DRAINED TESTS

FIG. 6·16 COMPARISON OF STRESS-STRAIN CURVES FROM UNDRAINED TESTS WITH A CRITICAL STATE MODEL (PENDER, 1978)
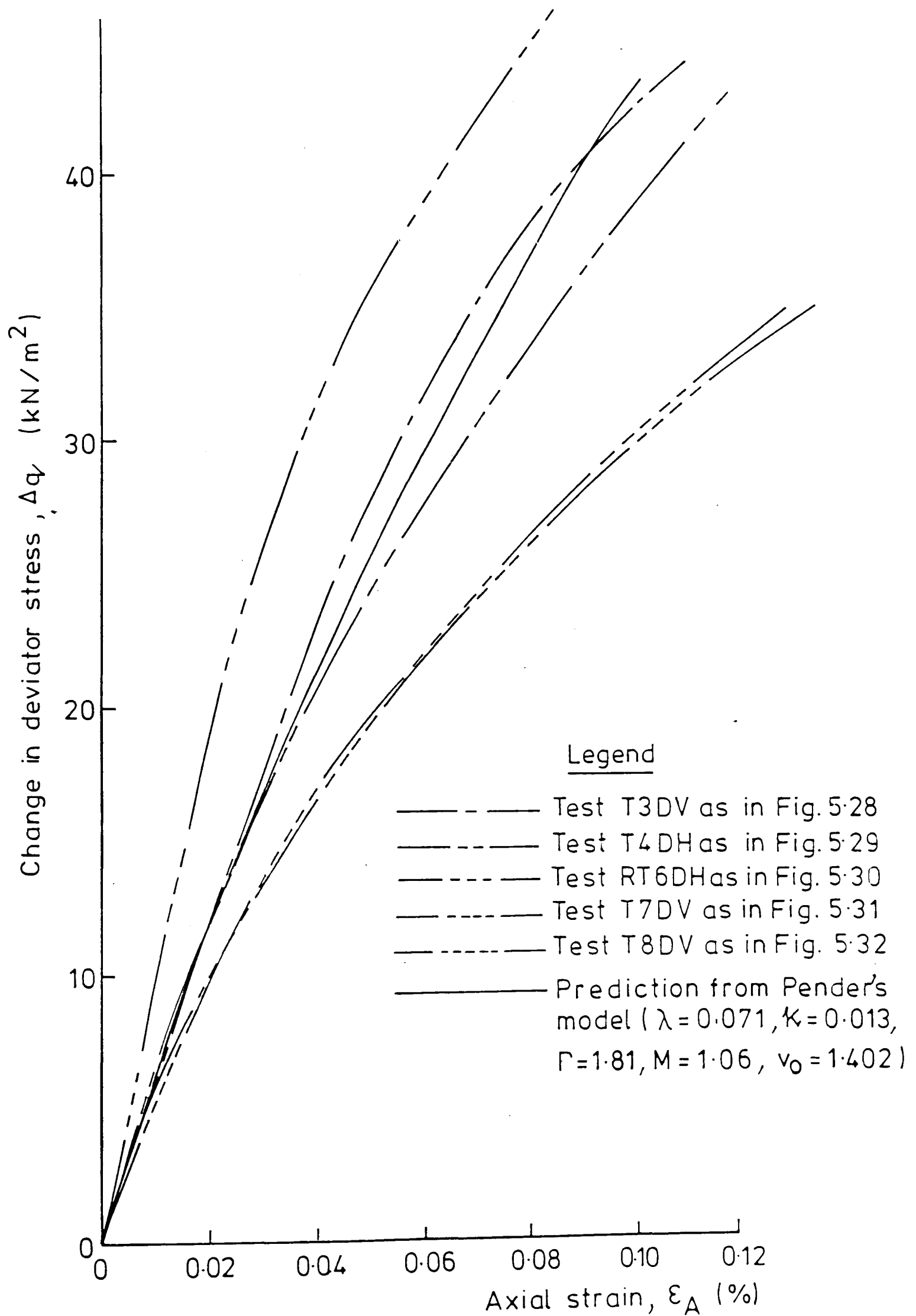
FIG. 6·17 COMPARISON OF STRESS-STRAIN CURVES FROM DRAINED TESTS WITH A CRITICAL STATE MODEL (PENDER,1978)
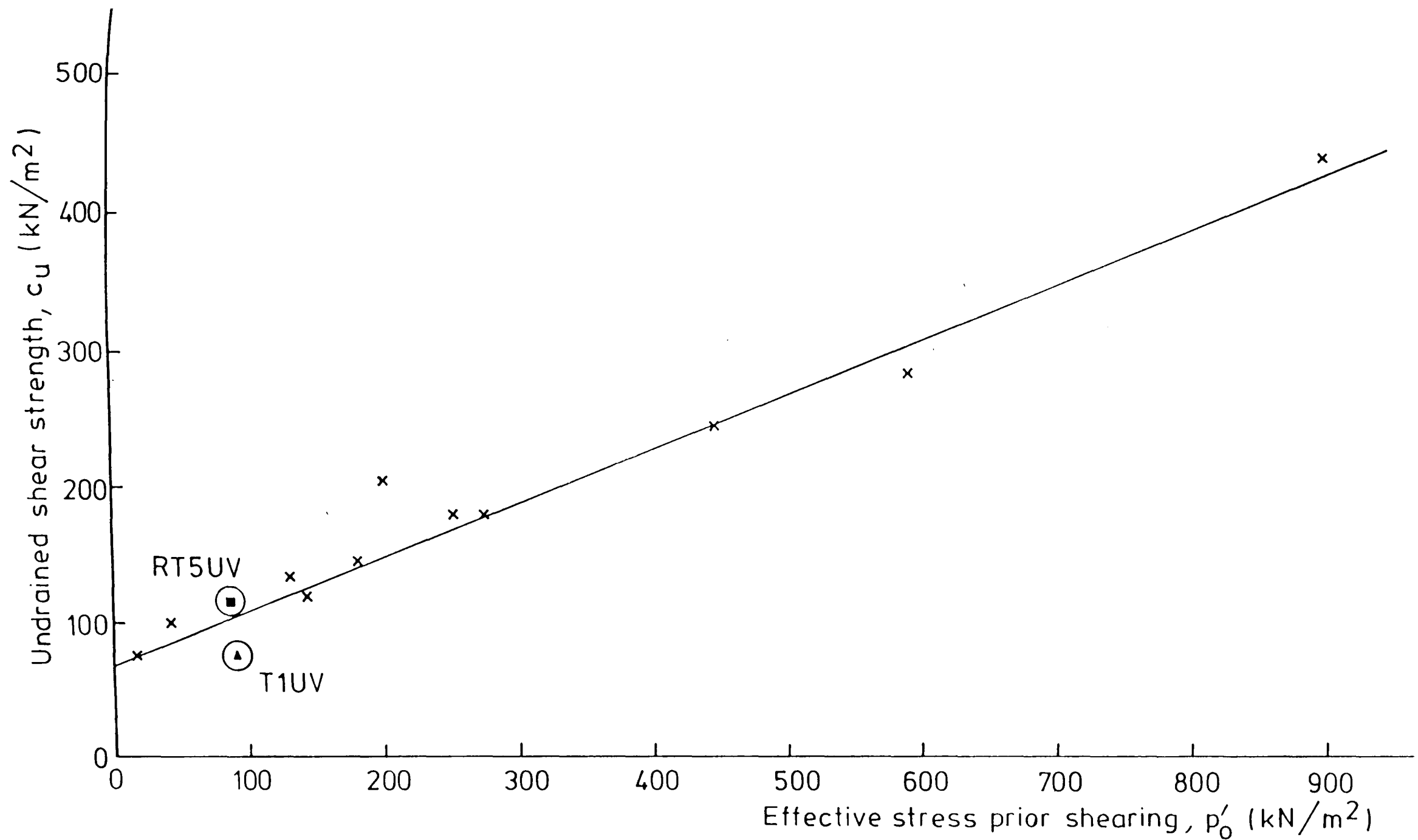
FIG. 6·18   COMPARISON OF UNDRAINED SHEAR STRENGTH FROM MAIN TESTS WITH
CONSOLIDATED UNDRAINED TESTS FROM MARSLAND AND POWELL (1985)

Undrained shear strength, c_u kN/m^2

● 98 mm Triaxial test
▲ 865 mm Plate test
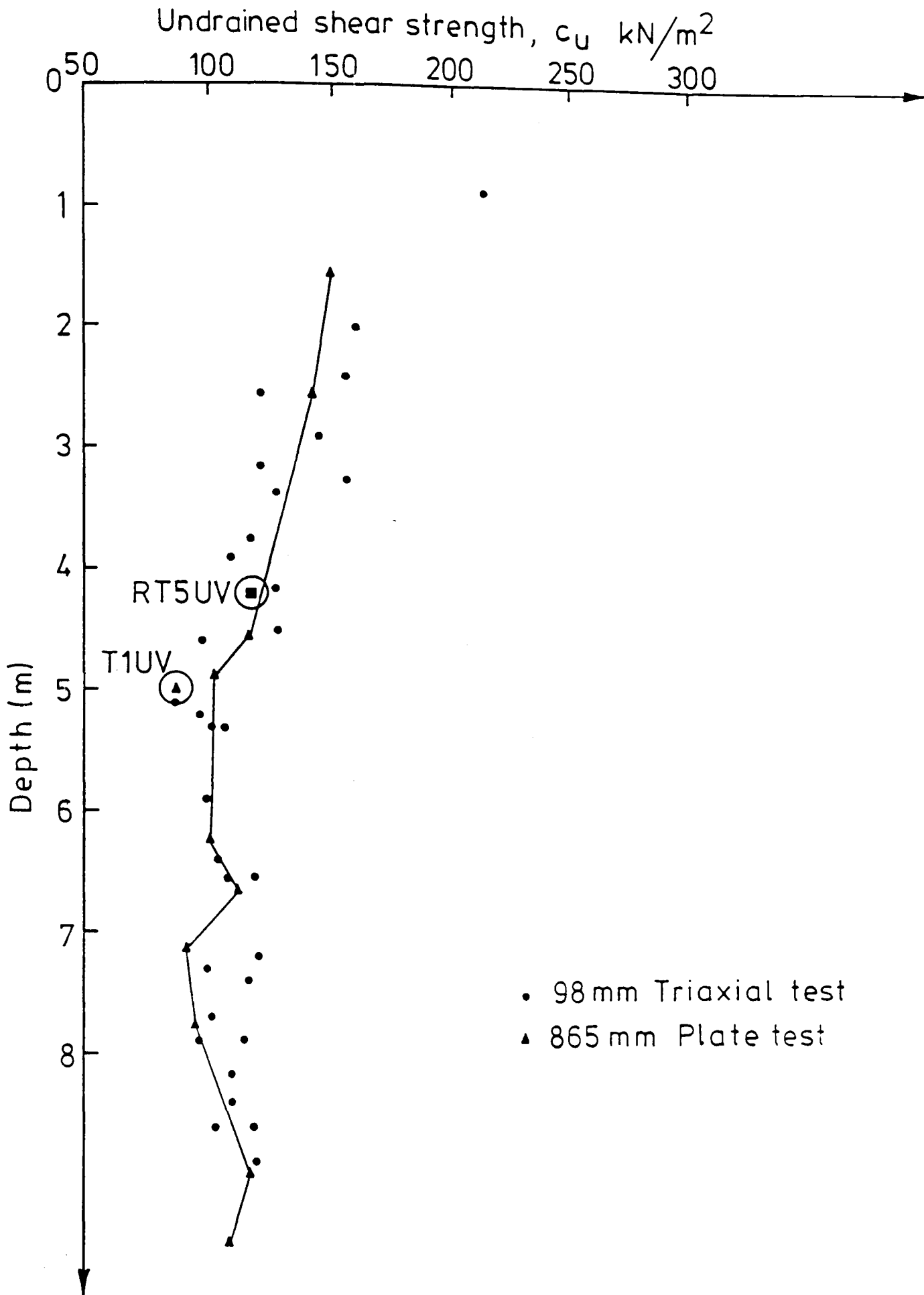
FIG. 6·19   COMPARISON OF UNDRAINED SHEAR STRENGTH FROM
MAIN TESTS WITH UNCONSOLIDATED UNDRAINED
TRIAXIAL TESTS AND PLATE TESTS FROM MARSLAND
AND POWELL (1979)
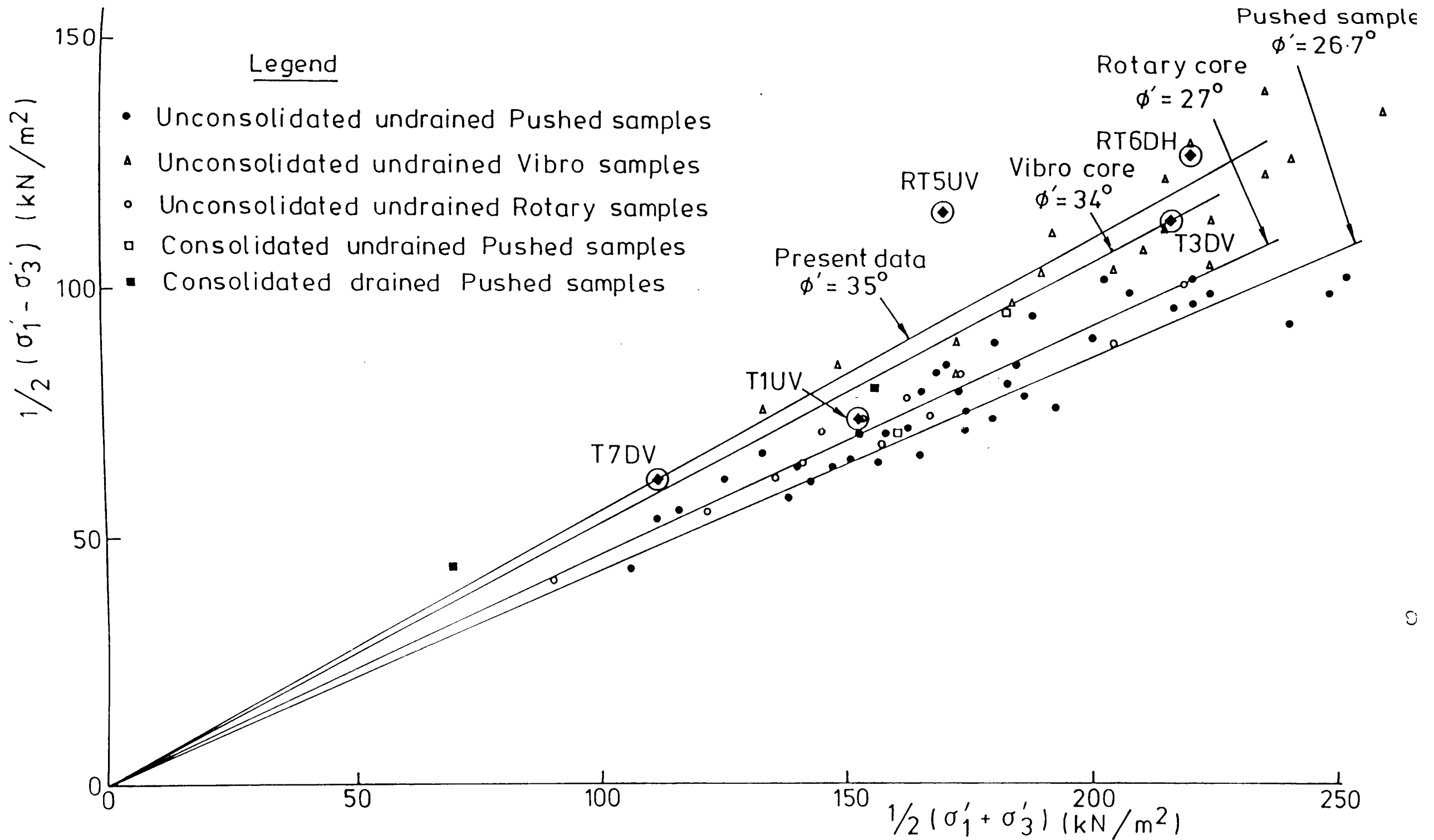
FIG.6·20   COMPARISON OF EFFECTIVE STRESS PARAMETERS WITH MARSLAND AND POWELL (1985)
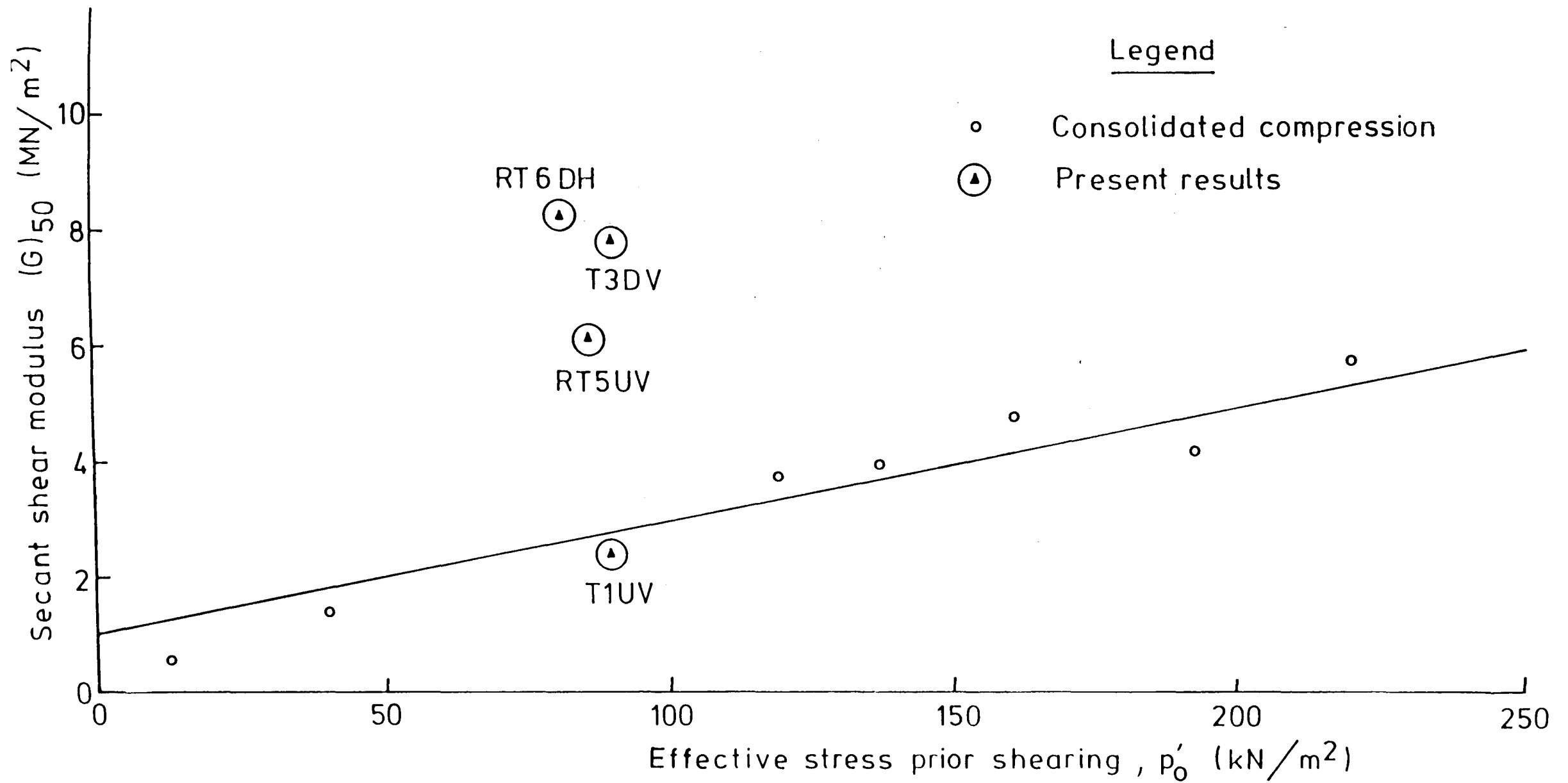
FIG. 6·21   COMPARISON OF SECANT SHEAR MODULI AT HALF OF MAXIMUM DEVIATOR STRESS WITH THOSE FROM MARSLAND AND POWELL (1985)
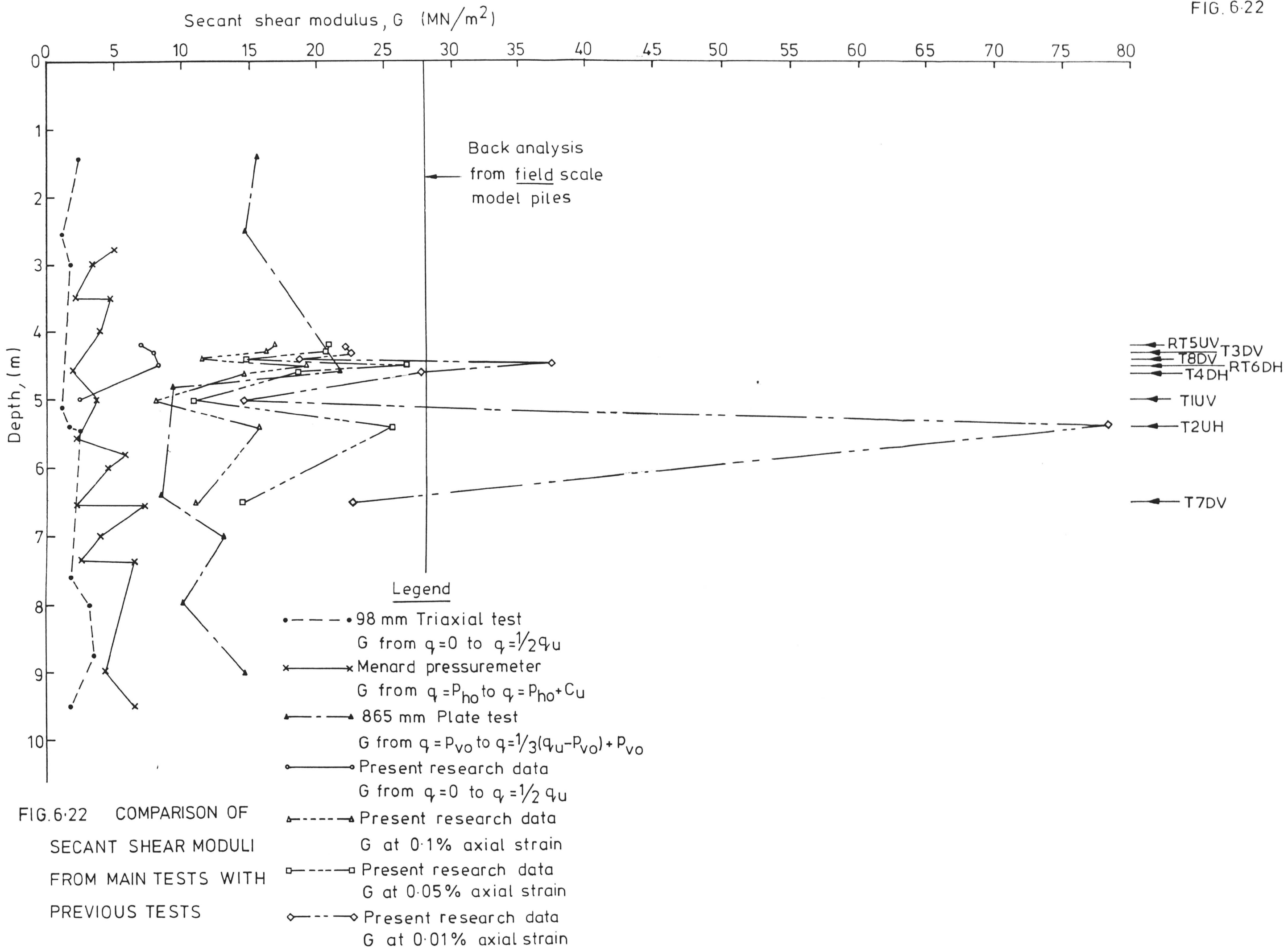
FIG. 6·22

FIG. 6·22   COMPARISON OF
SECANT SHEAR MODULI
FROM MAIN TESTS WITH
PREVIOUS TESTS
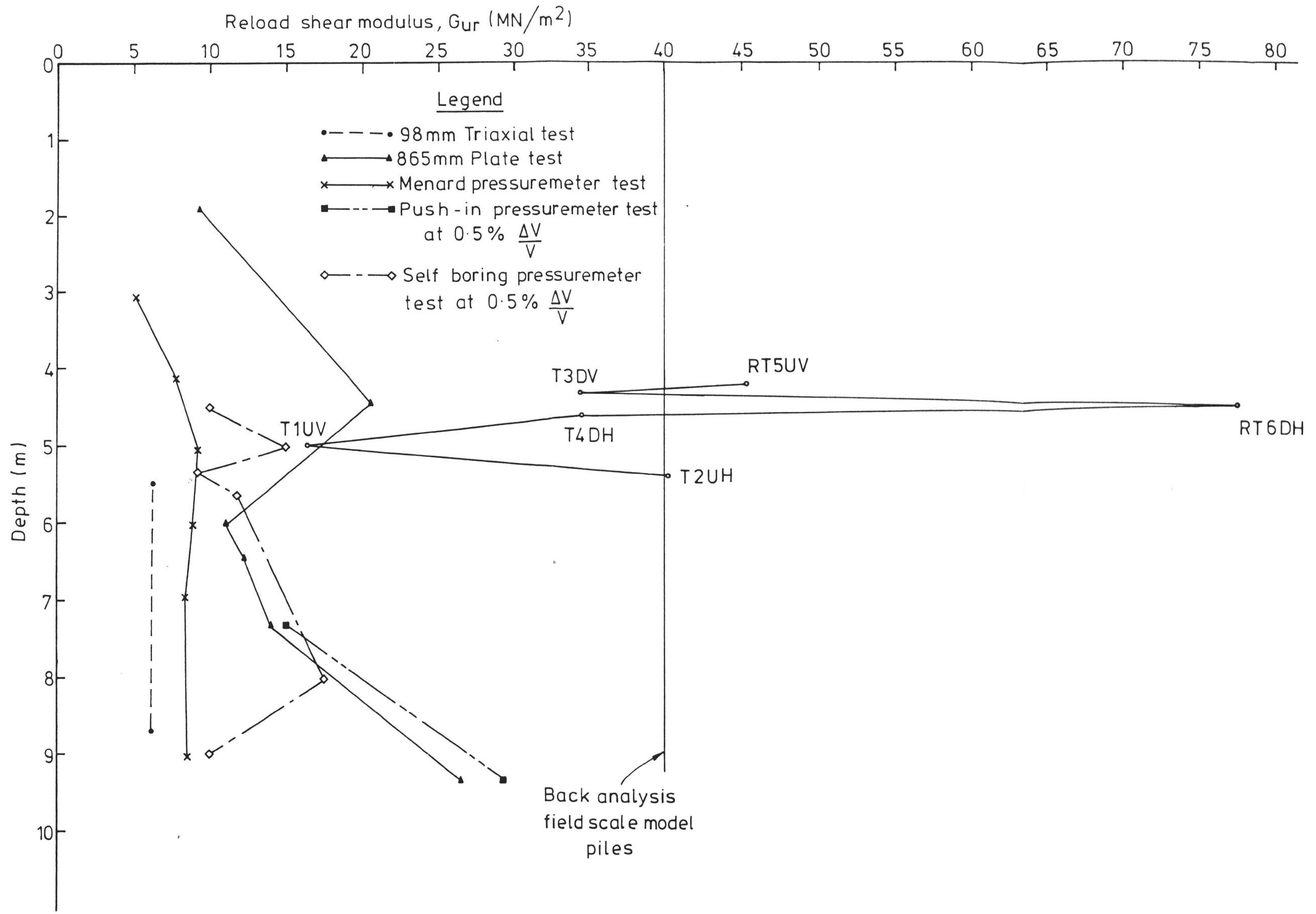
FIG. 6·23

FIG. 6·23   COMPARISON OF RELOAD SHEAR MODULI
FROM MAIN TESTS WITH PREVIOUS TESTS
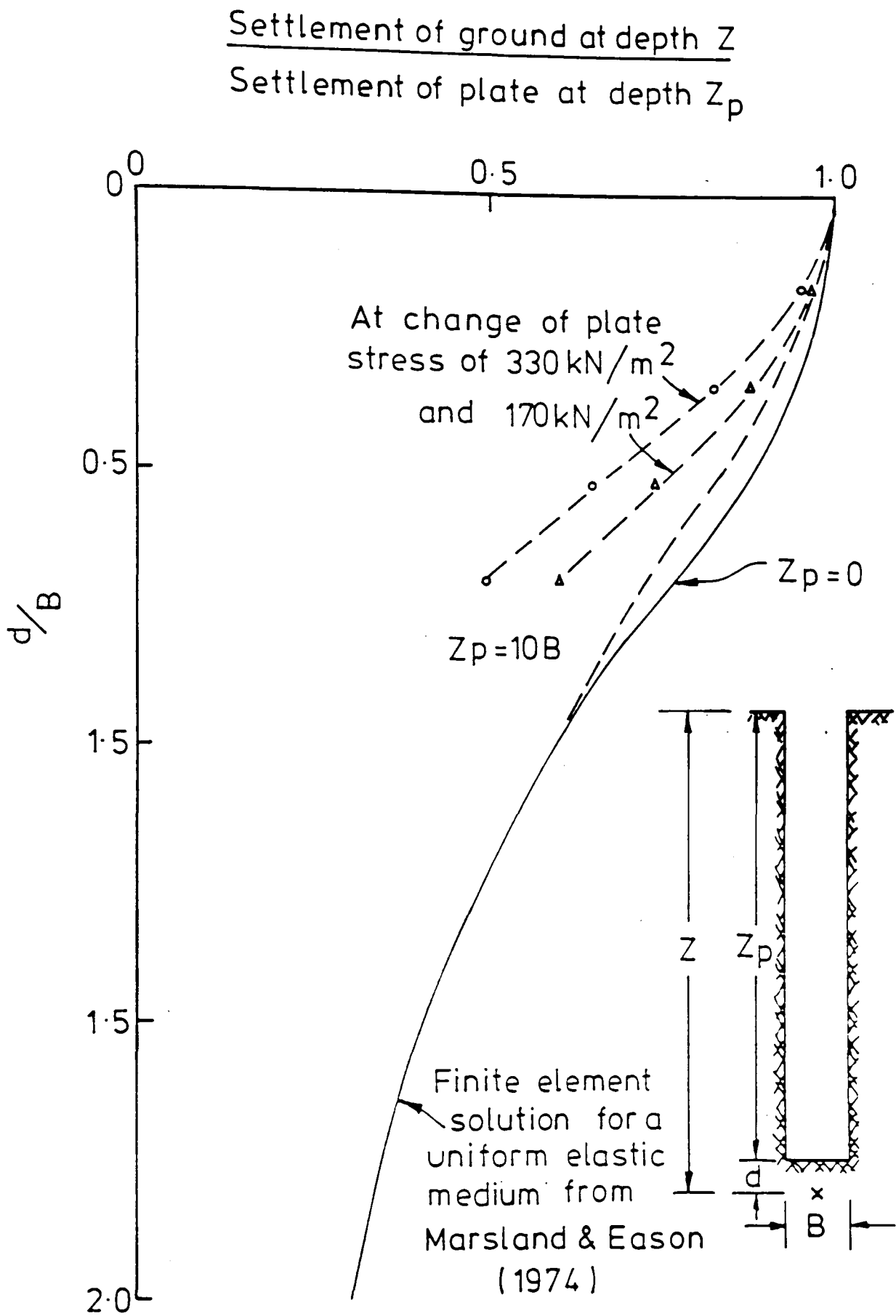
FIG. 6·24   COMPARISON OF PLATE TEST SETTLEMENT
RATIO WITH FINITE ELEMENT SOLUTION
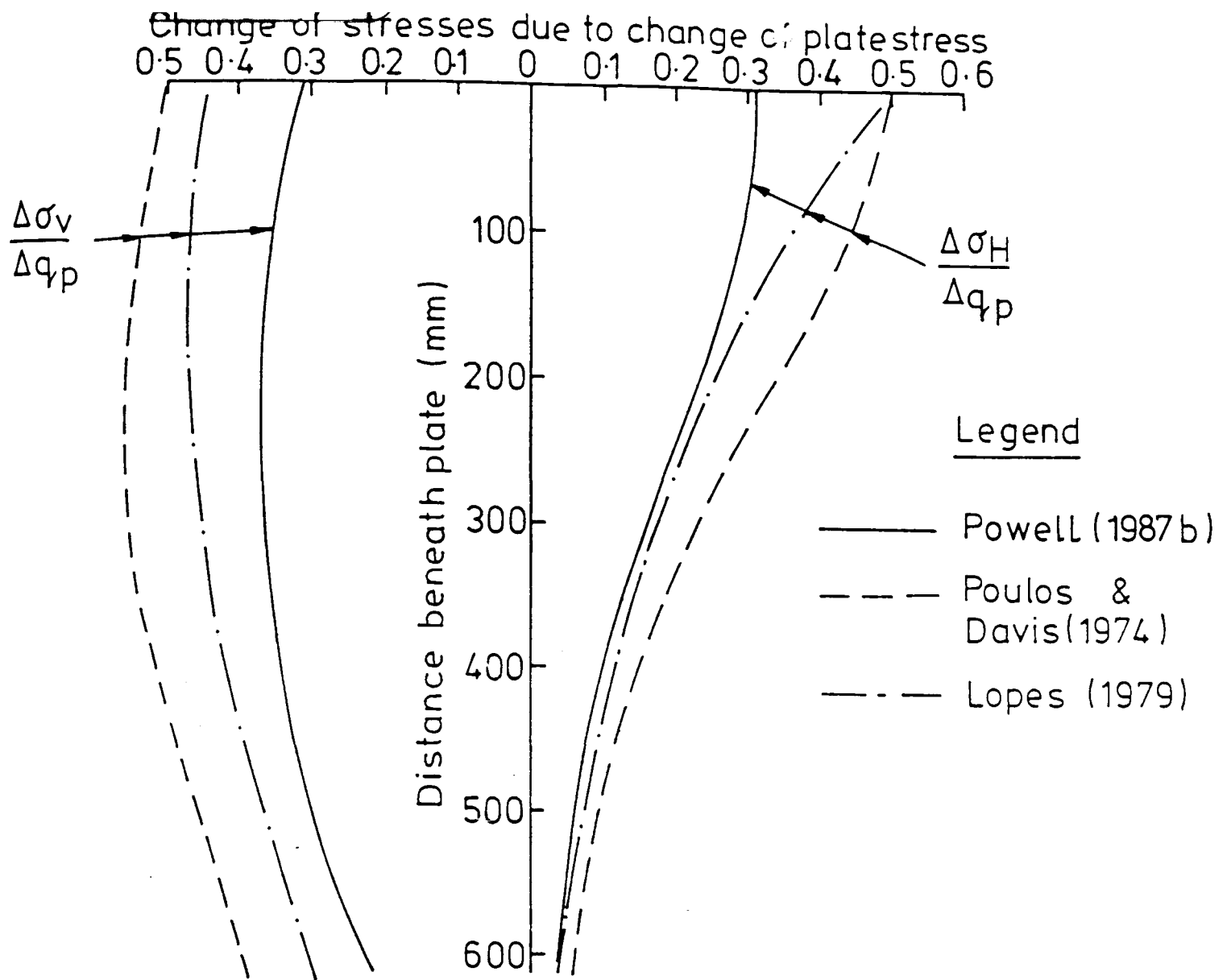
FIG. 6.25 STRESS DISTRIBUTION AT CENTRE LINE OF PLATE TEST (POWELL, 1987b)
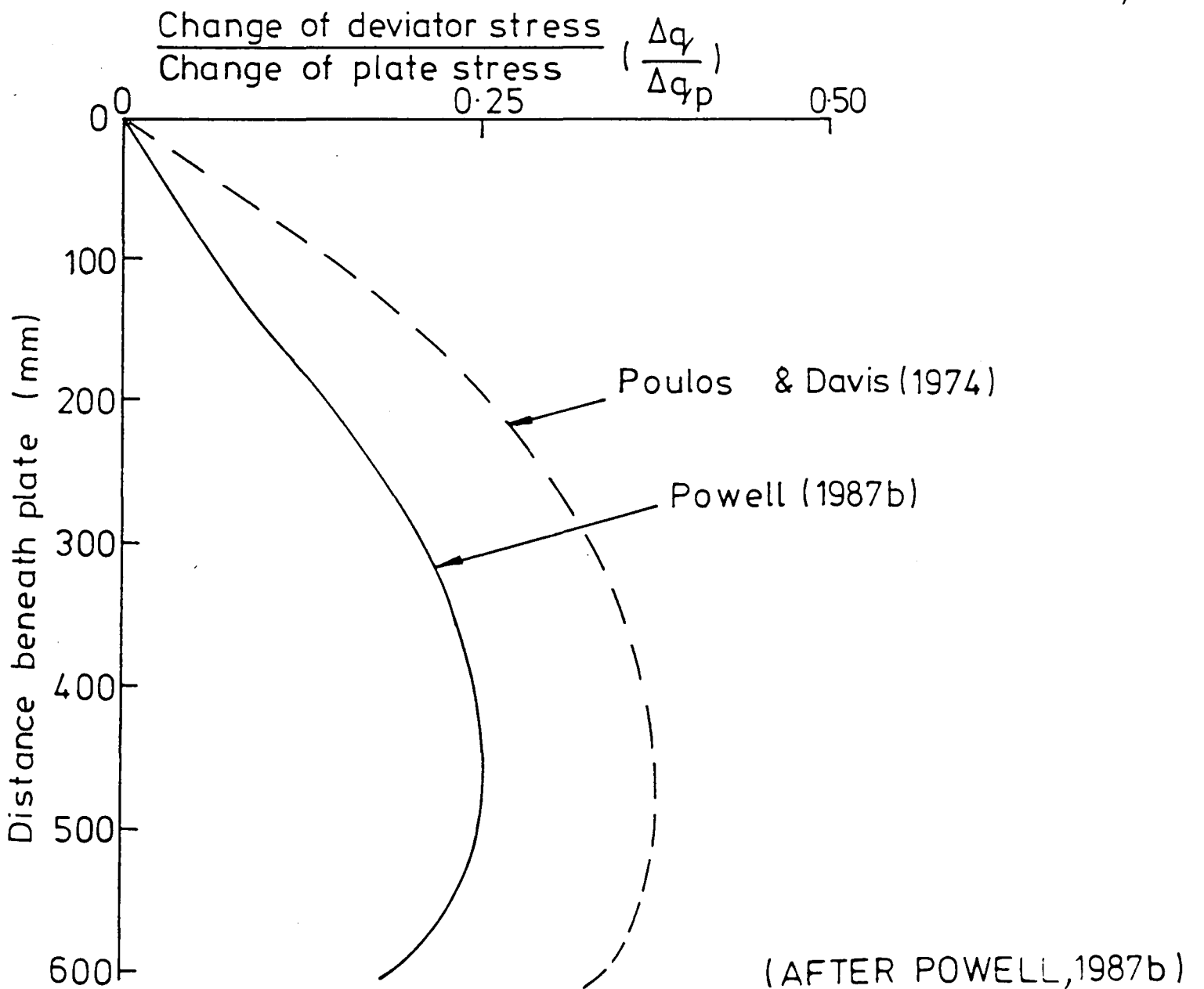
6.26 DISTRIBUTION OF DEVIATOR STRESS AT CENTRE LINE OF PLATE TEST
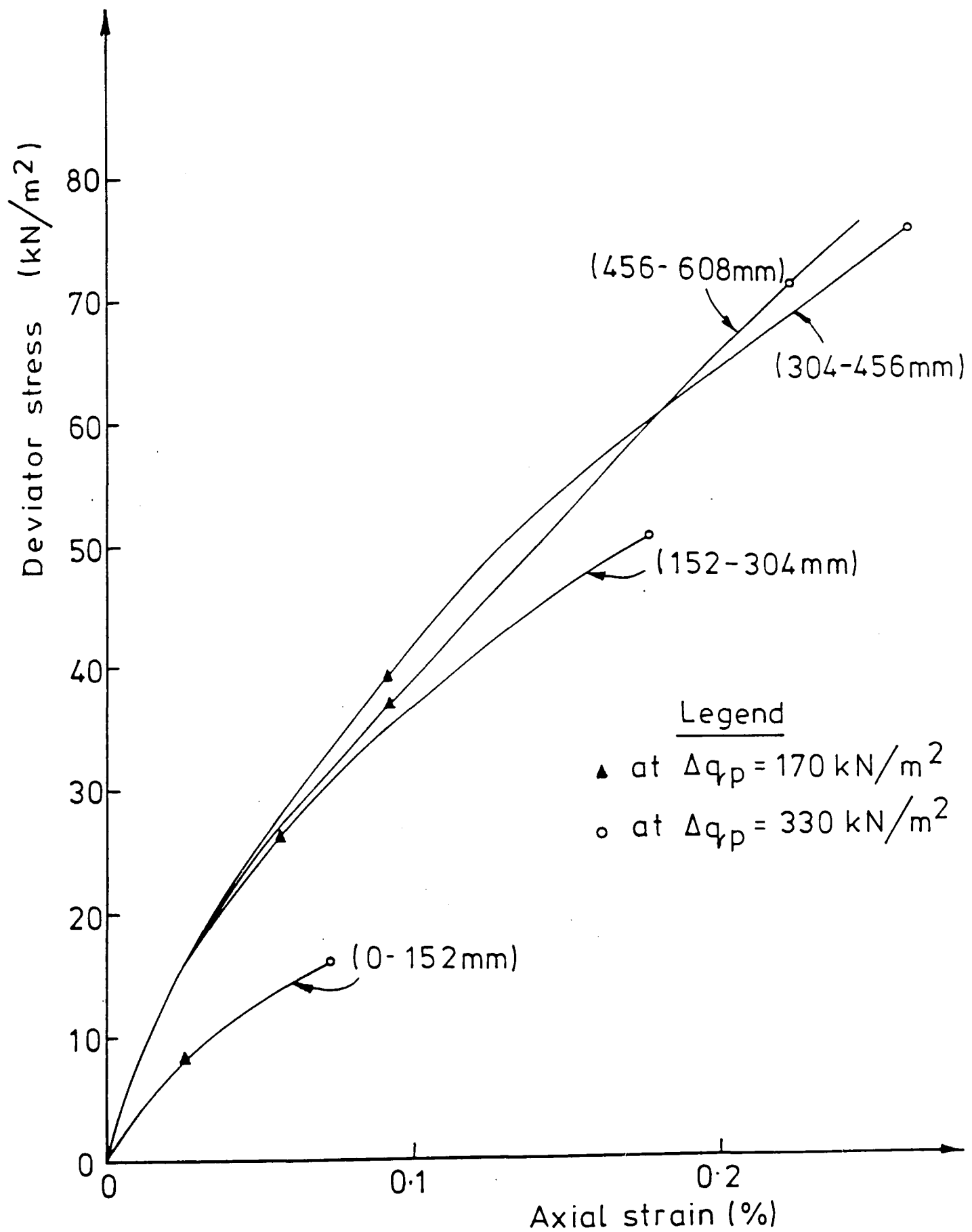
FIG. 6·27 STRESS-STRAIN CURVES DEDUCED FROM A
PLATE TEST WITH UNDER-PLATE INSTRUMENTATION
(POWELL 1987 a,b)
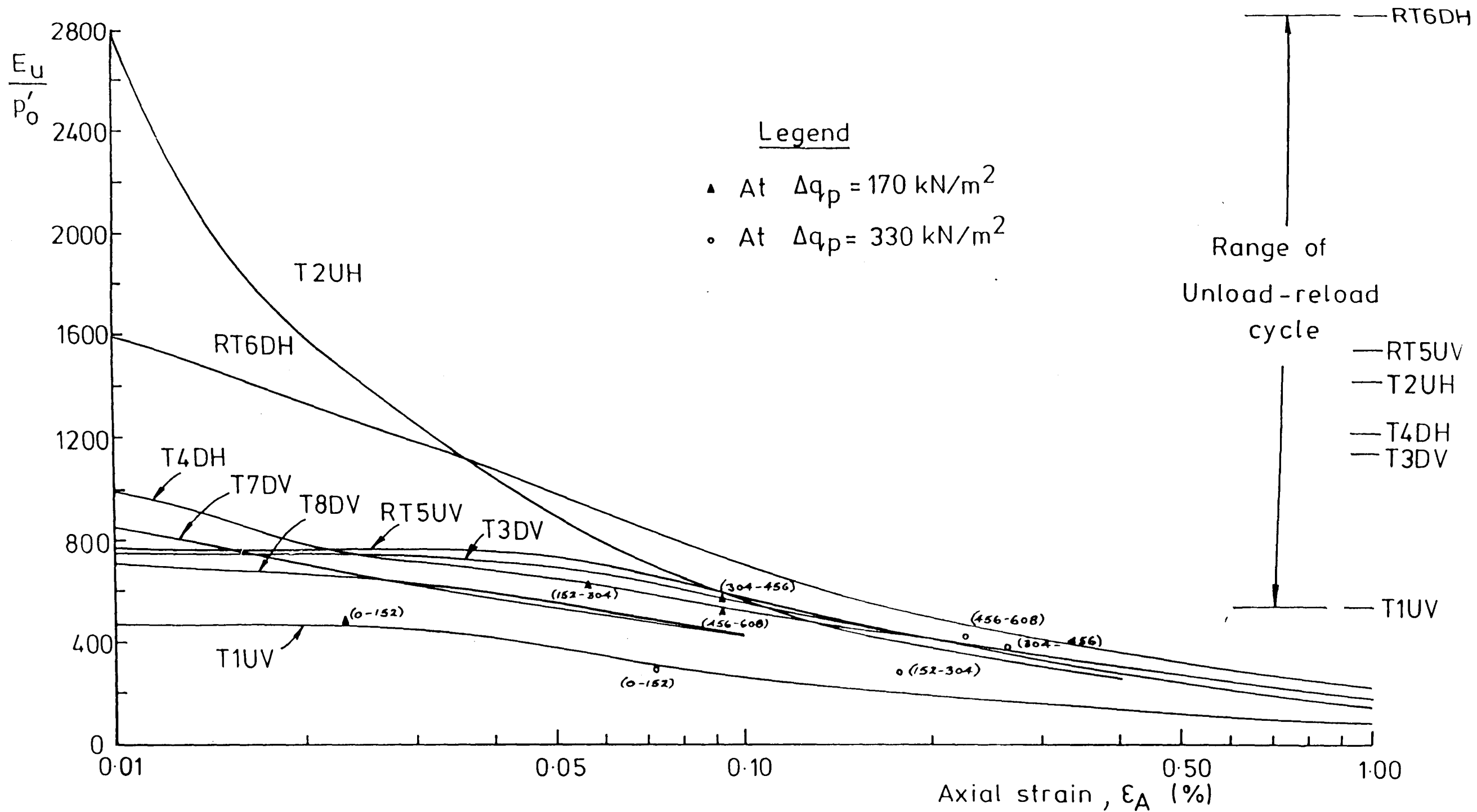
FIG. 6·28 COMPARISON OF STRESS-STRAIN CHARACTERISTICS FROM MAIN TESTS WITH A PLATE TEST (POWELL 1987 a,b)
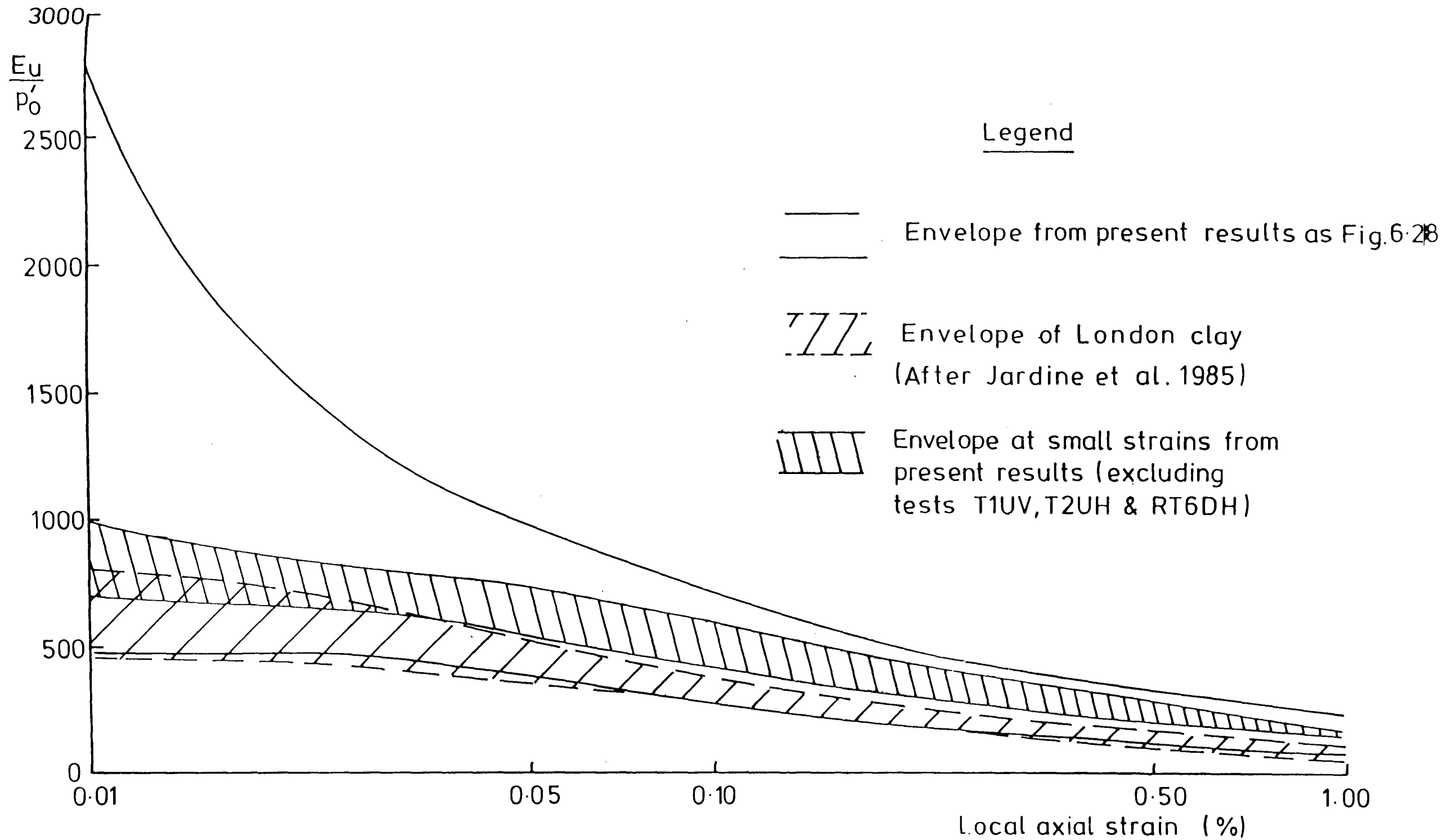
FIG.6·29   COMPARISON OF STRESS-STRAIN CHARACTERISTICS FROM MAIN TESTS WITH JARDINE ET AL (1985)

CHAPTER 7

CONCLUSIONS AND SUGGESTIONS FOR FURTHER WORK

This thesis has been concerned with the measurement of soil deformation generally and of the deformation of undisturbed Cowden Till at small strain levels (0.01 - 0.10%) in particular. In this chapter conclusions are drawn and suggestions are made concerning the equipment used, the experimental techniques and the results of the tests.

7.1   MAIN CONCLUSIONS

7.1.1 Equipment and Experimental Techniques

(1) It has proved possible to obtain 250mm diameter tube samples of Cowden Till, to extrude and store them under isotropic pressure, and to subject 100mm diameter specimens to stress path tests in a hydraulically controlled triaxial cell.

(2) A computerized control system has been successfully developed for compressive stress paths in the (p', q) plane. Difficulties were encountered in controlling the stress path accurately because of deficiencies in the design of the stress path cell (friction losses and unfavourable ratio between the upper and lower Bellofram sealed areas). These difficulties were most acute at small deviator stresses and upon reversal of the loading direction. Certain restrictions were also imposed by the computer capacity. For example, it was not possible to display the progress of a test graphically.

(3) Instrumentation has been developed to measure axial and radial strains locally in the central region of the triaxial specimen. Proximity transducers permit these local measurements to be made

within the small strain range with sufficient accuracy. The axial strain has also been measured between the specimen end caps by submersible displacement transducers (LVDTs). The local strain measurements have proved superior to the end cap measurements which have been adversely affected by bedding errors and misalignment of the LVDT's. External measurements of axial strain were inadequate at small strain levels but proved useful at larger strains in corroborating the local measurements.

(4) Difficulty was experienced in predicting suitable loading rates, due in part to uncertainty over the effectiveness of the peripheral spiral drainage employed. Consequently, some drained tests were carried out too quickly even though deviator stress was increased at only 0.7 kN/m^2/hour.

7.1.2 Results for Cowden Till

(1) The interpretation of the results has been done in the knowledge that they have been affected by non-homogeneity of the specimens due to the presence of gravel-sized particles. Also, only a limited amount of triaxial test data could be produced in the time available and data from only one field test could be directly compared.

(2) In the stress path tests on isotropically consolidated specimens, Cowden Till has been shown to exhibit strongly non-linear stress-strain behaviour, even at small strains, and most of the shear strain is irreversible (plastic). The stress-strain character-istics were in acceptable agreement with those derived from a 865mm diameter plate loading test with under-plate instrumentation providing the effect of strain level was considered. However,

some uncertainty remains concerning the interpretation of the plate test data, particularly in respect of the influence of stress relief during excavation of the borehole. Nevertheless, the present evidence suggests that plate tests provide no better information about the stiffness of Cowden Till than triaxial tests of the type described in this thesis.

(3)   At   large strains no development of localized shear zones was observed, the tests being terminated before any reduction of strength beyond the peak value could take place. The undrained strength was found to be close to that determined from plate loading tests. In terms of effective stress the strengths were higher than most of the previously published data. This is probably due to a reduction of moisture content which occurred during consolidation and storage.

(4)   Attempts have been made to analyse the compression which occurs at the end of a specimen as the axial stress is increased. This compression is part of the bedding error in conventional axial strain measurements. A quantification of the compression is hindered by the random nature of surface variations and by limitations of the presently existing theories. These theories apply for surface variations which are small in wavelength by comparison with the specimen width and are restricted to isotropic, linear elastic or rigid plastic material behaviour. The choice of equivalent linear elastic parameters to represent non-linear soil behaviour is difficult as the strains associated with the compression of the surface variations are unknown.

(5)   The experimental stress-strain behaviour at small strain levels has been compared with the predictions of a number of mathematical

models. The non-linear elastic model of Atkinson (1973) appears to be applicable to Cowden Till, for which the behaviour is approximately isotropic. Simple stiffness predictions on the basis of critical state soil mechanics (Atkinson and Bransby, 1978) are inadequate at small strains. However, the model of Pender (1978) developed for over-consolidated soils, gives a reasonable prediction of the stress-strain behaviour.

7.2   SUGGESTIONS FOR FURTHER WORK

7.2.1   Improvement of Equipment and Experimental Techniques

(1)   The stress cell path could be modified by reducing the lower Bellofram sealed area. This would permit a more sensitive control of deviator stress.

(2)   The equipment could be developed to permit extension tests to be conducted.

(3)   The control system could be improved by installing a more powerful computer. This would permit data of local strain to be processed immediately and used for control purposes. Tests could be conducted under strain control at larger strains, as suggested by Atkinson et al. (1985), and the loading rate could be adjusted in response to pore pressure information fed back from a central pore pressure transducer. A graphical display of the test's progress would also be desirable.

(4)   The mountings of the proximity transducers used for local strain measurement could be made adjustable, so that target distances could be optimized initially and maintained within

range throughout a test

7.2.2   Research on Cowden Till

(1)   Block samples could be taken, as originally intended, in order that mechanical disturbance is kept to a minimum. If similar triaxial tests were performed as on the 250mm diameter tube samples, the sensitivity of the results to sampling technique could be assessed.

(2)   Following the work undertaken by Powell (1987b), further analysis could be made of the plate loading test to clarify the stress changes taking place beneath the plate. It is particularly important to establish the extent to which the soil is being reloaded following construction of the borehole. Triaxial samples could be subjected to stress paths similar to those occurring beneath the plate.

(3)   Additional existing plate test data could be processed by the BRE to reinforce the conclusions drawn in this thesis.

REFERENCES

Allen, P.W. (1966). 'Use of Rubber in Engineering', Proc. Conf. the Use of Rubber in Engineering, London.

Atkinson, J.H. (1973). 'The Deformation of Undisturbed London Clay', Ph.D. Thesis, University of London.

Atkinson, J.H. (1975). 'Anisotropic Elastic Deformations in Laboratory Tests on Undisturbed London Clay', Geotechnique, Vol. 25, No. 2, pp. 357-374.

Atkinson, J.H. (1981). 'Foundations and Slopes', McGraw Hill Book Co., London.

Atkinson, J.H. (1984). 'Selection of Rates of Testing for Stress Path Tests', Research Report GE/84/1, The City University.

Atkinson, J.H. and Bransby, P.L. (1978). 'The Mechanics of Soils', McGraw Hill Book Co., London.

Atkinson, J.H., Evans, J.S. and Scott, C.R. (1983). 'Stress Path Testing Equipment: Spectra System Operating Manual', Research Report GE/83/1, The City University.

Atkinson, J.H., Evans, J.S. and Scott, C.R. (1985). 'Developments in microcomputer controlled stress path testing equipment for measurement of soil parameters', Ground Engineering, Vol. 18, No. 1, pp. 15-22.

Atkinson, J.H., Lewin, P.I. and Ng, C.L. (1985). 'Undrained Strength and Overconsolidation of a Clay Till', Proc. Int. Conf. on Construction in Glacial Tills and Boulder Clays, Edinburgh, pp. 49-54.

Baguelin, F., Jezequal, J.F., Le Mee, E. and Le Mchaute, A. (1972). 'Expansion of Cylindrical Probes in Cohesive Soils', Proc. ASCE, J., Soil Mech. and Found. Div., Vol. 98, No. SM11, pp. 1129-1142.

Balasubramaniam, A.S. (1976). 'Local Strains and Displacement Patterns in Triaxial Specimens of a Saturated Clay', Soils and Foundations, Vol. 16, No. 1, pp. 101-114.

Baligh, M.M. (1985). 'The Strain Path Method', Proc. ASCE, J., Geotech. Engng. Div., Vol. 111, No. 9, pp. 1108-1136.

Balla, A. (1960). 'Stress Conditions in Triaxial Compression'. Proc. ASCE, J., Soil Mech. and Found. Div., Vol. 86, No. SM6, pp. 57-84.

Barden, L. and McDermott, R.J.W. (1965). 'Use of Free Ends in Triaxial Testing of Clays', Proc. ASCE, J., Soil Mech. and Found. Div., Vol. 91, No. SM6, pp. 1-23.

Berre, T. (1983). 'Suggested International Code of Soil Engineering Practice for Triaxial Compression Test - 2nd Draft', Norwegian Geotechnical Institute.

Bishop, A.W. and Henkel, D.J. (1962). 'The Measurement of Soil Properties in the Triaxial Tests', Edward Arnold, London.

Bishop, A.W. and Wesley, L.D. (1975). 'A Hydraulic Triaxial Apparatus for _____ Path Testing', Geotechnique, Vol. 25, No. 4, pp. 657-670.

Blight, G.E. (1965). 'Shear Stress and Pore Pressure in Triaxial Testing', Proc. ASCE, J., Soil Mech. and Found. Div., Vol. 91, No. SM6, pp.25-39.

Bolton, M. (1979). 'A Guide to Soil Mechanics', Macmillan Publishers Ltd., London.

Boyce, J.R. and Brown, S.F. (1976). 'Measurement of Elastic Strain in Granular Material', Geotechnique, Vol. 26, No. 4, pp. 637-640.

British Standards Institution (1950). 'External Micrometer': BS 870.

British Standards Institution (1950). 'Slip or (Block) Gauges and their Accessories': BS 888.

British Standards Institution (1957). 'Determination of Hardness': BS 903, Part A7.

British Standards Institution (1975). 'Methods of Tests for Soils for Civil Engineering Purposes': BS 1377.

British Standards Institution (1978). 'Statistical Terminology Part 1 - Glossary of Terms Relating to Probability and General Terms Relating to Statistics': BS 5532.

British Standards Institution (1981). 'Code of Practice for Site Investigation': BS 5930.

British Standards Institution (1983). 'Precision Vernier Height Gauge': BS 1643.

British Standards Institution (1986). 'Terms used in Metrology'. BS 5233.

Broms, B.B. (1980). 'Soil Sampling in Europe: State-of-the-Art', Proc. ASCE, J., Geotechn. Engn. Div., Vol. 106, No. GT1, pp. 65-98.

Brown, S.F. and Snaith, M.S. (1974). 'The Measurement of Recoverable and Irrecoverable Deformations in the Repeated Load Triaxial Test', Geotechnique, Vol. 24, No. 2, pp. 255-259.

Burland, J.B. (1969). 'Contribution to Discussion', Proc. Conf. In-Situ Inv. in Soils and Rocks, British Geotechnical Society, London, pp. 61-62.

Burland, J.B., Broms, B.B. and De Mello, V.F.B. (1977). 'Behaviour of Foundations and Structures', Proc. 9th ICSMFE, Tokyo, Vol. 2, pp. 495-546.

Burland, J.B., Sills, G.C. and Gibson, R.E. (1973). 'A Field and Theoretical Study of the Influence of Non-homogeneity on Settlements', Proc. 8th ICSMFG, Moscow, Vol. 1.3, pp. 39-46.

Burland, J.B. and Symes, M.J. (1982). 'A Simple Axial Displacement Gauge for Use in the Triaxial Apparatus', Geotechnique, Vol. 32, No. 1, pp. 62-65.

Catt, J.A. and Penny, L.F. (1966). 'The Pleistocene Deposits of Holderness, East Yorkshire', Proc. Yorks. Geol. Soc., Vol. 35, pp. 375-420.

Clayton, C.R.I. and Khatrush, S.A. (1986). 'A New Device for Measuring Local Axial Strains on Triaxial Specimens', Geotechnique, Vol. 36, No. 4, pp. 593-597.

Costa Filho, L. de M. (1980). 'A Laboratory Investigation of the Small Strain Behaviour of London Clay', Ph.D. Thesis, University of London.

Daramola, O. (1978). 'The Influence of Stress-History on the Deformation of a Sand', Ph.D. Thesis, University of London.

Davis, R.O. and Salt, G.A. (1986). 'Strength of Undulating Shear Surfaces in Rocks', Geotechnique, Vol. 36, No. 4, pp. 503-509.

Duncan, J.M. and Dunlop, P. (1968). 'The Significance of Cap and Base Restraint', Proc. ASCE, J., Soil Mech. and Found. Div., Vol. 94, No. SM1, pp. 271-290.

El-Ruwayih, A.A. (1975). 'Stress-Strain Characteristics of Rockfill and of Clays under High Pore Water Tension', Ph.D. Thesis, University of London.

Fookes, P.G., Gordon, D.L. and Higginbottom, I.E. (1975). 'Glacial Landforms, their Deposits and Engineering Characteristics', Proc. Symp. The Engineering Behaviour of Glacial Material, Birmingham, pp. 18-51.

Gallagher, K.A. (1983). 'Research on the Behaviour of Piles as Anchorages for Buoyant Structure - Final Report, Appendix I, Section 3 - Soil Properties at Cowden', Building Research Establishment.

Gallagher, K.A. (1984). 'Tension Loading on Piles in a Glacial Till, Ph.D. Thesis, University of Sheffield.

Gallagher, K.A. and St. John, H.D. (1980). 'Field Scale Model Studies of Piles as Anchorages for Buoyant Structures', Proc. 2nd European Offshore Petroleum Conf. London.

Gens, A. (1983). 'Stress-Strain and Strength Characteristics of a Low Plasticity Clay', Ph.D. Thesis, University of London.

Gerrard, C.M. and Wardle, L. (1971). 'The Predicted Effect of Soil Sampling Disturbance on the Stresses and Strains Developed during Triaxial Testing', Proc. 4th Asian Reg. Conf. Soil Mech. and Found. Engng., Bangkok, pp. 40-48.

Gibson, R.E. (1950). 'Correspondence', J. Instn. Civ. Engrs., Vol. 34, pp. 382-383.

Gibson, R.E. and Anderson, W.F. (1961). 'In-Situ Measurement of Soil Properties with the Pressuremeter', Civil Engineering and Public Works Reviews, Vol. 56, No. 658, pp. 615-618.

Girijavallabhan, C.V. (1970). 'Stresses in a Restrained Cylinder under Axial Compression', Proc. ASCE, J., Soil. Mech. and Found. Div., Vol. 96, No. SM2, pp. 783-787.

Hadidi, F. (1984). 'The Total Fabric of Natural Clayey Soils and its Relevance to their Engineering Behaviour', Ph.D. Thesis, University of Strathclyde.

Hanna, T.H. (1985). 'Field Instrumentation in Geotechnical Engineering'. Trans. Tech. Publications, Germany.

Henderson, G., Smith, P.D.K. and St. John, H.D. (1979). 'The Development of the Push-In Pressuremeter for Offshore Site Investigation', Proc. Conf. Offshore Site Investigation, London, pp. 159-168.

Henkel, D.J. (1960). 'The Shear Strength of Saturated Remoulded Clay', Proc. Research Conf. on Shear Strength of Cohesive Soils', Colorado, pp. 533-554.

Hight, D.W. (1983). 'A Simple Piezometer Probe for the Routine Measurement of Pore Pressure in Triaxial Tests on Saturated Soils', Geotechnique, Vol. 33, No. 4, pp. 396-401.

Hight, D.W. (1983). 'Laboratory Investigations of Sea Bed Clays', Ph.D. Thesis, University of London.

Hight, D.W., Gens, A. and Jardine, R.J. (1985). 'Evaluation of Geotechnical Parameters from Triaxial Tests on Offshore Clay', Proc. Int.Conf.Offshore Site Investigation, London.

Hoare, D.J. (1978). 'Permeable Synthetic Fabric Membranes II - Factors Affecting their Choice and Control in Geotechnics', Ground Engineering, Vol. 11, No. 8, Nov., pp. 25-31.

Hoare, D.J. (1984). 'Geotextiles as Filters', Ground Engineering, Vol. 17, No. 2, March, pp. 29-44.

Hsieh, H.S. and Kavazanjian, E., Jr. (1985). 'An Automatic Triaxial Device for Measuring the At-Rest Earth Pressure Coefficient', Geotechnical Report No. GT3, University of Stanford.

Hvorslev, M.J. (1949). 'Subsurface Exploration and Sampling of Soils for Civil Engineering Purposes', Waterways Experimental Station, Mississippi River Commission, U.S. Army Corps of Engineers.

Jaeger, J.C. and Cook, N.G.W. (1976). 'Fundamentals of Rock Mechanics', John Wiley & Sons Ltd., New York.

Jardine, R.J., Symes, M.J. and Burland, J.B. (1984). 'The Measurement of Soil Stiffness in the Triaxial Apparatus', Geotechnique, Vol. 34, No. 3, pp. 323-340.

Jardine, R.J., Fourie, A., Maswoswe, J. and Burland, J.B. (1985). 'Field and Laboratory Measurements of Soil Stiffness', Proc. 11th ICSMFE, San Francisco, Vol. 2, pp. 511-514.

Johnson, K.L. (1985). 'Contact Mechanics', Cambridge University Press, Cambridge.

Kaye, G.W.C. and Laby, T.H. (1973). 'Tables of Physical and Chemical Constants', Longman Book Co., London.

Khan, M.H. and Hoag, D.H. (1979). 'A Noncontacting Transducer for Measurement of Lateral Strains', Can. Geotech. J., Vol. 16, pp. 409-411.

Kirkpatrick, W.M. and Khan, A.J. (1984). 'The Reaction of Clays to Sampling Stress Relief', Geotechnique, Vol. 34, No. 1, pp. 29-42.

Kirkpatrick, W.M., Khan, A.J. and Mirza, A.A. (1986). 'The Effects of Stress Relief on Some Overconsolidated Clays', Geotechnique, Vol. 36, No. 4, pp. 511-525.

Kubba, L.M. (1980). 'The Effect of Sampling Disturbance on the Deformation of Clay', Ph.D. Thesis, University of Wales.

Ladd, C.C., Foott, R., Ishihara, K., Schlosser, F. and Poulos, H.G. (1977). 'Stress-Strain Deformation and Strength Characteristics', Proc. 9th ICSMFE, Tokyo, Vol. 2, pp. 421-494.

Lambe, T.W. (1964). 'Methods of Estimating Settlement', Proc. ASCE, J., Soil Mech. and Found. Div., Vol. 90, No. SM5, pp. 43-67.

Lambe, T.W. (1967). 'Stress Path Method', Proc. ASCE, J., Soil Mech. and Found. Div., Vol. 93, No. SM6, pp. 309-331.

Lambe, T.W. and Marr, W.A. (1979). 'Stress Path Method: Second Edition', Proc. ASCE, J., Geotechn. Engng. Div., Vol. 105, No. GT6, pp. 727-738.

Lambe, T.W. and Whitman, R.V. (1979). 'Soil Mechanics', John Wiley & Sons Ltd., New York.

Lewin, P.I. (1970), 'Stress Deformation Characteristics of a Saturated Soil', M.Sc. Thesis, University of London.

Lopes, F.E. (1979). 'The Undrained Bearing Capacity of Piles and Plates Studied by the Finite Element Method', Ph.D. Thesis, University of London.

Maguire, W.M. (1975). 'The Undrained Strength and Stress-Strain Behaviour of Brecciated Upper Lias Clay', Ph.D. Thesis, University of London.

Marsland, A. (1971a). 'Large In-Situ Tests to Measure the Properties of Stiff Fissured Clays', Proc. 1st Aust. N.E. Conf. Geomechanics, Melbourne, Vol. 1, pp. 180-189.

Marsland, A. (1971b). 'Clays subjected to In-Situ Plate Tests', Ground Engineering, Vol. 5, No. 6, pp. 24-31.

Marsland, A. (1971c). 'The Shear Strength of Stiff Fissured Clays', Proc. of the Roscoe, Memorial Symposium, Cambridge, pp. 59-68.

Marsland, A. (1972). 'Model Studies of Deep In-Situ Loading Tests in Clay', Civil Engineering and Public Works Review, Vol. 67, No. 792, pp. 695-698.

Marsland, A. (1974). 'Comparisons of the Results from Static Penetration Tests and Large In-Situ Plate Tests in London Clay', Proc. European Symp. on Penetration Testing, Stockholm, Vol. 2/2, pp. 245-252.

Marsland, A. (1979). 'The Interpretation of In-Situ Tests in Glacial Clays', Proc. Conf. Offshore Site Investigation, London, pp. 217-228.

Marsland, A. and Eason, B.J. (1974). 'Measurement of Displacements in the Ground Below Loaded Plates in Deep Boreholes', Symp. Field Instrumentation in Geotechnical Engineering, British Geotechnical Society, pp. 304-317.

Marsland, A. and Powell, J.J.M. (1979). 'Evaluating the Large Scale Properties of Glacial Clays for Foundation Design', Proc. 2nd Int. Conf. on Behaviour of Offshore Structures, London, Vol. 1, pp. 193-214.

Marsland, A. and Powell, J.J.M. (1985). 'Field and Laboratory Investigations of the Clay Tills at the Building Research Establishment Test Site at Cowden, Holderness, Proc. Int. Conf. on Construction in Glacial Tills and Boulder Clays, Edinburgh, pp. 147-168.

Marsland, A. and Randolph, M.F. (1977). 'Comparisons of the Results from Pressuremeter Tests and Large In-Situ Plate Tests in London Clay', Geotechnique, Vol. 27, No. 2, pp. 217-243.

Maswoswe, J. (1985). 'Stress Paths for Compacted Soils during Collapse due to Wetting', Ph.D. Thesis, University of London.

Menard, L.F. (1957). 'Mesures In-Situ des Properties Physiques des Sols', Annales des Ponts et Chaussees, Vol. 127, No. 3, pp. 357-377.

Menard, L.F. (1975). 'The Interpretation and Application of Pressuremeter Test Results', Sols-Sols, No. 26.

Meyerhof, G.G. (1951). 'The Ultimate Bearing Capacity of Foundations', Geotechnique, Vol. 2, No. 4, pp. 301-331.

Meyerhof, G.G. (1961). 'The Ultimate Bearing Capacity of Wedged Shape Foundations', Proc. 5th ICSMFE, Paris, Vol. 2, pp. 105-109.

Miller, C.J. (1980). 'The Laboratory Determination of the Small Strain Behaviour for Lias Clay, and its Significance to Settlement Analysis', M.Sc. Thesis, University of London.

Moore, W.M. (1966). 'Effects of Variations in Poisson's Ratio on Soil Triaxial Testing', Highway Research REcord, No. 108, pp. 19-30.

Palmer, A.C. (1972). 'Undrained Plain-Strain Expansion of a Cylindrical Cavity in Clay: A Simple Interpretation of the Pressuremeter Test', Geotechnique, Vol. 22, No. 3, pp. 451-457.

Peck, R.B. (1969). 'Deep Excavation and Tunnelling in Soft Ground', Proc. 7th ICSMFE, Mexico, State-of-the-Art Volume, pp. 225-290.

Pender, M.J. (1978). 'A Method for the Behaviour of Overconsolidated Soil', Geotechnique, Vol. 28, No. 1, pp. 1-25.

Perloff, W.H. and Pombo, L.E. (1969). 'End Restraint Effects in the Triaxial Test', Proc. 7th ICSMFE, Mexico, Vol. 1, pp. 327-333.

Pickett, G. (1944). 'Application of the Fourier Method to the Solution of Certain Boundary Problems in the Theory of Elasticity', Journal of Applied Mechanics, ASME, Vol. 11, pp. A176-182

Poulos, H.G. and Davis, E.H. (1973). 'Elastic Solutions for Soils and Rock Mechanics', John Wiley & Sons Ltd., New York.

Powell, J.J.M. (1987a). Private Communication.

Powell, J.J.M. (1987b). 'In-situ Testing of Stiff Clays', Ph.D. Thesis, University of London (in preparation).

Powell, J.J.M., Marsland, A. and Al-Khafagi, A.N. (1982). 'Pressuremeter Testing of Glacial Clay Tills', Proc. Int. Symp. In-Situ Testing, Paris, Vol. 2, pp. 373-378.

Powell, J.J.M. and Uglow, I.M. (1985). 'A Comparison of Menard, Self-Boring and Push-In Pressuremeter Tests in a Stiff Clay Till', Proc. Int. Conf. Offshore Site Investigation, London, pp. 201-207.

Prince, A. (1986). 'The Development and Future of Computerization and Automation Data Logging in the Soil Mechanics Laboratory', Proc. Symp. Computer Applications in Geotechnical Engineering, Birmingham, pp. 147-156.

Radhakishnan, N. (1972). 'Analysis of Triaxial Tests by the Finite Element Method', Proc. Symp. Appl. Fin. El. Method. in Geotech. Engng., Vicksburg, Mississippi, pp. 949-1004.

Randolph, M.F. and Wroth, C.P. (1978). 'Analysis of Deformation of Vertically Loaded Piles', Proc. ASCE, J., Geotechn. Engng. Div., Vol. 104, No. GT12, pp. 1465-1488.

Rendulic, L. (1938). 'Pore-Index and Pore Water Pressure', Bauingenieur, Vol. 17, pp. 559.

Roscoe, K.H. (1970). 'The Influence of Strains in Soil Mechanics', Geotechnique, Vol. 20, No. 2, pp. 129-170.

Roscoe, K.H. and Burland, J.B. (1968). 'On the Generalized Stress-Strain Behaviour of Wet Clay', Engineering Plasticity, ed. J. Heyman and F.A. Leckie, Cambridge University Press, pp. 535-609.

Rowe, P.W. (1968). 'Failure of Foundations and Slopes on Layered Deposits in Relation to Site Investigation Practice', Proc. ICE, Supplementary Volume, pp. 73-131.

Rowe, P.W. (1971). 'Representative Sampling in Location, Quality and Site', ASTM, Spec. Techn. Publ. 483, pp. 77-106.

Rowe, P.W. and Barden, L. (1964). 'Importance of Free Ends in Triaxial Testing', Proc. ASCE, J., Soil Mech. and Found. Div., Vol. 90, No. SM1, pp. 1-27.

Sarsby, R.W., Kalezotis, N. and Hadded, E.H. (1980). 'Bedding Error in Triaxial Tests on Granular Media', Geotechnique, Vol. 30, No. 3, pp. 302-309.

Schmidt, B. (1966). 'Discussion of Earth Pressure at Rest Related to Stress History', Can. Geotech. J., Vol. 3, No. 4, pp. 239-242.

Schofield, A.N. and Wroth, C.P. (1968). 'Critical State Soil Mechanics', McGraw Hill Book Co., London.

Simpson, B., O'Riordan, N.J. and Croft, O.D. (1979). 'A Computer Model for the Analysis of Ground Movements in London Clay', Geotechnique, Vol. 29, No. 2, pp. 149-175.

Skempton, A.W. (1961). 'Horizontal Stresses in an Overconsolidated Eocene Clay', Proc. 5th ICSMFE, Paris, Vol. 1, pp. 351-357.

Skempton, A.W. and Bjerrum, L. (1957). 'A Contribution to the Settlement Analysis of Foundations on Clay', Geotechnique, Vol. 7, No. 4, pp. 168-178.

Skempton, A.W. and Sowa, V.A. (1963). 'The Behaviour of Saturated Clays during Sampling and Testing', Geotechnique, Vol. 13, No. 4, pp. 269-290.

Som, N.N. (1968). 'The Effect of Stress Path on the Deformation and Consolidation of London Clay', Ph.D. Thesis, University of London.

Sutton, H. (1979). 'Stress and Strain Paths in the Triaxial Cell', Ph.D. Thesis, University of Surrey.

Swedish Geotechnical Committee (1961). 'Standard Piston Sampling', Proc. Swedish Geotechnical Institute, No. 19.

Symes, M.J. and Burland, J.B. (1984). 'Determination of Local Displacements on Soil Samples', Geotechnical Testing Journal, ASTM, Vol. 7, No. 2, pp. 49-54.

Taylor, J.R. (1982). 'An Introduction to Error Analysis', University Science Books, Oxford University Press.

Tedd, P. and Charles, J.A. (1981). 'In-Situ Measurement of Horizontal Stresses in Overconsolidated Clay using Push-In Spade-Shaped Pressure Cells', Geotechnique, Vol. 31, No. 4, pp. 554-558.

Tedd, P. and Charles, J.A. (1983). 'Evaluation of Push-In Pressure Cell Results in Stiff Clay', Proc. Int. Symp. In-Situ Testing, Paris, Vol. 2, pp. 579-584.

Timoshenko and Goodier, J.N. (1971). 'Theory of Elasticity', McGraw Hill Book Co., New York.

Terzaghi, K. (1943). 'Theoretical Soil Mechanics', John Wiley & Sons Ltd., New York.

Windle, D. and Wroth, C.P. (1971). 'In-Situ Measurements of the Properties of Stiff Clays', Proc. 9th ICSMFE, Tokyo, Vol. 1, pp. 347-352.

Woods, R.I. and Clinton, D.B. (1986). 'A Microcomputer Stress Path Testing and Data Analysis System for Research and Practice', Proc. Symp. Computer Applications in Geotechnical Engineering', Birmingham, pp. 137-145.

Wroth, C.P. (1971). 'Some Aspects of the Elastic Behaviour of Over-consolidated Clay', Proc. of the Roscoe Memorial Symposium, Cambridge, pp. 347-361.

Wroth, C.P. (1982). 'British Experience with the Self-Boring Pressure-meter', Proc. Symp. Pressuremeter and its Marine Applications, Paris, pp. 143-164.

Wroth, C.P. and Huges, J.M.O. (1973). 'An Instrument for the In-Situ Measurement of the Properties of Soft Clays', Proc. 8th ICSMFE, Moscow, Vol. 1.2, pp. 487-494.